

Palaeovolcanic and present magmatic structures along the N-S trending Regensburg-Leipzig-Rostock zone

kumulative Dissertation
zur Erlangung des akademischen Grades
Doktor der Naturwissenschaften
doctor rerum naturalium - Dr. rer. nat.

vorgelegt dem Rat der Chemisch-Geowissenschaftlichen Fakultät
der Friedrich-Schiller-Universität Jena
von Diplom-Geophysiker Tobias Nickschick
geboren am 18.11.1985 in Wernigerode



Gutachter:

1. Prof. Dr. Lothar Viereck

2. Prof. Dr. Florian Bleibinhaus

Tag der Veteidigung: 18.01.2017

Vorwort

Diese Abschlussarbeit entstand während meiner Anstellung und Tätigkeit als wissenschaftlicher Mitarbeiter in der Sektion 3.2 Organische Geochemie am Helmholtz-Zentrum Potsdam - Deutsches GeoForschungsZentrum GFZ durch die Drittmittelfinanzierung der Deutschen Forschungsgemeinschaft DFG in einem gemeinsamen Projekt mit der Universität Leipzig. Diese kumulative Dissertation ist in zwei in sich geschlossene Teile aufgeteilt. Der erste Teil befasst sich mit dem übergreifenden Thema der Dissertation, der Regensburg-Leipzig-Rostock-Störungszone, der zweite Teil befasst sich mit den von meinen Coautoren und mir verfassten Fachpublikationen zu ausgewählten Einzelfallbeispielen innerhalb des Gesamtrahmens.

Um das Gesamtlayout dieser Dissertation nicht zu stören, werden die insgesamt vier Publikationen, von denen drei bereits publiziert sind und eine eingereicht ist, in einem separaten Teil zusammengefasst präsentiert, womit der Auflage der Promotionsordnung die Originalversionen der Publikationen zu präsentieren, erfüllt wird. Der erste Teil wurde von mir als alleinigem Autor verfasst, die Artikel, die im zweiten Teil zusammengefasst sind, entstanden in einem Autorenkollektiv. Die Anteile des jeweiligen Kollegen an der Erstellung der Publikationen sind im Anschluss an diese Arbeit zu finden. Da die Artikel sprachlich aufgrund des Autorenkollektivs auf die 1. Person Plural zurückgreifen, wird diese auch im ersten Teil verwendet.

Zusammenfassung

Die hier vorliegende Dissertation beschäftigt sich mit der Regensburg-Leipzig-Rostock Störungszone, einem etwa 700 km langen und rund 40 km breiten Verbund aus einzelnen Störungslineamenten unter besonderer Betrachtung der gegenwärtigen und vergangenen vulkanischen und magmatischen Aktivität. Die Regensburg-Leipzig-Rostock Störungszone wird häufig in der aktuellen Literatur verwendet um ein besonderes Phänomen rezenter Fluidaufstiegs zu charakterisieren, die sogenannten Erdbebenschwärme. Allerdings wird hierbei oft nicht auf die Hintergründe für den Auslösemechanismus eingegangen, welche die eben genannten, magmatisch bedingten Aufstiege von Fluiden sind. Häufig sind diese an Kreuzungsbereichen von tiefreichenden Störungen angesiedelt, welche Schwächezonen für aufsteigende Fluide und Magmen darstellen. In dieser Arbeit wird daher eine Kompilation aus bisher bekannten Vulkanfeldern und Einzelstrukturen entlang dieser Störungszone erstellt und um aktuelle Forschung in Form von Fachpublikationen des Promovenden erweitert.

Entlang der Regensburg-Leipzig-Rostock Störungszone lassen sich vor allem ultramafische bis karbonatitische, vulkanische oder sub-vulkanische Ausprägungsformen entdecken, wie beispielsweise Maar-Diatrem-Vulkane, tief erodierte Diatreme, Schlackekegel, verdeckte Intrusionen oder Gänge. Jener Mechanismus ist überwiegend mit einer Magmenherkunft aus dem lithosphärischen Oberen Mantel assoziiert. Auffällig dabei ist die hohe Variabilität der Alter der Vulkanfelder. Die ältesten Vorkommen bisher bekannter vulkanischer Tätigkeit sind dabei der Delitzsch- bzw. Delitzsch-Bitterfeld-Komplex und ein bisher unbekanntes Feld aus Diatremen in der Nähe des heutigen Erdbebenschwarmgebietes um Werdau, welches etwa 70 bis 80 km entfernt von Delitzsch liegt. Aktiver Vulkanismus im Tertiär (Paläogen und Neogen) entlang der Störungszone lässt sich unter anderem im Vogtland, in Nordostbayern und Nordwestböhmen finden, dessen Ursache möglicherweise in der Öffnung des Eger Grabens (Eger Riftes) zu suchen ist. Junge vulkanische Aktivität des Quartärs kann anhand von zwei bekannten Schlackekegeln und einem Maar-Diatrem-Vulkan im nordwestböhmischen Cheb-Becken untersucht werden und selbst gegenwärtig andauernde magmatische Aktivität ist unterhalb dieses Beckens zu verzeichnen. Insbesondere die Mofettenfelder um Hartoušov und Bublák im Cheb-Becken sind dabei besonders geeignete Untersuchungslokalitäten für die Beobachtung einer rezenter Magmenintrusion. Die Nähe zu dem durch fluidinduzierte Erdbebenschwärme seismisch aktivsten Gebiet, des Nový Kostel Hypozentralgebietes, welches sich direkt nördlich der Mofettenfelder entlang einer Nord-Süd-verlaufenden Störung befindet, ist dabei wissenschaftlich brisant. Die hier vorgestellte Übersicht der Vulkanfelder wird ergänzt um insgesamt vier Studien zu drei verschiedenen magmatisch-bedingten Strukturen: dem kretazischen, vermuteten Diatrem nahe Greiz, dem quartären Maar-Diatrem in der Nähe von Mýtina an der tschechisch-deutschen Grenze und dem durch magmatische Fluide stark entgasenden Mofettenfeld Hartoušov im Cheb-Becken. Der Einfluss einer derart tiefreichenden, über lange Zeit für Fluide und Magmen passierbaren Störungszone in Zentraleuropa ist bislang nicht geklärt, auch wenn das Vorhandensein dieser Störungszone in vielen Studien vorausgesetzt wird.

Summary

This PhD thesis focuses on the Regensburg-Leipzig-Rostock fault zone, a network of single fault lineaments of about 700 km length and about 40 km width in total, under special consideration of past and present volcanic and magmatic activity. The Regensburg-Leipzig-Rostock zone is often used in recent studies to explain a very well-researched and characteristic phenomenon of recent fluid ascent, the so-called earthquake swarms. However, these studies often do not account for the background of the actual trigger, which is the aforementioned magmatically induced migration of fluids. In most cases fluid ascent occurs at intersections of deep-reaching faults, which provide excellent ascent paths for migrating fluids. Within the frame of this thesis a compilation of currently known volcanic provinces and singular formations is created and supplemented by recent research results in form of scientific articles written by the author of this PhD thesis.

Along the Regensburg-Leipzig-Rostock zone mainly ultramafic and carbonatitic volcanic to subvolcanic formations can be found in the forms of maar-diatreme-volcanoes, deeply eroded diatremes, scoria cones, hidden and covered intrusions or dykes etc. The different volcanic provinces feature a high variability in their respective ages of formation. The oldest formations associated with this fault zone are the Cretaceous Delitzsch, or Delitzsch-Bitterfeld, complex and a yet unknown volcanic field of similar age near the seismically active area around Werdau, which is about 70 to 80 km away from the Delitzsch complex. Volcanic activity in the Tertiary (Palaeogene and Neogene) can be studied in the Vogtland area, in north-eastern Bavaria and north-west Bohemia, which are presumed to have been formed due to the rifting process of the Eger Graben (Eger rift). Young volcanism within the Quaternary has so far been found in the north-west Bohemian Cheb Basin in form of two scoria cones and one maar-diatreme-volcano. A recently ongoing magmatic intrusion has been observed beneath the Cheb Basin within two mofette fields (Hartoušov and Bublák) which are directly related to a N-S running lineament. In continuation of this lineament is the Nový Kostel focal area, which is characterized by recurring, fluid-triggered seismic activity in form of earthquake swarms. The compilation of volcanic provinces presented here is supplemented by new information from four studies on three separate magmatically influenced structures: an assumed diatreme of Cretaceous age near the city of Greiz, the Quaternary Mýtina maar at the German-Czech border and the mofette field of Hartoušov which is heavily influenced by the ascent of magmatic fluids. The impact of a deep-reaching fault zone which is passable for fluids and magma over such a long period of time has is not completely understood, even though many studies take the existence of this fault zone for granted.

Im Zusammenhang mit dieser Doktorarbeit entstanden die folgenden wissenschaftlichen Beiträge:

ISI-Standard-Publikationen

1. **Nickschick, T.**, Flechsig, C., Meinel, C., Mrlina, J., Kämpf, H. (submitted to International Journal of Earth Sciences) Architecture and temporal variations of a terrestrial CO₂ degassing site using electric resistivity and CO₂ gas measurements.
2. Flechsig, C., Heinicke, J., Mrlina, J., Kämpf, H., **Nickschick, T.**, Schmidt, A., Bayer, T., Günther, T., Rücker, C., Seidel, E., Seidl, M. (2015) Integrated geophysical and geological methods to investigate the inner and outer structures of the Quaternary Mýtina maar (W-Bohemia, Czech Republic). International Journal of Earth Sciences 104(8):2087-2105
3. **Nickschick, T.**, Kämpf, H., Flechsig, C., Mrlina, J., Heinicke, J. (2015) CO₂ degassing in the Hartoušov mofette area, western Eger Rift, imaged by CO₂ mapping and geoelectrical and gravity surveys. International Journal of Earth Sciences 104(8):2107-2129
4. **Nickschick, T.**, Kämpf, H., Jahr, T. (2014) The "Triasscholle" near Greiz, Germany - a volcanic origin? Bulletin of Volcanology 76(4):1-20

Andere Publikationen

1. Alawi, M., **Nickschick, T.**, Kämpf, H. (2015) Mikrobiologische Prozesse in CO₂-Aufstiegskanälen. System Erde 5(1):28-33

Konferenzbeiträge

1. **Nickschick, T.**, Flechsig, C., Kämpf, H. (2016) Architecture and seasonal variations of a terrestrial CO₂ degassing site using electric resistivity measurements and CO₂ gas measurements. 76. Jahrestagung der Deutschen Geophysikalischen Gesellschaft, 14.-17.03.2016 in Münster, Poster
2. **Nickschick, T.**, Kämpf, H., Flechsig, C., Mrlina, J., Heinicke, J. (2015) CO₂-Degassing in the Hartoušov Mofette Area, Western Eger Rift: CO₂ Mapping and Geophysical Surveys as a Multi-method Approach in a Non-volcanic Terrestrial Area. International Conference on Gas Geochemistry, 24.-31.08.2015, Chengdu, China, Vortrag
3. **Nickschick, T.**, Flechsig, C., Mrlina, J., Kämpf, H., Heinicke, J. (2015) 3D Modelling of the Mýtina maar (NW-Bohemia, Czech Republic) using geoelectric, gravity and geomagnetic data. 75. Jahrestagung der Deutschen Geophysikalischen Gesellschaft, 23.-26.03.2015 in Hannover, Poster
4. **Nickschick, T.**, Kämpf, H., Flechsig, C., Mrlina, J., Heinicke, J. (2014) CO₂-degassing in the Hartoušov mofette area, western Eger Rift, based on combined CO₂ soil gas, CO₂ gas flux, geoelectrical and gravimetric surveys, GeoFrankfurt 22.-24.9.2014, Frankfurt, Vortrag
5. Kämpf, H., Flechsig, C., **Nickschick, T.**, Heinicke, J., Mrlina, J. (2014) Die CO₂-Entgasungszone Hartoušov und das Mýtina Maar, westliches Eger Rift - neue Ergebnisse aus einem DFG-Projekt. Messel-Arbeitstreffen, 17.03.2014, Messel, Vortrag

-
6. **Nickschick, T.**, Kämpf, H., Schüller, I., Heinicke, J., Flechsig, C., Mrlina, J. (2013) Tracing and quantifying magmatic gas discharge in the diffuse degassing area of Hartoušov (western Eger Rift), based on combined CO₂ soil gas flux studies and geophysical surveys. International Conference on Gas Geochemistry, 01.-07.09.2013, Patras, Griechenland, Poster und Vortrag
 7. **Nickschick, T.**, Kämpf, H., Schüller, I., Heinicke, J., Flechsig, C., Mrlina, J. (2013) Tracing and quantifying magmatic gas discharge in the diffuse degassing area of Hartoušov (western Eger Rift), based on combined CO₂ soil gas flux studies and geophysical surveys. Tagung Basalt 2013: Cenozoic Magmatism in Central Europe, 24.-28.04.2013, Görlitz, Poster
 8. **Nickschick, T.**, Kämpf, H., Jahr, T. (2013), The Triasscholle near Greiz, E Thuringia - a volcanic based origin? Tagung Basalt 2013: Cenozoic Magmatism in Central Europe, 24.-28.04.2013, Görlitz, Poster
 9. Kämpf, H., **Nickschick, T.**, Schmidt, A., Schüller, I., und Nowaczyk, N. (2013) Das Diatrem Ebersbrunn und die Triasscholle Greiz: Kretazischer Vulkanismus in Westsachsen/Ostthüringen?, Messel-Arbeitstreffen, 18.03.2013, Messel, Vortrag
 10. Heinicke, J., Flechsig, C., Kämpf, H., Mrlina, J., **Nickschick, T.**, Seidel, E., Schmidt, A. (2013) Geophysical and geological survey of the inner and outer structure of the Mýtina maar, western Eger Rift. 73. Jahrestagung der Deutschen Geophysikalischen Gesellschaft, 04.-07.03.2013, Leipzig, Poster
 11. **Nickschick, T.**, Kämpf, H., Jahr, T. (2013), The "Triasscholle" near Greiz, E Thuringia - a volcanic origin? 73. Jahrestagung der Deutschen Geophysikalischen Gesellschaft, 04.-07.03.2013, Leipzig, Poster
 12. Heinicke, J., Flechsig, Ch., Mrlina, J., Kämpf, H., **Nickschick, T.**, C. Rücker (2012) Geophysikalische Strukturuntersuchungen am Maar Mýtina in W Böhmen. 72. Jahrestagung der Deutschen Geophysikalischen Gesellschaft, 05.-08.03.2012, Hamburg, Poster
 13. Kämpf, H., Bräuer, K., **Nickschick, T.**, Schüller, I., Schmidt, A., Jahr, T. (2012) Earthquake swarms, a sign of active magmatic processes in the Regensburg - Leipzig - Rostock zone, Central Europe? 4th International Maar Conference - a multidisciplinary congress on monogenetic volcanism, 20.-24.02.2012, Auckland, New Zealand, Poster
 14. **Nickschick, T.**, Kämpf, H., Jahr, T. (2012) The Triasscholle near Greiz, E Thuringia - a volcanic based origin? 4th International Maar Conference - a multidisciplinary congress on monogenetic volcanism, 20.-24.02.2012, Auckland, New Zealand, Poster

Contents

Part I	Magmatic and palaeovolcanic activity along the Regensburg- Leipzig-Rostock zone	7
1	Introduction	8
1.1	Statement of problem	8
1.2	Setting	8
2	Magmatic phenomena along the Regensburg-Leipzig-Rostock zone	10
2.1	Cretaceous volcanism	12
2.2	Cenozoic volcanism	13
2.3	Recent magmatic activity	14
3	Summary of own publications	16
4	Discussion of the articles within the Regensburg-Leipzig-Rostock zone	19
5	Conclusions and outlook	25
6	References	26
Part II	Own research	34
7	The "Triasscholle" near Greiz, Germany - a volcanic origin?	35
7.1	The "Triasscholle" near Greiz, Germany - a volcanic origin? Supplementary Data A - Details about the geophysical surveys	56
7.2	The "Triasscholle" near Greiz, Germany - a volcanic origin? Supplementary Data B - Detailed information about the IGMAS+ model of the TS	59
8	Integrated geophysical and geological methods to investigate the inner and outer structures of the Quaternary Mýtina maar (W-Bohemia, Czech Republic)	62
9	CO₂ degassing in the Hartoušov mofette area, western Eger Rift, imaged by CO₂ mapping and geoelectrical and gravity surveys	82
10	Architecture and temporal variations of a terrestrial CO₂ degassing site using electric resistivity and CO₂ gas measurements	106

Reprint permissions for listed articles	137
Declaration of personal contribution	141
Acknowledgements	146

PART I:

MAGMATIC AND PALAEOVOLCANIC
ACTIVITY ALONG THE REGENSBURG-
LEIPZIG-ROSTOCK ZONE

1 Introduction

1.1 Statement of problem

Within Central Europe a N-S trending fault zone has been proposed that is currently known as the so-called Regensburg-Leipzig-Rostock zone (RLRZ), as suggested by Bankwitz et al. (2003). It is part of a series of N-S zones in a 1000 km long belt which trend from the Massif Central in France to the Bohemian Massif (Bankwitz et al., 2003). The RLRZ is defined as a fault zone of about 700 km length and 40 km width loosely traceable between the German cities of Regensburg in the south and Rostock in the north. The seismically active, and thus best known, region is located in the center in a ca 150 km long zone between Cheb (Czech Republic) and Leipzig (Germany). The assumption of such a fault zone was based on multiple geological and geophysical studies from the second half of the 20th century, but to this day many of those have been forgotten and are rarely taken into account. Many of today's studies, especially seismological ones, are based on the assumption of N-S running faults within Germany and the Czech Republic but only focus on the most recent comprehensive study, which is Bankwitz et al. (2003).

This PhD thesis centers on the past and present magmatic and palaeovolcanic activity along this fault zone. Many authors have contributed to collecting data about formations and structures of magmatic origin and some have linked their work to other areas and studies, but a cohesive review has yet to be made. In chapter 1.2 the geological setting of the RLRZ will be explained, where observations for its existence from multiple disciplines of the geosciences are compiled. This serves as the necessary basis and the frame for my personal work on separate magmatic phenomena along the RLRZ, each presented in their own article in part II, chapters 7 - 10. Three different structures will be discussed in these chapters:

1. A Cretaceous formation in Thuringia, Germany, formerly interpreted to have formed by tectonic subsidence, which has been studied anew and is now interpreted as a diatreme.
2. A Quaternary maar-diatreme volcano near the border between Bavaria and the Czech Republic and
3. A mofette field in NW Bohemia which is driven by magmatic fluid ascent.

Chapter 3 provides a short summary of the most important results from these articles which are discussed within the context of the Regensburg-Leipzig-Rostock zone in chapter 4. Final thoughts on this topic and the area presented at the end of this thesis in chapter 5.

1.2 Setting

The RLRZ is a proposed fault zone of about 700 km length and 40 km width which connects the cities of Rostock, Leipzig and Regensburg in Germany in a N-S trending network of faults. Previous names used for this fault zone were Naab-Pritzwalk-Lineament (Behr, 1992; Behr et al., 2002; Kämpf, 2002; Neunhöfer and Hemmann, 2005) and, very uncommonly, Plauen/Klingenthal - Altenberg/Gera - Leipzig/Halle - Dessau/Bernburg (Kämpf et al., 1991). Often it also abbreviated to Regensburg-Leipzig zone due to this part being the most active one. The most comprehensive recent work on this particular fault zone was published by Bankwitz et al. (2003), where the name Regensburg-Leipzig-Rostock zone was used. Since then, this name seems to be the nomenclature that is mainly used when referring to this network of N-S running faults.

The currently most important geodynamic region is where the RLRZ intersects with the NE to ENE-striking Eger (Ohře) Graben, an active, non-volcanic rift system of about 50 km width and 300 km length belonging to the European Cenozoic Rift System that evolved in the Tertiary (Ziegler and Dezes, 2007). The western Eger Rift is related to a Paleozoic suture zone, originated by the collision of Laurasia (Laurentia-Baltica) and Africa (Gondwana), between the Saxothuringian zone in the north and the Teplá-Barrandian/Moldanubian zone in the south (Prodehl et al., 1995; Dézes et al., 2004; Geissler et al., 2007; Babuška and Plomerová, 2008). The Eger Rift is related to updoming of the lithosphere-asthenosphere boundary and the Mohorovičić discontinuity (Babuška and Plomerová, 2001; Babuška et al., 2007, 2010; Geissler et al., 2005; Heuer et al., 2006; Geissler et al., 2007) Recurring earthquake swarms have been registered, especially near the Nový Kostel focal zone (Fischer et al., 2014, and citations therein), but also smaller earthquake swarm focal zones are known within this central part of the RLRZ.

Different geoscientific methods have revealed the existence of N-S trending lineaments for different parts of this zone: Bankwitz et al. (2003) state that the central part of the RLRZ consists of many subparallel faults, as detected by satellite data and detailed structural analysis and geomorphology (Krull and Schmidt, 1990; Krentz et al., 1996), including data from trenches, mining pits and bore holes. A recent article (Andreani et al., 2014) also partially imaged the course of lineaments of the RLRZ. Due to that, the RLRZ can be found in geologic maps (Krull and Schmidt, 1990; LFUG, 1996; Krentz et al., 1996). Bankwitz et al. (2003) also mention that some of these faults also caused deep-seated offsets in Variscan granites, also reported by Kämpf et al. (1991) and Kämpf et al. (1992). They postulate that some of these faults are continuations of others and are traceable to more than 100 km in total length. Neotectonic activity along the Počátky-Plesná fault zone, a lineament of the RLRZ, has been discussed by (Bankwitz et al., 2003; Schunk et al., 2003; Peterek et al., 2011).

Geodetic evidence for movements along single lineaments within the fault zone have been reported. Wendt and Dietrich (2003) report horizontal surface deformation along a N-S lineament in the Vogtland area along the N-S trending Reichenbach - Schöneck - Erlbach fault during seismic activity and Mrlina (2000) mention motion on Czech side along a NNW-SSE, or rather N-S, trending fault by using long-term GPS measurement campaigns. While some lineaments show strike-slip movement, a clear and distinct sinistral or dextral orientation for the fault zone itself or its components could not be measured in the studies. Although, from a seismological point of view, the magnitudes of the earthquakes should be too small to cause measurable displacements, Mrlina and Seidl (2008) report distinct pre-, co- and post-seismic lateral motion. For example, for the earthquake swarm in 2000, the direction of the pre-seismic motion was dextral, while the post-seismic measurements clearly showed sinistral deformation. Wendt and Dietrich (2003) and Mrlina and Seidl (2008) report for their German and Czech long-term GPS campaigns that over extended periods of time different lithological blocks do not show a clear and steady direction of motion - the long-term trend along N-S fault lineaments remains not quite clear.

Geophysical indications were given in the original mention of a N-S- trending zone by Lauterbach (1952), who based his assumption on geomagnetic data. Later, Behr (1992) and subsequently Behr et al. (2002) used gravity data to trace and find N-S trending lineaments. Švancara et al. (2000) tested this as well and only found isolated elements between Altenburg and Nový Kostel and infer that the RLRZ is not a deep-seated steep lineament of significant density contrast. Also, Hofmann (2003) concluded in her gravimetric modelling of the Vogtland-NW-Bohemia region that one specific lineament, the Počátky-Plesná fault zone, cannot be seen due to a lack of density contrast. Well-researched and accepted is the RLRZ by seismotectonic studies due to recurring earthquake swarm activity. Numerous articles (e. g.

Neunhöfer and Hemmann (2005); Korn et al. (2008); Horálek and Fischer (2010); Fischer et al. (2014)) have correlated earthquake swarm activity with N-S- trending lineaments along the RLRZ in the Vogtland and Nový Kostel areas.

2 Magmatic phenomena along the Regensburg-Leipzig-Rostock zone

To this day, volcanic activity has not yet been discussed comprehensively in the context of the RLRZ. Some authors(e. g. Abratis et al. (2009); Kämpf (2002)) have discussed their respective study area in the tectonic context but a widespread review, linking different volcanic and magmatic phenomena does not exist yet. The N-S running RLRZ is dominated by a multitude of mainly Si-undersaturated volcanoes with ages from Lower Cretaceous to recent volcanism of Quaternary age and ongoing magmatic intrusions. A general map and schema of palaeovolcanic activity was given in Nickschick et al. (2014) and Schmidt et al. (2013) who refer to a classification from Ulrych et al. (2011) for the Czech part of the Bohemian Massif and extended it towards the German side. Fig. 1 provides an updated map from Nickschick et al. (2014) which provides an overview over the palaeovolcanic structures along the RLRZ.

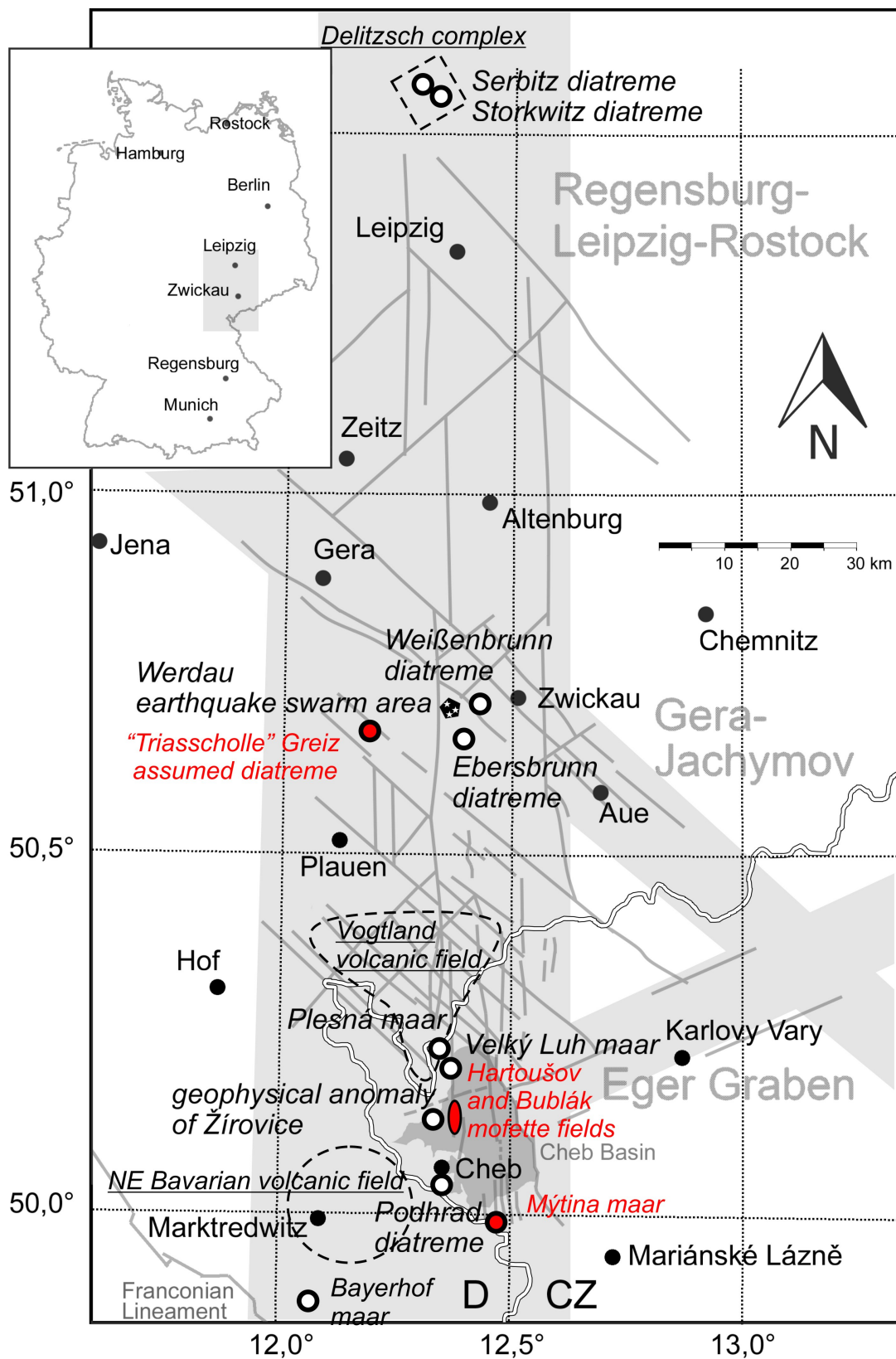


Fig. 1: Scheme of palaeovolcanic structures along the Regensburg-Leipzig-Rostock fault Zone, Eger Graben and the Gera-Jachymov Fault Zone, modified after Nickschick et al. (2014). Study areas that are part of this dissertation are marked red.

2.1 Cretaceous volcanism

A lot of the information available today about Cretaceous magmatic-volcanic activity is from uranium deposit exploration surveys in the 1960s and 1970 and not much has been published about, especially in relation to the RLRZ, in international journals. A large part of the information has either been classified as confidential information or has been forgotten due to not being published. Some of the few exceptions are the Delitzsch complex and three structures in the proximity of what is today known as the Werdau earthquake swarm region.

The Delitzsch complex (Seifert et al., 2000; Krüger et al., 2013), or Delitzsch-Bitterfeld volcanic field, can be found in the northern part of the RLRZ about 25 km NW of Leipzig, Saxony (Fig. 1). It is located within a heterogeneous series of Palaeozoic to lower Permian volcanic and sedimentary rocks at the intersection of the RLRZ and an E-W trending structural low (Röllig et al., 1989; Krüger et al., 2013). In this particular case Röllig et al. (1989) call it the intersection of meridional and equatorial running fault zones in the crystalline basement. The Delitzsch complex itself consists of late Cretaceous ultramafic rocks, such as aillikites, monchiquites, alnöites, and carbonatites, often occurring in the form of eruptive breccias Röllig et al. (1995). Dykes of eruptive breccias and lamprophyres have been found in more than 300 out of 5500 exploration drills by the former SDAG Wismut uranium mining company within an area of about 700 km² (personal communication L. Viereck, July 8th 2016, referring to B. C. Ehling) Two specific dolomite-carbonatite diatremes, Serbitz and Storkwitz have been researched more properly (Krüger et al., 2013, and citations therein). This study also determined an age of 75-71 Ma by sampling baddeleyite from the complex and derived a short duration of the magmatic and (sub-)volcanic activity for the main intrusion phase of the carbonatitic and ultramafic dykes.

In close vicinity to the Werdau earthquake swarm region, three (sub-)volcanic structures are currently known: The Weißenbrunn diatreme, the Ebersbrunn diatreme and the potential diatreme near Waldhaus, Greiz, the "Triasscholle". They all are located at the intersection of the RLRZ and the NW-SE trending Gera-Jachymov fault zone (Fig. 1).

The Weißenbrunn eruptive breccia is, according to the description of Alexowsky et al. (2007), a diatreme that was encountered by a SDAG Wismut drilling (drill 20008/3) at a depth of 535,8 m. It could be traced down to the final drilling depth of 790,1 m. It consists of a tuff with grey-green, dense, carbonatic matrix containing a mixture of granitic and quartzitic clasts and diabase, . At present, there is no clear age given for the Weißenbrunn diatreme, but according to Alexowsky et al. (2007) it is assumed to be of Tertiary or Cretaceous age.

The diatreme near Ebersbrunn, Saxony is, according to Schüller et al. (2012) and Schmidt et al. (2013), a deeply eroded Cretaceous diatreme. In the diatreme breccia spherical juvenile clasts covered by carbonatic and silicatic were found which hint at an ultramafic to carbonatitic composition for the magma within the Ebersbrunn diatreme (Schmidt et al., 2013). According to this and previous studies on the diatreme (e. g., Kroner et al. (2006); Matthes et al. (2010)) it was suggested that between 1.5 and 2 km of the upper part of the diatreme have been eroded since its formation. Schmidt et al. (2013) refer to Schüller et al. (2012), who ran (U-Th)/He age determination test measurements on apatite which resulted in a proposed age of ~113-96 Ma for the Ebersbrunn diatreme which is at the transition from the Lower Cretaceous to the Upper Cretaceous.

The so-called "Triasscholle" (lit. Triassic slab or Triassic block) near Greiz in Eastern Thuringia is a to this date not completely understood structure. Since its first thorough study in the 1960s (Puff, 1966, 1970) it has been considered as a block of Triassic sediments which has sunk into phyllitic shales

from the Lower Carboniferous due to tectonic uplift and consecutive subsidence. Since then, this tectonic hypothesis has been considered vague due to many inconsistencies that contradict a tectonic origin. In chapter 7 - Nickschick et al. (2014) - a detailed study is presented that attends this matter using geologic-tectonic, geophysical and geochemical information and questions the original interpretation. Nickschick et al. (2014) conclude that the Triasscholle near Greiz is most likely a deeply-eroded diatreme which originated from a series of phreatic or phreatomagmatic eruptions. Its age was derived from pollen analyses from the original report (Puff, 1966, 1970) where it was stated that the Triasscholle contains pollen from the Santonian (Late Cretaceous) which leads to a maximum age of ~ 85 Ma for its formation.

2.2 Cenozoic volcanism

The intersection of the RLRZ and the WSW-ENE striking Eger (Ohrě) Graben (or Eger Rift) marks a region for recurring volcanic activity within the Cenozoic. According to Ulrych et al. (2003, 2011) volcanic activity for the northern and western part of the Bohemian Massif can be classified in three distinct periods: (1) pre-rift period (Later Cretaceous to Mid Eocene, 79-49 Ma), (2) syn-rift period (Mid Eocene to Mid Miocene, 42-16 Ma) and (3) late-rift period (16-0.26 Ma).

According to Schmidt et al. (2013), Nickschick et al. (2014) and Flechsig et al. (2015) six confirmed or proposed maar-diatreme structures are located within the intersection of the RLRZ, the Eger Rift and the Cheb-Domažlice Graben: the Velký Luh maar (age: 49-37 Ma, Kvaček and Teodoridis (2007)), the Plesná maar (age: 33.5-28.5 Ma, Kvaček and Teodoridis (2007)), the Podhrad diatreme (unknown age, Šantruček et al. (1991)), the Bayerhof maar (age: 23.3-21.7 Ma, Rohrmüller (2003)), the Mýtina maar (age: 0.29 Ma, Mrlina et al. (2007)), and a geophysical anomaly (proposed maar) at Žírovice (unknown age, Dobeš et al. (1986)). In addition to these maar structures, Quaternary volcanic activity can also be seen by two scoria cones, the Komorní hůrka (Kammerbühl) and Železná hůrka (Eisenbühl).

Abratis et al. (2009) collected a large amount of different rocks from the Vogtland area (see Fig. 1). In this area, according to Abratis et al. (2009), two main fault systems intersect in the Vogtland and W-Bohemia area: the SW-NE trending Krušné hory and Litoměřice faults as the northern shoulders of the Eger Graben, and SE-NW trending faults such as the Aš-Tachov and Mariánské Lázně faults. Their petrological and geochemical analyses showed that many of their sampled rocks are heavily SiO₂-undersaturated and are enriched in incompatible elements and volatiles: a large number of the Vogtland volcanics are nephelinites, olivine melilithites, melanephelinites or tephrites. They also mention that carbonate droplets can be found within the rocks which is interpreted as an unmixing from the siliceous melt. In general, the igneous rocks found in the Vogtland area indicate that melting occurred at depths of over 80 km at a strongly metasomatized CO₂-enriched mantle and that the magma must have ascended quite rapidly due to the deep fault system in that area. Only one age for the whole Vogtland volcanic field is known from Potassium-Argon (K-Ar) age determinations. Kaiser and Pilot (1986); Abratis et al. (2009) state that an olivine-nephelinite from Breitenfeld near Markneukirchen (Saxony) has an age of 19.5 ± 1 Ma.

Rohrmüller et al. (2005) mention a K-Ar age determination campaign of Cenozoic volcanics in the area around Selb, Wunsiedel, Erbsdorf and Waldsassen (all Bavaria, Germany). Their investigations revealed of ages between 29.1 and 14.6 Ma for the eruption of the volcanics. Ackerman et al. (2013) measured 21.2-23.5 Ma old basanite lava flows in the same region (Zinst, Hirschentanz and Teichelberg). These ultrabasic rocks feature significant amounts of carbonate-bearing and silicate melt pockets within, marking another volcanic field of similar geochemical composition.

The youngest currently known sign for volcanic activity is marked by the Komorni hůrka scoria cone SW of Františkovy Lázně, the Železná hůrka scoria cone and the Mýtina maar at the German-Czech border near the villages Mýtina and Neualbenreuth. Especially the young Mýtina maar has seen some interest over the last years (Geissler et al., 2004, 2007; Mrlina et al., 2007, 2009; Flechsig et al., 2015). As of now it is the youngest known volcanic structure in the RLRZ and the western Eger Rift with an age of 290 ka, meaning it is younger than the Železná hůrka (519 ± 51 ka, Wagner et al. (2002)) or the Komorni hůrka (726 ± 59 ka, Wagner et al. (2002)). Another maar has been found near Neualbenreuth, just a few kilometres away from the Mýtina maar Bayerisches Landesamt für Umwelt (2015). It is assumed to be 200 ka years old, a final age has not been given for its initial time of origin. It is very likely that more, currently undiscovered maar-diatremes exist in the vicinity of these two maars.

2.3 Recent magmatic activity

Active mantle degassing occurs in NW Bohemia beneath the Cheb Basin, where the RLRZ intersects with the currently non-volcanically, but magmatically active Eger Rift (Weinlich et al., 1999; Bräuer et al., 2008; Nickschick et al., 2015, *subm.*). Fischer et al. (2014) recently summarized the level of understanding about the lithosphere in NW Bohemia from various articles. From a multitude of active and passive seismic experiments we know that:

1. The crust beneath the Cheb Basin is thinned to about 27 km (Geissler et al., 2005; Heuer et al., 2006)
2. The Moho varies in its thickness and seems to be laminated (Hrubcová and Geissler, 2009; Hrubcová et al., 2013)
3. The asthenosphere is characterized by decreased seismic velocities, which can be interpreted as a small plume similar to the Eifel and Massif Central or to an upwelling of the lithosphere-asthenosphere boundary - the situation remains unclear and is highly debated (Plomerová et al., 2007; Babuška et al., 2007; Babuška and Plomerová, 2013; Heuer et al., 2011).

Signs of hidden fluid ascent from a magmatic source have first been proven by isotopic analysis of $^3\text{He}/^4\text{He}$ ratios (Weinlich et al., 1999; Bräuer et al., 2005, 2008, 2011, 2014; Kämpf et al., 2013): Repeated measurements of the gas emitted in the central part of the so-called Hartoušov mofette field (HMF) and nearby Bublák mofette field (BMF) revealed that since at least the year 2000 a magmatic source from the Upper Lithospheric mantle has been degassing as indicated by a significant rise of the $^3\text{He}/^4\text{H}$ ratio to 6.32 Ra, which is typical for xenoliths from the European subcontinental mantle source (Gautheron et al., 2005).

The importance of fluid ascent from a magmatic source is also seen in the recurring earthquake swarms in NW-Bohemia. In general, earthquake swarms - a series of usually low-magnitude earthquakes - occur near ocean ridges in volcanically active or geothermal fields Wyss et al. (1997); Lees (1998); Dreger et al. (2000); Ibs-von Seht et al. (2008); Fischer et al. (2014). The Nový Kostel focal zone is the main area in which seismic energy is released. Focal mechanism analyses (Horálek and Fischer, 2008; Fischer, 2003; Fischer and Michálek, 2008; Vavryčuk, 2011; Fischer et al., 2014) show, that 90 % of the energy released show a rather N-S or WNW-ESE strike which hints at the importance of a sub-element of the RLRZ: The Počátky-Plesná fault zone (Bankwitz et al., 2003).

Both the Nový Kostel focal zone and the Hartoušov mofette field, two separate regions along one N-S striking fault zone show completely different kinds of fluid activity. In chapter 9 - Nickschick et al. (2015) - but also chapter 10 - (Nickschick et al., subm.) - we connect these two areas and discuss the relation of these regions which are linked to active magmatic degassing and fluid ascent.

3 Summary of own publications

In chapter 7 (Nickschick et al., 2014) we revised information about a formation of arguable origin, the "Triasscholle" near Greiz. In former times, this brecciated block of mixed Triassic sediments with an outcrop of about 200 m x 800 m has been considered the result of post-sedimentary tectonic movement. We re-evaluated this hypothesis by interpreting new gravity and magnetic data and combine them with existing gravity data and thorough studies of existing drill cores from the 1960s, and added petrological and mineralogical analyses and used geologic background information to test the original hypothesis. The results presented reveal that this particular structure cannot be the result of a simple tectonic event: A gravity anomaly as steep and laterally limited as measured in that area can only be caused by a small body such as a vertical vent or a cave. Absolute density measurements of core material and phyllites from the Carboniferous prove that the material within the gravity anomaly must be significantly less dense than the breccia or the phyllites. A gravity model using the IGMAS+ software (Götze et al., 2007) reveals a simple, yet possible geometry for the subsurface of the Triasscholle. As it seems the structure might be much larger than previously expected by geological mapping and a few exploration drillings. In our model we build a trough-like structure of 1,100 m x 500 m which fits the currently known assumptions made from the gravity survey and the petrophysical tests. As of now, the geomagnetic mapping of the innermost part of the Triasscholle has shown no significant magnetic anomalies. This remains unusual as in most cases diatremes are accompanied by distinct geomagnetic anomalies due to minerals with high susceptibilities such as magnetite or greigite. Petrographic analyses of thin sections from the brecciated parts of the SDAG Wismut drill cores reveal that the breccia at shallow depths differs from the breccia from the lower parts of the drill core material. While we find cataclastic fabric of the mainly carbonatic breccia material near the top, the material at the bottom seems to be overprinted hydrothermally. The clasts are now more idiomorphic in shape and do not show much exposure to mechanic stress which we interpret as signs for recrystallisations and new formations of crystals. Many clasts have a rims enriched in manganese and iron which is often observed in hydrothermal or metasomatic areas. Nickschick et al. (2014) also present indications found by other scientists for these assumed thermal events by looking at the surrounding phyllite and at a velocity anomaly found only few kilometers away from the Triasscholle in the subsurface by the GRANU95-B seismic profile (Enderle et al., 1998). With the addition of findings for oppositely directed transport we present a summary of why we think the Triasscholle cannot be the result of a tectonic uplift and subsidence scenario. It is much likelier that multiple events which involved a hydrothermal or magmatic source lead to the phenomenon currently known as the Triasscholle. Much of the information gained from our re-evaluation can be found in diatremes. Even though we did not find juvenile clasts within the drill from the assumed diatreme and cannot measure a significant magnetic anomaly, it might be possible that either the drill is too far to the margin in the unbedded diatreme facies (Lorenz, 2003; White and Ross, 2011) or phreatic eruptions happened with very little juvenile magma involved or that the magma involved had a carbonatic composition. Considering the time of the Triasscholle's origination (85 Ma or less) and its proximity to the ultrabasic to carbonatitic magma from the nearby Ebersbrunn diatreme (Schüller et al., 2012; Schmidt et al., 2013), this might also be a plausible explanation.

Chapter 8 presents the next logical step in the research around the Quaternary volcanism in NW Bohemia around the Mýtina maar and the Železná hůrka (Eisenbühl) scoria cone after the previous work presented in Geissler et al. (2004); Mrlina et al. (2007, 2009). This article marks an important step in

the understanding of recent volcanic activity within the RLRZ. Our research provides insight into the three-dimensional structure of the inner and outer maar-diatreme, and hence towards the potential of volcanic hazard in that area. We used a multitude of geophysical surveying strategies such as gravity, electric resistivity tomography, shallow seismics using a sledge hammer, and geochemical analyses from shallow (< 10 m) drills which were drilled in fall of 2012. The geophysical methods allowed a more specific reconstruction of the Mýtina maar's architecture: We observe an unsymmetrical filling of maar sediments, which are thicker on the eastern side, and can loosely trace the deposition of the volcanoclastic material. Both are observable due to their contrast in density and electric resistivity compared to the surrounding country rock. From the detailed surveys we also might have discovered one or two hidden structures within the maar, which are currently covered by the thick maar sediments. As of now, these are discussed as either post-eruptive, pre-sedimentation scoria cones or late intrusion dykes. The surveys also revealed "pocket" at the outside of the maar, which are interpreted as syn-eruptive fractures and consecutive subsidence (cone sheets). The geophysical methods themselves are incapable of differentiating between the tuff (consolidated) or tephra unconsolidated) of the volcanic deposits. At this point the analysis of the drill cores provides detailed insight into the maar's history: Using a similar, but advanced procedure compared to the one presented by Geissler et al. (2004), we considered the deposits to be consisting of a mixture of two separate end members: The volcanic, ultramafic end member in form of a volcanic bomb and the phyllitic country rock. By calculating the respective percentage along the drill cores we can trace different volcanic eruption characteristics and mark the transition from the phreatic to the (phreato-) magmatic phase. The article Flechsig et al. (2015) poses as a good example of how a multitude of different geophysical, geological and geochemical methods support each others' findings and improve the overall interpretation of how maar-diatremes can be studied in their spatial but also temporal position.

Nickschick et al. (2015, chapter 9) and Nickschick et al. (subm., chapter 10) contain recent information about the magmatically active CO₂ degassing system in the Hartoušov mofette field (HMF) and its tectonic context. The first of the two articles, Nickschick et al. (2015), focusses on the spatial relation of the heavy CO₂ degassing within the Cheb Basin in NW Bohemia. The heavy amounts of carbon dioxide are put into their regional context by evaluation the degassing pattern in the geologic frame. Large amounts of CO₂ are emitted via channels with diameters of less than one meter in form of dry mofettes. In some cases more than 100 kg of CO₂ per square meter are ejected each day via some of these small seepage sites. Our very detailed mapping of the carbon dioxide gas flux (more than 3700 points) and the content of CO₂ within the soil gas (about 3000 points) comprises a coarse mapping of the area as well as detailed measurements near strongly degassing CO₂ vents. This enormous data set was evaluated by using a statistical approach which, so far, has not been used to statistically estimate degassing patterns and amounts: the Trans-Gaussian-Kriging. However, this approach was a necessary step as the HMF is a very heterogeneously degassing mofette field and previous articles from scientists working in other degassing fields have used simpler approaches. The mathematical error is lower and interpolation result itself is much better using this method than other suggested methods. We estimate that between 23 and 97 tons of carbon dioxide are released from an area of about 350.000 m² in the HMF each day. We also found out that the CO₂ degassing is not steady over time but fluctuate quite significantly: High variations of up to one order of magnitude in the measured gas flux have been observed in the central part of the HMF. However, our estimation marks a milestone in the estimation of degassing patterns within the Cheb Basin: Previous studies relied on measurements assumptions based on that and/or concentrated their work on wet mofettes. The CO₂ degassing follows a certain schema: N-S- oriented degassing along a

steep morphological step and NW-SE along the central and northern part, where the morphological step is gentler. Using results from electric resistivity tomography and gravity measurement, we observe a slight shift in the lithology which is marked by the morphological step. Bankwitz et al. (2003) already suggested that the N-S trending Počatky-Plesná fault zone runs through that area and our findings support this hypothesis. Correlating drill logs from the Czech Geological Survey from the western and eastern side of this assumed fault zone also verifies this, as we can observe a shift of almost 30 m in the lithology in the Tertiary deposits, which is also in accord with Bankwitz et al. (2003).

Based on our results we developed a hypothesis in which the mofette fields of Hartoušov and Bublák are small pull-apart basins that have developed along the Počatky-Plesná fault zone and maybe parallel sub-faults. Other degassing- or fluid-related phenomena are located near the Plesná river, which roughly follows the fault zone's course (Kämpf et al., 2013). There are indications that this also continues in the region near. Flechsig et al. (2010) measured a subsided basin-like structure using electrical resistivity tomography parallel to the morphological step at U mostku, about 4-5 km north of the HMF. Halpaap (2014), using reflection seismic data, hypothesize a sinistral strike slip fault within the basement close to where the Počatky-Plesná fault zone or a parallel fault was assumed to be according to Bankwitz et al. (2003).

As magmatic, CO₂-dominated degassing within NW-Bohemia happens along one of the N-S- lineaments within NW Bohemia, it is of utmost importance to increase our knowledge about the fluid ascent from the Upper Lithospheric Mantle towards the surface. Since the last known volcanic event, which is the Mýtina maar, happen only roughly 300.000 years ago, further volcanic activity cannot be ruled out. The shift in the magmatic portion of the gas measured within the HMF, as indicated by the increase in the ³He/⁴He ratio (Bräuer et al., 2005, 2008) indicates a hidden magmatic intrusion, making it all the more important to study and understand fluids, their activity and their transport all the way to the surface. In Nickschick et al. (subm., chapter 10) we exemplarily tested the stability of mofettes in the HMF. The task was to test if changes within the mofettes' degassing variation, as shown by Nickschick et al. (2015), can be observed in the subsurface using a suitable method. Due to the good results from the previous studies, electrical resistivity tomography was used as even small variations of the subsurface architecture lead to a measurable change in the very conductive, clayey sediments. After the first measurements and evaluation of Meinel (2014), we systematically inverted the data again under special consideration of the results from Nickschick et al. (2015). Choosing a rather undisturbed degassing site, using the same setup every time and comparing it to self potential data, CO₂ gas measurements and the ground water level, we observe changes within the subsurface structure beneath two separate mofettes. Comparing our findings to a recent study from Flores et al. (2016) shows that mofettes show the mofettes' part beneath the surface degassing varies not significantly over time: Nickschick et al. (subm.) observe long-term trends while Flores et al. (2016) observe one mofette's activity stagnate from one day to the other. These changes in the fluids ascent can also loosely be seen in the changes of the self-potential.

4 Discussion of the articles within the Regensburg-Leipzig-Rostock zone

This thesis and the studies presented herein contribute to the understanding of the network of N-S running faults that is the Regensburg-Leipzig-Rostock zone. We present work on specific structures of ages from the Upper Cretaceous, the Quaternary and recent magmatic activity using a multitude of geophysical, geologic-tectonic and geochemical measurements and results, and use background information to put these new results into their appropriate context. Using a multitude of methods we developed and tested our hypotheses of:

1. A diatreme which was thought to be a tectonic collapse breccia (Nickschick et al., 2014).
2. Hazard potential of a Quaternary maar and the distribution of its volcanoclastics (Flechsig et al., 2015).
3. The existence of pull-apart basin-like structures along a N-S running fault at which magmatic degassing occurs as a possible weakening zone for potential future volcanic activity (Nickschick et al., 2015).
4. The (in-)stability of mofettes and therefore magmatic fluid ascent over time along aforementioned lineament (Nickschick et al., *subm.*).

By studying the Triasscholle near Greiz under special consideration of a hypothetical volcanic background, a multitude of different indicators support this hypotheses: The steeply-inclined blocks, the bimodal matrix within the breccia, the gravimetric anomaly, the signs of heating and thermal overprinting, the proximity to two other known formations of magmatic origin - the Ebersbrunn and Weißenbrunn diatreme - all these findings are signs of a magmatic-volcanic origin for the Triasscholle. The age, determined by pollen analyses, hints at a similar, Cretaceous age as the nearby Ebersbrunn diatreme. One major thing that remains enigmatic is the lack of juvenile clasts within the breccia of this proposed diatreme. The very heterogeneous breccia, which was studied in Nickschick et al. (2014), could only be partially analysed within the limited amount of time. From the geophysical model and the modelled extent, it can be assumed that the drills were sunk into the margin of the diatreme and that the drill core, due to erosion of more than 80 million years, retrieved sample material from the unbedded diatreme facies. Therefore, there is a high chance that juvenile, magmatic material has not been found yet and that thorough research under this aspect can separate the mixture of phyllite, Mesozoic sediments and granitic basement rocks from a potential juvenile component. One other possibility might be that the Triasscholle "diatreme" formed due to a carbonatitic intrusion. While this is a very bold assumption on its own, the findings of carbonatic juvenile material in the immediate vicinity in the Ebersbrunn diatreme (Schüller et al., 2012; Schmidt et al., 2013) and the Weißenbrunn diatreme (Alexowsky et al., 2007) support this hypothesis. Separating a possible mixture of Middle Triassic (Muschelkalk) limestone and dolomites from admixed carbonatic juvenile would be a challenging but possibly rewarding task. Due to the work presented in Nickschick et al. (2014), the Triasscholle should not be considered to be a purely tectonic phenomenon, but rather to be the eroded remnant of a diatreme. This also indirectly implies a potential sub-volcanic to volcanic field, consisting of the Ebersbrunn, Weißenbrunn and Greiz diatremes, which could have formed in the Cretaceous in an area, which is still today, after such a long time, characterized by fluid migration

in the Werdau earthquake swarm area (Hemmann et al., 2003; Neunhöfer and Hemmann, 2005). Knowing this, it is also to be expected that more, hidden or previously misinterpreted structures are to be found in this potential volcanic field, especially since the Weißenbrunn diatreme has only been encountered within a drill at a depth of more than 530 m (Alexowsky et al., 2007). The existence of a separate, second ultramafic to carbonatitic volcanic field 70 to 80 km south of the Delitzsch complex proves to be an exciting theory, considering the little amount of information about Cretaceous volcanism along the RLRZ and also Central Europe in general.

Our article Flechsig et al. (2015), continuing the previous examinations (Mrlina et al., 2007, 2009) of the Mýtina maar and its surrounding, provides a detailed look into the potential risk and hazard of a Quaternary volcano in Central Europe. Up to this day this maar and the Komorni hůrka and Źelezná hůrka scoria cones mark the most recent signs of volcanic activity within the RLRZ and the Eger Graben. Another maar is assumed to be located near Neualbenreuth (Bayerisches Landesamt für Umwelt, 2015, and pers. comm. with J. Rohrmüller) and its supposed age of 200 ka indicates that this not the only undiscovered maar of Quaternary age in that area.

The results from Flechsig et al. (2015) lead to a detailed three-dimensional geophysical modelling of the Mýtina maar and its surrounding. Flechsig et al. (2015) already presented a first three-dimensional model of the inversion from the electric resistivity tomographies. Currently, the gravity data and magnetic data is used to establish a refined 3D model with the IGMAS+ software package. This procedure was also already used and explained in Nickschick et al. (2014) and references therein. A first version of the gravity model has been realized which now considers the geologic situation and the volcanoclastic deposits from Flechsig et al. (2015) in contrast to the first model seen in Mrlina et al. (2009). A first version can be seen in Figs. 2 and 3. When all the geophysical data has been gathered the magnetic model will be implemented and help refining this model immensely. In the final step the gravity and magnetic model will be compared to the 3D inversion of the geoelectric data and both models will help finding boundary conditions for the geophysical parameters and extent of the maar-diatreme's structure. As the different methods provide answers to different problems, such as the question of hidden intrusions, distribution patterns of the volcanic deposits and the time-dependent sequence of the eruptions for the maar and the scoria cone - we expect a step forward in the understanding of the young volcanic activity within the RLRZ. While the two scoria cones are rather small structures with diameters of a few tens of meters, the Mýtina maar's phreatic to phreatomagmatic deposits were spread over several kilometres. In general, ultramafic, low-viscosity melilititic and nephelinitic magmas are considered to be less dangerous to their intermediate or felsic counterparts in regards to the volcanic risk. However, an event of this magnitude would pose a serious threat within Central Europe and studying this maar-diatreme volcano provides great asset in understanding the volcanic potential in the Cheb Basin, especially since we also witness ongoing magmatic activity in this area today and the area around NW Bohemia is not considered to be potentially dangerous.

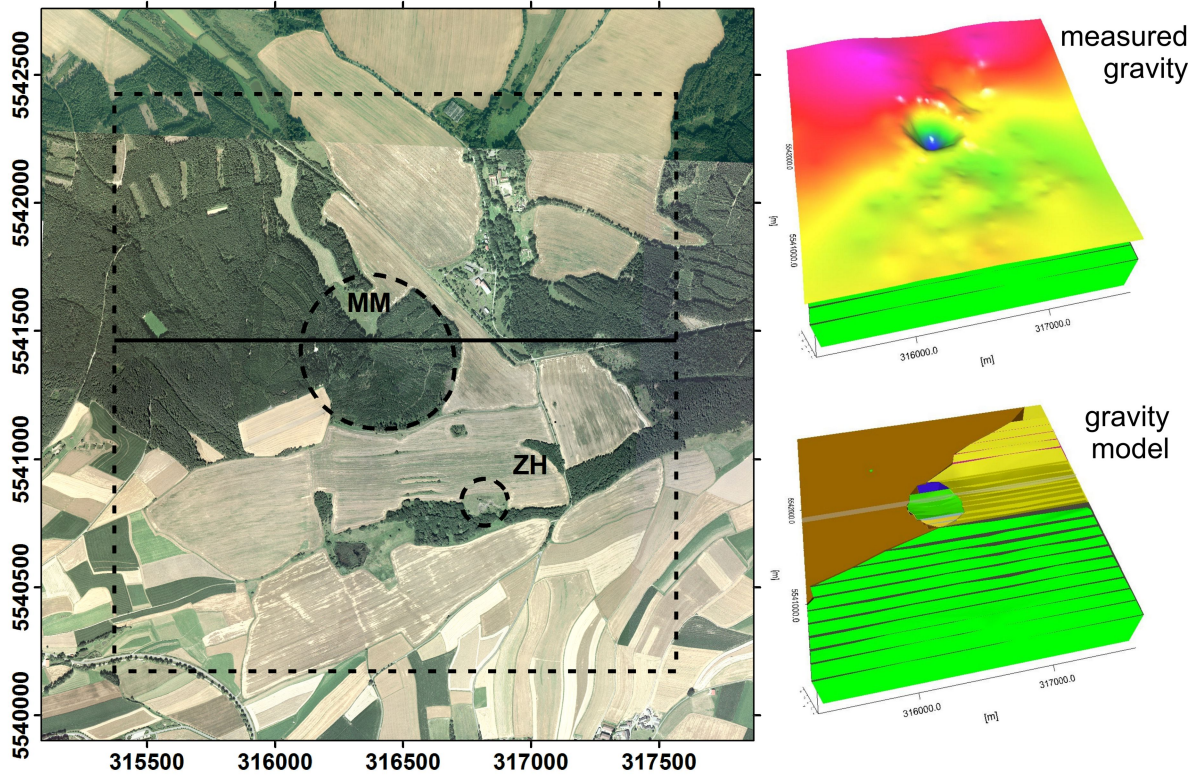


Fig. 2: Left: Extent of the gravity model (dashed outline) for the surrounding of the Mýtina maar (MM) and the Železná hůrka scoria cone (ZH). Right: Bouguer gravity map of the measured gravity data from Mrlina et al. (2009) and Flechsig et al. (2015) and the IGMAS+ gravity model, currently consisting of 30 E-W oriented sections and respecting the local geologic situation. Differently coloured sections represent different lithological blocks and densities. The solid E-W running line marks the location of the IGMAS+ section presented in Fig. 3. The map was compiled using different datasets leading to the different colouring of the northern part.

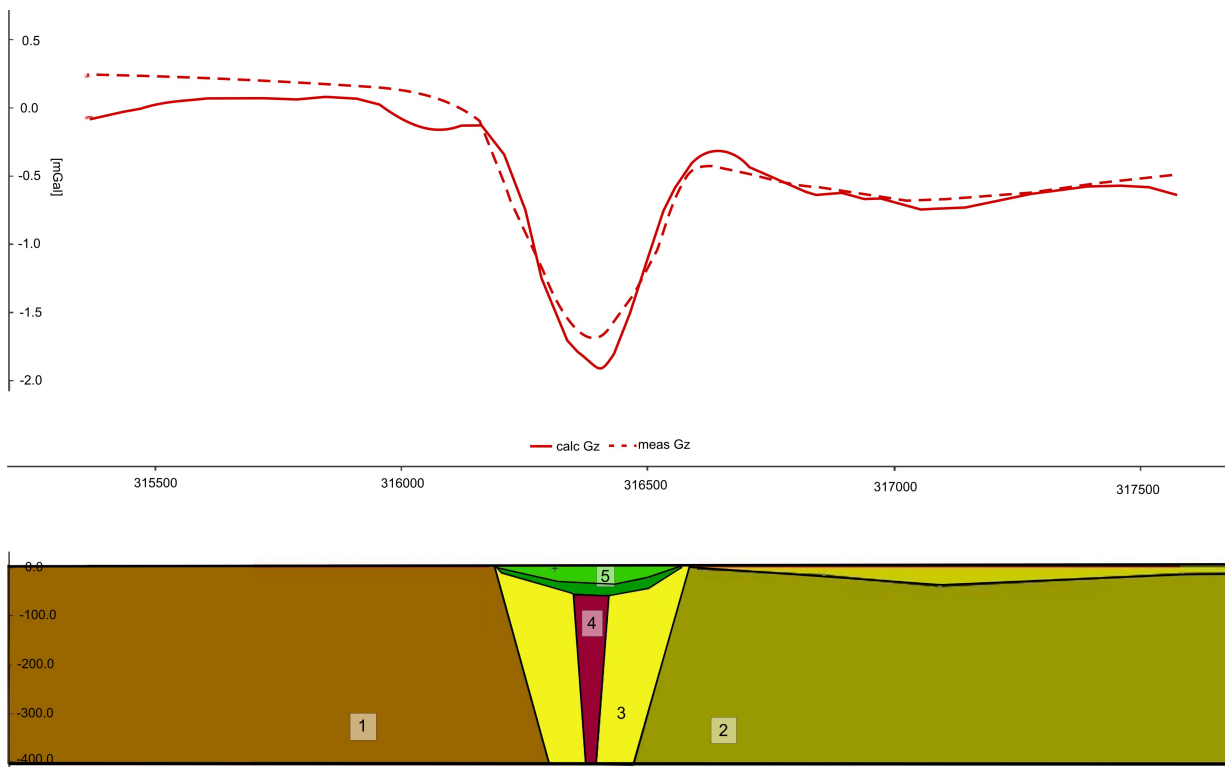


Fig. 3: Section of the 3D gravity model realized in IGMAS+. The position of the section is shown in Fig 2. The different bodies marked by numbers reflect the maar-diatreme's structure and the geologic situation with their respective modelled density : 1 - phyllitic schist, $2,660 \frac{kg}{m^3}$; 2 - quartzitic phyllite, $2,619 \frac{kg}{m^3}$; 3 - outer diatreme facies, $2,630 \frac{kg}{m^3}$; 4 - inner diatreme facies, $1,950 \frac{kg}{m^3}$; 5 - maar lake sediments, $2,000 \frac{kg}{m^3}$ for the upper part and $2,150 \frac{kg}{m^3}$ for the lower part to respect compaction.

The ongoing magmatic activity in NW-Bohemia in its most impressive form - the earthquake swarms in the Nový Kostel focal area - is a rather well-researched phenomenon (Vavryčuk, 1993; Fischer, 2003; Fischer and Michálek, 2008; Horálek et al., 2000; Horálek and Fischer, 2010; Fischer et al., 2014). Steady registration of seismic events allow a continuous recording of magmatic activity in the form of these fluid-triggered seismic events while the reason and the process of ascending fluids remains somewhat of a mystery. In Nickschick et al. (2015) a look onto the idea of the N-S trending Počatky-Plesná fault as part of the RLRZ (Bankwitz et al., 2003) and its tectonic control on the ascent of the CO₂-dominated magmatic fluids aimed at questioning this particular lineament, especially since it is morphologically rather unimpressive compared to the NE-SW trending Maránské Lázně fault. Nickschick et al. (2015) list a number of indications for its existence on a local scale. Rojik et al. (2014, Figs. 32 and 33) show in their compilation of geological maps an E-W trending profile which shows the basement-cutting faults of the northeastern Cheb basin, two of them being the N-S trending Skalná fault and "Plesná brook". (Halpaap, 2014) attempted to obtain a geophysically constrained model of the Počatky-Plesná fault and the Maránské Lázně fault near Kopanina by using reflection seismic data. The interpretation given there indicates a multitude of faults within the crystalline basement and no observable faults offsetting sedimentary layers near the Plesná valley, implying that it has not been active within the last 25 Ma. One has to consider, however, that the seismic profile bends a little and runs acute-angled and nearly parallel to the proposed course of the fault at the escarpment, which might lead to a slight error, but also

Nickschick et al. (2015) only noticed a small offset between the two sides of the assumed fault. Although all these studies and the studies already evaluated in Nickschick et al. (2015) are not able to find large displacements, the area around the mofette fields of Bublák and Hartoušov is the one with the highest amount of Upper Mantle-derived gas. The increase of the magmatic component in the gas, which has been observed in a very detailed fashion along this area (Weinlich et al., 1999; Bräuer et al., 2003, 2005, 2008, 2011, 2014; Kämpf et al., 2013) directly proves the ongoing magmatic activity and, furthermore, that fluids migrate from their source in the Upper Lithospheric Mantle towards the surface in the Bublák and Hartoušov mofette fields. Judging from the findings presented in Nickschick et al. (subm.) one can assume that the variability in the amount degassed as surface is highly variable. This currently ongoing, hidden magmatic intrusion derived from the change in the isotopic composition also marks the youngest sign of magmatic activity along a N-S trending fault - a clear sign that magmatic activity within the RLRZ is not phenomenon of the past but that also in the future this magmatic activity can change to active volcanism with characteristic formations such as the Mýtina maar and the potential danger linked with it.

By linking the articles presented in this thesis to existing studies from other structures along the RLRZ insight is gained about the temporal and spatial importance of the RLRZ: Although the RLRZ has found its way into the literature, it is still unknown how exactly this fault zone controls or is controlled by various magmatic and volcanic phenomena over at least 80 million years. We observe evidence for volcanic activity from the Upper Cretaceous in the northern part around the Delitzsch-Bitterfeld and Werdau areas, Tertiary volcanism in the Vogtland area, in NW Bohemia and NE Bavaria and also Quaternary volcanism and recent magmatic activity in NW Bohemia as well. Especially Cretaceous volcanic activity within this area is a very interesting finding. Comparable volcanics from northern Bohemia, eastern Eger Rift, of Cretaceous to Late Paleocene age were mentioned in Skála et al. (2015, and articles cited therein): At the intersection of the Eger Rift and the Lusatian Fault mainly melilititic or lamprophyric dykes were found and studied. Since especially the older structures are currently known from extensive drilling campaigns in the eastern part of Germany, there is a high possibility that other, similar structures are still hidden along the RLRZ, especially formations of Cretaceous or Palaeogene age. As of now, we do not know if the RLRZ has remained active constantly over time; but it is more likely that it has been active during certain phases in which the different volcanic and sub-volcanic structures were formed. It also seems that after the initial volcanic or plutonic phase no further signs of active volcanic activity have been found yet. Exceptions from this are the recurring earthquake swarms at shallow depths in the Vogtland area (Hemmann et al., 2003; Neunhöfer and Hemmann, 2005; Korn et al., 2008) and the Nový Kostel focal area (Vavryčuk, 1993; Fischer, 2003; Fischer and Michálek, 2008; Horálek et al., 2000; Horálek and Fischer, 2010; Fischer et al., 2014) The Werdau earthquake swarm area is, due to its proximity to the Weißenbrunn diatreme, the Triasscholle Greiz and the Ebersbrunn diatreme, a very interesting region: Although these structures are of (Late) Cretaceous age, seismic activity in form of these fluid-triggered swarms can still be measured today - a sign that fluid paths are still somehow open and accessible for ascending fluids. Even today, we can witness magmatic intrusions by observing variations in the isotopic composition of fluids that occur within a few years (Weinlich et al. (1999); Bräuer et al. (2003, 2009, 2014).

All these structures, which are discussed in this thesis, have in common that they are composed of ultramafic silicate or carbonate melts which are commonly found at depths of several tens of kilometres (Upper Mantle). This means that single faults within the fault zone reach deeply into the crystalline

basement and are weakening zones for ascending fluids at their respective times and, in the case of earthquake swarm activity, possibly still do. As of now, we mark the Delitzsch complex north of Leipzig as the northernmost palaeovolcanic structure within the RLRZ and the volcanic field in NE Bavaria (Rohrmüller et al., 2005; Ackerman et al., 2013) as the southernmost although one can assume that there are others. The northernmost formation - the Delitzsch complex - is at the same time also one of the oldest (Cretaceous). Continuing southward, the volcanic province consisting of the Weißenbrunn diatreme, the Ebersbrunn diatreme and the assumed diatreme near Greiz mark another zone of (most likely) Cretaceous age. Between these two complexes a gap of about 80 km exists where no comparable formation of magmatic-volcanic origin has been found yet. The southern Vogtland volcanic field marks a temporal jump from Cretaceous age to Oligocene-Miocene age. Together with the NE Bavarian field, which is about the same age, they enclose the magmatically active area beneath the Cheb Basin. The different ages of magmatic activity in different regions do not only hint at different stages of time of volcanic activity, they also hint at a spatial shift of more than 150 km over the time along the RLRZ. Even in recent times, we are able to relate a change of fluid migration paths over time. Fischer et al. (2014), for example, use seismic data from Knett (1899) and Credner (1876, 1898) and correlate them with new data. This way, spatial shifts in the earthquake swarm hypocenters have been traced back to more than a century ago and reveal a highly mobile zone for magmatic fluid migration.

5 Conclusions and outlook

This thesis as a whole and the articles herein stress the importance of studying the network of fault zones forming the Regensburg-Leipzig-Rostock zone in more detail. As of now, a multitude of volcanic fields and isolated structures exist with this N-S trending fault zone that have often been studied separately or just occasionally been connected with one or maybe two other volcanic fields. However, along a length of about 200 km along the RLRZ from Delitzsch-Bitterfeld in the north to NE Bavaria in the south a series of ultramafic to carbonatitic volcanic or subvolcanic structures can be found. This kind of magma composition is often linked to the Upper Mantle, so rather deep-reaching migration and fluid ascent paths can be assumed. While we observe Cretaceous activity in the Delitzsch complex and, most likely, also the Ebersbrunn-Greiz-Werdau area, Tertiary magmatic activity can be observed in the Vogtland and NE Bavarian area and even Quaternary and recent activity in the Cheb Basin, implying a rather long time of constant or recurring activity.

The Triasscholle certainly features a lot of the evidence for a volcanic history in the Cretaceous in Greiz. However, without a final step to prove this theory some more research needs to be done. One of the key questions is the actual size of the assumed diatreme and tomographic geophysical methods such as electrical resistivity tomography or seismics would be excellent tools to trace the contact of country rocks to the diatreme breccia. Isotopic analyses on carefully prepared samples from the existing drills from the breccia could potentially clarify the chemistry of the juvenile component and an exploration drill into the gravimetric minimum would surely and ultimately clear the cause for this anomaly and provide fresh core material to analyse. A modern re-interpretation of the GRANU95-B seismic profile considering a magmatic background could test the assumption we made in Nickschick et al. (2014). As a logical consequence the comparison of the Delitzsch complex and this Cretaceous volcanic field could help finding their spatial and temporal relation to each other.

Direct comparisons of the volcanic fields in the Vogtland area, the NE Bavarian area and similarly old ultramafic rocks from the Eger Rift might be able to relate their origin and position within the opening of the Eger Graben, since their age hint at the late stages of the rifting process Ulrych et al. (2011).

Even though the Mýtina maar has been researched in detail, many questions of scientific background can be studied there. One of the major steps is to establish a three-dimensional model of the Mýtina maar, as already suggested in chapter 4. Knowing the actual size and dimensions of a maar-diatreme allow calculations of the amount of the magmatic component, the general amount of ejected volcanoclastics and, derived from that, the danger such a maar poses to society. Aside from the hazard, this maar offers a great opportunity to study palaeoclimate in Central Europe (Mrlina et al., 2009) and together with the assumed maar near Neualbenreuth could benefit our current state of knowledge about it. Within the International Continental scientific Drilling Programme (ICDP) several deep drills will be sunk in NW-Bohemia. Some of the key questions can be answered by a drill into one or both of the maars and research linked to these drills should focus on finding more potential maar structures in the area. One of these ICDP drills is also planned to be sunk into one of the degassing fields around Hartoušov or Bublák, which are excellent natural laboratories to study and monitor the magmatic intrusion - a tremendous asset to the observations in the earthquake swarm area. The author of this thesis himself plans to submit a proposal to this circular of the ICDP priority programme to test his hypotheses about pull-apart basins along the Počátky-Plesná fault and how tectonically controlled magmatic fluids interact with the sediments in the Cheb Basin and how large this degassing zone is.

6 References

Literatur

- Abratis M, Munsel D, Viereck-Götte L (2009) Melilithite and Melilithit-führende Magmatite des sächsischen Vogtland: Petrographie und Mineralchemie. *Zeitschrift für Geologische Wissenschaften* 37(1-2):41–73
- Ackerman L, Špaček P, Magna T, Ulrych J, Svojtka M, Hegner E, Balogh K (2013) Alkaline and Carbonate-rich Melt Metasomatism and Melting of Subcontinental Lithospheric Mantle: Evidence from Mantle Xenoliths, NE Bavaria, Bohemian Massif. *Journal of Petrology* 54(12):2597–2633
- Alexowsky W, Berger HJ, Goth K, Hübner F, Junghanns C, Schneider JW, Wolf L, Brauer R, Joisten H, Kardel K, Kaufmann H, Riedel P, Rumbaur C, C S, Steinborn H, Temme L, Wenzel B, Witthauer B, Wolf P (2007) Geologische Karte des Freistaates Sachsen 1:25000, Erläuterungen Blätter 5240 Zwickau und 5241 Zwickau Ost, Saxon State Agency for Environment, Agriculture and Geology
- Andreani L, Stanek KP, Gloaguen R, Krentz O, Dominguez-Gonzalez L (2014) DEM-Based Analysis of Interactions between Tectonics and Landscapes in the Ore Mountains and Eger Rift (East Germany and NW Czech Republic). *Remote Sensing* 6, DOI 10.3390/rs6097971
- Babuška V, Plomerová J (2001) Subcrustal lithosphere around the Saxothuringian-Moldanubian Suture Zone - a model derived from anisotropy of seismic wave velocities. *Tectonophysics* 332:85–199
- Babuška V, Plomerová J (2008) Control of paths of Quaternary volcanic products in western Bohemian Massif by rejuvenated Variscan triple junction of ancient microplates. *Studia Geophysica et Geodetica* 52:607–629
- Babuška V, Plomerová J (2013) Boundaries of mantle-lithosphere domains in the Bohemian Massif as extinct exhumation channels for high-pressure rocks. *Gondwana Research* 23:973–987
- Babuška V, Plomerová J, Fischer T (2007) Intraplate seismicity in the western Bohemian Massif (central Europe): a possible correlation with a paleoplate junction. *Journal Of Geodynamics* 44:149–159
- Babuška V, Fiala J, Plomerová J (2010) Bottom to top lithosphere structure and evolution of western Eger Rift (Central Europe). *International Journal Of Earth Sciences* 99:891–907
- Bankwitz P, Schneider G, Kämpf H, Bankwitz E (2003) Structural characteristics of epicentral areas in Central Europe: study case Cheb Basin (Czech Republic). *Journal Of Geodynamics* 35:5–32
- Bayerisches Landesamt für Umwelt (2015) Quartäres Maar SE von Neualbenreuth, geotopkataster Bayern - Geotop-Nummer:377R041
- Behr HJ (1992) Lineare Krustenstrukturen im Umfeld der KTB-Lokation. KTB report 92 3:3–82
- Behr HJ, Conrad W, Miller A, Trzebski R (2002) Linsser filtering and interpretation of the gravity map of Germany and adjacent regions at a scale of 1:1,000,000. *Zeitschrift für Geologische Wissenschaften* 30:385–402

-
- Bräuer K, Kämpf H, Strauch G, Weise S (2003) Isotopic evidence ($^3\text{He}/^4\text{He}$, $^{13}\text{C}_{\text{CO}_2}$) of fluid-triggered intraplate seismicity. *Journal of Geophysical Research: Space Physics* 108(B2):2070, DOI 10.1029/2002JB002077
- Bräuer K, Kämpf H, Niedermann S, Strauch G (2005) Evidence for ascending upper mantle-derived melt beneath the Cheb basin, Central Europe. *Geophysical Research Letters* 32: L08303, DOI 10.1029/2004GL022205
- Bräuer K, Kämpf H, Niedermann S, Strauch G, Tesař J (2008) The natural laboratory NW Bohemia-comprehensive fluid studies between 1992 and 2005 used to trace geodynamic processes. *Geochemistry, Geophysics, Geosystems* 9: L17309, DOI 10.1029/2009GL039615
- Bräuer K, Kämpf H, Strauch G (2009) Earthquake swarms in non-volcanic regions: what fluids have to say. *Geophysical Research Letters* 36: L17309, DOI 10.1029/2009GL039615
- Bräuer K, Kämpf H, Koch U, Strauch G (2011) Monthly monitoring of gas and isotope compositions in the free gas phase at degassing locations close to the Novy Kostel focal zone in the western Eger Rift, Czech Republic. *Chemical Geology* 290:163–176, DOI 10.1016/j.chemgeo.2011.09.012
- Bräuer K, Kämpf H, Strauch G (2014) Seismically triggered anomalies in the isotope signatures of mantle-derived gases detected at degassing sites along two neighboring faults in NW Bohemia, central Europe. *Journal of Geophysical Research: Solid Earth* 119(7):5613–5632, DOI 10.1002/2014JB011044
- Credner H (1876) Das vogtländisch-erzgebirgische Erdbeben vom 23. November 1875. *Zeitschrift für die Gesamten Naturwissenschaften* 48:246–269
- Credner H (1898) Diesaächsischen Erdbeben während der Jahre 1889 und 1897, insbesondere das sächsisch-böhmische Erdbeben vom 24. Oktober bis 29. November 1897. *Abhandlungen der mathematisch-physischen Classe der Königlich Sächsischen Gesellschaft der Wissenschaft* 24(4):315–399
- Dézes P, Schmid S, Ziegler P (2004) Evolution of the European Cenozoic Rift System: interaction of the Alpine and Pyrenean orogens with their foreland lithosphere. *Tectonophysics* 389:1–33
- Dobeš M, Hercog F, Mazáč O (1986) Die geophysikalische Untersuchung der hydrogeologischen Strukturen im Cheb-Becken. *Sbornik Geologických Věd* 21:117–158
- Dreger DS, Tkalčić H, Johnston M (2000) Dilational processes accompanying earthquakes in the Long Valley Caldera. *Science* 288:122–125
- Enderle U, Schuster K, Prodehl C, Schulze A, Bribach J (1998) The refraction seismic experiment GRANU95 in the Saxothuringian belt, southeastern Germany. *Geophysical Journal International* 133:245–259
- Fischer T (2003) The August-December 2000 earthquake swarm in NW Bohemia: the first results based on automatic processing of seismograms. *Journal Of Geodynamics* 35:59–81
- Fischer T, Michálek J (2008) Post 2000-swarm microearthquake activity in the principal focal zone of West Bohemia/Vogtland: Space-time distribution and waveform similarity analysis. *Studia Geophysica et Geodetica* 52:493–511
-

-
- Fischer T, Horálek J, Hrubcová P, Vavryčuk V, Bräuer K, Kämpf H (2014) Intra-continental earthquake swarms in West-Bohemia and Vogtland: A review. *Tectonophysics* 611:1–27, DOI 10.1016/j.tecto.2013.11.001
- Flechsigt C, Fabig T, Rücker C, Schütze C (2010) Geoelectrical investigations in the Cheb Basin/W-Bohemia: An approach to evaluate the near-surface conductivity structure. *Studia Geophysica et Geodetica* 54:417–437
- Flechsigt C, Heinicke J, Mrlina J, Kämpf H, Nickschick T, Schmidt A, Bayer T, Günther T, Rücker C, Seidel E, Seidl M (2015) Integrated geophysical and geological methods to investigate the inner and outer structures of the Quaternary Mýtina maar (W-Bohemia, Czech Republic). *International Journal of Earth Sciences* 104(8):2087–2105, DOI 10.1007/s00531-014-1136-0
- Flores H Estrella, Umlauf J, Schmidt A, Korn M (2016) Locating mofettes using seismic noise records from small dense arrays and Matched Field Processing Analysis in the NW Bohemia/Vogtland Region, Czech Republic. *Near Surface Geophysics* 14(4):327–335
- Gautheron C, Moreira M, Allegre C (2005) He, Ne and Ar composition of the European lithospheric mantle. *Chemical Geology* 217:97–112
- Geissler W, Kämpf H, Seifert W, Dulski P (2007) Petrological and seismic studies of the lithosphere in the earthquake swarm region Vogtland/NW Bohemia, central Europe. *Journal of Volcanology and Geothermal Research* 159:33–69
- Geissler WH, Kämpf H, Bankwitz P, Bankwitz E (2004) Das quartäre Tephra-Tuff-Vorkommen von Mytina (Südrand des westlichen Eger-Grabens/Tschechische Republik): Indikationen für Ausbruch- und Deformationsprozesse. *Zeitschrift für Geologische Wissenschaften* 32:31–54
- Geissler WH, Kämpf H, Kind R, Bräuer K, Klinge K, Plenefisch T, Horálek J, Zedník J, Nehybka V (2005) Seismic structure and location of a CO₂ source in the upper mantle of the western Eger (Ohře) rift, Central Europe. *Tectonics* 24, TC5001, DOI 10.1029/2004TC001672
- Götze HJ, Schmidt S, Fichler C, Alvers MR (2007) IGMAS+ A New 3D Gravity, FTG and Magnetic Modeling Software. *AGU Fall Meeting Abstracts* pp A1+
- Halpaap F (2014) Seismic Structure of the Cheb Basin from a Reflection Survey. Master's thesis, University of Jena
- Hemmann A, Meier T, Jentzsch G, Ziegert A (2003) Similarity of waveforms and relative relocalisation of the earthquake swarm 1997/1998 near Werdau. *Journal Of Geodynamics* 35:191–208
- Heuer B, Geissler WH, Kind R, Kämpf H (2006) Seismic evidence for asthenospheric updoming beneath the western Bohemian Massif, central Europe. *Geophysical Research Letters* 33, L05311, DOI 10.1029/2005GL025158,2006
- Heuer B, Geissler WH, Kind R, the BOHEMA working group (2011) Receiver function search for a baby plume in the mantle transition zone beneath the Bohemian Massif. *Geophysical Journal International* 187:577–594

-
- Hofmann Y (2003) Gravimetrische und geodynamische Modellierungen in der Schwarmbeben-Region Vogtland/NW-Böhmen. PhD thesis, University of Jena
- Horálek J, Fischer T (2008) Role of crustal fluids in triggering the West Bohemia/Vogtland earthquake swarms: just what we know (a review). *Studia Geophysica et Geodetica* 52:455–478
- Horálek J, Fischer T (2010) Intraplate earthquake swarms in West Bohemia/Vogtland (Central Europe). *Jökull* 60:67–87
- Horálek J, Šileny J, Fischer T, Sláncová A, Boušková A (2000) Scenario of the January 1997 West Bohemia earthquake swarm. *Studia Geophysica et Geodetica* 44:491–521
- Hrubcová P, Geissler WH (2009) The crust-mantle transition and the Moho beneath the Vogtland/West Bohemian region in the light of different seismic methods. *Studia Geophysica et Geodetica* 53:275–294
- Hrubcová P, Vavryčuk V, Boušková A, Horálek J (2013) Moho depth determination from waveforms of microearthquakes in the West Bohemia/Vogtland swarm area. *Journal Of Geophysical Research-space Physics* 118:1–17, DOI 10.1029/2012JB009360.
- Kaiser G, Pilot J (1986) Weitere K-Ar-Datierungen an jungen Vulkaniten. *Zeitschrift für Geologische Wissenschaften* 14(1):121–124
- Kämpf H (2002) Comparison between the Ultramafic Delitzsch Complex and the active magmatic evolution in the western part of the Eger Rift: Interaction between fracture tectonics, migration of magmatic fluids and the structure of the seismogenic crust. In: *Mitteilungen des Naturwissenschaftlichen Vereines für Steiermark Band 132*
- Kämpf H, Franzke HJ, Neunhöfer H, Märten P, Röllig G, Schauer M (1991) Zur strukturellen Bedeutung der Nord-Süd-Bruchstörungszone Plauen/Klingenthal - Altenberg/Gera - Leipzig/Halle - Dessau/Bernburg. In: *Geologisch-tektonischer Bau der Gera-Jachymov (Joachimsthal)-Störungszone und die daran gebundenen Uranlagerstätten - Kurzfassungen der Vorträge und Poster*, pp 12–13
- Kämpf H, Bräuer K, Koch U, Malkovský M, Strauch G, Weinlich FH, Weise S (1992) Vulkanismus - Mineralwässer - Seismizität im Bereich der marienbader Störungszone. In: *Exkursionsführer zur 1. Jahrestagung der Gesellschaft für Geowissenschaften e.V. (i.G.), Falkenstein/Vogtland*, pp 129–155
- Kämpf H, Bräuer K, Schumann J, Hahne K, Strauch G (2013) CO₂ discharge in an active, non-volcanic continental rift area (Czech Republic): Characterisation (¹³C, ³He/⁴He) and quantification of diffuse and vent CO₂ emissions. *Chemical Geology* 339:81–83
- Knett J (1899) Das Erzgebirgische Schwarmbeben zu Hartenberg vom 1. Jänner bis 5. Feber 1824. *Sitzungsberichte der Deutschen Naturwissenschaft-Medizinischen Vereins für Böhmen* Lotos 19:167–191
- Korn M, Funke S, Wendt S (2008) Seismicity and seismotectonics of West Saxony, Germany - New Insights from recent seismicity observed with the Saxonian Seismic Network. *Studia Geophysica et Geodetica* 52:479–492
- Krentz O, Witthauer B, Eilers H, Neumann E (1996) General map of seismicity of Saxony (in German), scale 1:400.000, Freiberg.

-
- Kroner C, Jahr T, Kämpf H, Geissler WH (2006) Der "Tuffschlot" bei Ebersbrunn/Westsachsen, der partiell erodierte Rest eines Maar-Diatrem-Vulkans. *Zeitung für geologische Wissenschaften* 34:3–4
- Krüger JC, Romer RL, Kämpf H (2013) Late Cretaceous ultramafic lamprophyres and carbonatites from the Delitzsch Complex, Germany. *Chemical Geology* 353:140–150
- Krull P, Schmidt D (1990) Geological map of German Democratic Republic, Map of the foliations of cosmic images, Scale 1:500.000, Berlin.
- Kvaček Z, Teodoridis V (2007) Tertiary macrofloras of the Bohemian Massif: a review with correlations within Boreal and Central Europe. *Bulletin Geosciences* 82:383–408
- Lauterbach R (1952) Beiträge zur tektonische Deutung der geomagnetischen Übersichtskarte der Deutschen Demokratischen Republik. *Wissenschaftliche Zeitschrift der Karl-Marx-Universität Leipzig* 3:271–279
- Lees JM (1998) Multiplet analysis at Coso geothermal. *Bulletin of the Seismological Society of America* 8(5):1127–1143
- LFUG (1996) Seismologische Übersichtskarte des Freistaates Sachsen 1:400000, 1. Ausgabe Landesamt für Umwelt und Geologie, Freiberg
- Lorenz V (2003) Maar-Diatreme Volcanoes, their Formation, and their Setting in Hard-rock or Soft-rock Environments. *Geolines* 15:72–83
- Matthes H, Kroner C, Jahr T, Kämpf H (2010) Geophysical modelling of the Ebersbrunn diatreme, western Saxony, Germany. *Near Surface Geophysics* 8:311–319
- Meinel C (2014) Verifizierung saisonaler, oberflächennaher Einflussfaktoren auf geoelektrische Messungen zur Untersuchung von Aufstiegszonen von Kohlenstoffdioxid an drei Mofetten im Westteil des Egergrabens. Master's thesis, University of Leipzig
- Mrlina J (2000) Vertical displacements in the Nový Kostel seismoactive area. *Studia Geophysica et Geodetica* 44:336–345
- Mrlina J, Seidl M (2008) Relation of surface movements in West Bohemia to earthquake swarms. *Stud Geophys Geod* 52:549–566
- Mrlina J, Kämpf H, Geissler WH, van de Boogard P (2007) Proposed Quaternary maar structure at the Czech/German boundary between Mýtina and Neualbenreuth (Western Eger Rift, Central Europe). *Zeitschrift für Geologische Wissenschaften* 35:213–230
- Mrlina J, Kämpf H, Kroner C, Mingram J, Stebich M, Brauer A, Geissler WH, Kallmeyer J, Matthes H, Seidl M (2009) Discovery of the first Quaternary maar in the Bohemian Massif, Central Europe, based on combined geophysical and geological surveys. *Journal of Volcanology and Geothermal Research* 182:97–112
- Neunhöfer H, Hemmann A (2005) Earthquake swarms in the Vogtland/Western Bohemian region: Spatial distribution and magnitude-frequency distribution as an indication of the genesis of swarms? *Journal Of Geodynamics* 39:361–385

-
- Nickschick T, Kämpf H, Jahr T (2014) The “Triasscholle” near Greiz, Germany—a volcanic origin? *Bulletin of Volcanology* 76(4):1–20
- Nickschick T, Kämpf H, Flechsig C, Mrlina J, Heinicke J (2015) CO₂ degassing in the Hartoušov mofette area, western Eger Rift, imaged by CO₂ mapping and geoelectrical and gravity surveys. *International Journal of Earth Sciences* 104(8):2107–2129
- Nickschick T, Flechsig C, Meinel C, Mrlina J, Kämpf H (subm.) Architecture and temporal variations of a terrestrial CO₂ degassing site using electric resistivity and CO₂ gas measurements. *International Journal of Earth Sciences*
- Peterek A, Reuther CD, Schunk R (2011) Neotectonic evolution of the Cheb Basin (Northwestern Bohemia, Czech Republic) and its implications for the late Pliocene to Recent crustal deformation in the western part of the Eger Rift. *Zeitschrift für Geologische Wissenschaften* 5/6:335–365
- Plomerová J, Achauer U, Babuška V, Vecsey L, BOHEMA W (2007) Uppermantle beneath the Eger Rift (Central Europe): plume or asthenosphere upwelling? *Geophysical Journal International* 169:675–682
- Prodehl C, Mueller S, Haak V (1995) The European Cenozoic Rift System, in *Continental rifts: evolution, structure, tectonics*. In: Olsen, K.H. (Ed.), *Dev. Geotecton.* Elsevier
- Puff P (1966) Ergebnisbericht über die Kartierungsbohrung Ida- Waldhaus 1/64 und 2/64 bei Greiz, Bezirk Gera
- Puff P (1970) Die Triasscholle bei Greiz - Ein Beitrag zur postvariszischen Entwicklung des Ostthüringischen Schiefergebirges. *Geologie* 19:1135–1142, Berlin
- Rohrmüller J (2003) Die Forschungsbohrung Bayerhof-die Erkundungeines tertiären Maars im Steigerwald, Oberpfalz (NE Bayern). *Geologica Bavarica* 107:215–220
- Rohrmüller J, Horn P, Peterek A, Teipel U (2005) Specification of the Excursion Stops First day: Geology and structure of the lithosphere. In: Kämpf et al - *The KTB Deep Crustal Laboratory and the western Eger Graben* 46-63
- Rojik P, Fejfar O, Dašková J, Kvaček Z, Pešek J, Sýkorová I, Teodoridis V (2014) Krušné hory Piedmont basins - Cheb Basin. In: Pešek J (ed) *Tertiary Basins and Lignite Deposits of the Czech Republic, Tertiary Basins and Lignite Deposits of the Czech Republic*, Prague
- Röllig G, Viehweg M, Kampe A (1989) Zur Wirksamkeit von meridionalen und äquatorialen Strukturen im Gebiet der Mitteldeutschen Schwelle zwischen Halle und Schönnewalde. *Zeitschrift für Angewandte Geologie* 35:397–300
- Röllig G, Kampe A, Steinbach V, Ehling BC, Wasternack J (1995) Der Untergrund des deutschen Braunkohlereviere. *Zeitschrift für Angewandte Geologie* 23:3–26
- Šantruček P, Králík F, Kvičinský Z, Opletal M (1991) Geological map, scale 1:50.000, Czech Geological Survey, 1991
- Schmidt A, Nowaczyk N, Kämpf H, Schüller I, Flechsig C, Jahr T (2013) Origin of magnetic anomalies in the large Ebersbrunn diatreme, W Saxony, Germany. *Bulletin of Volcanology* 75(766), DOI 10.1007/s00445-013-0766-6
-

- Schüller I, Kämpf H, Schmidt A, Flechsig C, Jahr T (2012) Petrographic and thermochronometric investigation of the diatreme breccia of the Ebersbrunn Diatreme-W Saxony, Germany. In: Arentsen K, Németh K, Smid E (eds) 4th International Maar Conference a multidisciplinary congress on monogenetic volcanism, Auckland New Zealand, 20-24 February 2012, Abstract Volume, p. 139-140, ISBN: 978-1-877480-15-7.
- Schunk R, Peterek A, Reuther CD (2003) Untersuchungen zur quartären und rezenten Tektonik im Umfeld der Marienbader Störung und des Egerer Beckens (Tschechien) - erste Ergebnisse. *Mitteilungen des Geologisch-Paläontologischen Instituts der Universität Hamburg* 87:19–46
- Ibs-von Seht M, Plenefisch T, Klinge K (2008) Earthquake swarms in continental rifts - a comparison of selected cases in America, Africa and Europe. *Tectonophysics* 452:66–77
- Seifert W, Kämpf H, Wasternack J (2000) Compositional variation in apatite, phlogopite and other accessory minerals of the ultramafic Delitzsch complex, Germany: implication for cooling history of carbonatites. *Lithos* 53:81–100
- Skála R, Ulrych J, Ackerman L, Krmíček L, Fediuk F, Balogh K, Hegner E (2015) Upper Cretaceous to Pleistocene melilitic volcanic rocks of the Bohemian Massif: petrology and mineral chemistry. *Geologica Carpathica* 66(3):197–216
- Ulrych J, Lloyd FE, Balogh K (2003) Age Relations and Geochemical Constraints of Cenozoic Alkaline Volcanic Series in W Bohemia: A Review. *Geolines* 15:168–180
- Ulrych J, Dostal J, Adamovič J, Jelinek E, Špaček P, Hegner E, Balogh K (2011) Recurrent Cenozoic volcanic activity in the Bohemian Massif (Czech Republic). *Lithos* 123:133–144
- Vavryčuk V (1993) Crustal anisotropy from local observations of shear-wave splitting in West Bohemia, Czech Republic. *Bulletin of the Seismological Society of America* 83:1420–1441
- Vavryčuk V (2011) Principal earthquakes: Theory and observations from the 2008 West Bohemia swarm. *Earth and Planetary Science Letters* 305:290–296
- Švancara J, Gnojek I, Hubatka F, Dědáček K (2000) Geophysical field pattern in the west bohemian geodynamic active area. *Studia Geophysica et Geodetica* 44:307–326
- Wagner GA, Gögen K, Joonckheere R, Wagner I, Woda C (2002) Dating of the Quaternary volcanoes Komorná hůrka (Kammerbühl) and Železná hůrka (Eisenbühl), Czech Republic, by TL, ESR, alpha-recoil and fission track chronometry. *Zeitschrift für Geologische Wissenschaften* 30(3):191–200
- Weinlich FH, Bräuer K, Kämpf H, Strauch G, Tesař J, Weise SM (1999) An active subcontinental mantle volatile system in the western Eger rift, Central Europe: Gas flux, isotopic (He, C, and N) and compositional fingerprints. *Geochimica et Cosmochimica Acta* 63:3653–3671
- Wendt J, Dietrich R (2003) Determination of recent crustal deformations based on precise GPS measurements in the Vogtland earthquake area. *Journal Of Geodynamics* 35:235–246
- White JW, Ross PS (2011) Maar-diatreme volcanoes: A review. *J Volcanol Geotherm Res* 201:1–29
- Wyss M, Shimazaki K, Wiemer S (1997) Mapping active magma chambers by b values beneath the off-Ito volcano, Japan. *Journal of Geophysical Research* 102(B9):20,413–20,422

Ziegler P, Dezes P (2007) Cenozoic uplift of Variscan Massifs in the Alpine foreland: timing and controlling mechanisms. *Global and Planetary Change* 58:237–269

PART II:

OWN RESEARCH

7 The "Triasscholle" near Greiz, Germany - a volcanic origin?

Nickschick, T., Kämpf, H., Jahr, T.

published 2014 in Bulletin of Volcanology 76(4):1-20

The “Triasscholle” near Greiz, Germany—a volcanic origin?

T. Nickschick · H. Kämpf · T. Jahr

Received: 13 August 2013 / Accepted: 31 January 2014
© Springer-Verlag Berlin Heidelberg 2014

Abstract Near the city of Greiz in Eastern Thuringia, Germany, there is a stratigraphically non-coherent breccia encased in shales from the Lower Carboniferous that includes larger blocks of Triassic sediments, the so-called Triasscholle. The origin of this breccia has previously been interpreted tectonically. The geophysical methods of geomagnetics and gravimetry have recently been applied to the area. We found that the formation is characterised by a lack of a magnetic anomaly, but it has a distinct, spatially small gravity anomaly of approximately -2 mGal and whose shape hints at a structure about twice the previously suggested size. Most of the geological information available is derived from older drill cores located in the southwest part near the previously assumed margin. Scanning electron microscope (SEM) investigations on drill core samples from the polymict breccia at different depths show a cataclastic deformation of carbonate grains in the upper parts, while we find hypidiomorphic and idiomorphic zoned carbonate grains featuring a dolomitic/calcitic composition within the core as well as rims of ankeritic composition hinting at intense hydrothermal influence. The breccia itself contains granitoid xenoliths from greater depths, which indicate upward transport processes.

Editorial responsibility: K. Németh, Guest Editor

This paper constitutes part of a topical collection: Smith IEM, Németh K, and Ross P-S (eds) Monogenetic volcanism and its relevance to the evolution of volcanic fields.

Electronic supplementary material The online version of this article (doi:10.1007/s00445-014-0806-x) contains supplementary material, which is available to authorized users.

T. Nickschick (✉) · H. Kämpf
German Research Centre for Geosciences, GFZ Potsdam, Section 4.3
Telegrafenberg, 14473 Potsdam, Germany
e-mail: tobnic@gfz-potsdam.de

T. Jahr
Institute for Geosciences, Friedrich-Schiller-Universität, Burgweg
11, 07749 Jena, Germany

This and plastic deformation below 95m depth, both on macroscopic and microscopic scales, indicates an anomalous increase of heat with depth and material transport from depth. Judging from the gravimetric minimum and the SEM investigations on the breccia samples, we assume the Triasscholle near Greiz to be a deeply eroded maar-diatreme volcano. From pollen analysis results on the matrix, the formation can be considered Santonian or younger in age (≤ 85 Ma). Most interesting are the alteration of the mainly carbonatic components of the breccia, the deep erosion level of the diatreme and the multidisciplinary approach towards the reinterpretation of this formerly misinterpreted structure.

Keywords Maar-diatreme volcano · Gravimetry · Metasomatism · Polymict breccia · Thüringer Schiefergebirge · Upper Cretaceous volcanism

Introduction

Approximately 4 km northeast (NE) of Greiz, Eastern Thuringia, Germany, there is a geologically unique structure that has been known since the nineteenth century (Liebe and Zimmermann 1892). Encased in mainly phyllitic shales from the Lower Carboniferous is a southwest (SW)–NE-striking structure (Fig. 1) that mainly consists of brecciated Triassic sediments. This so-called Triasscholle (TS, literally: Triassic block) was mapped as only approximately 800×200 m in size and is nearly unexplored in terms of origin and extent, except for two exploration drill holes made in the 1960s and some local gravity surveys carried out by the former SDAG Wismut (Soviet/East-German Uranium Mining Co.) in the 1970s. Many of the results from these investigations have not yet been published. Most of the information available is described in Puff ("Ergebnisbericht über die Kartierungsbohrung Ida-Waldhaus 1/64 und 2/64 bei 1000 Greiz, Bezirk Gera," unpublished report, 1966, 1970), wherein the structure is assumed to

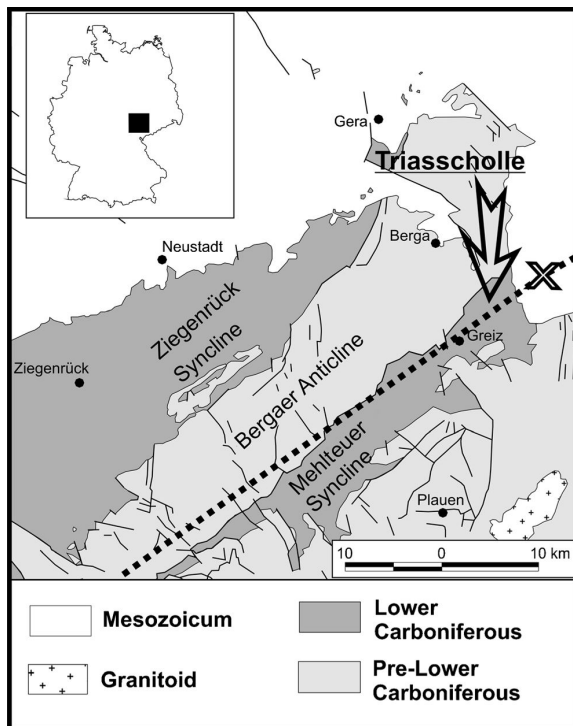


Fig. 1 Location of the TS in the western part of the Saxo-Thuringian Zone of the Variscan orogenic belt in Central Europe, modified after Hahn ("Erläuterungen zur geologischen Karte von Thüringen 1:25000, Blatt Greiz 5339", unpublished report. The *dotted line* represents the course of the profile B of the GRANU 95 experiment (Enderle et al. 1998) crossing the TS, where X marks the shot point F (see "Indications of a heating event" section)

result from tectonic processes due to the fact that the person in charge was a sedimentologist and volcanic structures were scarcely known in this area at that time (see "Seismic activity, fault zones and palaeo-volcanism" section). Later, the former SDAG Wismut performed some research on the region, including the area around the TS, in their search for uranium mineralisations. This also included some shallower exploration drilling as well as geophysical surveys.

In the 1990s, the crustal structure of the area was investigated by the way of seismic experiments (Enderle et al. 1998; DEKORP and Orogenic Processes Working Group 1999). These seismic profiles are located near this formation and thus represent an important source of information for this study. An updated geological map for the surrounding area is accessible from Hahn (2003, "Erläuterungen zur geologischen Karte von Thüringen 1:25000, Blatt Greiz 5339", unpublished report). Note that this map is based on the results from a few exploration drill holes and the assumption of a tectonic origin for the TS. According to Puff (2005), it remains unclear how this "Waldhaus" Formation (see Fig. 2) was formed, although he suggested that the breccia might have been the result of a magmatic or phreatomagmatic event. It had also been suggested that further insight into the structure could be provided

via the application of geophysical methods to the area. The geophysical surveys we conducted include the examination of both the local gravity and the magnetic field. As a result, a first simple three-dimensional (3D) model of the area was made using the Interactive Geophysical Modelling Assistant (IGMAS+) software, the successor of the IGMAS software package developed by Götze (1978), Götze and Lahmeyer (1988) and Götze et al. (2007). By combining the original drill logs, the results from recent geophysical surveys and petrographic and mineral-chemical investigations on samples of the WA 1/64 drill from a 30- to 260-m depth, we assume the Triasscholle near Greiz to be a deeply eroded, hydrothermally overprinted maar-diatreme volcano. Some preliminary results were also presented in Nickschick et al. (2012).

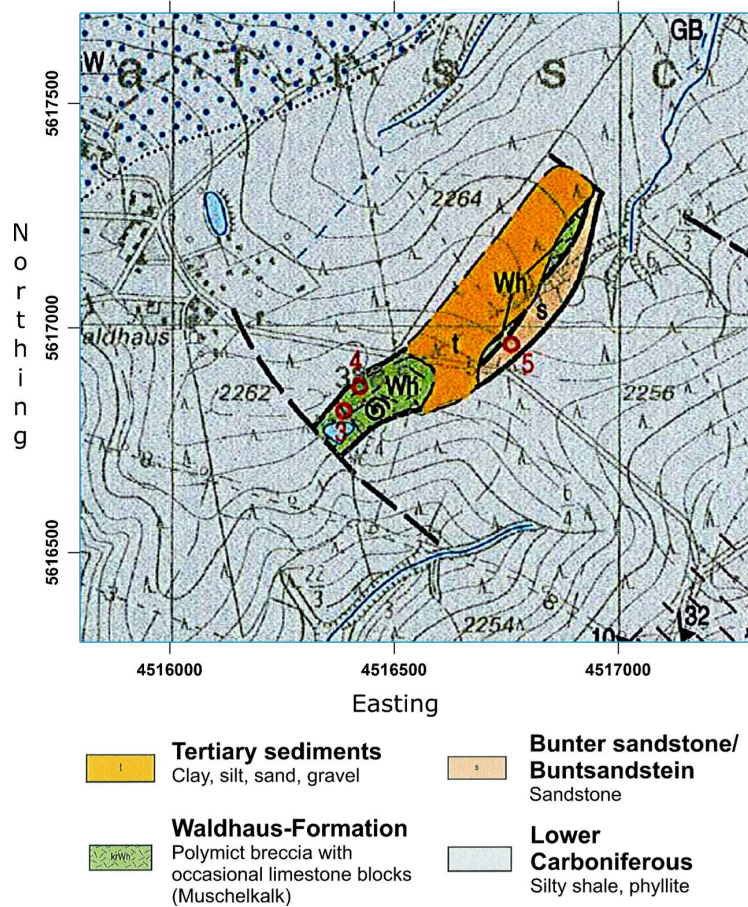
Geological, geophysical and volcanic settings

Seismic activity, fault zones and palaeo-volcanism

Over the last years, the TS has seen renewed interest because of its close proximity to the Werdau earthquake swarm region and to the Ebersbrunn diatreme, which is located ca. 14 km ENE of the TS (Fig. 3). Earthquake swarms are often associated with recent volcanism and/or are triggered by the migration of magmatic fluids entering the lithosphere, and they consist of a series of earthquakes with low magnitude (Bräuer et al. 2003, 2005, 2009; Hemmann and Kämpf 2002; Kämpf 2002; Kämpf et al. 2013; Ibs-von Seht et al. 2008). Swarms of the Werdau epicentral area occurred on September 1986, December 1997/January 1998 and August/September 2006 (Hemmann et al. 2003; Neunhöfer and Hemmann 2005; Korn et al. 2008). The Werdau earthquake swarm area is situated in the north (N)–south (S) trending Regensburg-Leipzig-Rostock Zone (RLRZ, Fig. 3). According to Bankwitz et al. (2003), the RLRZ is approximately 700 km long and ca. 40 km wide. Fossil paths for magma ascent are known at seismically active sections of the RLRZ near Zwickau and between Plauen and Marianske Lazne (Fig. 3). Three distinct periods of volcanic activity, including maar-diatreme volcanoes for the northern and western part of the Bohemian Massif, can be defined in the area of interest: (1) pre-rift period (Later Cretaceous to Mid Eocene, 79–49 Ma), (2) syn-rift period (Mid Eocene to Mid Miocene, 42–16 Ma) and (3) late-rift period (16–0.26 Ma) (Ulrych et al. 2011). Related to the occurrence of maar-diatreme volcanoes, the known volcanic activity in the seismically active central part of the RLRZ comprises the following (Fig. 3):

- Si-undersaturated ultramafic rocks (carbonatites, aillikites and alnöites) at the Delitzsch Complex N of Leipzig (Röllig et al. 1990) that occurred at 75–71 Ma (Krüger et al. 2013); Two carbonatite diatremes, Storkwitz and

Fig. 2 Geology of the TS and the surrounding area, modified after Hahn (2003). Red circles and numbers mark different drill holes: 3 = WA 1/64, 4 = WA 2/64 and 5 = Gr 41/79



- Serbitz, are known in the complex (Seifert et al. 2000; Krüger et al. 2013).
- The Ebersbrunn diatreme (age: Tertiary or Cretaceous; Berger 2008) the Weißenbrunn diatreme (unknown age; Alexowsky et al. 2007) and the TS are located at the intersection of the RLRZ and the Gera Jachymov fault zone (GJFZ).
 - Melilitites and melilitite-bearing igneous rocks including six confirmed or proposed maar structures are situated at the intersection of the RLRZ and the Eger Graben (EG): the Plesná maar (33.5–28.5 Ma, Kvaček and Teodoridis 2007), the Velký Luh maar (49–37 Ma, Kvaček and Teodoridis 2007), a geophysical anomaly (proposed maar) at Žírovice (unknown age, Dobeš et al. 1986), the Podhrad diatreme (unknown age, Šantrůček et al. 1991), the Bayerhof maar (21.7–23.3 Ma, Rohrmüller 2003) and the Mýtina maar (0.29 Ma; Mrlina et al. 2009).
 - At the intersection between the EG and the GJFZ, there are three maars: Hammerunterwiesenthal (31 Ma, Suhr and Goth 2008), Libouš (unknown age, Brus and Humík 1984) and Mrtvá Slatina (unknown age).

Geological setting

The Thüringer Schiefergebirge (Saxo-Thuringian Slate Mountains) forms the framework of the investigated area on a regional scale. On a more local scale, the TS is situated in the NE–SW striking Mehlteuer Syncline (Seidel 2003; Hahn and Meinhold 2005; Meinhold et al. 2005; Linnemann and Romer 2010) (Fig. 1). The area is characterised by an older Variscan NE–SW-directed thrust-sheet complex that was overprinted by younger Variscan NW–SE to NNW–SSE compressional tectonics (Hahn and Meinhold 2005; Hahn et al. 2010) and affected by an anchizonal to low-grade regional metamorphism. There are NE–SW-striking faults parallel to the fold axis of the syncline as well as perpendicularly oriented faults that may belong to the Gera-Jáchymov fault zone (Pohl et al. 2006; Neunhöfer 2009) (Fig. 3). The third type of faulting known to exist in this region is N–S-trending faults that belong to the Regensburg-Leipzig-Rostock fault zone (Bankwitz et al. 2003; Neunhöfer 2009). The area surrounding the TS is dominated by rocks of Lower Carboniferous age, mainly argillaceous and silty shales but also quartzites,

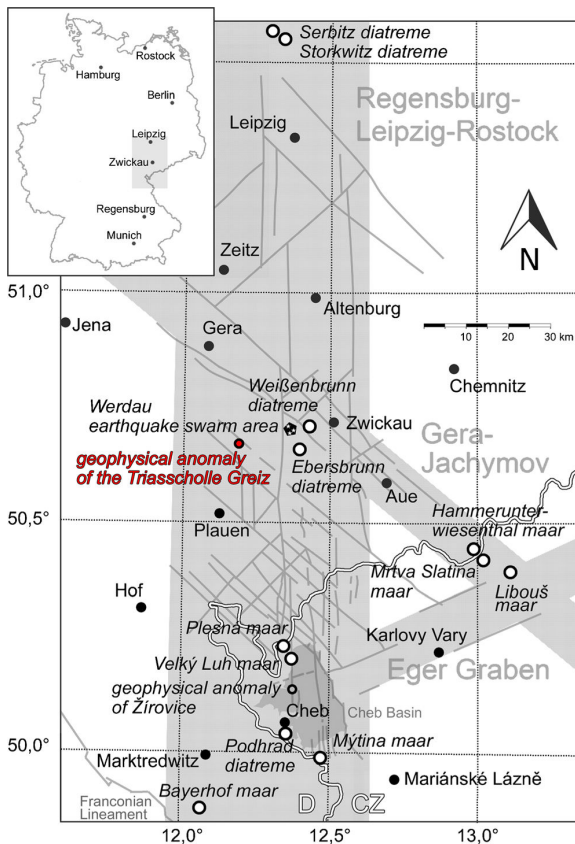


Fig. 3 Occurrence of maar-diatreme volcanism and earthquake swarm activity in the intersection area between Regensburg-Leipzig-Rostock Fault Zone, Eger Graben and the Gera-Jachymov Fault Zone (according to Brus and Humik 1984; Dobeš et al. 1986; Bankwitz et al. 2003; Rohmüller 2003; Neunhöfer and Hemmann 2005; Krvaček and Teodoridis 2007; Suhr and Goth 2008; Mrlina et al. 2009, Krüger et al. 2013, Suhr personal communication 2013). CZ Czech Republic

graywackes, sandstones and conglomerates (Seidel 2003; Hahn 2003; Hahn and Meinhold 2005). Figure 2 shows the near-surface geology of the area of interest.

The dominant rocks near the structure are phyllites from the Lower Carboniferous. Apart from these, none of the rocks described by Seidel (2003) can be found in the vicinity of the TS. Much of the available information for the TS is derived from two major drillings that were sunk in the 1960s: the deeper one, Ida-Waldhaus 1/64 (WA 1/64), has a total depth of 260.5 m, and Ida-Waldhaus 2/64 (WA 2/64) has a depth of approximately 100 m. Ida-Waldhaus 1/64 was supposed to have nearly reached the bottom of the TS (Puff unpublished report, 1970). WA 1/64 is located at E 4516379.3 and N 5616805.7, while WA 2/64 is just a few metres to the NE of WA1/64, at E 4516412.8 and N 5616861.0. The results were extensively discussed in Puff (unpublished report, 1970, 2005). These exploration drillings were supplemented by other, shallower drillings from the former SDAG Wismut; the most useful for us being drill hole Gr 41/79 at E 4516961 and N 5616752, with a total depth of 41 m. This drilling

and the report from Schulz and Krutzsch ("Bericht 47/66 über die sporenpaläontologische Untersuchung von Proben aus der Bohrung Ida-Waldhaus", unpublished report) are proof for the existence of Bunter sandstone (Buntsandstein, Lower Triassic) within this formation. The sandstone is described as strongly disintegrated. The locations of these three drillings can be seen in Fig. 2.

We stress the importance of the locations of the drillings, as WA 1/64 and WA 2/64 especially are located near the previously estimated margin of the TS.

Stratigraphy and petrography of drill cores

Stratigraphy

In this section, we combine the results from Puff (unpublished report, 1970) and the data described by Hahn (unpublished report). The first two are based on petrographic and biostratigraphic approaches (macroscopic research and transmitted light microscopy investigations). These results are supplemented by pollen analyses on a silty-clayey sediment clast in the breccia from Schulz and Krutzsch (unpublished report) (see Table 1).

The existence of the Upper Bunter sandstone is verified in one sample by the pollen analyses of Schulz and Krutzsch (unpublished report, Table 1). It forms a large amount of the breccia's matrix as grey dolomitic silts and clays. A considerable amount of Bunter sandstone has been confirmed in the TS from the results of the Gr 41/79 drilling (see Fig. 2, drilling no. 5), in which at least 30 m of the eventually achieved 41 m contained differently coloured sandstones. It is impossible to state at this time whether these sandstones belong to the Middle or Upper Bunter sandstone.

Different characteristic horizons of the Lower Muschelkalk (Early Middle Triassic) were found and could clearly be distinguished from rocks of the Middle Muschelkalk due to the higher porosity of the latter rocks. Larger blocks of massive, fine-grained limestone from the Wellenkalk (Lower Muschelkalk) are found within the breccia, sometimes reaching diameters of up to 20 m. The Middle Muschelkalk is represented by unfossiliferous and sometimes marly, dolomitic or massive limestones that are often accompanied by quartz grains with the individual grains being in the range of silt to fine sand (see Fig. 4). The transition from the Middle to Upper Muschelkalk is also verified by a conglomeratic dolomite that contains chalcedony. Rocks from the Upper Triassic (Keuper) were not detected in the initial research.

Most interesting, however, is the identification of sediments from the Upper Cretaceous within the drill cores (Schulz and Krutzsch unpublished report, sample from 65 m depth, Table 1), although no evidence for the existence of Permian and Jurassic rocks has been found yet. These Upper Cretaceous sediments were determined to have an age

Table 1 Summary of the results from Schulz and Krutzsch (unpublished report). One sample from each drilling (WA 1/64 and WA 2/64) was chosen for pollen and microflora analyses. These two samples were subdivided into five subsamples. Short summaries of the results can also be found in Puff (unpublished report, 1970)

Component	Classification	Encountered microflora
Silty-clayey sediment (taken from WA 1/64 65–66 m depth. Green olive to yellowish brown)	Upper Cretaceous (Coniacian to Campanian age)	<i>Pteridophyte spores: Leiotreiles, Intrapunctisporis, Concavisporites, Foveotriletes, Small Toroisporis, Gleicheniidites (Gleicheniidites), Gleicheniidites (Peregrinisporis), Camarotonosporites, Cicatricosisporites, Polypodiaceoisporites, Trilites, Foveasporis, Laevigatosporites haardtii, Monoletes ind.</i> <i>Angiosperm pollen: Latipollis, triangle-pollen type—indet., Subtriporopollanites, Quietoider pollentype, Plicapollis ex gr Seta PF., Vacuopollis, Trudopollis, Oculopollis, Pompeckjoidaepollenites ex gr subherycynicus, Pseudotrudopollis, Semioculopollis, Longaxoner, Tricolporopollenites, Dicolpopollis, Ginkgyoid-like pollentype</i>
Muschelkalk clasts (taken from WA 2/64 20.5–21.4 m depth)	Lower Muschelkalk	<i>Latosaccus latus, Platysaccus reticulatus, Protosacculina germanica, Striatizonites kelleri, Succimotisorites grandior</i>
Grey breccia (taken from WA 2/64 20.5–21.4 m depth. Bluish-grey cement)	Muschelkalk	<i>Tsugaepollenites oriens, Triadispora epigonia, Dacrycarpites europaeus, Illinites chitonoides</i>
	Upper Buntsandstein	<i>Triadispora faloata, Triadispora orassa, Voltziaceasporites nephrosaccus, Microsachryidites fastidiodes, Triadispora staplini, Voltziaceasporites heteromorpha</i>

between Coniacian and Campanian (Schulz and Krutzsch unpublished report).

All stratigraphic units occur without any noticeable correlation, especially apparent from the arbitrarily alternating different Muschelkalk horizons along the drill core. In the top-most parts of drillings WA 1/64 and WA 2/64, we find numerous poorly rounded clasts from the Muschelkalk of different sizes together with phyllites from the Lower

Carboniferous (mostly approximately 0.5–2 cm diameter) and quartz clasts (Fig. 5). In the lower parts of the drilling, WA 1/64, Puff (unpublished report) mentions an increasing amount of phyllite fragments, which are described as having diameters of approximately 1.5 cm (Fig. 5e, g, h). According to Puff (1970) and Hahn (2003), the whole area is mainly covered by a red to brown Tertiary clayey and marly soil. The largest part of the TS consists of a polymict breccia with

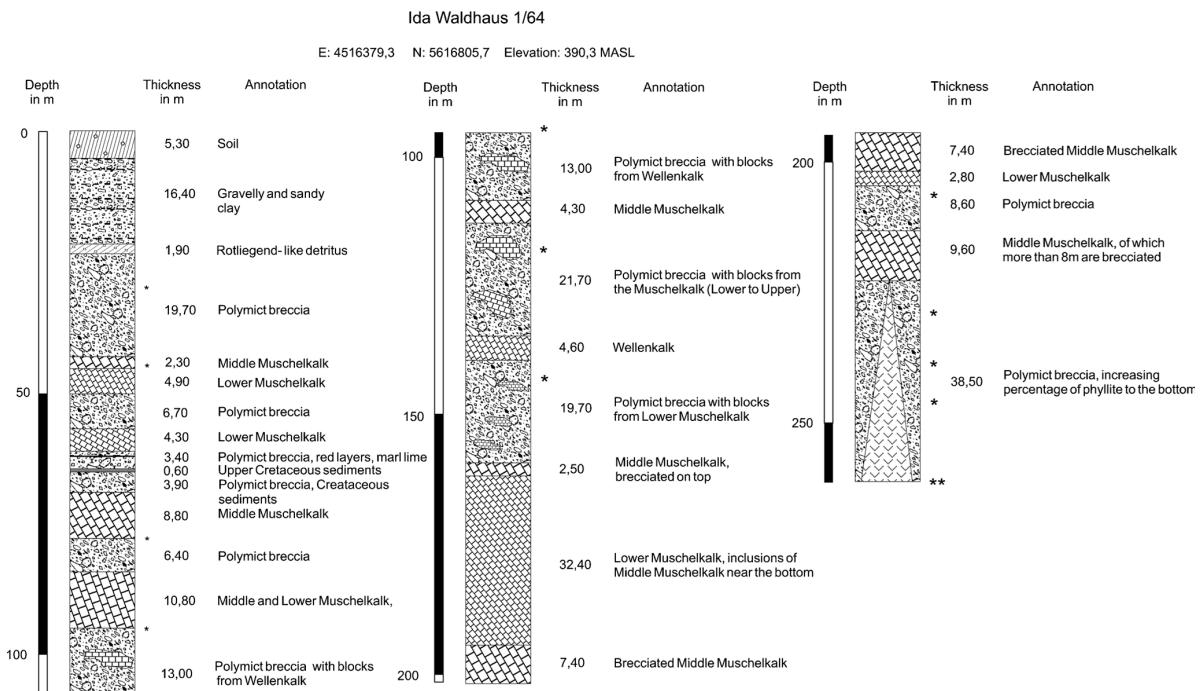
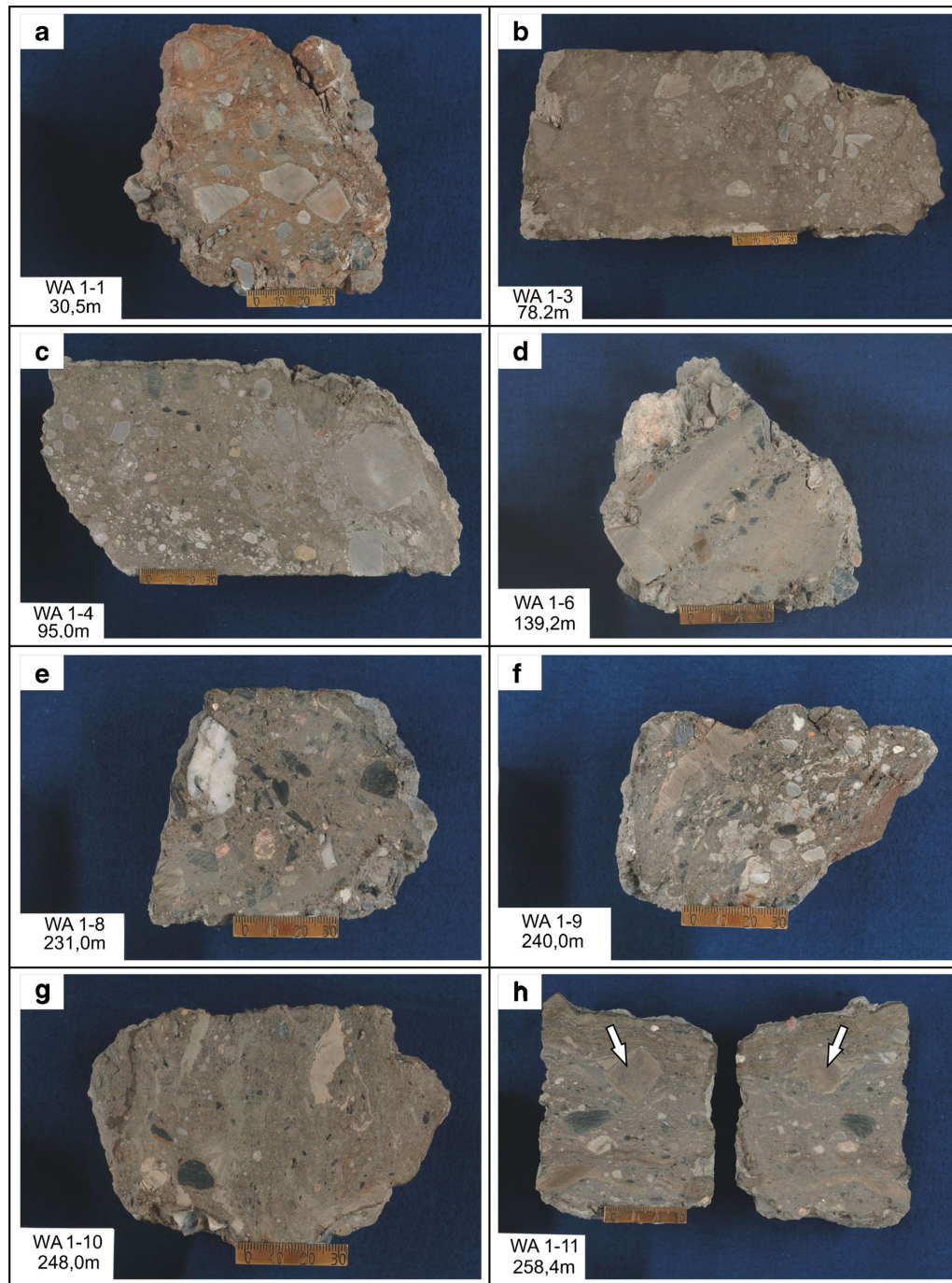


Fig. 4 Drill log of the WA1/64 drilling, after Puff (1970). Asterisk indicates that a polished thin section of the sample collected at this depth exists



varying amounts of milky quartz or shales from the surrounding rock mixed with a more or less “pure” limestone breccia. Within this breccia are blocks of solid limestone (Muschelkalk) with diameters ranging from a few decimetres to some metres (Fig. 4). This part differs from the polymict

parts in terms of the content of adjoining rocks within the breccia. The clasts are angular to sub-rounded and very poorly sorted and are sometimes aligned on a macroscopic scale; this happens very rarely, however. The solid limestone blocks show a very steep inclination towards a NW direction. It also

◀ **Fig. 5 a–h** Specimens of polymict breccia from different depths taken from the WA 1/64 drill core (Triasscholle Greiz, Germany). All photos were taken by E. Ganz (GFZ). **a** 30.5 m depth. Numerous angular carbonate and argillite clasts and a high degree of finely fragmented clasts. *Dark grey/black*: argillite clasts, *light grey*: carbonate clasts, light brown ground mass, irregular rock structure. **b** 78.2 m depth. Angular carbonate and argillite clasts and high percentage of finely fragmented clasts, *light grey*: carbonate clasts, light brown to grey ground mass, irregular rock structure. **c** 95.0 m depth. Angular carbonate (*light grey*) and argillite (*dark grey to black*) clasts, grey-coloured ground mass, irregular rock structure. **d** 139.2 m. Rounded-off carbonate (*light grey*) clast and some angular argillite (*dark grey/black*) clasts, greyish ground mass, rock structure: slightly regular. **e** 231.0 m depth. High degree of finely fragmented clasts and weakly developed flow structure. *White/light grey*: rounded quartzite clast, *dark grey/black*: argillite clasts, *rose*: kalifeldspar, greyish ground mass. **f** 240.0 m depth. Large portion of finely fragmented material and flow structure with a red to brown silty-clayey layer and angular resp. rounded argillite (*black/dark grey*) and few carbonate (*light grey*) clasts, grey ground mass. **g** 248.8 m depth. Finely fragmented material and weakly developed flow structure. *Red to brown*: silty-clayey layer, *black/dark grey*: argillite, *light grey*: carbonate, grey ground mass, *rock structure*: regular. **h** 258.4 m depth with clearly developed flow structure (*arrow*: rotated carbonate clast, flow texture and large portion of finely fragmented clasts, carbonate (*light grey*) and argillite (*black/dark grey*) clasts, grey ground mass)

seems as if the amount of massive blocks decreases to greater depths while the proportion of phyllite in the breccia increases (Puff 1970). The structure of the rocks from the drill core between 30 and 95 m appears irregular and chaotic. At greater depths, the structure tends to result in a regular “flow structure” at 260 m (Fig. 5h). A schematic figure of the whole WA 1/64 drilling is shown in Fig. 4.

Petrography of the polymict breccia

To extend knowledge about the petrographic composition and texture of the polymict breccia, we carried out scanning electron microscope (SEM) analyses at GFZ Potsdam (SEM Ultra 55 plus and NORAN System Seven (NSS)) on selected samples of the WA 1/64 drilling between a 30- and 260-m depth (Table 2). SEM was chosen as the breccia’s particle size is in the range of a few to some hundreds of micrometres. To prevent electrostatic charging of the SEM, the samples were sputtered with a carbon coating. The electron signals were

Table 2 Names of polished thin sections and their depths in the WA1/64 drilling

Name	Depth [m]	Name	Depth [m]
WA 1-1	30.50	WA 1-7	206.00
WA 1-2	45.50	WA 1-8	231.00
WA 1-3	78.20	WA 1-9	240.00
WA 1-4	95.00	WA 1-10	248.00
WA 1-5	118.50	WA 1-11a	258.40
WA 1-6	139.20	WA 1-11b	258.40

received by an angle-selective back-scattered electron detector with a 7–20-kV excitation voltage and a working distance of 6–7 mm between sample surface and objective.

SEM analyses of polished sections (Fig. 6a–h) show the following results: xenomorphic calcite grains in the groundmass occur up to a depth of 95 m and show no or thin ankeritic outer rims (Fig. 6a–c). At depths below 95 m, calcite and dolomite become steadily more idiomorphic and coated by an outer rim of ankerite (Figs. 6d–h and 7 and Tables 3 and 4). The grain size of the carbonate grains of the groundmass increases with depth from <5 to 20 μm (Fig. 6a–h). At depths of 140 and 260 m, we found zoned carbonate crystals up to 260 μm with a dolomitic composition in the core and an ankeritic composition at the rim (Fig. 7).

While dispersed apatite occurs at depth of 30 m, there is idiomorphically formed apatite, celestine and barite below 140 m (Fig. 6d). These minerals seem to have recrystallised in cavities, and there are larger accumulations of apatites at 258 m (Fig. 6g). At a 240-m depth, idiomorphic clay minerals are observed in fractures in quartzes and around quartz grains. These minerals are rimmed by hematite (Fig. 6f). All these phenomena hint at intense hydrothermal impact to depth.

To test the rearrangement of the breccia, we studied the occurrence of xenoliths and xenocrysts (apatite, garnet) from different depths. Some marble, phyllite, quartz and granitoid xenoliths can be found within breccia samples (Table 3). To assign apatite and garnet grains to types of xenoliths, we performed an analysis using the JXA-8230 Super Probe Electron Probe Microanalyser microprobe at GFZ Potsdam. The operating conditions for electron probe microanalysis of garnet were 15 kV at 20 nA with a 1- μm beam and 15 kV at 20 nA with a beam of 10 μm for apatite (20 kV, 40 nA, 10 μm beam for trace REEs). Two main groups of apatites can be distinguished:

1. Apatites with fluorine contents of 3–4.5 %
2. Apatites with fluorine contents ≤ 1.5 % and some per cent of H_2O

The apatites from group 1 can be found in paragenesis with quartz mobilisations in phyllite, and the apatites from group 2 are in paragenesis with the granitoids. Garnet (almandine) was found in granitoid xenoliths. Metamorphically remobilised apatite-bearing quartz can be found within parts of the breccia as described in Seidel (2003). However, no previous report mentions the occurrence of garnet in the vicinity of the TS.

Geophysical investigations

As numerous papers have shown (e.g. Büchel and Pirrung 1993; Gabriel 2003; Kroner et al. 2006; Mrlina et al. 2009; Matthes et al. 2010), the application of gravity and magnetic

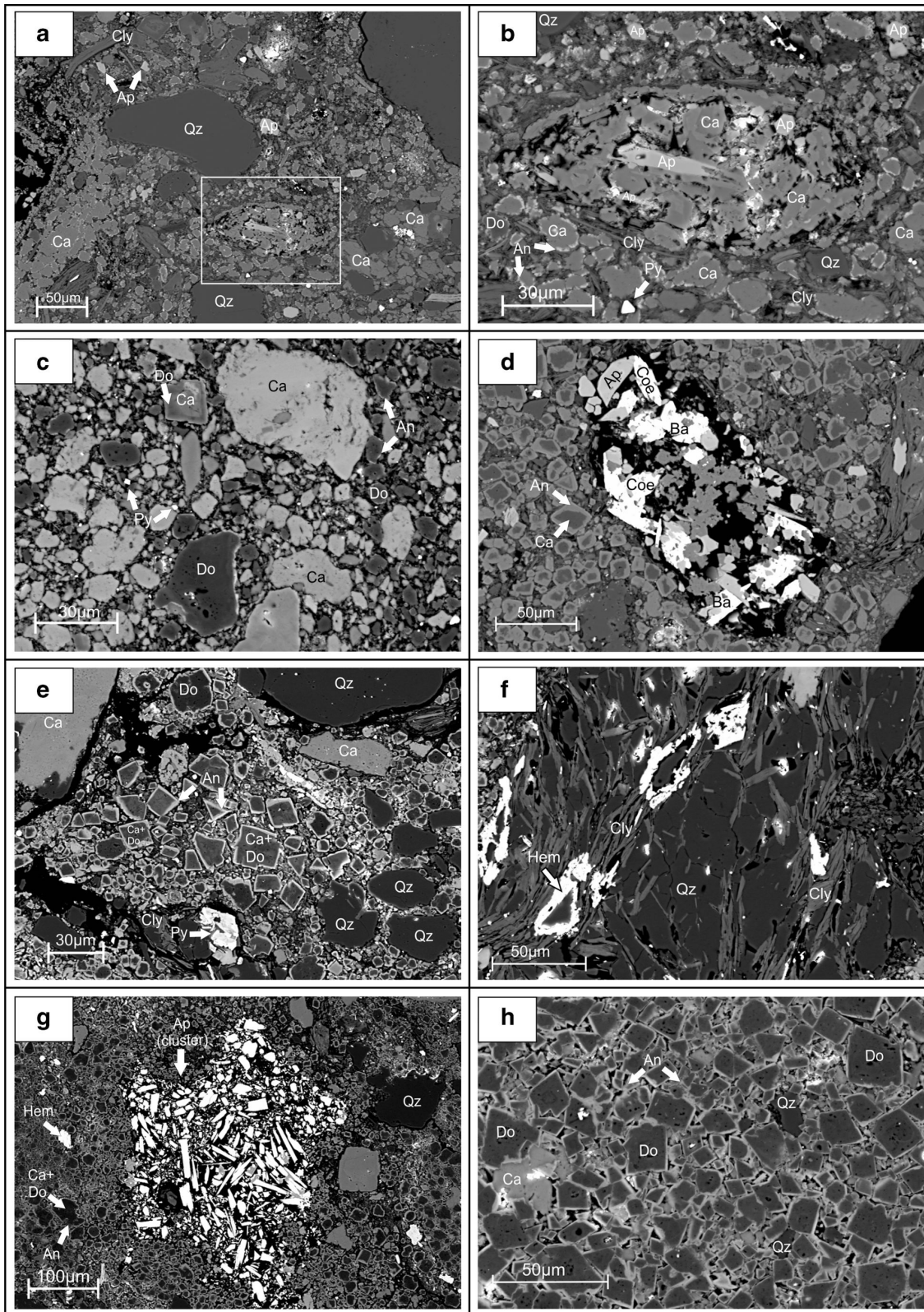


Fig. 6 a–h Scanning electron microscope (SEM) images from polished thin sections from the WA 1/64 drill hole (Triasscholle Greiz, Germany) at various depths. *Qz* quartz, *Cly* clay minerals, *Ca* calcium-dominated carbonate (calcite), *Do* calcium–magnesium carbonate (dolomite), *An* Ankerite, *Ap* apatite, *Coe* celestine, *Ba* barite, *Py* pyrite, *Hem* hematite. **a** Sample WA 1-1 (30.5 m depth). Cataclastic fabric. Predominantly xenomorphic clasts of calcite and dolomite ($\leq 10 \mu\text{m}$) with very fine fringed rims of ankerite; poorly rounded, larger quartz clasts and few dispersed apatites. Clayey matrix. Frame: see photo b. **b** Sample WA 1-1 (30.5 m depth). Detail of photo a (see above). *Centre*: Fossil of a shell with calcitic infilling paired with apatitic clasts and surrounded by clays. *Bright white*, diffuse areas in the fossil mark cavities filled with glue; *white*, sharp spots are pyrite. **c** Sample WA 1-4 (95.0 m depth). Poorly rounded clasts in a cataclastic fabric. Dolomite and calcite diameters vary between a few micrometres so some tens of micrometres. Some (dolomitic) grains feature fine rims of ankerite. Fine dispersed pyrites occur with diameters below $10 \mu\text{m}$. No larger clayey material can be seen. **d** Sample WA 1-6 (139.2 m depth). Calcites and dolomites feature a distinct (hyp-)idiomorphic rim of several micrometres. Larger cluster of sulphates (barite and celestine), paired with larger apatite crystals in a cavity. **e** Sample WA 1-9 (240.0 m depth). (Hyp-)idiomorphic carbonates of different sizes (few to some tens of micrometres) with distinct rims of ankerite. Few larger clasts of poorly rounded calcite clasts without rims. Quartzes feature accretions of clay minerals. A larger cluster ($\sim 30 \mu\text{m}$) of pyrite is located in a cavity. **f** Sample WA 1-9 (240.0 m depth). Large accretion of (hyp-)idiomorphic clay minerals along the edges of quartz grains. Note the occurrence of hematite. *Upper left*: smaller, rather xenomorphic calcites with ankeritic rims at the edge. **g** Sample WA 1-11b (258.4 m depth). Large cluster of (hyp-)idiomorphic apatite crystals. Total diameter of the apatite cluster is approximately $300\text{--}400 \mu\text{m}$. Occurrence of larger hematites. (Hyp-)idiomorphic carbonates feature a distinct ankerite rim. **h** Sample WA 1-11b (258.4 m depth). Idiomorphic crystals of mainly dolomite and few calcites with distinct ankeritic rims. Diameters vary between a few and a few tens of micrometres. Some small, poorly rounded quartz clasts are present

surveys has proven to be effective in the study of the lateral and vertical extent of maar-diatreme-like structures, e.g. in Ebersbrunn and Baruth, Saxony, the Eifel region (Germany) as well as in Western and Northern Bohemia (Czech Republic), as they are often characterised by distinct anomalies in their respective potential field. Until now, only these two geophysical methods have been applied, as they were expected to be the most useful and least costly considering time and effort for this initial geophysical investigation phase. The application of geophysics also serves as a verification of the geological assumptions that were derived from a few exploration drill holes and the initial tectonic interpretation of Puff (1970) and does not necessarily reflect the real geological situation.

Gravimetry and geomagnetics—methods

Both gravimetric and geomagnetic surveys were performed along nearly E–W-running profiles, wherein access was possible due to less dense vegetation. The database contains data from approximately 1,240 points for the magnetic survey and 261 observations for the gravity surveys in an irregular grid (for more information about the measurements, see [Supplementary Data A](#)). To further improve our database,

preexisting gravity data from the former SDAG Wismut have been included (SDAG Wismut unpublished data, 1972). To date, these data have never been used in any other official report. This additional dataset covers a large area in the N, NE and E of the TS in a $150 \times 200\text{-m}$ grid.

Unfortunately, no data from this source are available for the southern and western part of the TS. Combining both sets of data increases the number of available gravity stations to an overall number of 318 stations. The results of all measurements can be seen in Fig. 8.

Geophysical indication of a diatreme-like structure

The gravimetric surveys carried out within the area show that the TS is characterised by a depression in the local gravity field at E 4516750 and N 5617050, with a distinct minimum of approximately -2 mGal relative to the surrounding area. The general gravity anomaly correlates to the assumed outcrops by Hahn (2003) and is thus elongated. However, there is a distinct minimum in the centre of only 100 m in diameter with a very steep gravity gradient compared with the whole anomaly, which indicates a sudden change in the density of the rocks. This change can be explained as the transition from solid or slightly fractured rocks to heavily fractured rocks. From the centre of the gravity minimum, the gravitational gradient is steeper towards the NW–SE than in the perpendicular direction, as seen from the gravity minimum. The magnetic map of the area shows that the change in the total magnetic intensity throughout the area of investigation is less than 40 nT, which is negligible and is comparable to daily variations of the magnetic field in terms of magnitude. This is somewhat unusual, as diatremes are often accompanied by both gravimetric and magnetic anomalies at the same time (e.g. Büchel and Pirrung 1993; Mrlina et al. 2009; Matthes et al. 2010). Nevertheless, there is the possibility that the infill did not contain susceptible material in the first place, that the distribution of highly susceptible minerals within the area is more or less even or that a heating event has altered the juvenile clasts, which is discussed later (see “[Hydrothermal overprint with increasing depth](#)” and “[Indications of a heating event](#)” sections). Most variations seen in Fig. 6b are derived from near-surface phenomena such as remnants of a fence and similar objects. The largest variations (not shown here) were measured in the southernmost region but are related to the occurrence of a gas pipeline beneath the forest.

Petrophysical determination of mass and density

The mass and density of samples from various depths of the Ida-Waldhaus 1/64 drilling were determined. A few samples from the surrounding rocks of the TS were collected and measured as well. The investigation of the mass–density–porosity relation was carried out using Archimedes’ principle

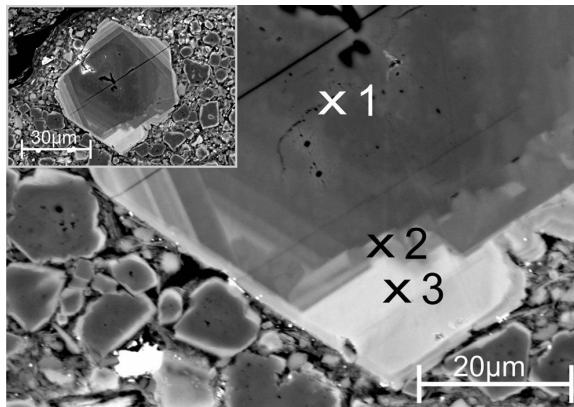


Fig. 7 Sample WA 1-11b (258.4 m depth): Zoned carbonate phenocryst. While the centre has a dolomitic composition, the Fe and Mn contents increase and Ca and Mg contents decrease with growing distance from the centre (see Table 4), resulting in an ankeritic composition at the clast's rim

at the GFZ Potsdam. The samples were heated in a vacuum to determine the dry mass before they were saturated with a fluid of known density. In the first attempt, saturation of the samples with distilled water led to their disintegration due to the occurrence of clay minerals within the samples. In the second attempt, the application of 2,2,4-trimethylpentane (isooctane) produced the necessary requirements, as it did not affect the samples. The results are reported in Table 5.

The most striking result is that the breccia's density varies between 2,665 and 2,799 kg/m³, with no correlation of density to depth. These variations are the result of the different

Table 4 Main components of the large carbonate clast from Fig. 7, determined via EDX

Sample point	MgO	Al ₂ O ₃	SO ₃	CaO	MnO	Fe ₂ O ₃
1	37.74	0.10	0.22	60.98	0.56	0.40
2	26.17	0.19	–	50.49	1.39	21.73
3	12.60	–	–	47.60	9.39	30.40

amounts of country rocks scattered within the breccia, especially sample WA 1-10 (Table 5). The average density of the breccia is slightly lower than the density of the phyllites. This observation is consistent with the small gravity difference detected across the southern limit of the TS with the surrounding rocks.

3D modelling

A 3D model of the area was constructed in an attempt to simulate the local gravity anomalies in favour of a hypothetical diatreme structure. A very simple model was established for this purpose. This model resembles a carrot-shaped, steep-walled body (diatreme) with a lower density in the upper part and a slightly higher density in the lower part to account for compaction. A more complex model reflecting the maar-diatreme scheme as featured in, e.g. Lorenz and Kurszlaukis (2007) or White and Ross (2011), is not fitting at this time, as further geological data (drillings) are needed as boundary conditions for refinement. The magnetic results are not suited for a combined gravity and magnetic interpretation. In the 3D

Table 3 Xenoliths and xenocrysts found within selected thin sections

Sample	Xenoliths			Xenocrysts			
	Limestone ^a	Phyllite ^b	Granitoid ^c	Apatite 1 ^d	Apatite 2 ^e	Garnet ^e	Quartz ^f
WA1-1	X	X	X	X	X	O	X
WA1-2	X	X	X	X	–	O	X
WA1-3	X	X	–	X	–	O	X
WA1-4	X	X	O	O	O	O	X
WA1-6	X	X	X	X	X	O	X
WA1-7	X	X	X	O	O	O	X
WA1-9	X	X	O	O	O	O	X
WA1-11a	X	X	X	X	X	O	X
WA1-11b	X	X	X	X	X	X	X

Xenoliths/xenocrysts are encountered (X), not encountered (–), or have yet to be looked for thoroughly (O)

^a Age: Trias (Muschelkalk), eroded, sunken material/blocks from palaeosurface

^b Age: Lower Carboniferous, country rock

^c Age: Upper Devonian (Gehmlich et al. 1998), outcropped at depth

^d In paragenesis with quartz mobilisations in phyllite

^e In paragenesis with granitoids

^f Quartz mobilisations in phyllite or quartz from granite

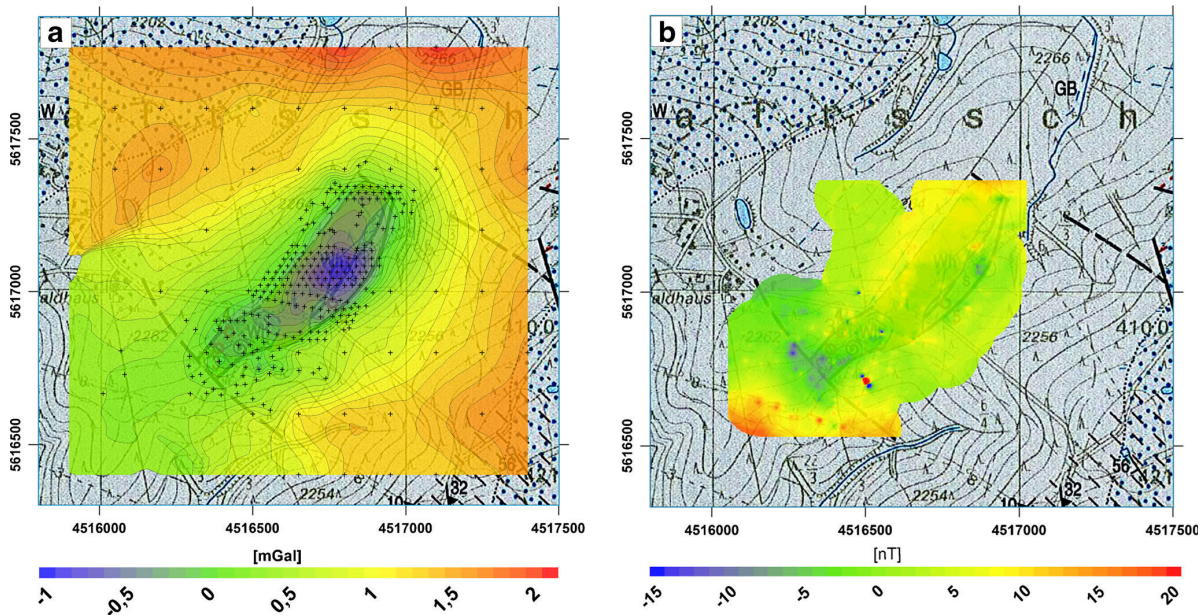


Fig. 8 Isoline maps for **a** the Bouguer gravity (*black crosses* indicate the locations of the observation stations) and **b** the geomagnetic field. While there is a distinct negative anomaly in the local gravity field, no distinct positive or negative anomaly can be detected

model, the subsurface mass distribution can be rebuilt, generating a theoretical gravity field that can be compared with the actual measured gravity values and modified by generating and altering the different bodies' shapes, extents and densities.

The IGMAS+ software package was used for forward modelling the local gravitational field of the TS. The IGMAS+ software is the successor of the IGMAS software, originally developed by Götze and Lahmeyer (1988). The model contains six different bodies that were partially split to make the process of modelling easier. A section containing all these bodies can be seen in Fig. 9 (for more information about the modelled sections, see [Supplementary Data B](#)).

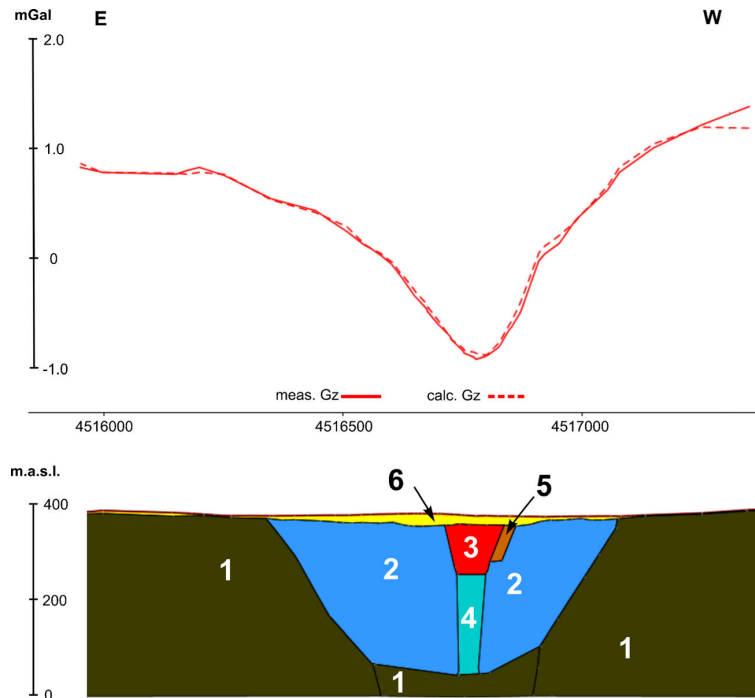
The six bodies can be described as follows:

1. A surrounding body of phyllites, $\rho=2,800 \text{ kg/m}^3$: For modelling purposes, the phyllite was split into three separate bodies with the exact same properties.
2. The breccia, representing the largest part of the TS, $\rho=2,730 \text{ kg/m}^3$
3. A body causing the distinct gravimetric minimum, $\rho=2,100 \text{ kg/m}^3$: This body refers to the diatreme's inner part, which consists of highly fractured rocks.
4. A body below no. 3: This body may or may not exist. Its existence cannot be verified due to the limited gravimetric data, $\rho=2,300 \text{ kg/m}^3$. This body accounts for the vertical extension of the inner diatreme structure (*sensu* Lorenz and Kurszlaukis 2007). The shape is slightly

Table 5 Results of the petrophysical determination of the density of the WA 1/64 drill samples and samples from the surrounding phyllites. Saturation fluid: isooctane, density $\rho=689.2 \text{ kg/m}^3$

Sample	Depth [m]	Density [kg m^{-3}]	Porosity	Sample	Depth [m]	Density [kg m^{-3}]	Porosity
WA 1-1	30.50	2,700.4	0.1431	WA 1-8 A	231.00	2,665.2	0.0112
WA 1-2 A	45.50	2,776.6	0.1399	WA 1-8 B	231.00	2,799.8	0.1375
WA 1-2 B	45.50	2,793.7	0.1366	WA 1-9	240.00	2,740.3	0.1021
WA 1-3 A	78.20	2,712.2	0.1779	WA 1-10	248.00	2,749.4	0.1649
WA 1-3 B	78.20	2,712.6	0.1735	WA 1-11a A	258.40	2,743.3	0.1039
WA 1-4 A	95.00	2,742.3	0.1194	WA 1-11a B	258.40	2,769.3	0.1046
WA 1-4 B	95.00	2,724.5	0.1079	WA 1-11b A	258.40	2,769.2	0.0919
WA 1-5 A	118.50	2,758.3	0.1397	WA 1-11b B	258.40	2,764.1	0.0994
WA 1-5 B	118.50	2,734.6	0.1243	Phy 1	–	2,795.5	0.1452
WA 1-6	139.20	2,759.8	0.1189	Phy 2	–	2,809.4	0.1731
WA 1-7	206.00	2,735.8	0.1442	Phy 3	–	2,791.7	0.1604

Fig. 9 IGMAS+ section running through the gravity minimum in an E–W direction. This section contains all the modelled bodies. Note that the outer body (no. 1) exceeds the area shown here and is, in fact, several hundreds of metres longer to minimise edge effects. For the position of the profile, see Fig. 10



cylindrical, and changes in its shape or density have minimal influence on the model, as changes in body no. 3 result in much stronger shifts in the gravitational field. The density is slightly higher than body no. 3 due to compaction.

5. Sandstone from the Upper Bunter as found in drilling Gr 41/79, $\rho=2,500 \text{ kg/m}^3$: The shape and extent are estimated from Hahn (2003) and Puff (1970).
6. A cover of Tertiary sediments and soil with a large portion of organic matter (forest), $\rho=1,700 \text{ kg/m}^3$: Note that due to the heterogeneity of the covering (unconsolidated Tertiary sediments, organic-rich coverage), the shape and density may change slightly over the area.

We assume that the sandstone has a density of $2,500 \text{ kg/m}^3$, indicating that we do not expect it to be heavily fragmented. This body, however, has only a minor impact compared with the other bodies, even if the density is changed, and it accounts for higher or lower grades of fragmentation. Because the Bunter sandstone has been encountered only in drill core Gr 41/79, a relatively small block of sandstone was simulated. Derived from the amplitude and extent of the anomaly, we expect a body of lower density compared with the rest of the breccia to be in the centre of the anomaly, which would indicate either heavily fragmented material or an accumulation of otherwise low-density material. Due to the limited amount of data available at this point, we can only make assumptions about the geometry of the deep parts of the

structure. The topmost layer also bears some uncertainty. Nothing in particular is known about the exact density or spatial distribution (especially the thickness) of the coverage of organic matter and Tertiary sediments. The only information is derived from the exploration drillings, which described a few metres of coverage of which a great portion was lost during the drilling. Nevertheless, we can estimate the thickness of this coverage from that source. On the other hand, a more or less evenly distributed coverage is assumed, thus leading to an offset of depth for the other bodies.

We projected the modelled bodies onto the surface to visualise their extensions, which can be seen in Fig. 10. We estimate the brecciated part to be larger than that estimated in the geological map in Fig. 2, as it was based on a few exploration drills and the idea of a tectonic origin. We assume a slow wedging out of the breccia to the N and S. However, because the breccia's density was measured from samples from one drilling, it is currently impossible to make a more accurate prediction of the breccia's spatial distribution or the position of the diatreme's margin. Nevertheless, a model consisting only of these six bodies is capable of generating a theoretical gravity field that resembles the measured gravity field. This means that a trough-like phyllite bed filled with brecciated material around a central low-density zone is a better explanation for the gravity anomaly than a wedge-like caving-in, as proposed by Puff (1970).

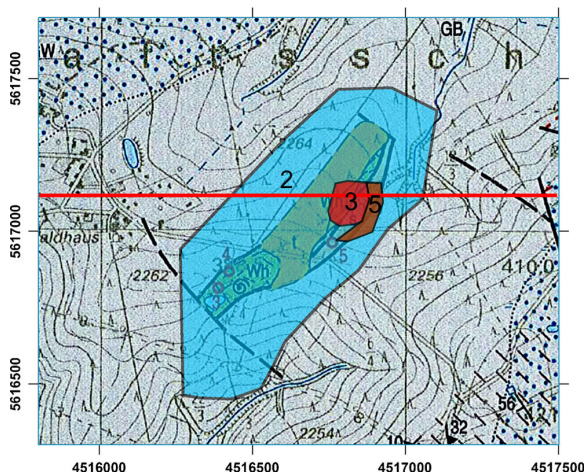


Fig. 10 Theoretical outcrop of modelled bodies 2 to 5 in IGMAS+ plotted on top of the map from Fig. 2. Bodies 1 and 6 from the model are not shown in order to retain the overview, and body 4 lies underneath body 3. The colours of the bodies are the same as in Fig. 9. Note that the blue structure in the NW is a lake and does not belong to the model. From the current model, we expect the brecciated part to be larger than expected (1,100×500 m)

Discussion

Geophysical aspects

A wedge-like cave-in, as proposed by Puff (1970), would generate an elongated negative gravity anomaly in the area without large variations in the gravity gradient. However, we find a more isometric, considerably higher negative anomaly of approximately -2 mGal with higher gradients relative to the surroundings within the centre, indicating an area of low-density material as derived from the gravity gradients. This argument is strengthened by the absolute determination of the density of the surrounding phyllites as well as the breccia from the drilling, although the latter is taken from the estimated margin of the formation. The small difference between the densities of the phyllite and the breccia cannot produce this type of gravity anomaly. We also consider the brecciated part (“Waldhaus Formation” in Fig. 2) to be larger than previously estimated. Derived from our IGMAS+ model, we built a brecciated body that is approximately 1,100×500 m close to the surface. This body is derived from the gravity model and does not necessarily imply that it has the same petrographic composition as found in the drill cores (differentiation between inner diatreme facies and the so-called halo); rather, it means there should be a larger area of fractured rocks nearby. The more elongated than round form of the anomaly is most likely due to the distribution of the breccias along the preexisting Variscan folding.

At the same time, we do not record any larger geomagnetic anomaly near the gravity low, which indicates a lack of

material with a moderate to high magnetic susceptibility. As most of our assumptions are made from the WA 1/64 and WA 2/64 drillings, which are close to the margin of the structure, we cannot make more precise predictions about the extent of the breccia. Without further information, statements about the shape and structure of the TS below 200 m depth cannot be made.

Petrographic, mineral, chemical and geological aspects

Hydrothermal overprint with increasing depth

From the investigations with the SEM (Figs. 6 and 7), one can see the composition of the breccia alters with increasing depth. In the topmost section, at approximately 30.5 m below the surface, we see a cataclastic fabric of the carbonatic matrix, as could be expected from a tectonic breccia that resembles a relic from a sedimentary deposit (Triassic-Muschelkalk). We also encounter dispersed sulphides within the breccia, containing mostly iron and sometimes lead and even a few apatites. Between 95 and approximately 139 m, a sudden change in the carbonate particles can be observed within the thin sections. Whereas the grains at shallower depths are rather xenomorphic, we suddenly observe hypidiomorphic and idiomorphic carbonate grains featuring distinct ankeritic rims. In the lowermost thin section, from approximately 258.5 m, the carbonate particles seem to have the most idiomorphic shape amongst all the studied thin sections with ankeritic rims. These particles are also idiomorphic and do not show any evidence of abrasion by cataclasis or mylonitisation. Another feature encountered in the SEM analysis is the accumulation of pyrite and apatite. Although no increase in the phosphorous and even a decrease in the sulphur contents were measured, we find few, but larger, clusters of these minerals in the deeper regions of the drill core. We also found clay minerals in fractures of quartz grains, and we interpret them as a post-genetic product and not as an initial feature already present before the breccia’s genesis. On a more macroscopic scale, we also find indications for a plastic or ductile deformation of the material (Fig. 5f–h). All these phenomena lead us to believe that the lower parts of the breccia were exposed to higher temperatures or high-temperature fluids, leading to the assumption of an anomalous geothermal or/and magmatic source. Although many of the encountered minerals can also occur in a sedimentary surrounding, such as pyrite, celestine, apatite or barite, we interpret the occurrence and appearance of fewer but larger clusters of these minerals at greater depths in drilling WA 1/64 as the result of a hydrothermal overprint, including recrystallisations and new formations of, e.g. clay minerals or the iron and manganese-rich rims at the carbonates, as often observed in hydrothermal, metasomatic environments.

Indications of a heating event

Kunert (Die Frankenwalder Querzone: Entwicklung einer thermischen Anomalie im Saxothuringikum, unpublished report) and Kosakowski et al. (1999) also mention a higher grade of illite crystallinity in the phyllites from the Lower Carboniferous in the area around Greiz, indicating the presence of a high-temperature environment (Table 6), which cannot be explained by a heat and pressure increase via compaction of the overlying sediments. The nearby sample K104 (E 4518600, N 5614800, approximately 3 km SW from the TS) was determined to have undergone temperatures of approximately 300 °C (Kunert unpublished report). However, this might also be related to either the Variscan orogenesis or to volcanism in the Rotliegend (Lower Permian), and it still needs to be verified by samples from the TS sediments (personal communication Torsten Hahn). However, several kilometres of sediment coverage cannot explain the increased temperature via compaction.

Enderle et al. (1998) mention a low-velocity anomaly at a shooting point from a seismic profile (GRANU95-B, see Enderle et al. 1998). This point is located at E 12° 17.582' and N 50° 43.002' (E 4520800, N 5620169) and is thus 5–6 km NE of the TS and approximately 6 km NNE from the measured sample K104 from Kunert (unpublished report) (Fig. 1). Enderle et al. (1998) measured an unusual increase of the velocity below, a deviation from the felsic granulites that were expected to be at that locality and they indicate the presence of a body featuring higher velocities. This would apply to our idea of a yet unknown magmatic intrusion in this region. For a more detailed overview of the depth profiles, see Fig. 7 in Enderle et al. (1998).

Indications for oppositely directed transport

Different types of xenoliths occur in the depth range from 30 to 260 m in the WA 1/64 drill core (Table 4):

- Limestone (Trias/Muschelkalk) has not been recently outcropped at the surface due to the Tertiary coverage

Table 6 Samples from Kunert (1999) featuring temperature, position and relative distance to the TS on illite crystallinity. Note that the closest samples, K103 and K104, feature temperatures of 335 and 300 °C, respectively

Sample	Easting	Northing	Dist. [m]	Temp. [°C]
K103	5,613,750	4,513,950	4,380	335
K104	5,614,800	4,518,600	2,900	300
K105	5,609,800	4,512,400	8,500	275
K106	5,607,750	4,512,200	10,400	325
K108	5,609,900	4,508,800	10,750	245
K109	5,606,000	4,509,800	13,100	300
K110	5,606,600	4,507,800	13,810	260

(Fig. 2). Puff (2005) assumes that massive blocks of limestone subsided from the palaeosurface. The chaotic stratigraphy (Fig. 4) hints at multiple subsidence events.

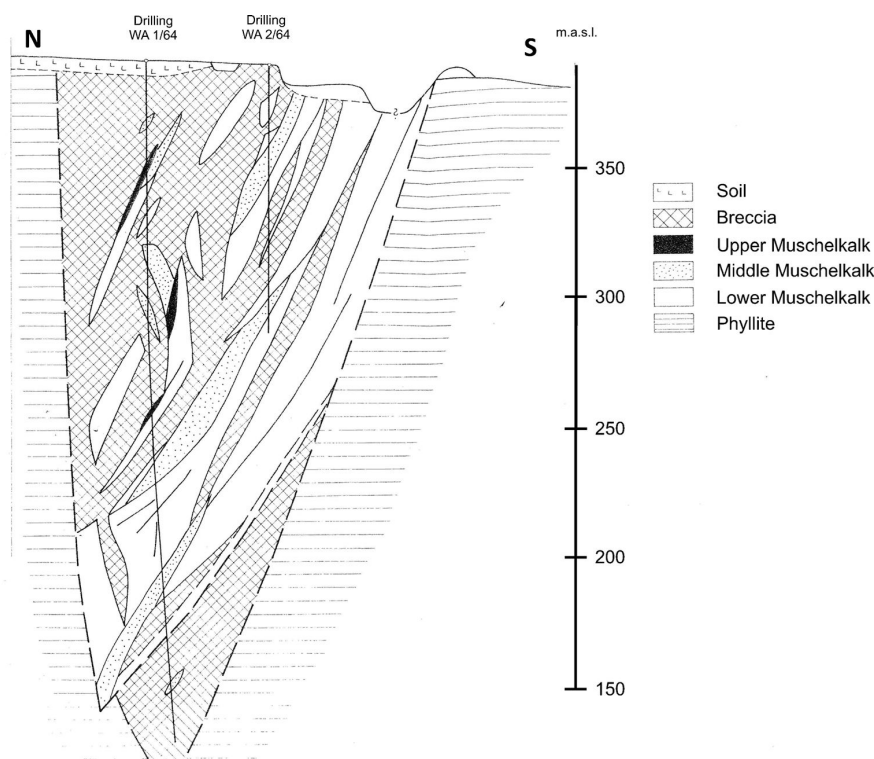
- Phyllite and metamorphic quartzites (Lower Carboniferous) form the recently outcropped country rock of the TS. Fragments of these rocks are found within the entire WA 1/64 drill core.
- Granitic xenoliths, most likely belonging to small dykes or minor intrusions from the Upper Devonian (Eigenfeld 1938; Gehmlich et al. 1998; Hahn unpublished report), occur within the TS's breccia. No other granite intrusions or granite conglomerate horizons are known in the phyllitic country rock (Lower Carboniferous). Thus, the occurrence of granitoid xenoliths in the breccia of the TS speaks for upward material transport.

Summing up, the occurrence of different xenolith types in the polymict breccia indicates opposing transport directions of the xenoliths (downwards from the palaeosurface, from the margin of the TS and upwards from below). This is a major criterion for the reinterpretation of the TS's origin.

Summary

This additional information and our own results hint at a high-gradient temperature increase from 30 to 260 m depths and at material transport from the palaeosurface, the margin and below. This interpretation, as well as the form and amplitude of the gravity anomaly, is a major indication for interpreting the TS as the result of a volcanic-based origin. The most obvious origin would make the TS the lower (unbedded) part of a maar-diatreme volcano, as suggested by, e.g. Lorenz (1986, 2003), Lorenz and Kurszlaukis (2007) and White and Ross (2011), as maar-diatreme volcanoes are "the second most common volcano in subaerial environments" (Lorenz and Kurszlaukis 2007). If we interpret the structure in this way, then most of the encountered facts fit the hypothesis that maar-diatreme volcanoes are accompanied by oval to round gravity anomalies, as in Mrlina et al. (2009), Matthes et al. (2010) and Schmidt et al. (2013), to name studies from nearby representatives. The heat involved in the process is also able to explain the mineralogical features previously shown (mineralisation of clays and ankerite). The steep inclination of the Muschelkalk blocks mentioned in the drill log can also be explained in this way. Because of instability, the maar crater's, the diatreme's and the conduit's walls start slumping. This leads to such a feature as described by, e.g. Hearn (1968), Lorenz (1986, 2003), Barnet (2004, 2008) and White and Ross (2011). Puff (unpublished report) has already attempted to correlate the limestone blocks between the WA 1/64 and WA 2/64 drillings (Fig. 11). Considering the TS to be the result of a volcanic eruption leads to the idea that this original proposal also fits the hypothesis of a diatreme's margin that

Fig. 11 Correlation and interpretation of the WA 1/64 and WA 2/64 drillings and the enclosed, steeply inclined blocks of the Muschelkalk limestone, translated from Puff (unpublished report)



has partially and repeatedly slumped in the direction of the eruptions (towards the gravity low), although it was initially interpreted as a tectonic feature.

As mentioned in, e.g. Hearn (1968), Lorenz (1982, 2003) and Geshi et al. (2011), consecutive eruptions may widen the diameter and depth of a maar-diatreme volcano and/or lead to multiple slumpings and, thus, to the nonlinear stratigraphy. Considering the subsidence mechanisms described by White and Ross (2011), a classification of the larger blocks of the Muschelkalk limestone into wall rock slides or the so-called Sinkschollen, as originally proposed by Cloos (1941), or “floating reefs”, as in, e.g. Lorenz (1975), Clement (unpublished report) and Barnet (2008), is not clear at this time, although the latter scenario is more likely. Additionally, the rather elongated shape of the Waldhaus formation is not an unusual phenomenon (Kurszlaukis and Lorenz 1997; Kurszlaukis and Barnet 2003) and is most likely related to the structural background of Variscan folding and preexisting faults.

In Puff (2005), a possible scenario for a volcanic origin was already given: a (phreatic) eruption without the ejection of juvenile magma (phreatic) occurred when sediments from the Lower and Middle Triassic still covered the area of the TS, most likely during the Upper Cretaceous. It was also mentioned that this event must have happened at least before the Tertiary, as considerable time is needed for the erosion of at least 200 m of Triassic sediment coverage as well as the Upper Cretaceous rocks, the maar and the upper diatreme. Upper

Cretaceous age was also determined for the ultramafic rocks (alnöite, aillikite, carbonatite) of the Delitzsch Complex (Röllig et al. 1990; Seifert et al. 2000; Wasternack 2008; Krüger et al. 2013) and in a preliminary investigation of apatite in the Ebersbrunn diatreme (Schüller et al. 2012).

The most prominent facts that speak against this genesis are the missing magnetic anomaly and the missing juvenile clasts. We do not observe a distinct anomaly from the geomagnetic surveys, and there is no indication of a general presence of higher-susceptibility material, as igneous rocks often show susceptibilities of some orders higher than limestone or phyllite. This characteristic, however, can also be caused by an intrusion that lacks minerals of high susceptibility (e.g. magnetite). The occurrence of massive iron-bearing ankerite rims around the carbonate particles (mainly dolomite, Table 4) strongly argues for a remobilisation of Fe, Mn and Mg. In this case, we assume that iron is transported by hydrotherms from juvenile material in the diatreme and precipitated as ankerite in the mainly carbonatic environment of the breccia (YiQun et al. 2012). To this point, it is unclear whether juvenile clasts are absent or if the iron-bearing rims around the carbonatic particles are of juvenile origin.

We came to the following conclusions:

1. The above-mentioned facts can be explained if we assume a series of phreatic or hydrothermal explosions with no

juvenile magmatic material involved. The difference to a phreatomagmatic is whether there was direct water–magma contact or if a stable, but high-temperature and high-pressure system existed that was somehow destabilised and thus started boiling and exploding (Browne and Lawless 2001; Tămaş and Milési 2003).

2. The other idea is an intrusion of magma resulting in a sustained phreatomagmatic eruption.

Tămaş and Milési (2002, 2003) summarised the characteristics for phreatomagmatic and phreatic breccias. Tămaş and Milési (2003) mention some characteristics that fit the TS's quite well. One very important fact, which matches our observations, is the lack of juvenile magmatic clasts in the breccia. However, some facts speak against this origin. Phreatic breccias are mainly clast-dominated and have <50 % of matrix and rock flour. The TS, however, is a matrix- and rock flour-dominated breccia (~60–80 %). The authors also mention only minor movement of the fragments within the breccia, which does not fit the stratigraphy and the description of the drill core WA 1/64. Additionally, phreatic breccias are smaller compared to phreatomagmatic breccias, and considering the TS's age and the erosion, which might be comparable to the Ebersbrunn diatreme (Schmidt et al. 2013), the TS's must have been a very, very large phreatic breccia pipe originally.

Some characteristics from Tămaş and Milési (2002) describing phreatomagmatic breccias also fit our observations. They mention very large rock fragments—a description that fits the large blocks of Triassic limestone in the drill WA 1/64 (Fig. 4). They also mention a long distance transport for clasts within the breccia pipe. This also matches the stratigraphy encountered in the drill core WA 1/64, where the clasts from different stratigraphic units were moved several tens to hundreds of metres up- and downward. Additionally, and in contrast to the description of phreatic breccias, the TS's breccia is also dominated by matrix and rock flour and the amount of larger clasts increases with depth (Puff 1970).

Both articles mention a grade of mineralogical alteration and layering around the minerals due to presence of hot fluids. In our case, ankerite rims and clay minerals were found that speak for an alteration of preexisting minerals. From the available rock samples, it is impossible at the moment to determine the origin of those newly precipitated and altered minerals as both processes lead to a similar result when hot and aggressive fluids are present within the breccia.

As the TS was formed during the Santonian, juvenile clasts could have been altered by metasomatism. Clear evidence for the occurrence of a hydrothermal overprint of the original breccia can be seen in Figs. 6 and 7. If the TS contained a rather small percentage of juvenile clasts in a predominantly calcitic-dolomitic environment, they could have been altered into ankerite and/or the large amount of clayey cement within

the breccia. Hydrothermal overprinting and mineral alteration of silicates were shown by, e.g. Steiner (1968), Ugolini (1974) and Hawkins (1981). Research on ankerite precipitation in hydrothermal systems was shown in Zimák et al. (2002), and YiQun et al. (2012) report that fluids from the Upper Mantle caused serpentinization in the Upper Crust and provided Fe²⁺ and Mg²⁺ ions for the precipitation of dolomite and ankerite.

Although the chemistry of the possibly intruded magma is unknown at this point, a first assumption can be made. The Delitzsch Complex (Röllig et al. 1990; Seifert et al. 2000; Kämpf 2002; Wasternack 2008; Krüger et al. 2013) and the Ebersbrunn diatreme (Schüller et al. 2012; Schmidt et al. 2013), which both feature carbonatitic, aillikitic or alnöitic melts, are also located at the intersection of the Regensburg-Leipzig-Rostock fault zone and other fault zones (more information about volcanic structures and their chemical composition in “Seismic activity, fault zones and palaeo-volcanism” section). Additionally, these rocks were determined to be of Upper Cretaceous age. For a better determination of the original magmatic chemistry, the preexisting drills are insufficient because they are located at the diatreme's margin.

Regardless of which hypothesis is correct, what we are convinced of is the time of the TS's genesis. From pollen analyses of multiple samples made by Schulz and Krutzsch (unpublished report), we know that no microflora younger than Santonian age (Late Cretaceous, 85 Ma) was found within the cores, so we expect the TS to be approximately the same age as that mentioned by Puff (2005). This would lead to the idea that a magmatic body, or at least a phase of anomalous high temperatures, was present below the area of investigation at that time.

Evaluation of the TS genesis hypotheses

Although many features speak for a volcanic origin of the TS, it is necessary to rule out other mechanisms that lead to the formation of breccia-filled pipes. Ollier (2007) summarises the characteristics of breccia pipes of different origins: volcanic, non-volcanic and hydrothermal breccias. However, it should be mentioned that Ollier (2007) clearly favours a gas-driven brecciation mechanism for the formation of volcanic breccias. We use these characteristics in combination with Puff (2005), who offered different hypotheses in an attempt to find a possible origin for the TS and included volcanic eruptions as a mechanism for its formation:

1. The original idea of the formation being a tectonic breccia is supported by the occurrence of different striking fault zones assumed to intersect near the formation as well as recrystallisations and shear planes found in the lower parts of the drillings (Puff 2005). This theory, however, is unable to explain other phenomena. It fails to explain the round gravity anomaly and the bimodal and well-

mixed distribution of a fine-grained matrix together with huge, steeply inclined blocks of limestone that require multiple events for the petrographic and petrologic composition. This hypothesis is impossible in an uplift-subsidence scenario: Several hundreds of metres of sediments must be moved up- and downward several times, which would result in a more homogeneous, non-alternating breccia. The encountered sediments from the Upper Cretaceous (downward transport) and the underlying granitoid xenoliths (upward transport) together cannot be explained at all with this approach and only in a volcanic or halokinetic process (Ollier 2007). Furthermore, we found several indicators for increased heat at deeper parts of the TS, which would require several kilometres of overlying sediments. This, however, was not the case and can be ruled out as a cause for the massive mineralisation of clays and ankerite in the lower part of the TS.

- Another hypothesis suggests a genesis via debris flows after, as similar horizons can be seen within the drilling, as in, e.g. the Wellenkalk (Lower Muschelkalk). This idea can explain the fine-grained matrix and the smaller clasts within it. However, it was unable to explain the gravity low, the large

blocks of limestone and the strongly increased heat at greater depths. In this scenario, it is also completely impossible to arrange the stratigraphy as encountered in the drill WA 1/64.

- A comparison of the TS's breccia with meteor impact breccias, such as the Nördlinger Ries, shows some resemblances and would also feature a rather round gravity anomaly. A striking point against this hypothesis is the lack of weathered glasses (tectites) and shocked rocks. Additionally, the relatively small extension of the formation is rather unlikely for an impact remnant (Stöffler et al. 2002).
- The final idea is the previously discussed hypothesis of a volcanic/phreatomagmatic origin, with the exception of the lack of juvenile clasts. This theory fits best in our view.

Conclusions and outlook

We conclude that the TS may look like the structure shown in Fig. 12 and is thus a maar-diatreme volcano eroded to the unbedded diatreme level. This conclusion is based on the interpretation of the 3D model under special consideration of

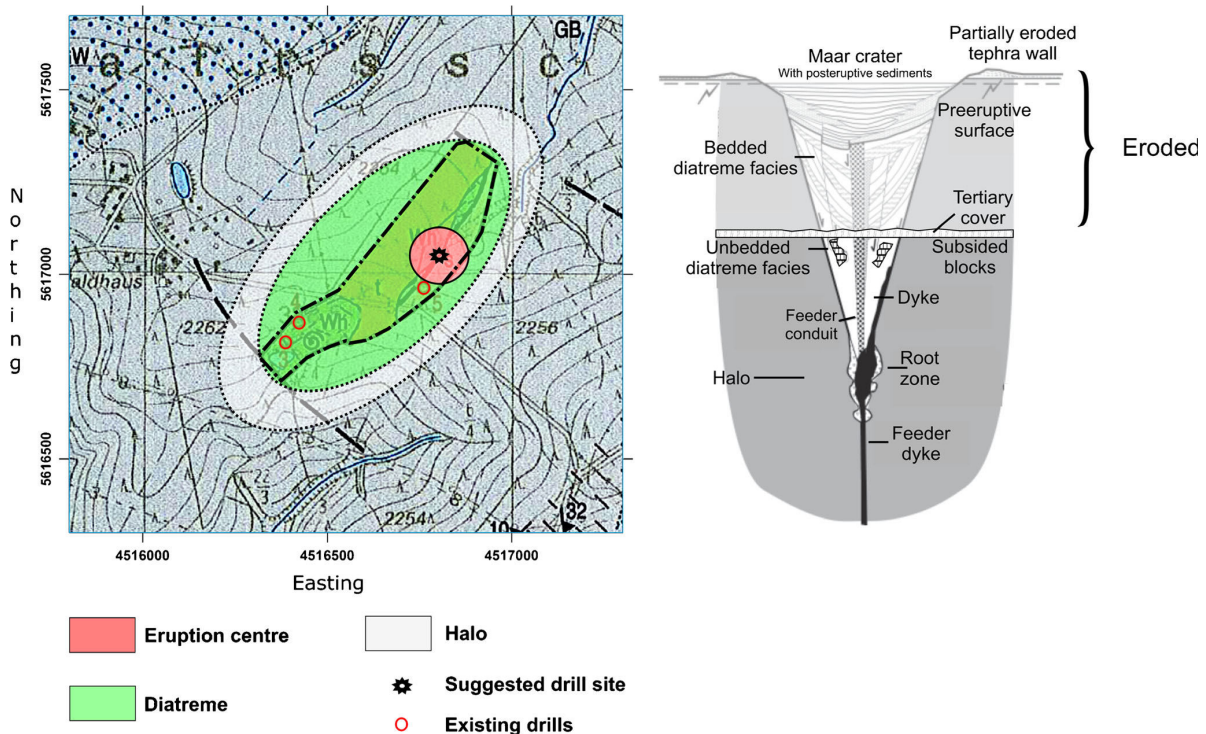


Fig. 12 Left: Assumed size of the diatreme and the position of the eruption centre and the brecciated area surrounding it (*halo*). The existing drillings and a new drilling site, essential for further research, stress the importance of a new deep drilling. Note that at this point, it is impossible to exactly determine the diatreme–halo contact. Diatreme and halo are

encircled by *dotted lines* to stress the fact that their extents cannot be determined exactly at this time. Right: Model of a maar-diatreme volcano, modified after Lorenz et al. (2003). We expect the topmost part to be eroded to (at least) the sub-maar area and to be surrounded by a halo

the maar-diatreme model from Lorenz et al. (2003). The existing deep drillings WA 1/64 and WA 2/64 are located at the expected margin of a possible maar-diatreme volcano but are too far away from the assumed centre of eruption to make any further statements about the TS's origination, which most likely occurred in the Santonian (Schulz and Krutzsch unpublished report; Puff 1970). The Gr 41/79 drilling (no. 5 in Fig. 2) is closer, but is shallow and only presents sandstone, which is also most likely the result of a gravitational syneruptive slumping.

Although we find many strong indications for the existence of a maar-diatreme structure NE of Greiz, we do not have any definite proof or evidence to declare the TS is the result of a volcanic eruption. Further investigations have to be performed to unequivocally determine its origin. Therefore, we recommend a new drilling of at least 300 m within or near the gravity low (Fig. 12). With a new drilling, it might also be possible to find juvenile clasts to infer the magma's chemistry and age. Further investigations focusing on an approach as described in Kunert (unpublished report) and Kosakowski et al. (1999) might also reveal further information about the palaeotemperature environment, especially when applied to samples from a new drilling. With further geophysical methods, such as seismics or geoelectrics, the topmost layer could be researched more intensively to refine the gravity model and thus improve its validity. This approach, however, is limited because the whole area is covered by forest and is thus difficult to access.

Acknowledgments First, H.K. would like to dedicate this paper in memoriam to Dr. habil. Erich Schroeder in honour of his collective fieldwork in Greiz and for calling attention to open questions regarding the genesis of the Triasscholle near Greiz and to Peter Puff for his effort and initial work on the TS.

We would like to express our gratitude to Dr. Karoly Nemeth for his intense work as a guest editor and reviewer and to Prof. Volker Lorenz, Dr. Marie Noëlle-Guilbaud and two additional anonymous reviewers who improved this article a lot. We thank the German Research Foundation (DFG) for funding this project (JA 542/21 and KA 902/17) and A. Hiller (Wismut GmbH, Geologisches Archiv Chemnitz), T. Hahn (Bayerisches Landesamt für Umwelt), T. Heuse, L. Katzschmann and (Thüringer Landesanstalt für Umwelt und Geologie, Jena), A. Schmidt (University of Leipzig), G. Meinhold (University of Göttingen), D. Markwart (Berlin), T. Hermann (Alfred-Wegener-Institute, Bremerhaven) and several people from the GFZ Potsdam, including I. Schüller, E. Spangenberg, E. Gantz, M. Ospald, H. Liep and I. Schäpan. Also, special thanks go to GFZ Potsdam for supporting this research project in multiple ways. We would also like to express our gratitude to C. Kroner (Physikalisch-Technische Bundesanstalt Braunschweig) for the initial surveys prior to our measurements.

References

- Alexowsky W, Berger H-J, Goth K, Hübner F, Junghanns C, Schneider JW, Wolf L in cooperation with Brauer R, Joisten H, Kardel K, Kaufmann H, Riedel P, Rumbaur C, Schubert H, Steinborn H, Temme L, Wenzel B, Withauer B Wolf P (2007) Geologische Karte des Freistaates Sachsen 1:25000, Erläuterungen Blätter 5240 Zwickau und 5241 Zwickau Ost, Saxon State Agency for Environment, Agriculture and Geology, in German
- Bankwitz P, Schneider G, Kämpf H, Bankwitz E (2003) Structural characteristics of epicentral areas in Central Europe: study case Cheb Basin (Czech Republic). *J Geodyn* 35:5–32
- Barnet WP (2004) Subsidence breccias in kimberlite pipes—an application of fractal analysis. *Lithos* 76:299–316
- Barnet WP (2008) The rock mechanics of kimberlite volcanic pipe excavation. *J Volcanol Geotherm Res* 174:29–39
- Berger H-J (2008) Eruptivbrekzie von Ebersbrunn. In: Pälchen W, Walter H (eds) *Geologie von Sachsen: Geologie von Sachsen: Geologischer Bau und Entwicklungsgeschichte*. Schweitzerbart, Stuttgart, pp 482–483, in German
- Bräuer K, Kämpf H, Strauch G, Weise SM (2003) Isotopic evidence ($^3\text{He}/^4\text{He}$, $^{13}\text{C}/^{12}\text{C}$) of fluid-triggered intraplate seismicity. *J Geophys Res* 108(B2):2070. doi:10.1029/2002JB002077
- Bräuer K, Kämpf H, Niedermann S, Strauch G (2005) Evidence for ascending upper mantle-derived melt beneath the Cheb basin, Central Europe. *Geophys Res Lett* 32, L08303. doi:10.1929/2004GL022205
- Bräuer K, Kämpf H, Strauch G (2009) Earthquake swarms in non-volcanic regions: what fluids have to say. *Geophys Res Lett* 36, L17309. doi:10.1029/2009GL039615
- Browne P, Lawless J (2001) Characteristics of hydrothermal eruptions, with examples from New Zealand and elsewhere. *Earth Sci Rev* 52(4):299–331
- Brus Z, Hurnik S (1984) Explosive volcanic structures in the North Bohemian brown-coal basin. *Cas Mineral Geol* 29:255–269, in Czech
- Büchel G, Pirrung BM (1993) Tertiary maars of the Hocheifel Volcanic Field, Germany. In: Negendank JFW, Zolitzschka B (eds) *Paleolimnology of the European Maar Lakes*. Springer, Berlin, pp 447–465
- Cloos H (1941) Bau und Tätigkeit von Tuffschloten. Untersuchungen an dem Schwäbischen Vulkan. *Geol Rundsch* 32:709–800, in German
- DEKORP and Orogenic Processes Working Group (1999) Structure of the Saxonian granulites: geological and geophysical constraints on the exhumation of high-pressure/high-temperature rocks in the mid-European Variscan belt. *Tectonophysics* 18:756–773
- Dobeš M, Hercog F, Mazáč O (1986) Die geophysikalische Untersuchung der hydrogeologischen Strukturen im Cheb-Becken. *Sbor geol věd Užité geofyz* 21:117–158, in German
- Eigenfeld R (1938) Die granitführenden Konglomerate des Oberdevon und Kulms im Gebiet altkristalliner Sattellagen in Ostthüringen. *Frankenwald und Vogtland. Abh Sächs Akad Wiss Math Naturwiss Kl* 42(7):7–150
- Enderle U, Schuster K, Prodehl C, Schulze A, Bribach J (1998) The refraction seismic experiment GRANU95 in the Saxothuringian belt, southeastern Germany. *Geophys J Int* 133:245–259
- Gabriel G (2003) Die gravimetrische Anomalie Baruth (Sachsen)—Aussagen über die Struktur eines verdeckten Maars. *Z Angew Geol* 49:18–25, in German
- Gehmlich M, Linnemann U, Tichomirova M, Todt W, Bombach K (1998) Geochronologie und geochemische Signaturen devonischer Granitoidgerölle des Saxothuringikums und deren potentielle Liefergebiete (Hirschberger Granit und Porphyroide von Neumühle Greiz). *Z Geol Wiss* 26(3/4):421–444, in German
- Geshi N, Németh K, Oikawa T (2011) Growth of phreatomagmatic explosion craters: a model inferred from Suoana crater in Miyakejima Volcano, Japan. *J Volcanol Geotherm Res* 201:30–38
- Götze HJ (1978) Ein numerisches Verfahren zur Berechnung der gravimetrischen Feldgrößen dreidimensionaler Modellkörper. *Arch Meteorol Geophys Bioclimatol* 25:195–215, in German
- Götze HJ, Lahmeyer B (1988) Application of three-dimensional modelling in gravity and magnetics. *Geophysics* 53:1096–1108

- Götze HJ, Schmidt S, Fichler C, Alvers MR (2007) IGMAS+ a new 3D gravity, FTG and magnetic modeling software. AGU Fall Meeting Abstracts
- Hahn T (2003) Geologische Karte von Thüringen 1:25000, Blatt 5339 Greiz, 2nd edn. Thüringer Landesanstalt für Umwelt und Geologie, Jena
- Hahn T, Meinhold G (2005) Revision der Unterkarbonstratigraphie der Mehtheuerer Mulde (Vogtland, Saxothuringikum). *Geowiss Mitt Thüringen* 12:51–70, in German
- Hahn T, Kroner U, Melzer P (2010) Early carboniferous synorogenic sedimentation in the Saxo-Thuringian Basin and the adjacent allochthonous domain. In: Linnemann U, Romer RL (eds) *Pre-Mesozoic geology of Saxo-Thuringia—from the Cadomian active margin to the Variscan Orogen*. Schweizerbart, Stuttgart, pp 171–192
- Hawkins DB (1981) Kinetics of glass dissolution and zeolite formation under hydrothermal conditions. *Clays Clay Minerals* 29(5):331–340
- Hearn CB Jr (1968) Diatremes with kimberlitic affinities in North-Central Montana. *Science* 159:622–625
- Hemmann A, Kämpf H (2002) Seismicity in the central part of the Naab-Pritzwalk-Rostock lineament, related to mantle fluid activity? EGS XXVII General Assembly, Nice, 21–26 April 2002, abstract #5193
- Hemmann A, Meier T, Jentzsch G, Ziegert A (2003) Similarity of waveforms and relative relocalisation of the earthquake swarm 1997/1998 near Werdau. *J Geodyn* 35:191–208
- Ibs-von Seht M, Plenefisch T, Klinge K (2008) Earthquake swarms in continental rifts—a comparison of selected cases in America, Africa and Europe. *Tectonophysics* 452:66–77
- Kämpf H (2002) Comparison between the Ultramafic Delitzsch Complex and the active part of the Eger Rift: interaction between fracture tectonics, migration of magmatic fluids and the structure of the seismogenic crust. *Mitt Naturwiss Ver Steiermark* 132:14–15
- Kämpf H, Bräuer K, Schumann J, Hahne K, Strauch G (2013) CO₂ discharge in an active, non-volcanic continental rift area (Czech Republic): characterisation ($\delta^{13}C$, 3He/4He) and quantification of diffuse and vent CO₂ emissions. *Chem Geol* 339:71–83
- Korn M, Funke S, Wendt S (2008) Seismicity and seismotectonics of west Saxony, Germany—new insights from recent seismicity observed with the Saxonian network. *Stud Geophys Geod* 52:479–492
- Kosakowski G, Kunert V, Clauser C, Franke W, Neugebauer HJ (1999) Hydrothermal transients in Variscan crust: palaeo-temperature mapping and hydrothermal models. *Tectonophysics* 306:325–344
- Kroner C, Jahr T, Kämpf H, Geissler WH (2006) Der “Tuffschlot” bei Ebersbrunn/Westsachsen, der partiell erodierte Rest eines Maar-Diatrem-Vulkans. *Z Geol Wiss* 34:3–4, in German
- Krüger JC, Romer RL, Kämpf H (2013) Late Cretaceous ultramafic lamprophyres and carbonatites from the Delitzsch Complex, Germany. *Chem Geol* 353:140–150
- Kurszlaukis S, Barnet WP (2003) Volcanological and structural aspects of the Venetia kimberlite cluster—a case study of South African kimberlite maar-diatreme volcanoes. *S Afr J Geol* 106:165–192
- Kurszlaukis S, Lorenz V (1997) Volcanological features of a low-viscosity melt: the carbonatitic Gross Brukkaros Volcanic field, Namibia. *Bull Volcanol* 58:421–431
- Kvaček Z, Teodoridis V (2007) Tertiary macrofloras of the Bohemian Massif: a review with correlations within Boreal and Central Europe. *Bull Geosci* 82:383–408
- Liebe KT, Zimmermann E (1892) *Geologische Spezialkarte von Preußen und den Thüringischen Staaten, Blatt Greiz (Reichenbach)*. Berlin, [Explanation.: Berlin 1893], in German
- Linnemann U, Romer RL (eds) (2010) *Pre-Mesozoic geology of Saxo-Thuringia*. Schweizerbart, Stuttgart, 485 pp
- Lorenz V (1975) Formation of phreatomagmatic maar-diatreme volcanoes and its relevance to kimberlite diatremes. *Phys Chem Earth* 9: 17–27
- Lorenz V (1982) Zur Vulkanologie der Tuffschlote der Schwäbischen Alb. *Jahresber Mitt Oberrhein Geol Ver NF* 64:167–200, in German
- Lorenz V (1986) On the growth of maars and diatremes and its relevance to the formation of tuff-rings. *Bull Volcanol* 48:265–274
- Lorenz V (2003) Maar-diatreme volcanoes, their formation, and their setting in hard-rock or soft-rock environments. *Geolines* 15:72–83
- Lorenz V, Kurszlaukis S (2007) Root zone processes in the phreatomagmatic pipe emplacement model and consequences for the evolution of maar-diatreme volcanoes. *J Volcanol Geotherm Res Spec* 150:4–32
- Lorenz V, Suhr P, Goth K (2003) Maar-Diatrem-Vulkanismus—Ursachen und Folgen. Die Guttauener Vulkangruppe in Ostachsen als Beispiel für die komplexen Zusammenhänge. *Z Geol Wiss* 31:267–312, in German
- Matthes H, Kroner C, Jahr T, Kämpf H (2010) Geophysical modelling of the Ebersbrunn diatreme, western Saxony, Germany. *Near Surf Geophys* 8:311–319
- Meinhold G, Hahn T, Heuse T, Mingram B (2005) Geochemistry and palynology of metasediments from the phyllite complex in the Greiz area (Saxo-Thuringia, Germany). *N Jb Geol Paläont (Abh)* 237(3): 423–452
- Mrlina J, Kämpf H, Kroner C, Mingram J, Stebich M, Brauer A, Geissler WH, Kallmeyer J, Matthes H, Seidl M (2009) Discovery of the first Quaternary maar in the Bohemian Massif, Central Europe, based on combined geophysical and geological surveys. *J Volcanol Geotherm Res* 182:97–112
- Neunhöfer H (2009) Erdbeben in Thüringen, eine Bestandsaufnahme. *Z Geol Wiss* 37:1–14, in German
- Neunhöfer H, Hemmann A (2005) Earthquake swarms in the Vogtland/Western Bohemia region: spatial distribution and magnitude-frequency distribution as an indication of the genesis of swarms? *J Geodyn* 39:361–385
- Nickschick T, Kämpf H, Jahr T (2012) The Triasscholle near Greiz, E Thuringia—a volcanic based origin?, In: Arentsen K, Németh K, Smid E (Eds) *Abstract Volume of the Fourth International Maar Conference—A Multidisciplinary Congress on Monogenetic Volcanism, Auckland N.Z.*, p. 132
- Ollier CD (2007) Breccia-filled pipes: distinguishing between volcanic and non-volcanic origins. *Geogr Fis Dinam Quat* 30:63–76
- Pohl D, Wetzel HU, Grünthal G (2006) Tektonische Untersuchungen im Raum Vogtland-Leipzig mit Hilfe von Fernerkundung. *Geoinformatik Erdbeobachtung Vorträge* 26:277–286, in German
- Puff P (1970) Die Triasscholle bei Greiz—Ein Beitrag zur postvariszischen Entwicklung des Ostthüringischen Schiefergebirges. *Geologie* 19:1135–1142, in German
- Puff P (2005) Die Triasscholle bei Greiz—ein vulkanischer Explosionskrater? In: *Exkursionsführer: Geologie des Thüringischen Schiefergebirges im Gebiet von Greiz*. Thüringer Geologischer Verein, Jena, pp 22–24, in German
- Rohrmüller J (2003) Die Forschungsbohrung Bayerhof—die Erkundung eines tertiären Maars im Steigerwald, Oberpfalz (NE Bayern). *Geol Bav* 107:215–220, in German
- Röllig G, Viehweg M, Reuter N (1990) The ultramafic lamprophyres and carbonatites of Delitzsch/GDR. *Z Angew Geol* 36:49–54
- Šantrůček P, Králík F, Kvičinský Z, Opletal M (1991) Geological map, scale 1:50.000. Czech Geological Survey, 1991
- Schmidt A, Nowaczyk N, Kämpf H, Schüller I, Flechsig C, Jahr T (2013) Origin of magnetic anomalies in the large Ebersbrunn diatreme, W Saxony, Germany. *Bull Vol* 75:766. doi:10.1007/s00445-013-0766-6
- Schüller I, Kämpf H, Schmidt A, Flechsig C, Jahr T (2012) Petrographic and thermochronometric investigation of the diatreme breccia of the Ebersbrunn Diatreme—W Saxony, Germany. In: Arentsen K, Németh K, Smid E (eds) *Abstract Volume of the Fourth International Maar Conference—A Multidisciplinary Congress on Monogenetic Volcanism, Auckland N.Z.*, p 139
- Seidl G (2003) *Geologie von Thüringen*, vol 2. Schweizerbart, Stuttgart, 601 pp., in German

- Seifert W, Kämpf H, Wasternack J (2000) Compositional variation in apatite, phlogopite, and other accessory minerals of the ultramafic Delitzsch complex, Germany: implications for cooling history of carbonatites. *Lithos* 53:81–100
- Steiner A (1968) Clay minerals in hydrothermally altered rocks at Wairakei, New Zealand. *Clays Clay Minerals* 16:193–213
- Stöffler D, Artemieva NA, Pierazzo E (2002) Modeling the Ries-Steinheim impact event and the formation of the moldavite strewn field. *Meteorit Planet Sci* 37:1893–1907
- Suhr P, Goth K (2008) Tertiäre Maare. In: Pälchen W, Walter H (eds) *Geologie von Sachsen: Geologie von Sachsen: Geologischer Bau und Entwicklungsgeschichte*. Schweizerbart, Stuttgart, pp 484–486, in German
- Tămaş C, Milési JP (2002) Hydrovolcanic breccia pipe structures—general features and genetic criteria—I. Phreatomagmatic breccias. *Stud UBB Geol XLVII(1)*:127–147
- Tămaş C, Milési JP (2003) Hydrothermal breccia pipe structures—general features and genetic criteria—II. Phreatic breccias. *Stud UBB Geol XLVIII(1)*:55–66
- Ugolini FC (1974) Hydrothermal origin of the clays from the upper slopes of Mauna Kea, Hawaii. *Clays Clay Minerals* 22:189–194
- Ulrych J, Dostal J, Adamovič J, Jelínek E, Špaček P, Hegner E, Balogh K (2011) Recurrent Cenozoic volcanic activity in the Bohemian Massif (Czech Republic). *Lithos* 123:133–144
- Wasternack J (2008) Ultramafit-Karbonatit-Komplex von Delitzsch. In: Pälchen W, Walter H (eds) *Geologie von Sachsen: Geologischer Bau und Entwicklungsgeschichte*. Schweizerbart, Stuttgart, pp 478–482
- White JW, Ross PS (2011) Maar-diatreme volcanoes: a review. *J Volcanol Geotherm Res* 201:1–29
- YiQun L, Xin J, Hong L, MingSheng Y, Wan Y, XiaoHu Z, Hao L, DingWu Z, ChaoYang Z, Qin S, ShuangShuang W (2012) Primary dolostone formation related to mantle-originated exhalative hydrothermal activities, Permian Yuejingou section, Santanghu area, Xinjiang, NW China. *Sci China Earth Sci* 55(2): 183–192
- Zimák J, Losos Z, Novotný P, Dobeš P, Hladíková J (2002) Study of vein carbonates and notes to the genesis of the hydrothermal mineralization in the Moravo-Silesian Culm. *J Czech Geol Soc* 47(3–4):111–122

7.1 The "Triasscholle" near Greiz, Germany - a volcanic origin?
Supplementary Data A - Details about the geophysical surveys

The "Triasscholle" near Greiz, E Germany - A volcanic origin?

T. Nickschick^a*, H. Kämpf^a, T. Jahr^b

^a German Research Centre for Geosciences GFZ Potsdam, Section 4.3 Telegrafenberg, 14473 Potsdam, Germany

^b Friedrich-Schiller-Universität, Institute for Geosciences, Burgweg 11, 07749 Jena, Germany

* Corresponding author, Email address: tobias.nickschick@gfz-potsdam.de

Online Resource 1: Details about the geophysical surveys

The distance between profiles was about 25 m on average. The spacing between each point of measurement along the profiles was 25 m for the gravimetric and 5 m for the geomagnetic surveys.

The first set of geophysical research was done in a preliminary investigation in the fall of 2009 (Hermann and Markwart, 2009). During that time, most of the northern and central part of the TS were explored. This set of data was enlarged by data taken in the time span from winter 2010 to late spring in 2011. This time, most of the remaining (southern) area was investigated. Due to the higher grade of vegetation in this area, an even coverage with especially gravimetric data is not granted. Most of the data gathered are derived from isolated observation points. This leads to an irregular coverage of data for the southern part but without any major gaps (<100 m). Most of the magnetic data were acquired with two proton magnetometers from the Institute of Geosciences, Jena, measuring the total magnetic intensity. To reduce the daily variation of the magnetic field, repeating measurements were made on an hourly basis. After the reductions have been applied, all values have been correlated to our base point. The gravimetric surveys were performed with LaCoste & Romberg gravimeters from the Institute of Geosciences, University of Jena (G-896 and D-187) and, later on, TU Berlin (G-85, replacing the G-896) with a resolution of a few μGals ($10^{-8} \frac{m}{s^2}$). The application of two separate gravimeters increased the accuracy for that point and showed any potentially made mistake. On the gravity data the following corrections were applied: tidal correction, instrumental drift, normal gravity, free air, latitude and Bouguer plate. No terrain correction has been applied yet. The northern and central parts do not show any larger topography, whereas the southern part features a flat slope and some minor depressions, the biggest one having a diameter of about 20 m. The occurring deviation thereby is estimated to be less than 80 μGal , considering the fact that no

elevation or depression was immediately close to the observation points. For the correction of the Bouguer plate the standard density of $2670 \frac{kg}{m^3}$ has been applied.

7.2 The "Triasscholle" near Greiz, Germany - a volcanic origin?
**Supplementary Data B - Detailed information about the IGMAS+ model
of the TS**

The "Triasscholle" near Greiz, E Germany - A volcanic origin?

T. Nickschick ^a*, H. Kämpf ^a, T. Jahr ^b

^a German Research Centre for Geosciences GFZ Potsdam, Section 4.3 Telegrafenberg, 14473 Potsdam, Germany

^b Friedrich-Schiller-Universität, Institute for Geosciences, Burgweg 11, 07749 Jena, Germany

* Corresponding author, Email address: tobias.nickschick@gfz-potsdam.de

Online Resource 2: Detailed information about the IGMAS+ model of the TS

For modelling the area is divided into a finite number of parallel sections (planes), consisting of closed polygon lines. These lines separate the model bodies within the section, characterised by different densities or/and susceptibilities. The actual bodies are formed by triangulation between the vertices of the corresponding bodies between the section and its neighbours. The model consists of 22 sections, running in E-W direction, which are shown here. This is a compromise between the strike of the structure and the gravity values from the former SDAG Wismut, which were measured in an E-W/N-S running grid, so the best coverage of these data is provided.

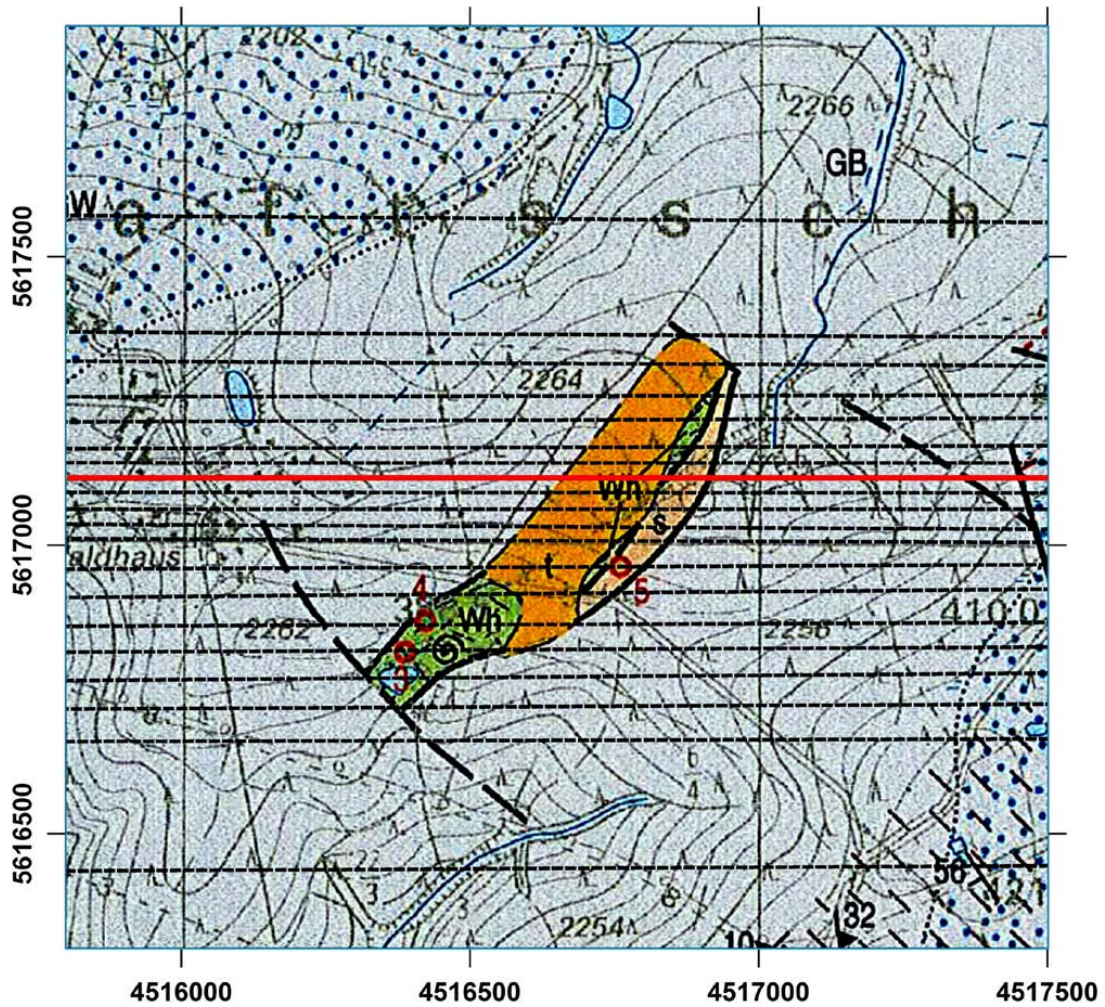


Fig.: Position of 20 of the 22 IGMA_s+ vertical sections, plotted over a slightly changed version of Fig 2. The remaining two sections are about 1km to the north and south, respectively, and not shown here to retain an overview. The red line marks the selected section shown in Fig 9.

8 Integrated geophysical and geological methods to investigate the inner and outer structures of the Quaternary Mýtina maar (W-Bohemia, Czech Republic)

Flehsig, C., Heinicke, J., Mrlina, J., Kämpf, H., Nickschick, T., Schmidt, A., Bayer, T., Günther, T., Rücker, C., Seidel, E., Seidl, M.

published 2015 in International Journal of Earth Sciences 104(8):2087-2105

Integrated geophysical and geological methods to investigate the inner and outer structures of the Quaternary Mýtina maar (W-Bohemia, Czech Republic)

Christina Flechsig · Jens Heinicke · Jan Mrlina · Horst Kämpf · Tobias Nickschick · Alina Schmidt · Tomáš Bayer · Thomas Günther · Carsten Rücker · Elisabeth Seidel · Michal Seidl

Received: 16 June 2014 / Accepted: 17 December 2014 / Published online: 9 January 2015
© Springer-Verlag Berlin Heidelberg 2015

Abstract The Mýtina maar is the first known Quaternary maar in the Bohemian Massif. Based on the results of Mrlina et al. (J Volcanol Geother Res 182:97–112, 2009), a multiparametric geophysical (electrical resistivity tomography, gravimetry, magnetometry, seismics) and geological/petrochemical research study had been carried out. The interpretation of the data has provided new information about the inner structure of the volcanic complex: (1) specification of the depth of post-volcanic sedimentary fill (up to ~100 m) and (2) magnetic and resistivity signs of one (or two) hidden volcanic structures interpreted as intrusions or remains of a scoria cone. The findings at the outer structure of the maar incorporate the (1) evidence of circular fracture zones outside the maar, (2) detection and distribution of volcanic ejecta and tephra-fall deposits at the surface, and (3) indications from electrical resistivity tomography and gravity data in the area between the Mýtina maar and

Železná hůrka scoria cone, interpreted as a palaeovalley, filled by volcanoclastic rocks, and aligned along the strike line (NW–SE) of the Tachov fault zone. These findings are valuable contributions to extend the knowledge about structure of maar volcanoes in general. Because of ongoing active magmatic processes in the north-east part of the Cheb Basin (ca. 15–30 km north of the investigation area), the Mýtina maar-diatreme volcano and surroundings is a suitable key area for research directed to reconstruction of the palaeovolcanic evolution and assessment of possible future hazard potential in the Bohemian Massif.

Keywords Eger Rift · Quaternary maar volcanism · Mýtina maar · Geophysical and geological survey

Motivation and state-of-the-art of maar investigation

A maar-diatreme volcano is a product of a series of small volume subsurface phreatic or phreatomagmatic eruptions and represents the second most common volcano type on continents and islands (Lorenz 2007; White and Ross 2011; Valentine and White 2012). The best chance to reconstruct and understand maar eruptions are historical records, but only a few examples exist worldwide (e.g. Ukinrek, the best studied maar eruption worldwide, occurred early April 1977: see Barnes and McCoy 1979; Kienle et al. 1980; Büchel and Lorenz 1993; Pirrung et al. 2008; Evans et al. 2009).

The Eifel and the Massif Central, both parts of the European Cenozoic Rift System, represent the two classical European regions for Quaternary maar eruptions (e.g. Nowell et al. 2006). However, the most active part of the European Cenozoic Rift System is the western Eger Rift (see Fig. 1) where indications for a presently active magma

C. Flechsig (✉) · J. Heinicke · A. Schmidt · E. Seidel
Institute for Geophysics and Geology, University of Leipzig,
Talstrasse 35, 04103 Leipzig, Germany
e-mail: geoflec@uni-leipzig.de

J. Mrlina · T. Bayer · M. Seidl
Institute of Geophysics, Academy of Sciences of the Czech
Republic, Boční II, 141 31 Praha 4, Czech Republic

H. Kämpf · T. Nickschick
German Research Centre for Geosciences GFZ Potsdam,
Section 4.3 Telegrafenberg, 14473 Potsdam, Germany

T. Günther
Leibniz Institute for Applied Geophysics, Stilleweg 2,
30655 Hannover, Germany

C. Rücker
Institute for Applied Geosciences, Technische Universität,
Ernst-Reuter-Platz 1, 10587 Berlin, Germany

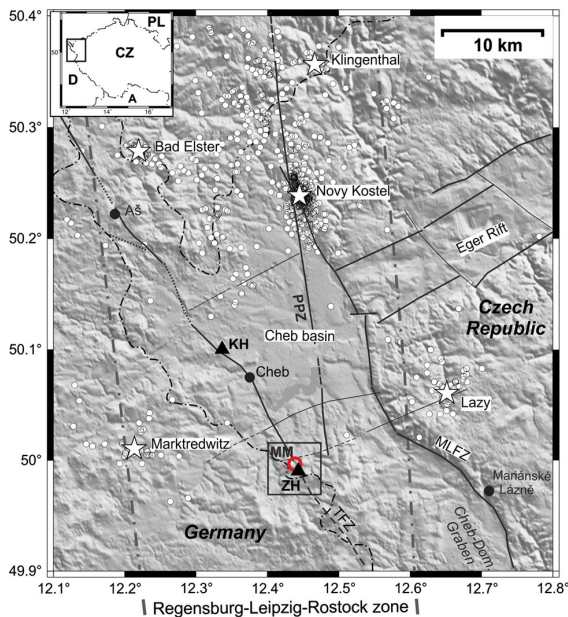


Fig. 1 Location of survey site Mýtina maar and Železná hůrka scoria cone in the western Eger (Ohře) Rift with the main fault zones and areas of recent seismic activity; *inset* position of the area under investigation in Central Europe; *triangles* Pleistocene scoria cones Železná hůrka (ZH) and Komorní hůrka (KH); *red circle* Mýtina maar (MM); *PPZ* Počátky Plesná fault zone, *MLFZ* Mariánské Lázně fault zone, *TFZ* Tachov fault zone; *stars* location of main swarm earthquake epicentral areas; *black square* survey site

intrusion from the lithospheric mantle into the crust were found by repeated isotopic investigations ($^{13}\text{C}_{\text{CO}_2}$, $^3\text{He}/^4\text{He}$) of the free gas phase in mineral water springs and mofettes (Bräuer et al. 2011). Between 1993 and 2005, an increase in mantle-derived helium was observed beneath the eastern part of the Cheb Basin (Bräuer et al. 2009). From 2005 to 2011, the helium isotopic ratio was at the same high level (Fischer et al. 2014). The north-east and east parts of the Cheb Basin, the area of hidden magmatic and earthquake swarm activity with magnitudes of possibly up to 4.5 (Fischer et al. 2014), are located only 15–30 km north of the Mýtina maar (age: 290 ka, Mrlina et al. 2007), which was detected by combined geophysical and geological surveys (Mrlina et al. 2009). Indications of presently active magmatic processes mean that potential future hazards (phreatomagmatic eruptions) for that area cannot be excluded. This study considers structural features of the Mýtina maar-diatreme volcano and surroundings as base for reconstructing the palaeovolcanic evolution.

We apply geophysical techniques combined with information from field geology and shallow drill cores to provide an insight into the shallow structure of the Mýtina

maar and Železná hůrka scoria cone, the distribution of volcanic ejecta (tephra), and the palaeovolcanic reconstruction.

Geological settings

The area under investigation is located ca. 10 km south-east of the city of Cheb at the southern periphery of the Cheb Basin, in the western part of the Bohemian Massif (Fig. 1). The Cheb Basin is a small intra-continental basin filled with sediments of Tertiary and Quaternary age and lies within the western part of the Eger (Ohře) Rift (Kopecký 1978). The crystalline basement of the area is dominated by Upper Cambrian to Ordovician muscovite–biotite mica schists, part of the Saxothuringian zone of the Variscan orogeny (Fiala and Vejnar 2004). The upper crust of the area is further characterised by granites of late Variscan age.

The Cenozoic alkaline volcanic activity in the western part of the Bohemian Massif (Fig. 1) is situated at the junction of three major neotectonic fault systems: the WSW–ENE-trending Eger Rift, the NNW–SSE-trending Cheb–Domažlice Graben, and the N–S-trending Regensburg–Leipzig–Rostock lineament (Bankwitz et al. 2003). According to Ulrych et al. (2011), three periods of volcanic activity, including maar-diatreme volcanoes for the northern and western part of the Bohemian Massif, can be defined in general: (1) pre-rift period (late Cretaceous to mid-Eocene, 79–49 Ma), (2) syn-rift period (mid-Eocene to mid-Miocene, 42–16 Ma), and (3) late-rift period (16–0.26 Ma). Related to the occurrence of maar-diatreme volcanoes, the known volcanic activity in the western part of the Eger Rift comprises mostly silica-undersaturated igneous rocks such as melilitites, melilitite-bearing nephelinites, and basanites. Six confirmed or proposed maar structures are situated at the intersection of the Regensburg–Leipzig–Rostock lineament, Eger Rift and the Cheb–Domažlice Graben: the Velký Luh maar (age: ~49–37 Ma), the Plesná maar (age: ~33.5–28.5 Ma) (Kvaček and Teodoridis 2007), the Podhrad diatreme (unknown age, Šantrůček et al. 1991), the Bayerhof maar (age: 23.3–21.7 Ma, Rohrmüller 2003), the Mýtina maar (age: 0.29 Ma, Mrlina et al. 2007), and a geophysical anomaly (proposed maar) at Žírovice (unknown age, Dobeš et al. 1986). The Quaternary volcanic activity of the Cheb Basin is also documented by the Komorní hůrka (Kammerbühl) and Železná hůrka (Eisenbühl) scoria cones. The neotectonic activity along fault systems has continued since the Middle Pleistocene (Peterek et al. 2011) and is still persistent as the occurrences of swarm earthquakes along N–S (e.g. the Počátky Plesná fault zone according to Bankwitz et al. 2003) and NW–SE-trending fault systems (Horalek and Fischer 2008; Fischer et al. 2014). Degassing of magmatic-originated CO_2 with mantle signature (He

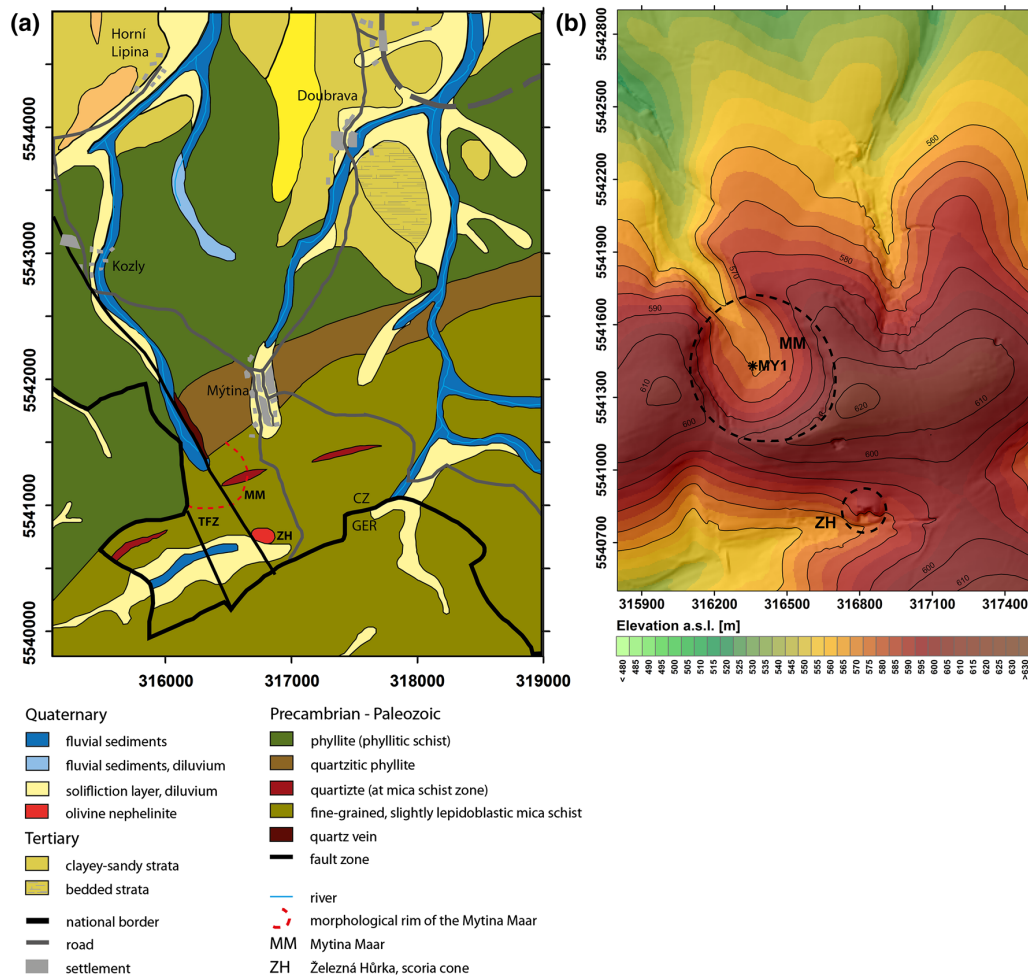


Fig. 2 Geological map and digital elevation model (DEM) of the investigation area; map display: WGS84/UTM zone 33N. **a** Simplified geological map of the region surrounding Mýtina maar and the Železná hůrka scoria cone (after Fiala and Vejnár 1997; Tonica et al. 1998; Stettner 1999); TFZ Tachov fault zone. **b** Digital elevation model (DEM) showing the morphology of the Mýtina maar (MM) as

an anomalous depression of about 50 m (black dashed line). A valley that breaches the maar is aligned in north-west direction (Kozly brook) and marks a tectonic structure: the Tachov fault zone. The cone of the Železná hůrka scoria cone (ZH) SE of the Mýtina maar is located in the same striking line. MY1: drill site MY1/85.5 m (Mrlina et al. 2009)

and C isotopes) denotes the ongoing magmatic activity in the western Bohemian Massif (e.g. Weinlich et al. 1999; Bräuer et al. 2009, 2011).

The object of this study, the volcanic complex, comprised of the Mýtina maar and the Železná hůrka scoria cone, which is located near the village Mýtina (Czech Republic) at the head of the NNW–SSE- and NW–SE-trending Kozly brook valley that traces the Tachov fault zone according to Geissler et al. (2004) (Fig. 2a). In the southern direction of the valley lies the well-studied Železná hůrka scoria cone (e.g. Proft 1894; Lochmann 1961; Schwarzkopf and Tobschall 1997) that is also situated on the Tachov fault zone (Mrlina et al. 2009). Both

volcanoes are part of the Plio-Pleistocene melilititic series (Ulrych et al. 2013). The crystalline basement surrounding the maar consists of phyllite, quartzitic phyllite, and mica schist of Precambrian to Palaeozoic age. The mica schist contains elongated lenses of quartzite following the orientation of the Eger Rift. A NNW–SSE-trending quartz vein had been found north-west of the Mýtina maar that indicates a strike direction of the Tachov fault zone. North of the study area, younger sediments of Quaternary and Tertiary age cover the older units. The valleys of small rivers and streams are filled with prevailing sandy-loamy fluvial sediments (Fiala and Vejnár 1997; Tonica et al. 1998; Galadi-Enriquez et al. 2009).

Methods

Over the last 15 years, there has been an increasing number of examples of geophysical methods being used successfully to image and to model the structure of maar volcanoes (e.g. Brunner et al. 1999; Schulz et al. 2005; Cassidy et al. 2007; Nicollin et al. 2006; Loera et al. 2008; Revil et al. 2008; Skácelová et al. 2010; Blaikie et al. 2012, 2014; De la Cruz-Reyna and Yokoyama 2011; Bolós et al. 2012; Barde-Cabusson et al. 2013).

At Mýtina maar, ground-based geophysical methods (magnetics and gravity measurements) have been used for the first investigation of the maar structure that was unknown before (Mrlina et al. 2007, 2009). Based on the results of the geophysical, geological, and petrological survey in the Mýtina maar area from 2004 to 2009 (Geissler et al. 2004, 2007; Mrlina et al. 2007, 2009), a further comprehensive field campaign was performed during the period between 2011 and 2013. Geophysical methods applied in this study were as follows: the electrical resistivity tomography (ERT), gravity and magnetic surveys, and a seismic survey on one selected profile. The data provide the necessary consolidation and spatial extension of the existing database (gravity, magnetics). In particular, we expected novel results from the comprehensive ERT surveys, as well as from the shallow seismic profile, about structural features inside and outside the maar and characteristic features of the fault zone. It was necessary to use an irregular grid of measurement profiles due to restrictions caused by dense forest areas, intensive agricultural use, and settlements. The compilation of the previous data sets and the new performed geophysical and geological investigations provide the opportunity for a detailed image of the Mýtina maar and the surrounding geological and volcanic structures to be obtained. The digital elevation model with 1-m resolution composed from the database of the Czech Office of Surveying and Cartography, Prague, serves as a background map for the presentation of the results and their interpretation (Fig. 2b).

Geological information (lithologic composition of the cores and amount of juvenile components) and measurements of the magnetic susceptibility of core samples were derived from six drill cores of shallow boreholes with a maximum depth of 9.5 m, which were drilled south-west, south, and south-east of the maar (locations in Fig. 3). They give the opportunity to describe and support the uppermost part of volcanoclastic deposits in relation to the geophysical prospecting. An additional mapping of magnetic susceptibility and ^{40}K content of soil samples improved the knowledge about the distribution of tephra/pyroclastic deposits at the surface.

Specific technical details of the instrumentation, measuring methods, and acquisition parameters are listed in Table 1.

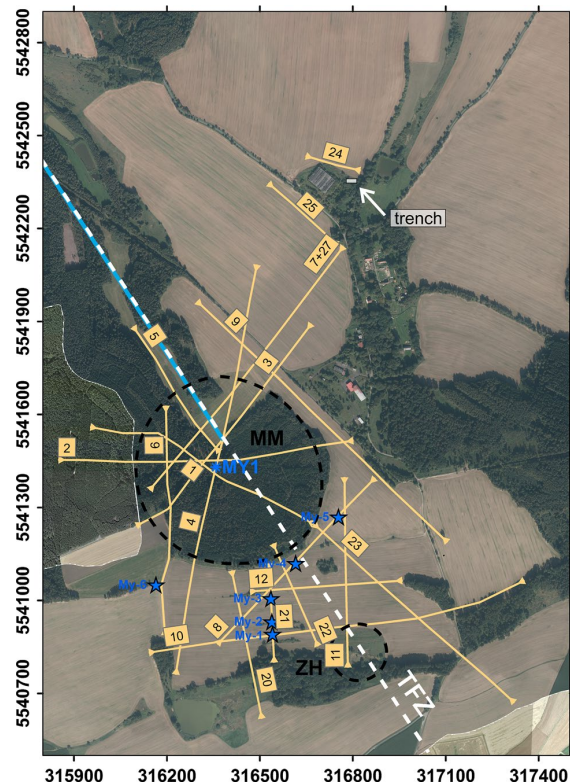


Fig. 3 Aerial view of the study area Mýtina maar and Železná hůrka scoria cone with the ERT profiles (yellow lines) and the six drill sites My-1 to My-6 (blue stars); MY1: drill site MY1/85.5 m (Mrlina et al. 2009); square near profile 24: trench (Geissler et al. 2004); MM Mýtina maar, ZH Železná hůrka; white dashed line Tachov fault zone (TFZ), blue dashed line Kozly brook valley; for information on distribution of geophysical measuring points, the used devices, and data quality, see Table 1; map source combination of several maps of the ČÚZK (Czech Office for Surveying, Mapping and Cadastre, Prague/CR); map display WGS84/UTM zone 33N

Electrical resistivity tomography (ERT)

The survey with the electrical resistivity tomography (ERT) was carried out in 2011 and 2012 and involved both field measurements on linear outlays (Fig. 3) by combining sounding and profiling techniques and the data inversion via software code. In the central part of the maar depression, the ERT profiles are the same as for magnetic and gravity measurements. Field measurements were taken with a combination of Wenner-alpha (CPPC) configuration and a special case of the dipole–dipole configuration: the Wenner-beta (CCPP). The Wenner-alpha configuration was chosen for its advantages: good signal-to-noise ratio to perform measurements with larger offsets and high sensitivity to vertical resistivity variations. The Wenner-beta configuration involves higher sensitivity for lateral resistivity

Table 1 Technical parameters of the geophysical and element geochemical methods

Method	Instrument	Measuring interval	Measuring accuracy/error	Total stations, samples
Geoelectrics/ERT	GeoTom	Most 5 m mpd, for details 2 m mpd	SD < 5 %	n/a (~22 km profiles)
Gravity	LCR D-188	10–40 m mpd, 50–200 m mpd	0.011 mGal	1,035
Magnetics	GTL TM-4 GEM GM-19	0.2–5 m mpd 1–10 m mpd 20–50 m spatial	0.1 nT, final 1 nT < 2 nT	~266,000 2,550 50 + 191
Magnetic susceptibility	Bartington MS-2	Laboratory samples from drill cores (10–30 cm distance), laboratory soil samples	1×10^{-5} (SI) 1×10^{-5} (SI)	360 92
Seismics	4 Geode = 96 channels 10 and 14 Hz geophones (vertical), source: sledgehammer	2 m geophone distance 2 m shot distance		0.72 km profile
Gamma spectrometry	Low-level gamma spectrometer, high-purity Ge detector	Laboratory soil samples	<10 %	49
Surveying	GPS Garmin 76S and 62S Total station Leica TCR403 Level metre Zeiss Ni025 GPS Trimble 5700 (DGPS)	Accordingly mpd Accordingly mpd Accordingly mpd Accordingly mpd	3 m (XY) 0.020 m (Z) 0.050 m 0.025 m (Z)	Surveying of gravity, magnetic, and geoelectric profiles
XRF	Siemens SRS 303	Samples from drill cores (10–30 cm distance)	Results were quantified using calibration curves (105 reference standards)	99

mpd Measurement point distance

contrasts, e.g. in fault zones. The maximum depth of penetration of electrical methods depends on the maximum electrode spacing and the chosen electrode configuration (Dahlin and Zhou 2004). In our case, an investigation depth of approximately 80–100 m could be achieved.

The inversion of the data was performed using either the 2D finite difference inversion code DC2DInvRes (Günther 2004) or the 2D–3D finite element inversion code BERT (Günther et al. 2006; Rücker et al. 2006; www.resistivity.net). The local topography was included for all ERT profile analyses. The inversion result delivers a model of the subsurface resistivity distribution and gives information on spatial averages of subsurface resistivity values in 3D or 2D sections.

Gravity

Gravity data have been collected since 2004, when a reconnaissance double profile indicated a very distinct negative anomaly inside the morphological depression (Mrlina et al. 2007). Between 2004 and 2012, more than 1,000 gravity points were observed, providing a striking negative anomaly of a volcanic diatreme/maar character (Mrlina et al. 2009). Gravity points were distributed in an irregular grid respecting difficult access at the earlier stage of the surveys, with distances between points reduced from 100 to 20 m in the central area of the depression (Fig. 4a, b). This spatial point distribution was replaced in the later stage of survey by profile measurements on P1–P4, P8, P21, and other profiles. This method was selected to allow correlations between gravity, magnetic, seismic, and geoelectric data. We consider that the main geological structures were covered very sufficiently by these gravity measurements.

Special software code DRIFT was used for accurate data processing, as described by Mrlina et al. (2007); we only list the principal reductions and corrections applied: tidal correction, instrumental drift, normal gravity (latitude correction), free air, Bouguer slab, and terrain corrections. As the maximum vertical altitude difference was about 100 m, terrain corrections were calculated to 30 km from each point; estimated terrain correction accuracy is below 0.020 mGal. For the Bouguer correction, the standard density of 2.67 g/cm³ was used, as the area is composed of metamorphic basement rock with densities of 2.65–2.75 g/cm³ (Mrlina et al. 2007). The map of Bouguer gravity anomalies was treated with various regional–residual separation procedures. As the vertical derivatives or upward continuation seemed to be affected by the data from the target anomaly of the maar, we ended up using polynomial planes of the order of 1–3 fitting the regional gravity trend, while second-order residuals were most reasonable. However, we intend to consider the original Bouguer anomaly map as the main working material for interpretation, as there is no artificial mathematical deformation.

Magnetics and petromagnetics

Magnetic points, like the gravity stations, were distributed in an irregular grid in the early-stage survey. However, in the later stages, concentrated magnetic measurements were performed in the almost continuously mode (walking modus) all over the structure and also around. At the last stage, the same profiles as the gravity profiles were surveyed and other detailed investigations especially between the maar and the Železná hůrka scoria cone were conducted. About 266,000 records of the magnetic field with a sampling rate of 1–2 m on profiles were performed in the walking modus in the past 6 years. In total, more than 53 km of detailed magnetic observations were completed. The instrumentation and survey parameters are listed in Table 1. The magnetic field data (total magnetic intensity) were corrected for temporal variations of the earth's total magnetic field intensity using data from a continuously running magnetometer base station, or using data from the magnetic observatory in south-west Bohemia. The area does not exhibit any industrial noise. Considering the very small extent of the investigation area, we did not apply the IGRF correction, but rather referenced all data to the same magnetic base station.

Various techniques were used to enhance the magnetic anomalies, e.g. reduced-to-pole (RTP), graphical/numerical range extraction, and derivatives. Final values of the complete Bouguer anomalies were used as input for various filtering techniques in order to enhance local features characterising the structures under study. The original total magnetic intensity (TMI) map, reduced-to-pole, and the tilt derivative map are the principal basis for interpretation. Magnetic grids/maps are, of course, affected by irregular distribution of high-density measurement profiles and some “empty” areas.

Ninety-two soil samples from depths of approximately 10 cm were collected around the maar structure (randomly distributed), and their mass specific magnetic susceptibility was analysed in the laboratory. The lateral distribution of the magnetic susceptibility values will be used as indication for tephra distribution.

The magnetic susceptibility of basaltic bombs found in the close surroundings of the maar was analysed in a laboratory, as well as density and porosity. These results were already presented by Mrlina et al. (2007).

Shallow seismic (refraction tomography)

A shallow seismic refraction survey of 720 m length was carried out coincident with the ERT and gravity profile 8 (see Fig. 3) to identify tectonic structure of the Tachov fault zone and tephra–tuff deposits in combination with other geophysical results. Because of high P-wave velocities

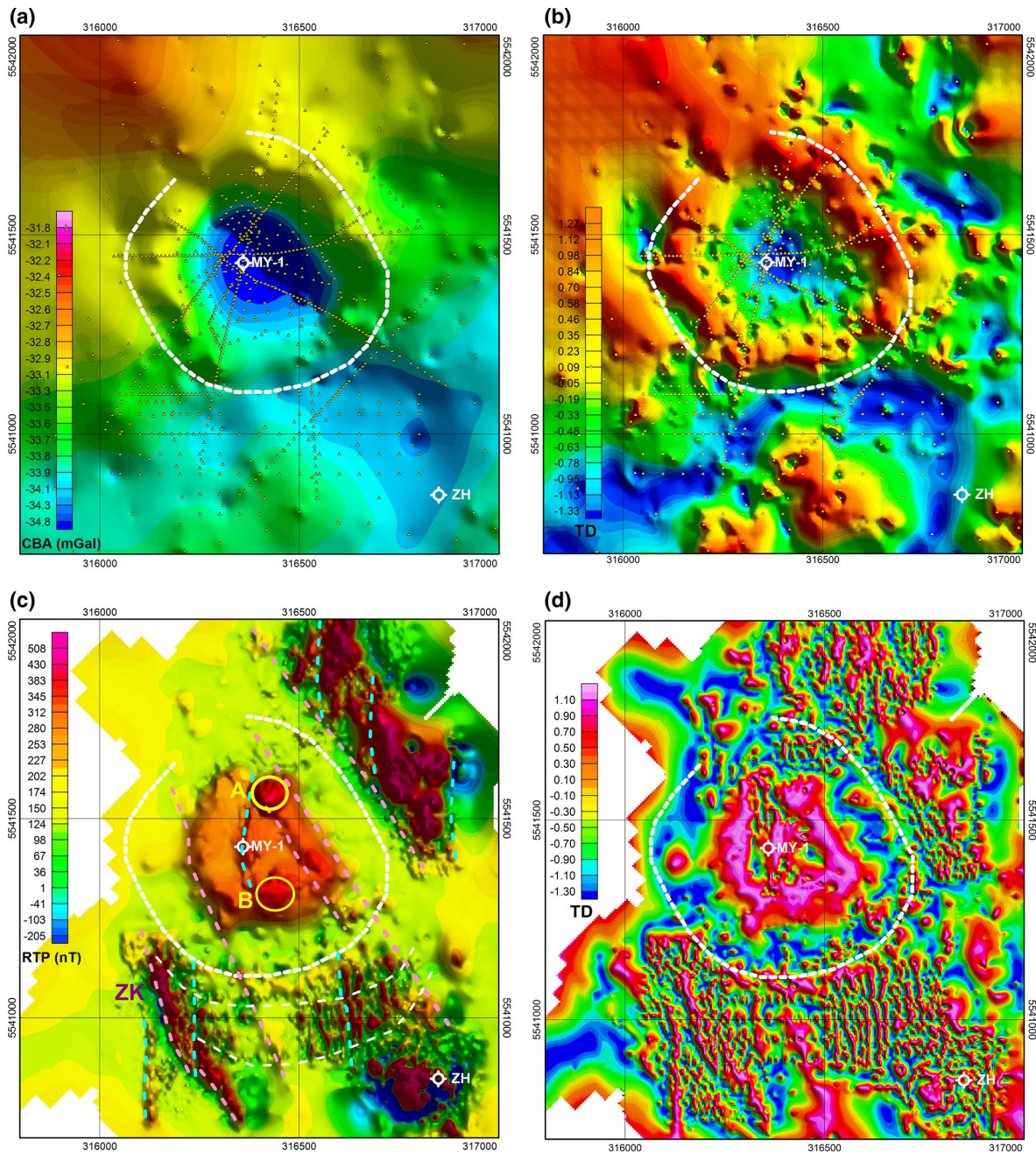


Fig. 4 Gravity and magnetic survey maps; *white hashed line* morphological rim of the maar; MY-1: position of the drill site MY1/85.5 m (Mrlina et al. 2009); ZH Železná hůrka; *map display* WGS84/UTM zone 33N. **a** Complete Bouguer gravity (CBA) map (sunlighted from NE) of the maar and near surroundings, with location of gravity measurement points (*yellow points*). Contour interval: 0.1 mGal; reduction density: 2.670 g/cm³. **b** Residual tilt derivative map (TD) indicates relative gravity highs and lows—the ring of high TD values reflects the bedrock without any volcanic products on the slopes of crater. *Yellow points* gravity measurement points. **c**

Reduced-to-pole (RTP) magnetic field intensity showing the central maar anomaly with a relative peak, A, on the northern side, another one, B, in the south part, and three areas of sharply disturbed RTP field, NE, SSW (ZK), and SSE; and Železná hůrka scoria cone (ZH) with a strong positive–negative anomaly. Some of the NNW–SSE oriented magnetic lineaments or zones are shown as *pink hashed lines* (direction of the Tachov fault zone) and N–S trends in *cyan hashed lines*. In the southern side, *dashed white circles* identified from the magnetic map highlight the limit breaks of magnetic strips. **d** Showing enhanced magnetic features in tilt derivative map (TD)

Table 2 Element content of juvenile (magmatic) and crustal end member

Type of end member	TiO ₂ (%)	MgO (%)	CaO (%)	P ₂ O ₅ (%)	Sr (ppm)	V (ppm)
Juvenile end member*	3.0	13.6	12.4	0.7	889.0	313.0
Crustal end member**	0.749	0.83	0.03	0.066	0	0

* Sample number: 72/2013 MYBO-1-2, ** Sample number: 41/2013 My-5-3.80 m

close to the surface and the lack of significant reflectors, a tomographic processing routine of the data was performed (software codes ReflexW and Rayfract) to generate a P-wave velocity model of the subsurface up to a depth of 60–80 m.

Laboratory gamma spectrometry

Near-surface soil samples from a depth of 10 cm were investigated with a low-level gamma spectrometer. The qualitative ⁴⁰K content (expressed in its activity Bq/kg) of 49 samples has been determined. A low content of ⁴⁰K could be expected in the case of primitive basaltic composition of the material.

Surveying

For the points' positioning, various geodetic techniques were applied according to access and visibility, mainly differential GPS and a total station. GPS observations were tied to the Czech reference stations (both position and altitude) in the WGS84/UTM 33N datum in order to form a local reference network. The survey points inside the maar depression were measured with a level metre in order to achieve good accuracy in vertical coordinates even in dense forest (Table 1). The coordinates of the points were also used to improve the local digital elevation model.

Geological mapping and drill core investigations (macroscopic description, magnetic susceptibility measurements, and petrochemical investigation)

The distribution of tephra-fall deposits around a volcano is a function of several parameters including atmospheric influences (wind direction and speed), palaeotopography, deposition, and eruption parameters (plume height, eruption volume, duration of eruption, particle size distribution, and aggregation processes) (e.g. Mastin et al. 2009). The deposition is further influenced by weathering, erosion, and transport processes in the surrounding of a maar diatreme (e.g. Pirrung et al. 2008). To assess the extent of the volcanoclastic deposits around the Mýtina maar and Železná hůrka scoria cone, the distribution of lapilli and bombs on the surface had been mapped (bombs > 64 mm, lapilli > 2 cm, and lapilli < 2 cm). The final completion of

the map was restricted by dense forest cover, vegetation, and settlements.

The core samples from the six shallow boreholes up to 9.5 m depth (see Fig. 3) were macroscopically inspected and documented (e.g. colour, grain size, texture, and structure properties). Further, the mass-specific magnetic susceptibility κ_m of 360 samples from drill core material My-1 to My-6 with a sampling distance of 0.1–0.3 m was measured and the geochemical element content determined. For the latter, the samples were grounded in an agate mill to <62 μ m and homogenised. Major element oxides (TiO₂, MgO, CaO, and P₂O₅) and trace elements (Sr and V) were analysed on 105 °C dried samples. The samples were prepared as fused discs of Li tetraborate–metaborate and were quantified using calibration curves generated from 105 reference standards.

The petrochemical results (the data set and the detailed discussion will be published separately) had been used to estimate the amount of juvenile components in the core samples. Based on the TiO₂, MgO, CaO, P₂O₅, Sr, and V contents, the juvenile (magmatic) content A_j has been used by means of a mixture calculation (1) because of a wide spread of element content between the crustal and the juvenile end member (after Geissler et al. 2004; Mrlina et al. 2007). A subsample of a volcanic bomb (MYBO 1–2 = 100 % juvenile) and a phyllite sample from a drill core (My-5: 3.80 m = 100 % crustal) are used as the end members (Table 2).

$$\text{Juvenile (magmatic) content } A_j(\%) = 100(X_{\text{sample}} - X_{\text{crustal}}) / (X_{\text{juvenile}} - X_{\text{crustal}}) \quad (1)$$

with X = sum of the mean contents of the elements TiO₂, MgO, CaO, P₂O₅, Sr, and V.

Results and interpretation

Gravity and magnetics

Final values of the complete Bouguer anomalies (CBA) (Fig. 4a), as well as magnetic total intensity map and reduced-to-pole (RTP) values were used as input for various filtering techniques in order to enhance local features characterising the structures under study.

The negative gravity anomaly of -2.3 mGal, centred in the maar depression (Fig. 4a), is the most prominent structure of the investigation area with a slightly elliptical extension in NW–SE direction. It is caused by limnic sediments with a drilled thickness of ~ 84 m (Mrlina et al. 2009) and assumed underlying diatreme breccia of low density. While a regional gradient of approximately 1.5 mGal/km (increasing gravity from south-east to north-west) was recognised in the maar's surrounding (with a sharper gradient in the north-west part of the investigation area and a lower in the SE), the steep gradient inside the maar is approximately 1.3 – 1.5 mGal/100 m.

The residual anomalies of different wavelength showed a remarkable zoning feature (see Fig. 4b)—the central negative anomaly is surrounded by a circular strip of positive gravity values about 100 m wide (see Fig. 4b) and located mainly on the steepest slopes of the maar depression. Then, on top of the morphological edge of the maar depression, there is a negative gravity rim around most of the maar (except north to north-west, where the maar depression is opened by the Kozly brook valley). The two (positive and negative) features do not represent a typical halo zone, which may surround directly some volcanic diatremes and express rather negative gravity. The positive circle reflects the gravity effect of the relatively higher density of the bedrock. The outer negative 'rim' located outside of the depression on fields (north-east, east, and south) and in forest (west) can be interpreted as an effect of mechanical stress (shock waves) during the eruption of the Mýtina maar (Diele 2000; White and Ross 2011). From sharp gravity gradients (Fig. 4b), it is possible to delineate the subsurface circular contact of the diatreme with country rock inside the maar depression. It is more difficult to determine whether there is any volcanic breccia accumulation around the maar lake sediments in the near subsurface, as a result of back falling.

The accurate position of the principal magnetic anomaly of the maar is clear from the map in Fig. 4c. It is evident that it is not caused by a simple singular source, such as regular volcanic breccia deposits; actually, there are a few zones of increased magnetic intensity. The anomaly inside the maar structure does not exhibit sharp spikes and reaches only about 200 nT of relative amplitude, which means that all sources are hidden at some depth. The relatively quiet character of the local field is also caused by the maar lake sediments cover, confirmed down to 84 m in the MY-1 well (Mrlina et al. 2009). Most of the magnetic sources inside the maar are located along the outer part of the predicted maar diatreme as indicated in Fig. 4d. However, these magnetic sources do not form a ring-like structure, but rather a set of NW–SE striking features or bended zones (Fig. 4c, d). Very low magnetic values characterise the space between the maar anomaly and the contour of the

depression (white circle in Fig. 4c, d). Most likely, these are weakly magnetic rocks of the bedrock, which was exposed during the maar-diatreme formation.

A notable circular anomaly at the northern side of the maar depression (see A in Fig. 4c) is located on the north-west edge of a linear NNW–SSE-trending magnetic anomaly (Fig. 4c pink dashed lines)—assumed to be related to a fault of the Tachov fault zone. However, there is only a very tiny increase in gravity values (~ 0.10 mGal) at the site of magnetic anomaly A. These findings may indicate either remains of a debris or scoria, or more likely a small hidden basaltic intrusion (further discussion in Sect. 5.1.2). The magnetic map in Fig. 4c suggests that a similar source may be present in near subsurface along all of the southern side of the gravity anomaly, too (magnetic anomaly B). This may also be a dyke(s) that have not protruded to surface and ended at the depth of some tens of metres.

Outside of the maar depression, there is another gravity low between the maar and the Železná hůrka volcano (Fig. 4a, b). This low-amplitude anomaly may indicate a weakened fractured zone between the two volcanic structures. Moreover, it is parallel to the trend of the regional Tachov fault zone. This gravity low is very well documented on gravity profile 8 (Fig. 3). Gravity data further indicate a perpendicular zone of lower density extending in a WSW–ENE direction, similar to the strike of the Eger Rift. This low between the two volcanic structures is parallel to the valley south of Železná hůrka (see geological trends in Fig. 2), but located higher on the slope, closer to the maar rim (see blue zone in Fig. 4a, b). Considering the above, we may assume that the maar is located on the crossing of the Tachov fault zone and a perpendicular geological zone that is indicated by gravity low of the direction WSW–ENE, corresponding with geological contacts in Fig. 2.

The magnetic image is also completely different on fields outside the maar. Extremely detailed magnetic surveying in this area, in many cases profiling with 0.2-m sampling interval, revealed short-wavelength spike-like anomalies (up to 1,000 nT) forming very local and narrow magnetic strips. Such magnetic pattern indicates accumulations of near-surface magnetic rocks [magnetic susceptibility of tephra bombs was high, about 30×10^{-3} (SI) on average (see Mrlina et al. 2007)]. They could be formed by solifluction of the volcanic material. In a few places, however, the larger extent and amplitude of anomalies may indicate basaltic dykes, like in case of Završský kout (ZK in Fig. 4c).

In fact, there are three areas with such characteristics of the magnetic field:

1. NE–NNE—the area of a former garrison and agricultural fields on the northern downhill slope from the maar rim with high values of magnetic field in general.

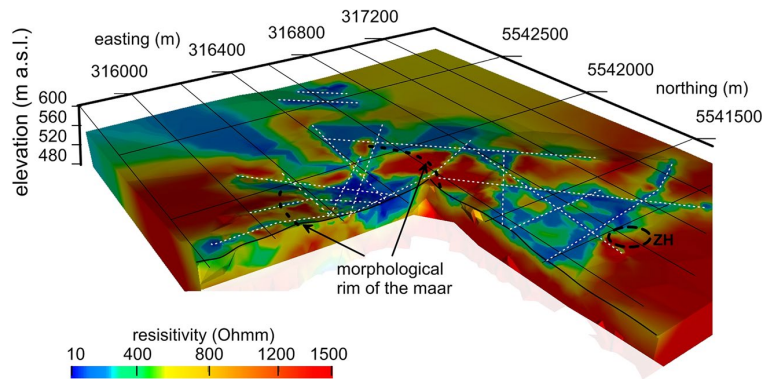


Fig. 5 3D resistivity model of the investigation area Mýtina maar–Železná hůrka scoria cone as result of 3D inversion of the measured apparent resistivity data of profiles 1–12 and 20–25 with software code BERT (Günther et al. 2006; Rücker et al. 2006; www.resistivity.net).

The model response for inversion result fits the measured data within the data error of $\chi^2 = 6.9\%$ and $\text{rms} = 9.3\%$. ZH Železná hůrka; white dotted lines location of the inverted profiles; map display WGS84/UTM zone 33N

2. SW—Završský kout (ZK in Fig. 4c), a prolonged strip of sharp magnetic anomalies, about 500 m long; confirmed by the My-6 shallow borehole with maximum core magnetic susceptibility of all six drill holes (see Sect. 4.5). This strip is diagonal to the slope, so it is not simply a down-hill movement of volcanic material from the maar rim. It may follow a fracture of the Tachov fault zone direction, and the presence of a dike intrusion cannot be excluded.
3. S–SSE—between the Mýtina maar and the Železná hůrka scoria cone, an area with high variability in the magnetic field and with many sharp local anomalies prolonged and oriented N–S, or partly NNW–SSE, as the Tachov fault zone. With respect to the higher elevation of the maar rim (~600–610 m a.s.l.) relative to the scoria cone (~580–590 m a.s.l.), the linear magnetic strips seem most likely to indicate volcanic tephra movement on the slope.

Considering all of the above indications, the magnetic field seems to be affected mainly by two trends: (1) a general principal NW–SE direction parallel to the Tachov fault zone (ZK strip/fracture, limits of the maar anomaly, see pink dashed lines in Fig. 4c) and (2) a N–S striking orientation according to the Regensburg–Leipzig–Rostock lineament (blue dashed lines in Fig. 4c). Simple downhill flow of tephra could be assumed, but the morphological gradients are of slightly different directions. The features are enhanced by the tilt derivative map (Fig. 4d).

In the south-east corner of the map in Fig. 4c, the Železná hůrka basaltic scoria cone (second extrusive phase) is indicated by high magnetic intensity (RTP values), positive over the main scoria cone (north and west sides) and negative in the south and south-east parts of the body, within a former

quarry, formed by the first-phase intrusion containing a significant volume of country rock fragments. Whether the local magnetic N–S strips NNW of the scoria cone are related to its effusive activity or to the maar products remains questionable.

Electrical resistivity tomography: 3D resistivity model

The near-surface volcanic and geologic units (limnic sediments inside the maar depression, pyroclastic deposits, and crystalline schist of the basement outside) provide sufficient resistivity contrasts due to their differences in clay content, porosity, and water saturation to obtain quantitative information about the 3D resistivity distribution.

The measured field data were inverted with the modelling and inversion code BERT (Rücker et al. 2006; Günther et al. 2006; www.resistivity.net) which allows the use of unstructured meshes to include arbitrary topography and subsurface structures. Considering that the electrode spacing is 5 m, the maximum length of the profiles is up to 1,500 m and the coverage of the area with profiles is not regular. We used the non-equidistant parameterisation of this code for the inversion. BERT combines a finite element forward operator (Rücker et al. 2006) and a Gauss–Newton inversion algorithm (Günther et al. 2006) and has been successfully used in several case studies (e.g. Flechsig et al. 2010; Udphuay et al. 2011). The 3D resistivity distribution (Fig. 5) had been recognised in a cube model of $2.1 \text{ km} \times 1.5 \text{ km} \times 120 \text{ m}$ with the data of the geoelectrical profiles 1–12 and 20–25 (Th. Günther/LIAG Hannover). A cut block in the south-west part of the area under investigation allows an insight into the resistivity distribution of the maar itself and the units in the surrounding.

The proven sedimentary infill (Mrlina et al. 2009) of the maar with resistivity values $<150 \text{ Ohm m}$ forms a circular

crater, which is detectable up to a depth of approximately 90–100 m. Very high resistivities (>1,000 Ohm m) outside of this anomaly—located directly around the maar except in NNE and north-west direction—are aligned in a “circular” shape. They are most likely caused by non-weathered mica schist, quartzitic phyllite, and quartzite, found in outcrops near to the surface (see Fig. 2a: Fiala and Vejnar 1997; Tonica et al. 1998). The resistivity distribution to the south-east shows thicker layers of lower resistivity (100–300 Ohm m) near to the surface (thickness of 30–40 m) between Mýtina maar and Železná hůrka scoria cone. The same situation can be determined north-eastward of the maar, where, at 1.2 km distance from the maar centre, in a trench, a tephra and tuff deposit of 4 m thickness had been exposed (Geissler et al. 2004). The deposits of lower resistivity are extended in a north-east direction approximately 1.5 km, to the south-east approximately 500 m. Potential causes of this feature are volcanoclastic deposits near the surface and weathered country rock at depth (<1,000 Ohm m after Dobeš et al. 1986). The heterogeneous resistivity structure NW–NNE of the maar is mainly caused by the bad coverage with profiles due to very dense brush and forest.

Seismic (refraction tomography): 2D P-wave velocity model

The seismic survey was designed to image and to characterise the Tachov fault zone between Mýtina maar and Železná hůrka scoria cone, where the fault zone is thought to be covered by tephra/tuff deposits. The model generated by seismic refraction tomography shows the variation of P-wave velocity to a depth of 60–80 m depending on the ray coverage and is discussed together with geoelectrical and gravity results in Sect. 5.2.2 (Fig. 10). The P-wave velocity along the entire profile ranges from about 300 m/s to about 5,500 m/s. High velocities >3,000 m/s are associated with hardly or unweathered bedrock (phyllite) and values between 2,000 and 3,000 m/s with weathered phyllite (Dobeš et al. 1986). In the south-west (10–90 m) and north-east (475–625 m) of the profile, high velocities (1,500–2,500 m/s) can be recognised in a depth of just 5–10 m relative to the surface. Values lower than 500 m/s occur to a maximum depth of 3 m. The 2D tomogram revealed a broad zone of lower seismic velocities (<1,500–2,000 m/s) that extends between 150 and 450 m to greater depth of 30–40 m. There are also dipping structures with steps of ~10 m at 150, 250, 380, and 600 m visible in the depth.

Mapping of fragmental ejecta (lapilli and bombs), magnetic susceptibility κ_m , and ^{40}K content of soil samples

Based on the geological description of a trench profile and aerial photographs, Geissler et al. (2004) and Mrlina et al.

(2007) provided a first attempt at mapping the distribution of the tephra deposits. Two surface mapping campaigns during autumn 2012 and 2013 defined the general distribution more precisely and delivered information about frequency and dominating grain sizes of lapilli (differentiating between diameter < 2 cm and > 2 cm) and volcanic bombs (diameter > 6.4 cm). Figure 6a shows the mapped distribution of volcanic ejecta on the surface.

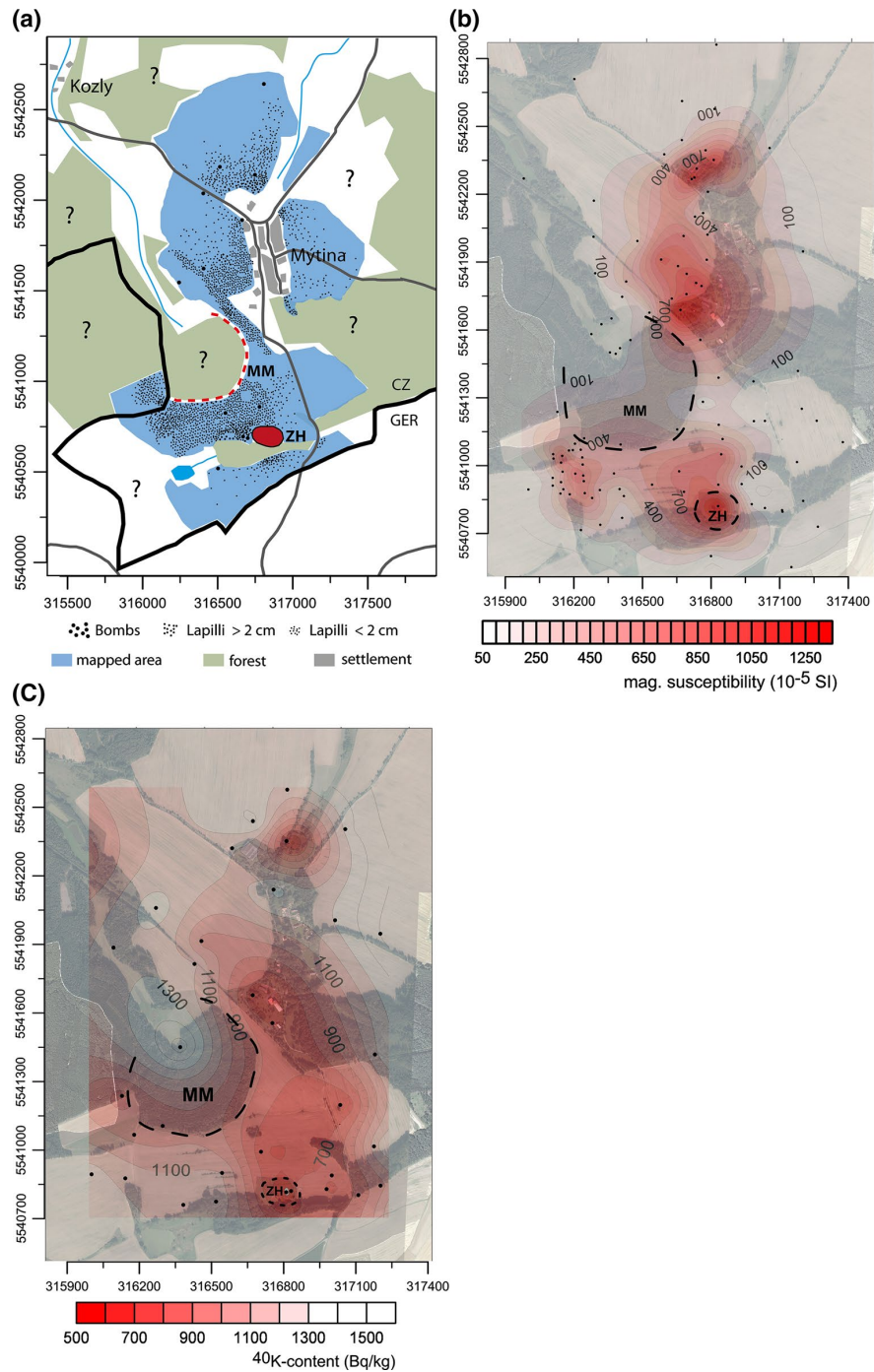
In addition to many finds south-west and south of the Mýtina maar (especially between Mýtina maar and Železná hůrka scoria cone), an elongated zone (~1.8 km length) of numerous finds from the maar to the NNE is clearly evident. The mapping also revealed an inhomogeneous distribution of amphibole and clinopyroxene xenocrysts as substantial components in the ejecta. South-west of the maar structure, as well as east and north of the Mýtina settlement, amphibole, clinopyroxene, phlogopite, and olivine megaxenocrysts are common features in the tephra deposits (Geissler et al. 2007). In contrast, lapilli on the field between the maar and the scoria cone rarely show this attribute. The distribution east of Mýtina is unknown. Accessibility of the fields did not allow detailed mapping, but isolated findings of lapilli give reason to expect further tephra deposits.

The investigation of tephra distribution around the Mýtina maar is supported by measurements of the mass-specific magnetic susceptibility κ_m of 92 soil samples (from a depth of ~10 cm). It is assumed that tephra and tuff deposits represent different stages of the eruption. Consolidated, tuffitic deposits usually contain large portions of the country rock from the initial and early stages of the maar genesis. Later stages are characterised by higher portions of juvenile material forming the tephra. Therefore, they should exhibit different magnetic properties. However, in some cases (see Sect. 4.5), we were able to identify juvenile-rich tephra underneath country rock-rich tuff deposits. The resulting map (Fig. 6b) shows the correlation of areas with samples of high susceptibility κ_m to the locations and findings of ejecta fragments (Fig. 6a). Several soil samples were also measured from sampling points where dense forest impeded the surface mapping of lapilli and bombs (westward of the maar).

A further indication for the surface distribution of tephra but also of tuff comes from the mapping of the ^{40}K content of 49 soil samples (Fig. 6c). The tephra with a higher amount of juvenile components and K_2O percentage of 1–2 % [see Geissler et al. 2004; Mrlina et al. 2007, and unpublished data from drill holes My-1 to My-4, and My-6 (Fig. 7)] has low contents of ^{40}K —expressed by its activity < 800 Bq/kg—whereas tuff with lower percentage of magmatic components and K_2O percentage of 3–7 % has a higher ^{40}K content (activity > 800 Bq/kg).

With the information above, the pattern of the tephra deposits could be verified: the deposition of tephra is not

Fig. 6 Results of surface mapping; map display WGS84/UTM zone 33N. **a** Mapping of ejecta fragments (volcanic bombs and lapilli) at the surface in the Mýtina maar–Železná hůrka scoria cone investigation area; red hashed line Mýtina maar (MM), red ellipse Železná hůrka scoria cone (ZH). **b** Mapping of mass specific magnetic susceptibility κ_m of soil samples. Black dots represent the sampling points. MM Mýtina maar, ZH Železná hůrka scoria cone. **c** Mapping of ^{40}K activity in Bq/kg of soil samples. Black dots represent the sampling points. MM Mýtina maar, ZH Železná hůrka scoria cone



only concentrated in a ring shape around the Mýtina maar and Železná hůrka scoria cone but also covered a NNE–SSW directed elongated zone with a length of approximately 1.8–2.0 km. In the deep valley with steep slopes in north-west

direction from the maar with the Kozly brook (Figs. 3, 6a), no signs for tephra deposits have been found (according to the sample results of magnetic susceptibility κ_m and activity of ^{40}K), probably caused by erosion by the brook.

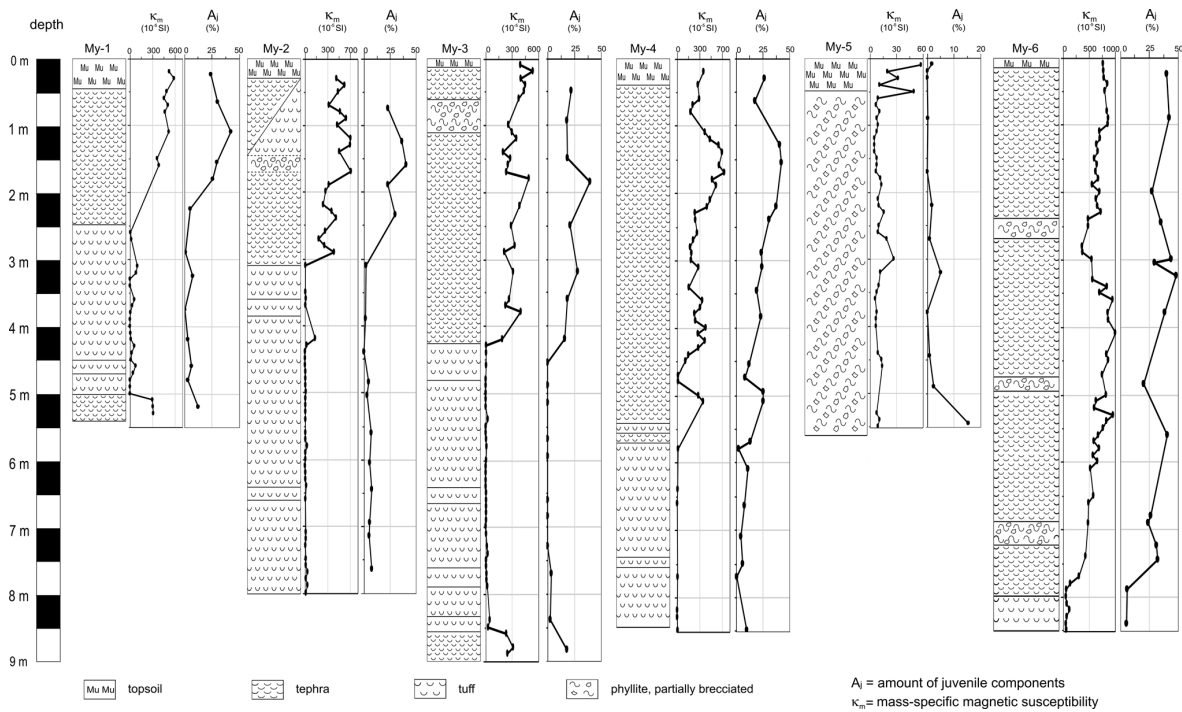


Fig. 7 Core description of drill cores My-1 to My-6 (see Fig. 3), variation in the mass specific magnetic susceptibility κ_m , and the determined amount of juvenile proportion of core samples A_j (mean value

of magmatic components TiO_2 , MgO , CaO , P_2O_5 , Sr , and V). The sampling interval is indicated as dots

Geological investigations of shallow drillings: core description, magnetic susceptibility κ_m , and juvenile components A_j

Following the outcome of geophysical investigations, six shallow drill holes with a maximum depth of 9.5 m were drilled south-west, south, and south-east of the maar (Fig. 3). Stratigraphic logs of the drill core (occurrence of tephra, tuff, and phyllite), the values of magnetic susceptibility κ_m , and the amount of juvenile components A_j are shown in Fig. 7.

The drill cores My-1 to My-4 show tephra (unconsolidated) deposits in the overlying part (~2.5–5.5 m thick) and tuff (consolidated) in the deeper layers (~2.9–>5 m thick). The thickness of tephra in the overlying parts decreases with distance between maar rim and the drill sites: in My-4 near rim ~5.5 m, in My-3 ~4 m, in My-2 ~3 m, and ~2 m in a distance of ~200 m to the rim in My-1. In the drill holes My-1 and My-3, tephra is shown to underlie the tuff (~0.5 m thick) at their base (at a depth of 5 m in My-1 and 8.5 m in My-3).

The tephra thickness in My-6, which had been drilled in the edge region of the magnetic anomaly ZK to the south-west of the maar (Fig. 4c), is ~8 m, maximum in all drill

holes, whereas in My-5, drilled approximately 80 m to south-east of the maar on a topographic high of 622 m, unweathered phyllites were already found at a depth of 0.5 m instead of volcanic deposits. The tephra deposits of My-1, My-2, My-3, and My-4 feature high amounts of juvenile components, A_j , and a higher magnetic susceptibility, κ_m , compared with tuff and phyllite. These data are consistent with local maxima of magnetic field measurements TMI/RTP (e.g. maximum ZK in Fig. 4a). Shallow drill holes (<10 m) of the Czech Geological Survey Prague (GEOFOND) from 1975 (V-3/ID 549493, V-4/ID 549494, V-5A/ID 549495, V-6/ID 549496, V-8/ID 549496, and V17/ID 549401) exploited the partly inaccessible magnetic anomaly area north-east of the maar (former garrison area). Tephra/tuff deposits of up to 8 m were also found in these drill cores (commonly referred in internal sample descriptions as “tuffite”).

Measurements of mass-specific magnetic susceptibility κ_m of core samples (Fig. 7) from the drill holes My-1 to My-6 reveal the significant differences of the magnetic susceptibility κ_m for tephra on the one hand and tuff or country rock on the other hand: tephra with $\kappa_m > 200 \times 10^{-5}$ (SI), tuffitic deposits, mica schist, and phyllite with low susceptibilities $\kappa_m < 20 \times 10^{-5}$ (SI). The determination of the

amount of juvenile components (see Fig. 7) is the quantitative proof that a higher average content of magmatic components A_j is linked with the higher magnetic susceptibility κ_m and a lower activity caused by ^{40}K of the soil samples (Fig. 6b, c). These results confirmed the interpretation of the surface mapping of κ_m .

The content of magmatic components, A_j , (Fig. 7) is low (<10 %) in tuffitic layers, whereas it is about 19–45 % in tephra layers (Fig. 7). Similar trends were detected in a trench, located ca. 800 m north of the Mýtina maar (see Geissler et al. 2004; Mrlina et al. 2007). These results reflect the downward propagation of the root zone of the Mýtina maar, in which the deepening and widening of the root zone leads to lower amounts of ejected country rock (and higher amounts of juvenile material) towards shallow depths when the maar-diatreme dries or phreatomagmatic explosions occur in the open diatreme (Lorenz and Kurszlaukis 2007; Mrlina et al. 2007).

Discussion of special features

Inner structure of Mýtina Maar

Post-volcanic sedimentary maar infill

Figure 8 shows the 2D resistivity distribution on profile 4 (see Fig. 3) which crosses the maar centre and the location of the research drill hole MY1. The inner part of the Mýtina maar is characterised by a pronounced anomaly caused by the lower resistivity of limnic sediments (10–150 Ohm m: water-saturated sand and silty clay with

high content of clay minerals; Mrlina et al. 2009) in relation to the resistive host rock units. The low resistivity structure (<150 Ohm m) is detectable up to the investigation depth of about 80–100 m.

The ERT model on profile 4 shows high resistivity values (>1,000 Ohm m) matching the areas where the profile intersects the areas where basement rocks occur near the surface (quartzitic phyllite, quartzite, and mica schist after Fiala and Vejnar 1997 and Tonica et al. 1998), especially in the east, south, and west of the maar. The Kozly brook valley to the north-west is deeply eroded (~40–50 m compared with the highest part of morphological maar rim) where the weathered basement phyllitic rocks feature resistivity values of 200–600 Ohm m.

The lithological description of the exploratory drill hole MY1 (Mrlina et al. 2009) near the centre of the gravity anomaly, with a depth of 85.5 m, provides a link to the modelled resistivity values with the material composition of the sediments. Highly water-saturated, unconsolidated sand (S) has resistivity values of 10–50 Ohm m and silty clay (C) 30–200 Ohm m and pebbles/cobbles with some silty clay (P) can be assigned with resistivity values >200 Ohm m, whereas different clay and pore water content could lead to overlapping value ranges. Comparable results for maar sediments are available from research drill holes of maar structures in the Upper Lusatia region Baruth, Kleinsaubernitz, and Kreckwitz (Bücker et al. 2003; Schulz et al. 2005). In the case of the Baruth maar, the resistivity values are 10–100 Ohm for clay-rich limnic sediments, water-saturated ash layers, and collapse breccia. Lapilli tuff, found in depth of 240–250 m, is characterised by very low resistivity of 3–12 Ohm m. The resistivity of the bedrock granodiorite is >2,000 Ohm m (Brunner et al. 1999; Bücker et al. 2003).

A statement on the precise thickness of the sediment layers is restricted by the potential low resistivity contrast between sediments and diatreme breccia. The breccia could be water saturated, and therefore, ERT cannot distinguish between these units. According to the studies of Ross et al. (2011), the younger maars (<10–70 ka) of each substrate type (hard or soft rock environment) have diameter/depth ratios in the same range of 3–7, whereas older maars (>70 ka) tend to be shallower due to erosion (>7). The average Ar–Ar age of the Mýtina maar is 288 ± 17 ka (mid-Pleistocene) (Mrlina et al. 2007), and the maar crater is up to ~550 m in diameter. Taking this into account, the increase in resistivity to values >500–800 Ohm m in deeper horizons of the Mýtina maar at 80–90 m could mark the transition zone from limnic sediments to phyllitic debris and the diatreme.

ERT profile 4 (Fig. 8) crosses both the sediment deposits and the flanks of the maar rim in the south-west and north-east. We observe differing slope angles of the crater

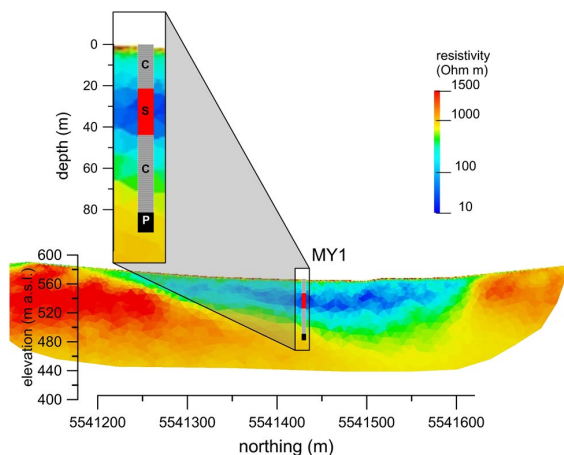


Fig. 8 2D resistivity model on profile 4 (see Fig. 3) in the sector of the post-eruptive sediments of the Mýtina maar and lithological description of drill core MY1 (Mrlina et al. 2009), C—silty to clayey material, S—sandy material, P—pebbles/cobbles with some silty clay

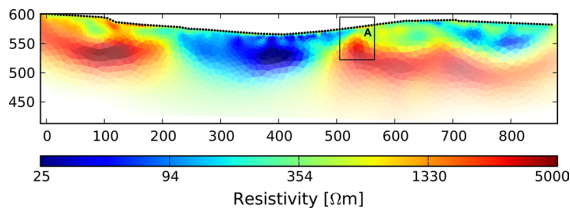


Fig. 9 2D resistivity distribution on profile 3 (see Fig. 3): local resistivity anomaly (A) in the north part of the Mýtina maar

flanks with a steeper slope on the north-east side compared with the south-west. It is also evident that the low resistivities of the maar sediments extend from the research drill hole MY1 towards the north-east to a greater depth than reached in MY1 (~84 m). From ERT results, the greatest thickness of the post-eruptive sedimentary fill is expected to occur 50 ± 10 m towards the ENE–NE direction from the MY1 borehole. In the case of an extended thickness of limnic layers than that of the drill record of MY1 (Mrlina et al. 2009), a more extensive drill record could be available for palaeoclimatic investigation. Results of palynological analyses from MY1 confirm the presence of a palaeoclimatic archive with at least three successive warmer periods of most probably interstadial character from the upper Quaternary Saalian glacial complex (Stebich et al. 2009).

Hidden volcanic structures inside the Mýtina maar

Two notable magnetic anomalies (A and B in Fig. 4c) located at the northern and southern sides of the maar depression (easting = 316,450) may indicate hidden structures. These anomalies could mark accumulations of breccia/tephra or small basaltic intrusion. In the case of the anomaly A, there is a very slight increase in gravity values on profile 3 (see Fig. 3), which crosses the area of the anomaly, of about 0.1 mGal, but indicates a minor increase in the density. Resistivity distribution on profile 3 reveals a local structure with high resistivity values $>2,000$ Ohm m below a depth of approximately 40 m (anomaly A in Fig. 9).

Based on the findings, the positive anomaly in the magnetic field intensity (see Sect. 4.1), high resistivity, and increased density, we infer a hidden basaltic intrusion from the final eruption phases of the maar rather than a local accumulation of breccia/tephra (Schmidt et al. 2013; Blaikie et al. 2014). Concerning anomaly B the lack of additional information from gravity and especially resistivity measurements does not allow to draw any specific conclusions, but might be also related to a small shallow intrusion branching off from the feeder dyke.

Structural features in the outer zone of the Mýtina maar

Circular structures in the outer zone of the Mýtina maar

A remarkable aspect of the structural resistivity patterns in the outer zone of the Mýtina maar is the local more conductive, pocket-like structures, which subdivide the higher resistive areas near to the surface. They could reach a maximum lateral extension and depth of 20–50 m. Figure 10 shows this phenomenon as examples on 2D resistivity distributions at the right side. The local low resistivity features on the sample profiles in Fig. 10 are indicated as red crosses. Taking into account the radial and near to the maar placed ERT profiles, the signatures seem to reveal a systematic arrangement especially in the south, in the south-east, but also in the north-east of the maar (yellow dashed lines in Fig. 10). We interpret these “circular” structures as a possible spatial correlation pattern unknown hitherto. Their strike is roughly concentric around a central complex, comparable to cone sheets (e.g. Phillips 1974).

The finding could qualify concentric fracture structures or systems, which are closely related to the formation of the maar (pre-, syn- or post-genetic). Ring fault structures and ring dykes are common at the periphery of explosive collapse calderas but not well known from the outer zone of maar structures (Lipman 1997; Geshi et al. 2011; White and Ross 2011; Lorenz and Suhr 2012). Ring fault structures of explosive collapse calderas provide insights concerning subsidence processes, roof geometry, and depths of the magma chambers (Lipman 1997). The fracturing in the outer zone of maar structures could be a result of geodynamic processes during magma ascent, such as shock waves during the eruptive period (Diele 2000). The generated fractures with increased permeability, probably partly filled by tuff/tephra deposits and consecutive infiltration of subsurface water, increased weathering with the consequence of reduced resistivity and density in these areas in comparison with the undisturbed/unweathered country rock. The structural ERT information is supported by indications of the gravity survey. A negative gravity ‘rim’ was detected outside of the maar depression on fields (north-east, east, and south), or in the forest (west), parallel to the circular morphological limit of the maar (Fig. 4b). The appearance of the anomaly is even and smoothed, depending on the greater distance up to 50 m between the gravity measurement points outside of the maar compared with the electrode distance of 5 m of the geoelectric measurements.

Further investigations, also supported by additional boreholes, are necessary to get more evidence and detailed indications about extend and origin of the phenomenon.

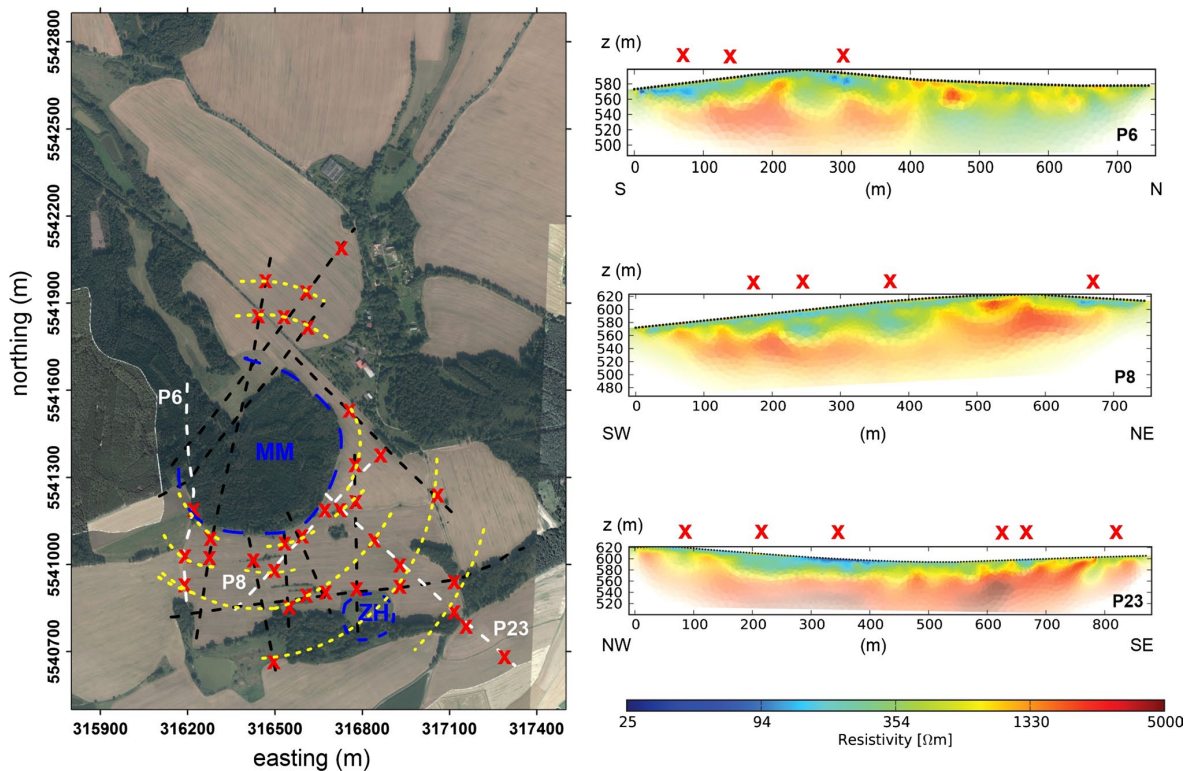


Fig. 10 Indications for circular structures in the outer zone of the Mýtina maar (yellow dashed lines) defined by means of small-scale local minima of resistivity (red crosses) on 2D resistivity models (profiles see Fig. 3)

Tachov fault zone between Mýtina maar and Železná hůrka scoria cone

A further aspect of this region of interest is the missing link between Mýtina maar and Železná hůrka scoria cone. We assume that the geodynamic or palaeoseismic activation of the NW–SE-trending Tachov fault zone after Fiala and Vejnar (1997) and Tonica et al. (1998) could be the trigger process for the maar and scoria cone eruptions or vice versa (Geissler et al. 2004). The local geological situation (Fig. 2a) with quartz veins leads to the assumption that the Tachov fault zone is linked to a NW–SE-trending system of volcanic structures. A further Quaternary volcano, Komorní hůrka scoria cone (KH in Fig. 1), confirms this prolongation of the Tachov fault zone in a north-west direction.

We have applied a combination of geophysical methods (gravity measurements, refraction seismic, and 2D electrical resistivity tomography) to identify possible structural features of the Tachov fault zone between both volcanic structures on the profile 8 (see Fig. 3), approximately perpendicular to the supposed direction of the Tachov fault zone. The compiled results are presented in Fig. 11.

The most important result is that both, seismic and geoelectric methods, show a consistent flat depression in the centre of the profile (150–480 m), which is also indicated by a significant gravity minimum. The maximum depth of this structure is approximately 30–40 m. In particular, the seismic P-wave velocities in the depression zone are reduced (<1,500–2,000 m/s) in comparison with the country rock >3,500 m/s. These reduced velocities can be interpreted as fractured/weathered rock matrix and overlying deposits of tuff and tephra. The minimum in the gravity analysis of -0.4 mGal confirms the variation in the material properties as well as the decrease in the resistivity (<300–400 Ohm m) which are caused for the same reason.

The shallow drill holes (Fig. 7) give necessary evidence for volcanoclastic deposits in the upper 5–10 m. With the exception of My-5, drilled nearby the topographic height 622 m (Fig. 2a), where unweathered phyllites occur at 0.5 m depth, all other drill holes exhibit volcanoclastic records of tephra and tuff. In neither case do these shallow drill holes reach the non-weathered host rocks. In addition, a second tephra layer has been recovered from the drill cores My-1 and My-3 at their base. It infers that several consecutive eruptions could have taken place and

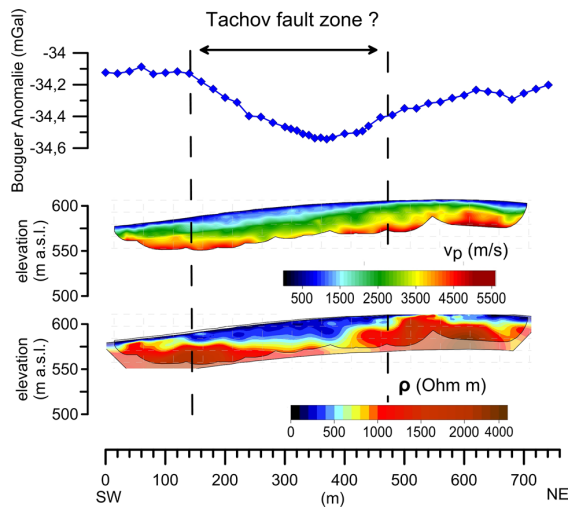


Fig. 11 Compilation of the geophysical results of gravimetry, ERT, and refraction seismic on the SW–NE running profile 8 (length 720 m; see Fig. 3) across the Tachov fault zone: Bouguer gravity anomaly (mGal), P-wave velocity distribution (m/s), and electrical resistivity distribution (Ohm m)

thicknesses of tephra and tuff >10 m is very likely. At the end of the profile 8 (near 680 m), another example of the before-mentioned indications of small pocket-like sub-structures is recognisable by a minimum in gravity, seismic velocity, and electrical resistivity, possibly belonging to the circular structures, discussed in Sect. 5.2.1.

Further investigations (deeper drill holes than 10 m, which should be drilled through the deposits from Mýtina maar and Železná hůrka scoria cone and an age determination of Železná hůrka scoria cone volcanics) are necessary to clarify whether both volcanic centres are related as being one volcanic event or had been formed by separated eruptions.

Conclusions

The western Eger Rift is of specific volcanological interest because of indications for a presently active magma intrusion from the lithospheric mantle into the crust beneath the eastern part of the Cheb Basin and intense, long-lasting earthquake swarm activity in the upper crust over the last three decades.

In this context, one possibility to evaluate volcanic hazard potential is the palaeovolcanic reconstruction of existing volcanic complexes like Mýtina maar/Železná hůrka scoria cone as most prominent example of Quaternary volcanic eruptions in the Bohemian Massif. Hence, the first step is a multiparametric geophysical and geological

analysis of the inner and outer structure of the Mýtina maar, presented in this publication.

The electrical resistivity tomography, gravity, magnetic, and seismic surveys of the Mýtina maar–Železná hůrka complex; data from six shallow drill holes, up to 9.5 m deep; and geological surface mapping of the outer structure of the Mýtina maar extend the findings of Mrlina et al. (2009) and generate new features associated with this volcanic complex.

In particular, we were able to reveal and determine:

1. the extension of the post-eruptive sedimentary maar infill that is deeper than the 84 m retrieved in the research drill MY1 (Mrlina et al. 2009) and volcanoclastic deposits and areas of near-surface country rock in the surrounding of the Mýtina maar could be found, based on resistivity models;
2. one (or two) hidden volcanic structures inside the maar covered by sedimentary layers, which are interpreted as basaltic intrusions, rather than remains of scoria or of a debris;
3. hitherto unknown circularly arranged structures in the external/outer zone of the Mýtina maar around the central maar depression, comparable to cone sheets and interpreted to be caused by fracturing during maar genesis (possibly a proof of palaeoseismicity, see Geissler et al. 2004);
4. indications from electrical resistivity tomography, seismic, and gravity survey of a palaeovalley, filled with volcanoclastic rocks aligned along the strike line (NW–SE) of the Tachov fault zone, in the area between the Mýtina maar and the Železná hůrka scoria cone; and
5. tephra deposits within the drill cores in the overlying part (My-1 to My-4: ~2.5–5.5 m, My-6: ~8 m thick) and tuff in the underlying layers (~2.9–>5 m thick) and low juvenile component proportions, A_j , (<10 %) in tuffitic layers and about 19–45 % in tephra layers. The identification of one more sequence of juvenile-rich tephra below country rock-rich tuff at the base of My-1 and My-3 infers that several consecutive eruptions with long periods of quiescence could have taken place.

Deposition of tephra is not only concentrated in a ring shape around the Mýtina maar and Železná hůrka scoria cone but also covered a NNE–SSW directed elongated zone with a length of approximately 1.8–2.0 km, based on the distribution of lapilli and bombs, magnetic susceptibility, and ^{40}K content of soil samples.

This study shows that the applied geophysical and geological techniques represent a very efficient tool for the detection of volcanic structures as a first step in reconstructing the palaeovolcanic evolution of maar-diatreme volcanoes.

Because of the indications from isotope (C_{CO_2} , He, N_2) research to a presently active magmatic process in combination with earthquake swarm activity located ~15–30 km north of the working area (Bräuer et al. 2009, 2011; Kämpf et al. 2013), a potential for future hazards (phreatomagmatic eruptions) for the eastern part of the Cheb Basin cannot be excluded. Therefore, the most suitable key area for future work of reconstruction of the palaeovolcanic evolution and assessment of possible future hazard potential in the Bohemian Massif is the Mýtina maar-diatreme volcano and surroundings along the NW–SE striking Tachov fault zone.

Acknowledgments We would like to express our gratitude to the German Research Foundation (DFG) for funding this project (FL271/13 and KA902/16). Gravity measurements were partly supported by the project CzechGeo/EPOS, Grant No. LM2010008. Thanks to R. Naumann, D. Berger, F. Körting, H. Liep, M. Ospald, V. Polák, I. Schüller and J. Wondrak. At last, we would like to express our gratitude towards K. Nemeth, our editor, and A. Pittari and J. van Otterloo, our reviewers, for helpful suggestions that improved this article.

References

- Bankwitz P, Schneider G, Kämpf H, Bankwitz E (2003) Structural characteristics of epicentral areas in Central Europe: study case Cheb Basin (Czech Republic). *J Geodyn* 35:5–32
- Barde-Cabusson S, Bolós X, Pedrazzi D, Lovera R, Serra G, Martí J, Casas A (2013) Electrical resistivity tomography revealing the internal structure of monogenetic volcanoes. *Geophys Res Lett* 40:2544–2549. doi:10.1002/grl.50538
- Barnes I, McCoy GA (1979) Possible role of mantle-derived CO_2 in causing two “phreatic” explosions in Alaska. *Geology* 7:434–435
- Blaikie TN, Ailleres L, Cas RAF, Betts PG (2012) Three dimensional potential field modelling of a multi-vent maar-diatreme—The Lake Coragulac maar, Newer Volcanics Province, south-eastern Australia. *J Volcanol Geother Res* 235–236:70–83. doi:10.1016/j.jvolgeores.2012.05.002
- Blaikie TN, Ailleres L, Betts PG, Cas RAF (2014) Interpreting subsurface volcanic structures using geologically constrained 3-D gravity inversions: examples of maar-diatremes, Newer Volcanics Province, southeastern Australia. *J Geophys Res Solid Earth* 119:3857–3878. doi:10.1002/2013JB010751
- Bolós X, Barde-Cabusson S, Pedrazzi D, Martí J, Casas A, Himi M, Lovera R (2012) Investigation of the inner structure of La Crosa de Sant Dalmai maar (Catalan Volcanic Zone, Spain). *J Volcanol Geother Res* 247–248:37–48. doi:10.1016/j.jvolgeores.2012.08.003
- Bräuer K, Kämpf H, Strauch G (2009) Earthquake swarms in non-volcanic regions: what fluids have to say. *Geophys Res Lett* 36:L17309. doi:10.1029/2009GL039615
- Bräuer K, Kämpf H, Koch U, Strauch G (2011) Monthly monitoring of gas and isotope compositions in the free gas phase at degassing locations close to the Nový Kostel focal zone in the western Eger Rift, Czech Republic. *Chem Geol* 290:163–176
- Brunner I, Friedel S, Jacobs F, Danckwardt E (1999) Investigation of the Tertiary maar structure using three-dimensional resistivity imaging. *Geophys J Int* 136:771–780
- Büchel G, Lorenz V (1993) Syn- and post-eruptive mechanism of the Alaskan Ukinrek Maars in 1977. *Lect Notes Earth Sci* 49:15–60
- Bücker C, Wonik T, Schulz R (2003) Physikalische Eigenschaften einer tertiären Maarfüllung—Ergebnisse von Bohrlochmessungen in den Forschungsbohrungen Baruth (Sachsen). *Z Angew Geol* 49:43–51
- Cassidy J, France SJ, Locke CA (2007) Gravity and magnetic investigation of maar volcanoes, Auckland volcanic field, New Zealand. *J Volcanol Geother Res* 159:153–163. doi:10.1016/j.jvolgeores.2006.06.007
- Dahlin T, Zhou B (2004) A numerical comparison of 2D resistivity imaging with 10 electrode arrays. *Geophys Prosp* 52:379–398
- De la Cruz-Reyna S, Yokoyama I (2011) A geophysical characterization of monogenetic volcanism. *Geofis Int* 50(4):465–484
- Diele LM (2000) Der Pulvermaar-Vulkan: Struktur und Massenbilanzen auf der Basis von geophysikalischen Messungen und Volumenberechnungen. International Maar Conference, Daun/Vulkan-eifel, Germany, Terra Nostra 106
- Dobeš M, Hercog F, Mazáč O (1986) Die geophysikalische Untersuchung der hydrogeologischen Strukturen im Cheb—Becken. *Sbor Geol ved* 21:117–158
- Evans W, Bergfeld D, McGimsey RG, Hunt AG (2009) Diffuse gas emissions at the Ukinrek Maars, Alaska: implications for magmatic degassing and volcanic monitoring. *Appl Geochem* 24:527–535. doi:10.1016/j.apgeochem.2008.12.007
- Fiala J, Vejnar Z (1997) The Cheb-Dylen Crystalline Unit, relations to the Moldanubian Zone. In: Vrana S, Stedra V (eds) *Geologic model of Western Bohemia related to the KTB borehole in Germany*. *J Geol Sci Geology* 47:56–57
- Fiala J, Vejnar Z (2004) The lithology, geochemistry, and metamorphic gradation of the crystalline basement of the Cheb (Eger) Tertiary Basin, Saxothuringian Unit. *Bull Geosci* 79:41–52
- Fischer T, Horálek J, Hrubcová P, Vavryčuk V, Bräuer K, Kämpf H (2014) Intra-continental earthquake swarms in West-Bohemia and Vogtland: a review. *Tectonophysics* 611:1–27. doi:10.1016/j.tecto.2013.11.001
- Flechsich C, Fabig T, Rücker C, Schütze C (2010) Geoelectrical investigations in the Cheb Basin/W Bohemia: an approach to evaluate the near-surface conductivity structure. *Stud Geophys Geod* 54:417–437
- Galadi-Enriquesz E, Kroemer E, Loth G, Pürner T, Raum G, Teipel U, Rohrmüller J (2009) *Erdgeschichte des Oberpfälzer Waldes*. Geologische Karte 1:150 000, Augsburg. ISBN: 978-3-936385-55-7
- Geissler WH, Kämpf H, Bankwitz P, Bankwitz E (2004) Das quartäre Tephra-Tuff-Vorkommen von Mýtina (Südrand des westlichen Eger-Grabens/Tschechische Republik): Indikationen für Ausbruch- und Deformationsprozesse. *Z Geol Wiss* 32:31–54
- Geissler WH, Kämpf H, Seifert W, Dulski P (2007) Seismic and petrological studies of the lithosphere in the earthquake swarm region Vogtland/NW-Bohemia, Central Europe. *J Volcanol Geother Res* 159:33–69
- Geshi N, Nemeth K, Oikawa T (2011) Growth of phreatomagmatic explosion craters: a model inferred from Suoana crater in Miyakejima Volcano, Japan. *J Volcanol Geother Res* 201:30–38. doi:10.1016/j.jvolgeores.2010.11.012
- Günther T (2004) Inversion methods and resolution analysis for the 2D/3D reconstruction of resistivity structures from DC measurements. Dissertation, University of Mining and Technology Freiberg. <http://nbn-resolving.de/urn:nbn:de:swb:105-4152277>
- Günther T, Rücker C, Spitzer K (2006) 3-d modeling and inversion of DC resistivity data incorporating topography—Part II: inversion. *Geophys J Int* 166:506–517
- Horálek J, Fischer T (2008) Role of crustal fluids in triggering the West Bohemia/Vogtland earthquake swarms: just what we know (a review). *Stud Geophys Geod* 52:455–478
- Kämpf H, Bräuer K, Schumann J, Hahne K, Strauch G (2013) CO_2 discharge in an active, non-volcanic continental rift area (Czech

- Republic): characterisation (^{13}C , $^3\text{He}/^4\text{He}$) and quantification of diffuse and vent CO_2 emissions. *Chem Geol* 339:81–83
- Kienle J, Kyle PR, Self S, Motyka RJ, Lorenz V (1980) Ukinrek Maars, Alaska, I. April 1977 eruption sequence, petrology and tectonic setting. *J Volcanol Geother Res* 7:11–37
- Kopecky L (1978) Neoidic taphrogenic evolution and young alkaline volcanism of the Bohemian Massif. *J Geol Sci* 31:91–107
- Kvaček Z, Teodoridis V (2007) Tertiary macrofloras of the Bohemian Massif: a review with correlations within Boreal and Central Europe. *Bull Geosci* 82:383–408
- Lipman PW (1997) Subsidence of ash-flow calderas: relation to caldera size and magma-chamber geometry. *Bull Volcanol* 59:198–218
- Lochmann Z (1961) Železná hůrka (Eisenbühl). *Anthropozoikum* 11:69–81
- Loera HL, Aranda-Gómez JJ, Arzate JA, Molina-Garza SR (2008) Geophysical surveys of the Joya Honda maar (México) and surroundings; volcanic implications. *J Volcanol Geother Res* 170:135–152
- Lorenz V (2007) Syn- and post-eruptive hazards of maar-diatreme volcanoes. *J Volcanol Geother Res* 159:285–312
- Lorenz V, Kurszlauskis S (2007) Root zone processes in the phreatomagmatic pipe emplacement model and consequences for the evolution of maar-diatreme volcanoes. *J Volcanol Geother Res* 150:4–32
- Lorenz V, Suhr P (2012) On differences and similarities between maar-diatreme volcanoes and explosive collapse calderas. In: Arentsen K, Németh K, Smid E (eds) 4th International Maar conference a multidisciplinary congress on monogenetic volcanism, Auckland New Zealand 2012, abstract volume 58–59. ISBN: 978-1-877480-15-7
- Mastin L, Guffanti M, Servranckx R, Webley P, Barsotti S, Dean K, Durant A, Ewert JW, Neri A, Rose WI, Schneider D, Siebert L, Stunder B, Swanson G, Tupper A, Volentik A, Waythomas CF (2009) A multidisciplinary effort to assign realistic source parameters to models of volcanic ash-cloud transport and dispersion during eruptions. *J Volcanol Geother Res* 186:10–21
- Mrlina J, Kämpf H, Geissler WH, van den Bogaard P (2007) Proposed Quaternary maar structure at the Czech/German boundary between Mýtina and Neualbenreuth (western Eger Rift, Central Europe): geophysical, petrochemical and geochronological indications. *Z Geol Wiss* 35:213–230
- Mrlina J, Kämpf H, Kroner C, Mingram J, Stebich M, Brauer A, Geissler WH, Kallmeyer J, Matthes H, Seidl M (2009) Discovery of the first Quaternary maar in the Bohemian Massif, Central Europe, based on combined geophysical and geological surveys. *J Volcanol Geother Res* 182:97–112
- Nicollin F, Gibert D, Beauducel F, Boudon G, Komorowski JC (2006) Electrical tomography of LaSoufrière de Guadeloupe Volcano: field experiments, 1D inversion and qualitative interpretation. *Earth Planet Sci Lett* 244:709–724
- Nowell DAG, Jones MC, Pyle DM (2006) Episodic quaternary volcanism in France and Germany. *J Quat Sci* 21:645–675. doi:10.1002/jqs.1005
- Peterek A, Reuther CD, Schunk R (2011) Neotectonic evolution of the Cheb Basin (Northwestern Bohemia, Czech Republic) and its implications for the late Pliocene to Recent crustal deformation in the western part of the Eger Rift. *Z Geol Wiss* 5(6):335–365
- Phillips WJ (1974) The dynamic emplacement of cone sheets. *Tectonophysics* 24:69–84
- Pirring M, Büchel G, Lorenz V, Treutler HC (2008) Post-eruptive development of the Ukinrek East Maar since its eruption in 1977 A.D. in the periglacial area of south-west Alaska. *Sedimentology* 55:305–334
- Proft E (1894) Kammerbühl und Eisenbühl, die Schichtvulkane des Egerer Beckens. *Jahrb Geol Reichsanstalt Wien* 44:25–85
- Revil A, Finizola A, Piscitelli S, Rizzo E, Ricci T, Crespy A, Angeletti B, Balasco M, Barde Cabusson S, Bennati L, Bolève A, Byrdina S, Carzaniga N, Di Gangi F, Morin J, Perrone A, Rossi M, Rouleau E, Suski B (2008) Inner structure of La Fossa di Vulcano (Vulcano Island, southern Tyrrhenian Sea, Italy) revealed by high resolution electric resistivity tomography coupled with self-potential, temperature, and soil CO_2 diffuse degassing measurements. *J Geophys Res* 113:B07207. doi:10.1029/2007JB005394
- Rohrmüller J (2003) Die Forschungsbohrung Bayerhof—die Erkundung eines tertiären Maars im Steigerwald, Oberpfalz (NE Bayern). *Geol Bav* 107:215–220
- Ross PS, Delpit S, Haller MJ, Németh K, Corbella H (2011) Influence of the substrate on maar-diatreme volcanoes—an example of a mixed setting from the Pali Aike volcanic field, Argentina. *J Volcanol Geother Res* 201:253–271
- Rücker C, Günther T, Spitzer K (2006) 3-d modeling and inversion of DC resistivity data incorporating topography—Part I: modeling. *Geophys J Int* 166:495–505
- Šantrůček P, Králík F, Kvičinský Z, Opletal M (1991) Geological map, scale 1:50,000. Czech Geological Survey, 1991
- Schmidt A, Nowaczyk N, Kämpf H, Schüller I, Flechsig C, Jahr T (2013) Origin of magnetic anomalies in the large Ebersbrunn diatreme, W Saxony, Germany. *Bull Volcanol* 75:766. doi:10.1007/s00445-013-0766-6
- Schulz R, Buness H, Gabriel G, Pucher R, Rolf C, Wiederhold H, Wonik T (2005) Detailed investigation of preserved maar structures by combined geophysical surveys. *Bull Volcanol* 68:95–106
- Schwarzkopf LM, Tobschall HJ (1997) Železná hůrka (Eisenbühl)—volcanology and geochemistry of a quaternary scoria and lapilli cone in the Ohře (Eger) Rift. *J Geosci* 42:73
- Skácelová Z, Rappich V, Valenta J, Hartvich F, Šrámek J, Radon M, Gazdová R, Nováková L, Kolínský P, Pécskay Z (2010) Geophysical research on structure of partly eroded maar volcanoes: miocene Hnojnice and Oligocene Rychnov volcanoes (northern Czech Republic). *J Geosci* 55:333–345
- Stebich M, Mingram J, Mrlina J, Kämpf H (2009) The Mýtina Maar, west Bohemia, Czech Republic—Preliminary results from ongoing sedimentological and palynological investigations. *Asociación Geologica Argentina, Publicaciones especiales Series Dn No 12*, pp 118–119
- Stettner G (1999) Geologische Karte Bayern, Blatt 6040/6041 Neualbenreuth/Märing 1:25,000, Bayerisches Geologisches Landesamt Augsburg
- Tonica J, Opletal M, Cicha I, Cihelk M (1998) Geologica Mapa ČR, 11-32 Lázně Kynžvart 1:25,000. Český geologický ústav Praha
- Udphuay S, Günther T, Everett ME, Warden RR, Briaud JL (2011) Three dimensional resistivity tomography in extreme coastal terrain amidst dense cultural signals: application to cliff stability assessment at the historic D-Day site. *Geophys J Int* 185:201–220
- Ulrych J, Dostal J, Adamovič J, Jelínek E, Špaček P, Hegner E, Balogh K (2011) Recurrent Cenozoic volcanic activity in the Bohemian Massif (Czech Republic). *Lithos* 123:133–144
- Ulrych J, Ackerman L, Balogh K, Hegner E, Jelínek E, Pécskay Z (2013) Plio-Pleistocene basanitic and melilititic series of the Bohemian Massif: K–Ar ages, major/trace element and Sr–Nd isotopic data. *Geochemistry* 73:429–450
- Valentine GA, White JDL (2012) Revised conceptual model for maar-diatremes: subsurface processes, energetics, and eruptive products. *Geology* 40:1111–1114. doi:10.1130/G33411.1
- Weinlich FH, Bräuer K, Kämpf H, Strauch G, Tesář J, Weise SM (1999) An active subcontinental mantle volatile system in the western Eger rift, Central Europe: gas flux, isotopic (He, C, and N) and compositional fingerprints. *Geochim Cosmochim Acta* 63:3653–3671
- White JW, Ross PS (2011) Maar-diatreme volcanoes: a review. *J Volcanol Geother Res* 201:1–29

9 CO₂ degassing in the Hartoušov mofette area, western Eger Rift, imaged by CO₂ mapping and geoelectrical and gravity surveys

Nickschick, T., Kämpf, H, Flechsig, C., Mrlina, J., Heinicke, J.

published 2015 in International Journal of Earth Sciences 104(8):2107-2129

CO₂ degassing in the Hartoušov mofette area, western Eger Rift, imaged by CO₂ mapping and geoelectrical and gravity surveys

Tobias Nickschick · Horst Kämpf · Christina Flechsig · Jan Mrlina · Jens Heinicke

Received: 9 April 2014 / Accepted: 28 December 2014
© Springer-Verlag Berlin Heidelberg 2015

Abstract Strong, subcontinental mantle-dominated CO₂ degassing occurs in the Hartoušov and Bublák mofette fields in the western Eger Rift. The combination of CO₂ gas flux and soil gas measurements as well as gravity and geoelectric surveys provides insight into the surface and subsurface of this unique mofette area. CO₂ soil gas and gas flux measurements reveal that large amounts of carbon dioxide are released via channels with diameters below 1 m. Carbon dioxide emissions of several tens and up to more than 100 kg day⁻¹ are ejected via these small seeps. Measurements with small spacings are necessary to account for the point like, focused gas discharge in the lesser degassing surrounding. We estimate that between 23 and 97 tons of CO₂ are released over an area of about 350,000 m² each day in the Hartoušov mofette field. The application of widely used geostatistical tools leads to estimations of the CO₂ discharge with very high standard deviations due to the strong positive skewness of the data distribution. Geophysical investigations via electrical resistivity tomography and gravity measurements were carried out over areas of strong seepage and reveal distinct anomalies in the subsurface below mofettes, indicating rock and sediment alterations and/or sediment transport by pressurised, ascending CO₂ and water mobilised by it. This study reveals that the

gas emanations only occur west of a morphological step which is related to a N–S-oriented fault zone, the Počátky-Plesná fault zone. The results of CO₂ mapping and the geophysical studies can track the course of this fault zone in this area. Our results fit into a tectonic model in which the mofette fields are in the centres of two independent pull-apart basin-like structures. We hypothesise that the sinistral strike-slip movement of the Počátky-Plesná fault zone leads to a pull-apart basin-like opening, at which the strong, mantle-derived CO₂ degassing occurs nowadays. Since the Hartoušov and Bublák mofette fields only illustrate examples along the N–S-striking Počátky-Plesná fault zone, its role and other N–S-striking faults' roles of the Regensburg–Leipzig–Rostock zone for upper mantle degassing might have been underestimated previously.

Keywords Cheb Basin · Magmatic CO₂ · Eger Rift · CO₂ gas flux studies · Geoelectrics · Gravity

Introduction

The West Bohemia/Vogtland region is the geodynamically most active area near the European Cenozoic Rift showing persistent seismic activity in the form of recurring earthquake swarms and intense CO₂-degassing at the surface with mantle-derived He-isotope signatures. These intra-plate earthquake swarms are characterised by magnitudes up to ML 4.5 and focal depths between 4 and 20 km (Horálek and Fischer 2010). The area is known as “locus typicus” for the term “earthquake swarm”, established by Credner, more than 100 years ago (Credner 1876). Historical data document earthquake activity even since the twelfth century in Bohemia (Kárník et al. 1957) and since the sixteenth century in Saxony (Grünthal 1989). The epicentres are not equally

T. Nickschick (✉) · H. Kämpf
German Research Centre for Geosciences GFZ Potsdam,
Section 4.3 Telegrafenberg, 14473 Potsdam, Germany
e-mail: tnickschick@gmx.de

C. Flechsig · J. Heinicke
University Leipzig, Institute for Geophysics and Geology,
Talstraße 35, 04103 Leipzig, Germany

J. Mrlina
Czech Academy of Sciences, Institute of Geophysics,
Bočni II 1401, 14131 Prague, Czech Republic

distributed over the study region, but are concentrated in some clusters in the Southern Vogtland, the Fichtelgebirge/Oberpfalz and the area of the Cheb Basin and Slavskovský Les (Neunhöfer and Hemmann 2005; Horálek and Fischer 2010; Fischer et al. 2014). Most of the earthquake activity is concentrated at the Nový Kostel focal zone (NKFZ), located at the intersection between the N–S-trending Počátky-Plesná Fault Zone (PPZ) and the NW-trending Mariánské Lázně Fault Zone (MLFZ) (Fischer 2003; Fischer et al. 2012, 2014). About 90 % of the total seismic moment was released in the NKFZ, which was formed by an NNW-striking and steeply dipping fault plane (Horálek and Fischer 2010). Alexandrakakis et al. (2014) investigated the v_p/v_s ratio of the NKFZ and its surrounding by double-difference tomography. They found structures that may reflect changes in the lithology and/or fluid concentration in the hypocentral area and that an overlying body of granitic intrusion acts as a fluid trap. Swarm-like seismic activity near Nový Kostel was recorded in 1985/1986, 1997, 2000, 2008, 2011–2012 (Fischer et al. 2014) and in 2014 (ML = 4.5).¹

Results of seismological investigations prove that the structure of the lithosphere of this area is anomalous compared to the surroundings. The results were interpreted as crustal thinning to about 27 km (Geissler et al. 2005; Heuer et al. 2006). Hrubcová and Geissler (2009) found a ca. 5-km-thick layer in the lower crust (Moho reflective zone), while Hrubcová et al. (2013) found out that the thickness of the Moho reflective zone varied between 2 and 4 km within depth range of 27/28–31.5 km. Heuer et al. (2006) detected a zone of lower velocity at ca. 65 km depth which was interpreted as asthenospheric up-doming and/or may be caused by the occurrence of partial melt. Heuer et al. (2011) assumed a small plume structure with only weak imprint on the 410 km discontinuity beneath this area.

Most earthquake swarms in rifting regimes are related to magmatic dike intrusion or fluid transport processes in crustal faults. Earthquake swarms often form vertically oriented, planar shapes tracing the outline of the dike or fault, e.g. in Iceland (Jakobsdóttir et al. 2008; Key et al. 2011; White et al. 2011), in the western Eger Rift (ER), Central Europe (Bräuer et al. 2003; Dahm et al. 2008; Horálek and Fischer 2008; Fischer et al. 2014) and in Western Saxony SW of Zwickau, Central Europe (Hemmann and Kämpf 2002; Hemmann et al. 2003; Korn et al. 2008), Afar (Ebinger et al. 2008), the southern Kenya Rift (Ibs-von Seht et al. 2001) or the Long Valley Caldera, California/USA (Hill and Prejean 2005).

Weinlich et al. (1998, 1999, 2003) and Kämpf et al. (2007) carried out initial mappings of the gas and isotope

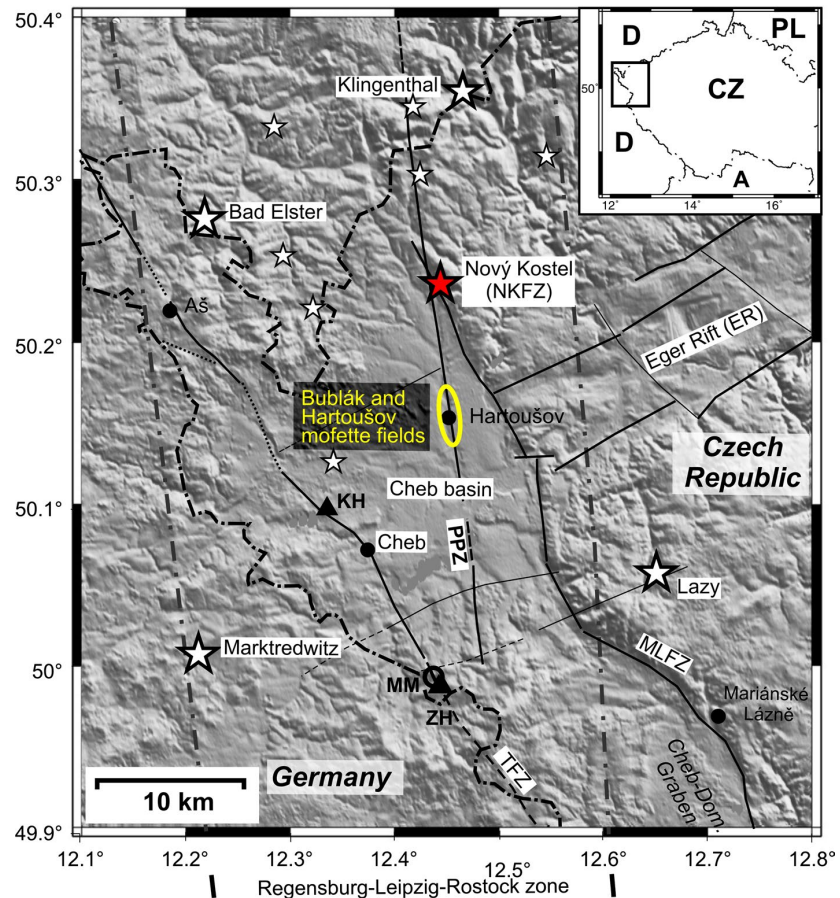
($^3\text{He}/^4\text{He}$, $\delta^{13}\text{C}_{\text{CO}_2}$) composition of free gas at mofettes and mineral springs in the western ER and provided a first estimation of the vent-bound CO_2 emission rate. Three different degassing centres could be distinguished in the region: Karlovy Vary, Mariánské Lázně and surroundings, and the Tertiary Cheb Basin. They showed a similar $\delta^{13}\text{C}_{\text{CO}_2}$ signature between -4 and -2 ‰, but different levels of mantle-derived helium: Karlovy Vary (≈ 2.4 Ra), Mariánské Lázně (≈ 4.6 Ra) and Cheb Basin (≈ 6 Ra), which covers the range of the subcontinental lithospheric mantle (SCLM) according to Gautheron et al. (2005). $^3\text{He}/^4\text{He} > 6$ Ra reflects a high percentage of mantle-derived helium and little mixing with helium from the crust (Bräuer et al. 2008). Several time series of gas isotope measurements of N, He and C indicated that an active hidden magmatic process has been ongoing since ca. 2000 beneath the eastern part of the Cheb Basin (Bräuer et al. 2005, 2008, 2009, 2011, 2014; Fischer et al. 2014). The increase in mantle-derived helium is both temporally and spatially progressive. Increases were first observed at the Bublák mofette field (BMF), then at Hartoušov, which is just about 1.5 km south of Bublák, along the PPZ, and subsequently along the MLFZ at Dolní Častkov (Bräuer et al. 2009). In addition, a 3-month-lasting increase of mantle-derived helium up to 6.3 Ra was observed at the Bublák mofette in March–May 2006. From the high gas flux and high $^3\text{He}/^4\text{He}$ ratios (covering the SCLM range), the mofette fields surrounding Bublák and Hartoušov appear to act as deep-seated fluid migration zones along the PPZ (Bräuer et al. 2011). The distinct increase in the $^3\text{He}/^4\text{He}$ ratios over a 3-month period at the monitoring locations was interpreted as an indication of a dike intrusion with fresh magma from the deeper reservoir probably located in the lithospheric mantle at ca. 65 km depth (Bräuer et al. 2009, 2011). Geissler et al. (2005) argue that all these observations are somehow interrelated by an active zone of mantle melting and magmatic underplating associated with recent extensional tectonics.

One of the open questions regarding the understanding of geodynamics—especially triggering mechanisms of earthquake swarms—is a profound knowledge of the magma intrusion/fluid migration in the earth's lithosphere via dikes, conduits or faults (Caine et al. 1996). However, since the terrestrial CO_2 conduits—unlike their marine hydrocarbon counterparts (Loseth et al. 2009)—are hard to detect by seismic profiling, information on the evolution, geometry—including permeability—and the constancy of the small-scale, terrestrial degassing structures in space and time is scarce.

According to the results of former investigations (Flechsigt et al. 2008; Kämpf et al. 2013), this degassing area represents an excellent example for studying the relationship between the emission of fluids from the lithospheric mantle and near-surface structural and lithological controls. In

¹ <http://www.ig.cas.cz/en/structure/observatories/west-bohemia-seismic-network-webnet/earthquakes-west-bohemia-2014>. Access on June 2nd, 2014.

Fig. 1 Schematic map with main fault zones, Quaternary volcanoes and the location of the survey site in the western Eger Rift zone (yellow ellipse). *MLFZ* Mariánské Lázně fault zone, *PPZ* Počátky-Plesná fault zone, *TFZ* Tachov fault zone, *ZH* Železná hůrka scoria cone, *MM* Mýtina maar, *KH* Komorní hůrka scoria cone. Large white stars mark the most active earthquake swarm areas, smaller ones mark areas with less activity. Modified after Ibs-von Seht et al. (2008), Mrlina et al. (2009), Horálek and Fischer (2010), Fischer et al. (2014)



order to extend the geophysical investigation in the CO₂ degassing and fault zone area and to correlate the subsurface information to the CO₂ study, a combination of resistivity surveys and microgravity measurements was chosen. Multidisciplinary approaches of combined gas studies and geophysical surveys have been carried out mainly in volcanically active areas (Carapezza et al. 2009; Finizola et al. 2006, 2009, 2010; Revil et al. 2008, 2011). Integrated studies are also known in case of degassing structures caused by thermometamorphic alteration of carbonate units (Arts et al. 2009; Pettinelli et al. 2008, 2010). Byrdina et al. (2009) have applied CO₂, radon, SP mapping, as well as ERT measurements in a non-volcanic area in a tectonically active zone in central Nepal, characterised by an intense microseismicity and deep CO₂ emissions. Thus, the application and combination of different geological, geochemical and geophysical methods are well suited in the research of diffuse degassing structures (DDS, Chiodini et al. (2001)).

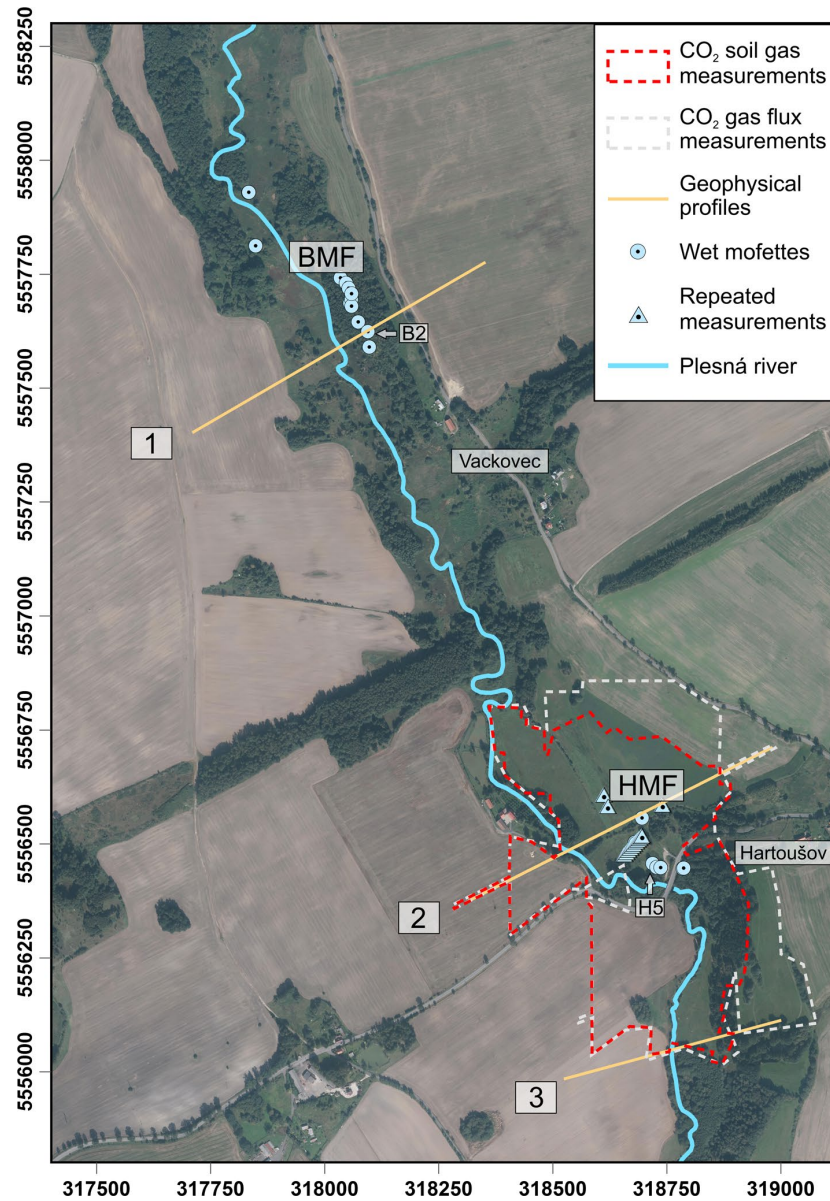
Based on preliminary investigations of Flechsig et al. (2008) and Kämpf et al. (2013), the aim of the presented study was to localise and quantify the mantle-derived

CO₂ emission and to evaluate the geological and tectonic background of the gas pathways inside diffuse degassing structures using different geoscientific methods, such as CO₂ soil gas and gas flow measurements, electric resistivity tomography and gravimetry. This combination provides a meaningful approach in the observation of near-surface fluid transport and migration ways, useful for the detection and monitoring along active faults.

Geological and geophysical setting

The area under investigation is located in the northeastern Cheb Basin (Fig. 1, inset map) in the Bohemian Massif. There, the dominating rocks are rock sequences from Upper Cambrian to Ordovician age and areas with Late Variscan intrusions dominated by granites. The Cheb Basin is a small intra-continental basin and lies within the western part of the ER. The crystalline basement of the Cheb Basin consists of muscovite granites of the Smrčiny/Fichtelgebirge Pluton (Hecht et al. 1997) and

Fig. 2 Aerial view of the study area with locations of CO₂ soil gas, CO₂ gas flux, geoelectrical and gravimetric surveys. BMF is the Bublák mofette field, HMF is the Hartoušov mofette field. B2 and H5 are isotope sample locations (see inset in Fig. 10). All coordinates in WGS84/UTM zone 33



crystalline schists of the Saxothuringian Zone of the Variscan Orogene (muscovite–biotite mica-schists of phyllitic appearance) (Fiala and Vejnar 2004). The Cheb Basin, located in the intersection of the ENE-trending ER and the N–S-trending Regensburg–Leipzig–Rostock Zone (RLRZ, Fig. 1), was formed during the Late Tertiary and Quaternary as a result of the reactivation of Hercynian faults and/or separated microplates, present within the basement (Bankwitz et al. 2003b; Mičoch 2003; Babuška and Plomerová 2008). The NW-trending pre-Neogene

MLFZ forms the eastern boundary of the Cheb Basin and is marked by a 50- to 100-m-high escarpment that can be traced along strike for over 100 km. The basin was filled with fluvial and lacustrine sediments (≤ 300 m thick) (Špicáková et al. 2000; Mičoch and Skácelová 2009; Rojčík et al. 2010).

Locally, Eocene clastics were first deposited and followed by Oligocene–Middle Miocene volcanoclastics, sands, clays and lignites. After a period of erosion in the Late Pliocene fluvial gravel, sand and kaolinitic clay

were deposited followed by Pleistocene sand and gravel. Holocene sand, silt and peat were the prevailing deposits in river valleys (Malkovský 1987; Špicáková et al. 2000; Flechsig et al. 2008, 2010; Rojík et al. 2010). The investigation area, the Hartoušov mofette field (HMF), is located in the flood plain of the Plesná river, at the eastern part of the Cheb Basin. HMF stretches approximately 500 m in NW direction and 350 m in NNW direction, (Fig. 2, all coordinates in the article are WGS84/UTM zone 33). According to Flechsig et al. (2008), the uppermost sediment units in the central part of HMF up to 10 m depth can be subdivided into three lithological units: (1) a basal fine-grained unit consisting predominantly of clay, silty clay and silt (age: Pliocene, thickness: >3 m), overlain by (2) a coarse-grained unit with sharp grain-size contrast dominated by sand and gravel (age: Pleistocene, thickness: ≈3–4.5 m) and (3) an uppermost, rather heterogeneous unit, consisting of clay, silt, sand and peat (age: Holocene, thickness: 2–3.6 m).

According to Ulrych (2011) and Krüger et al. (2013), three periods of volcanic activity, including maar-diatreme volcanism for the northern and western part of the Bohemian Massif, can be defined: (1) pre-rift period (Later Cretaceous to Mid Eocene, 79–49 Ma), (2) syn-rift period (Mid Eocene to Mid Miocene, 42–16 Ma) and (3) late-rift period (16–0.26 Ma). At the Quaternary volcanic centres close to the Cheb Basin (see Fig. 1), two main stages of volcanic activity are recognised: explosive, phreatomagmatic initial stage and eruptive final stage with lava fountains and lava flows. Age determinations using different methods indicate that the Quaternary volcanic activities occurred in the Mid Pleistocene 0.78–0.12 Ma ago (Mrlina et al. 2009). $^{230}\text{Th}/^{234}\text{U}$ determinations of Karlovy Vary travertine deposits cover a wide time span ranging between 0.23 Ma BP and the present (Vylita et al. 2007) and give evidence that magmatic CO_2 escape dates back to about 0.23 Ma (Fischer et al. 2014).

As a first local comparative geoelectric, soil gas and sedimentological study of a magmatic CO_2 degassing vent in the Hartoušov mofette field, near-surface structures had been investigated by Flechsig et al. (2008). The investigations reveal structural and substantial features that are thought to be directly or indirectly related to CO_2 flow (anomalies of electrical resistivity and self-potential, sediment properties). In the same area Schütze et al. (2012, 2013), Sauer et al. (2013) and Sandig et al. (2014) tested several diagnostic monitoring tools at different scales to monitor processes taking place during CO_2 migration and seepage. Flechsig et al. (2010) also featured the application of geoelectric methods along the PPZ at “U Mostku”, just a few kilometres to the north of the Hartoušov mofette area and across the assumed course of the MLFZ to identify characteristic features of these faults.

Methods

CO_2 gas flux and CO_2 soil gas concentration

Field measurements

In the HMF, detailed mappings of the CO_2 content in the soil and the CO_2 gas flux at the surface were carried out to define the extent of diffuse degassing structures (Chiodini et al. 2001) and the amount of ejected CO_2 in soil gas. These methods have been successfully used in other volcanically and non-volcanically active areas, such as Bergfeld et al. (2001), Chiodini and Frondini (2001), Chiodini et al. (2010), Finizola et al. (2006, 2009), Lewicki et al. (2012), Schütze et al. (2012). The database used in this article comprises 3,003 measurements of the CO_2 content in the soil gas over an area of 310,000 m^2 and 3,770 measurements of the CO_2 gas flux [including the database of Kämpf et al. (2013)] over an area of 352,000 m^2 . The CO_2 gas fluxes (762 measurements) and contents in soil (682 measurements) from Kämpf et al. (2013) were measured between 2007 and 2008, while the other measurements were carried out in 2009 and between 2012 and 2013. In all three field campaigns, measurements were carried out between April and October.

Measurements of the content of CO_2 soil gas were performed with an infrared gas analyser BM2000 (Ansyco/Germany) at depths of 0.6–0.8 m in order to avoid atmospheric influence. Saßmannshausen (2010) and Rennert et al. (2011, Tab.1) show that the partial pressure of CO_2 can significantly change from the surface to 0.6 m depth. In dry summer seasons, it was possible to perform measurements at these depths most of the time even in areas where the ground water level is high during rainy seasons. The BM2000 gas analyser's accuracy is 0.5 % for up to 5 % CO_2 , 1.0 % between 5 and 15 % CO_2 and 3 % for more than 15 % CO_2 , as given by the manufacturer. However, we experienced larger variations in our measurements after carrying out additional repeated measurements at the same spot. This is in agreement with the findings of Kämpf et al. (2013), who report variations from 15 to 50 % from the mean for concentrations of less than 20 %, whereas the deviation was at about 5 % for higher CO_2 soil concentrations.

The rate of discharge at surface was measured using the closed-chamber method; an easy and fast way of estimating the discharge rate of CO_2 as shown in numerous examples in volcanically (Chiodini and Frondini 2001; Carapezza et al. 2009; Inguaggiato et al. 2012) and non-volcanically active degassing zones (Bergfeld et al. 2001, 2006; Byrdina et al. 2009; Chiodini et al. 2010; Lewicki et al. 2012). For this purpose, a West Systems (Italy) device was used. The device uses a LiCOR 820 infrared gas

Fig. 3 Example of the change in the gas flux in $10^3 \text{ g m}^{-2} \text{ day}^{-1}$ and the CO_2 content in soil gas in % around one dry CO_2 vent in the Hartoušov mofette area (DDS), measured on 29 June 2012. The scheme illustrates that the measured gas flux varies within decimetres and centimetres and depends on the placement of the gas flux chamber

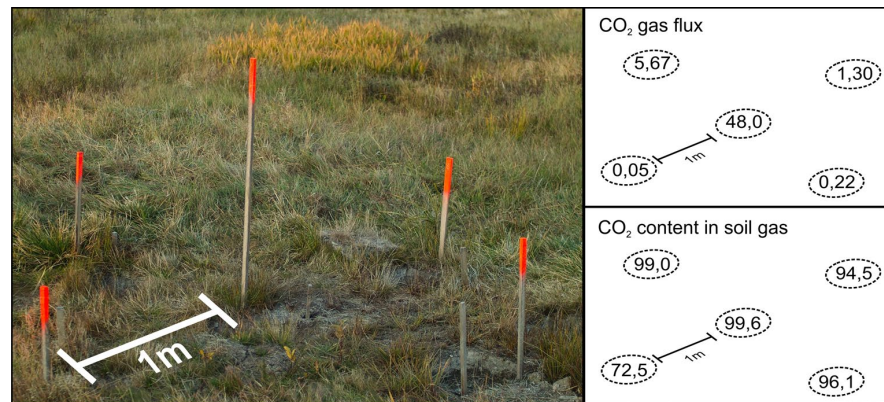
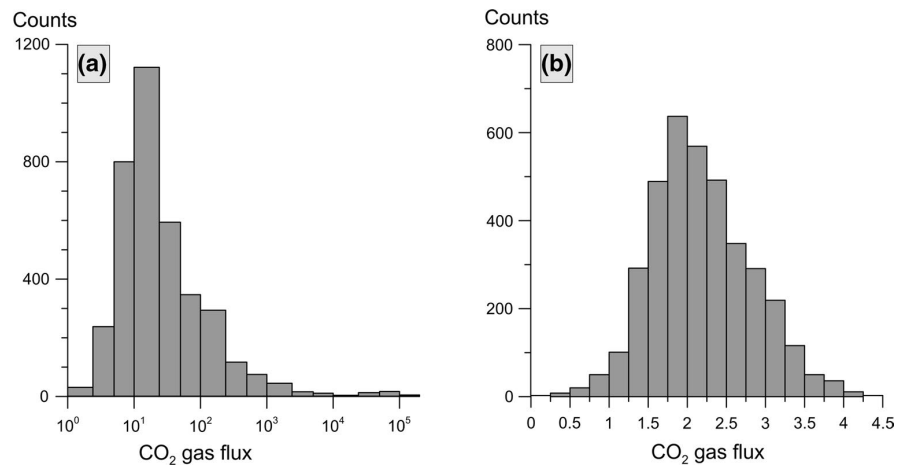


Fig. 4 Histograms of the distribution of 3,770 CO_2 gas flux measurements in the Hartoušov mofette field. **a** Untransformed distribution of the observations with gas fluxes on a logarithmic scale (gas flux in $\text{g m}^{-2} \text{ day}^{-1}$). Even on this logarithmic scale, the distribution is strongly positively skewed. **b** Gas fluxes after the transformation using the Box-Cox transformation with $\lambda = -0.23$

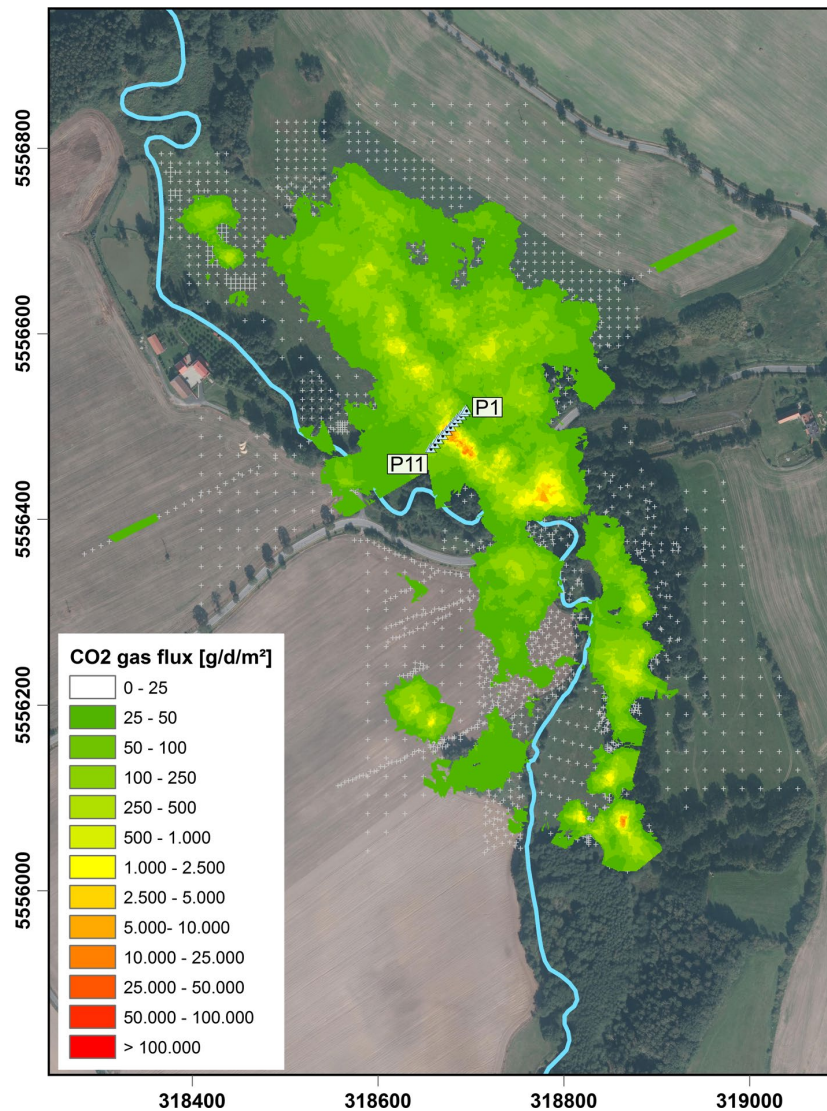


analyser for CO_2 discharge quantification, and the usage of two accumulation chambers ($\text{VA} = 2,756 \times 10^{-3} \text{ m}^3$ and $\text{VB} = 6,186 \times 10^{-3} \text{ m}^3$) allows for the high-accuracy measurements of gas fluxes up to $600 \text{ mol m}^{-2} \text{ day}^{-1}$ ($\approx 26.5 \times 10^3 \text{ kg m}^{-2} \text{ day}^{-1}$), according to the manufacturer. Within this range, the device has an accuracy of 4 %, higher fluxes increase the uncertainty as the chamber is saturated faster. Air temperature and barometric pressure were recorded and used to calculate the actual gas flux. Fifteen to twenty centimetres of soil coverage was removed several hours before measurement. This way, most of the surface vegetation was removed to establish more equal conditions for the gas flux mapping and to remove most of the influence of biogenic CO_2 input.

Point-to-point spacings varied from $20 \text{ m} \times 20 \text{ m}$ in areas with little CO_2 content soil gas and low fluxes to finer measuring grids ($10 \text{ m} \times 10 \text{ m}$, $5 \text{ m} \times 5 \text{ m}$ and finer spacings below $<1 \text{ m}$) in areas of strong degassing. This procedure accounted for a fast mapping but also aimed at encompassing gas chimneys. Kämpf et al. (2013) claimed that $>95 \%$ of the total emitted CO_2 can be attributed to CO_2 vents in the

Hartoušov area, although their diameter is often $<1 \text{ m}$ at the surface (Fig. 3). Detailed measurements around the gas vents were necessary due to the fact that the amount of CO_2 discharged by single vents can be over- or underestimated if the sampling position is shifted only by a few decimetres, which leads to an incorrect evaluation of the CO_2 balance for the area of investigation. This feature was already mentioned in Chiodini et al. (1998), Carapezza and Granieri (2004), who claimed that degassing occurs along microfractures and that consecutive flooding and drying can lead to a different spatial distribution of these microfractures, especially in areas of advanced argillaceous alteration. This is true in our area of interest, the Plesná valley, where clays or clayey sediments dominate as described in drills from GEOFOND (Czech Geological Survey, Fig. 9) and Flechsig et al. (2008). As this vent-bound degassing was exceeding the high-accuracy limitations of our gas flux metre, high gas fluxes bear higher uncertainties: the highest gas fluxes would fill the accumulation chamber within 5 s and the actual flux can only be approximated. In these locations, several measurements were taken to at least partly compensate this effect (Fig. 4).

Fig. 5 Quantified gas flux for 1 m² after interpolation of 3,770 measuring points in the Hartoušov mofette field using trans-Gaussian kriging. White dots indicate the measuring position; small triangles mark the locations of the repeated measurement stations (Table 1). Gas fluxes below 25 g m⁻² day⁻¹ are not displayed. *P1* and *P11* mark the first and last station of the reference profile for repeated measurements (Table 1)



Repeated measurements were carried out along a NE–SW-striking profile perpendicular to the main degassing area in the HMF in 2012. The profile consisted of 11 stations (P1 to P11) with 5 m distance to each other (Fig. 5). P1 was located at E: 318694; N: 5556518 and P11 was located at E: 318656; N: 5556478. The location of the profile was chosen to encompass low-, medium- and strong-degassing spots. Sandig et al. (2014) used also repeated measurements to evaluate the CO₂ degassing behaviour (analysing the gas composition) at the HMF but used a GPS tool with an accuracy of ±5 m as a reference and, thus, different sample spots each time. The repetition of measurements on fixed locations helps evaluating the consistency of the gas flux over the different field campaigns. Hence,

we established fixed sample stations in our measurements. These measurements were carried out in the morning and late afternoon (Table 1). The gas flux was not measured after rain events to keep the alteration of gas paths within the topmost centimetres as little as possible.

Data analysis

For the quantification of the totally discharged CO₂ in the HMF, we applied different, statistical methods using the geostatistical analysis tools in ArcGis: arithmetic mean, inverse distance weighting, radial basis function, ordinary kriging and trans-Gaussian kriging (utilizing ordinary kriging after data transformation using a power function).

Table 1 Results of repetition measurements of CO₂ gas fluxes during field campaigns along a profile consisting of 11 stations across the main mofette in the HMF in 2012

Date	P1	P2	P3	P4	P5	P6	P7	P8	P9	P10	P11	Sum P1–P11
23/06 PM	15	12	7	72	2,119	27,860	582	12	8	8	49	30,744
24/06 AM	22	14	5	108	2,480	27,562	549	15	11	11	53	30,829
24/06 PM	9	7	6	73	888	19,490	490	8	8	11	61	21,050
25/06 AM	12	7	6	51	1,526	16,792	403	10	8	12	55	18,881
26/06 AM	8	7	5	78	1,659	20,110	412	7	9	12	74	22,380
26/06 PM	5	7	7	67	1,707	29,104	415	9	6	10	60	31,396
27/06 AM	12	9	7	113	2,237	24,268	481	15	10	12	84	27,247
27/06 PM	10	9	5	98	1,683	21,694	437	7	8	11	78	24,039
28/06 AM	18	12	7	129	2,091	32,783	457	14	8	12	73	35,606
29/06 AM	30	13	7	72	1,297	26,542	430	13	12	14	87	28,517
28/08 AM	21	11	8	109	177	13,378	315	42	24	21	258	14,364
29/08 AM	23	7	12	167	1,507	15,335	301	55	30	25	226	17,688
30/08 AM	17	10	3	91	1,733	54,383	334	50	31	20	267	56,939
31/08 AM	10	4	6	64	708	37,298	277	13	17	9	42	38,449
01/09 AM	18	3	3	58	1,007	33,196	255	16	19	7	19	34,602
02/09 AM	18	8	6	103	1,019	17,482	307	23	20	10	23	19,019
08/10 AM	23	3	3	62	388	39,235	26	8	16	3	8	39,774
11/10 AM	19	5	3	33	1,190	46,797	114	7	8	9	9	48,194
Mean	16.1	8.1	5.8	86.0	1,411.9	27,961.6	365.9	17.9	14.2	12.1	84.8	29,984.3
Standard deviation	6.5	3.2	2.1	32.0	635.1	11,152.1	141.9	14.9	7.9	5.2	80.3	11,122.9
Standard deviation (%)	40.1	39.7	36.6	37.3	45.0	39.9	38.8	83.4	55.7	42.9	94.7	37.1

All numbers are gas fluxes in $\text{g m}^{-2} \text{ day}^{-1}$ except for the percentage-based standard deviation. High variations of up to one order of magnitude in the measured gas flux occurred within the course of a day

Arithmetic mean The simplest method for estimations of the total CO₂ discharge in the area is the arithmetic mean. According to Gilbert (1987) and Lewicki et al. (2005), this method can, in the case of a normally distributed population, be used to estimate the amount of ejected CO₂ after calculating the arithmetic mean and standard deviation for 1 m² and multiplying this by the size of area. This method, however, is very susceptible to few very high or low values.

Radial basis function The radial basis function method is an exact interpolator, which means that the interpolated surface has to go through every measured sample value. The method calculates the surface by combining circular hyperboloids, where each hyperboloid is centred on a sampled unit (Lewicki et al. 2005). The continuous surface created this way was then separated into parcels of 1 m², and the specific, calculated gas flux was attributed to each parcel. The closer data points are together, the more weight they have in the interpolation process. Radial basis functions are also applicable to large datasets. However, they are inappropriate when large changes occur within short distance as over- and underestimations will occur in the process.

Kriging Kriging is based on interpolation between sampled points using spatial covariance values. Observations closer to each other are given more weight in the process than observations further away. In this case, we used ordinary kriging, as it is an unbiased estimator that minimises variations in the estimations. Ordinary kriging also often is used in soil science and CO₂ gas studies (Bergfeld et al. 2001; Rogie et al. 2001; Lewicki et al. 2012; De Bortoli Teixeira et al. 2011). Kriging in general underestimates maxima and overestimates minima in the interpolation process (averaging). After the interpolation, the surface was split into 1 m² parcels, and the calculated gas flux was attributed to each parcel.

Trans-Gaussian kriging Most geostatistical approaches are based on the assumption of a Gaussian distribution of the data. This means that the skewness of the dataset should be exactly or close to zero. In our case, this was not the case as it was strongly, positively skewed (see “CO₂ gas flux and CO₂ soil gas concentration” section). Transformation of the dataset before geostatistical analysis and a consecutive back transformation afterwards can be performed to get normally distributed data. A fast way to achieve this is to transform the original data by using a power transform, such as the

Box–Cox transformation [e.g. Box and Cox (1964); Sakia (1992)], where the observed dataset $Z(s)$ is transformed to a normally distributed dataset $Y(s)$ using a suitable parameter λ . The Box–Cox transformation is:

$$Y(s) = \left(Z(s)^\lambda - 1 \right) \lambda^{-1} \quad \text{for } \lambda \neq 0$$

A special case is the so-called log-transformation in case when $\lambda = 0$. In our case, using $\lambda = -0.23$ yielded the best results. After the transformation, ordinary kriging was applied to the transformed dataset (see above). This process is also known as trans-Gaussian kriging.

Geophysical investigations: geoelectrical and gravity measurements

Geoelectrical methods are often the first choice for the investigation of near-surface sedimentary structures and processes within these because of their sensitivity to porosity, water and gas saturation of the pore space, salinity and temperature of the pore fluids expressed by the conductivity of the pore fluid and the presence of clay minerals. However, the same factors cause difficulties in the unequivocal interpretation of electrical resistivity images. Complementary information to electrical resistivity measurements is essential to improve their interpretation and is provided in this study by microgravity, CO_2 measurements, and the sedimentological results of drillings [Flechsigt et al. 2008, GEOFOND (Czech Geological Survey)]. Modern electrical imaging techniques (or electrical resistivity tomography/ERT) are based on the concept of remapping the same profile with a wide range of electrode spacings and involved both the field measurements by combining sounding and profiling techniques and the algorithms for data inversion. ERT has proven to be reliable for providing realistic images of the spatial distribution of electrical resistivity in the subsurface and has successfully been applied to a wide variety of problems such as environmental survey (Clifford and Binley 2010), characterization of fault zones (Nguyen et al. 2007; Wise et al. 2003; Suski et al. 2010) and geothermal regions (Finizola et al. 2006, 2009, 2010; Revil et al. 2008, 2011). The geoelectrical investigation aimed at detecting characteristic structures, which could be related to CO_2 ascent and the possible evidence of the PPZ in the resistivity distribution.

The aim of microgravity measurement was to determine whether the degassing zones in the Cheb Basin exhibit some mass deficit due to the degassing process. We decided to perform microgravity measurements that could detect zones of mass deficit or decreased rock density related to these phenomena. It may be expected that the gas emission would enlarge the pores in soft near subsurface sediments, as well as contribute to widening of the gas channelling

fractures. Another hypothesis is that uprising fluids are capable of transporting sediments (Flechsigt et al. 2008) which leads to a lateral deformation and thus leads to a deformation of the local gravity field. To our knowledge, the application of gravity measurements for research purposes on volcanically non-active, dry degassing sites has not been done before.

Electrical resistivity tomography

The geoelectrical research, which involved the survey of three profiles perpendicular to the assumed course of the PPZ as postulated by Bankwitz et al. (2003b) and the Plesná valley with its diffuse degassing sites of different degassing rates (HMF and BMF), was carried out between April and June 2012 (Fig. 2). They cross the river Plesná valley and the assumed course of the PPZ from W to E with fault scarps of approximately 15–20 m, running roughly parallel to the river. The valley slopes are asymmetric: flat in the west and steeper in the east. Profile No. 1 crosses the PPZ in the vicinity of the Bublák degassing area with several vents of high degassing rates, No. 2 crosses a meadow and fallow land with flatter slopes than on profiles 1 and 3 and lateral expanded degassing zones, and profile No. 3 crosses the valley 500 m south of profile 2, where small, dispersed CO_2 vents were discovered. Using a multi-electrode-device GeoTom (Geolog Fuß and Hepp, Germany), multi-core cables and conventional steel electrodes, the measurement was taken with the Wenner-alpha ($C_1 P_1 P_2 C_2$) and Wenner-beta ($C_1 C_2 P_1 P_2$) configuration, where the electrical potential difference caused by an electrical current, which is injected at electrodes $C_1 C_2$, is measured at $P_1 P_2$. The electrode spacing was 5 m. The used electrode arrays are different in their horizontal and vertical resolution, penetration depth and signal-to-noise ratio. The former has advantage in the signal-to-noise ratio even for measurements with larger offsets, whereas the latter has a higher sensitivity to lateral variations in the resistivity. The lateral position was determined in the field using a Garmin GPS with a precision of ± 3 m.

Different combinations of current and potential pairs of electrodes with increasing separation are measured and result in the combination of sounding and profiling sections with a maximum investigation depth of approximately 80–90 m. The stacking routine of the measurement device ensures a high data quality. In general, the measured values had a standard deviation of less 5 %. The resistivity field data (resistance values obtained from potential measurements and injected current and related geometry information depending on electrode spacing) were inverted in a 2D subsurface model of resistivity distribution. The inversion code DC2DInvRes [Th. Günther, www.resistivity.net and Günther et al. (2006)] which uses a nonlinear

smoothness-constrained least-squares technique to calculate the resistivity of the model blocks and a fast finite-difference operator to generate apparent resistivity values was used to determine a model that adjusted the measured data optimally. An optimization process tries to reduce iteratively the difference between the calculated and measured apparent resistivity values. The per cent error, considering N points of measurements was calculated as a data fit indicator. The final model was obtained using a combined inversion of data from Wenner-alpha and Wenner-beta configurations.

Gravity

A LaCoste and Romberg D-188 gravimeter was used for the gravity surveys after marking each station with wooden pegs. The standard error was about 0.011 mGal in swampy areas (e.g. BMF), while on hard field and hard meadow surface, the error was only 0.004 mGal. The elevation was measured by levelling, while end points were also tied to the national geodetic system by RTK GPS observations, using Trimble hardware. Some points in forest were observed by total station. The spacing between each measurement station was 5 m in the central zones and higher (10–40 m) at the ends of each profile. The accuracy of all these measurements was better than 3 cm in vertical component. Terrain corrections were calculated from an accurate DTM (1 m resolution) to the distance of 2.5 km, and the outer part of the correction to 167 km from SRTM90 DTM. Anyway, there were almost no steep slopes in the area, so that terrain effects were properly compensated, except for the nearest surrounding of the river bed. Because the Plesná valley is part of the Cheb Basin, the reduction density of $2,300 \text{ kg m}^{-3}$ was applied in the formula for the Bouguer gravity anomaly. The regional trend was removed from the data. Different filtering techniques were applied to separate small-scale from large-scale signals. A high-pass filter with 40 m wavelength (“HP40”) was chosen to visualise the effect of the degassing zone. Additionally, a filter with 100 m wavelength and smoothing by trends of the 9th order (“Hp100-Pol9”) was chosen to visualise the change in the overall subsurface geology.

Results

CO₂ gas flux and CO₂ soil gas concentration

Figures 5 and 6 show linear distributions of CO₂ gas efflux and concentrations. In the southern part of the area, the degassing regime is N–S oriented, while in the northern part, the orientation changes to NNE–SSW-oriented degassing. The N–S-oriented degassing occurs in a spatially

narrow area and is lower than in the NW–SE-oriented degassing part, where the emission is stronger and also occurs over a larger area. Furthermore, strong degassing occurs near the bridge/road which crosses the Hartoušov mofette field. Although this could be a naturally occurring phenomenon, it is most likely linked to a disturbance of the natural degassing regime due to the construction works.

The distribution of the measured gas fluxes can be seen in Fig. 4. Measured gas fluxes varied from $<10 \text{ g m}^{-2} \text{ day}^{-1}$ at the margin of the mofette field up to $125,000 \text{ g m}^{-2} \text{ day}^{-1}$ in the centre of CO₂ vents. Most of the measured gas fluxes in the HMF were in the range of $1\text{--}100 \text{ g m}^{-2} \text{ day}^{-1}$. Of the 3,770 measurements in the database, about 96 % of the totally discharged CO₂ could be related to 10 % of the measurements (377 values, $2.53 \times 10^6 \text{ g day}^{-1}$) and 84 % of the total CO₂ could be related to only 37 spots, which is ≈ 1 % of all measurements. On the other hand, 3,172 of the 3,770 measurements (≈ 84 %) could be related to gas fluxes $<100 \text{ g m}^{-2} \text{ day}^{-1}$ revealing the non-Gaussian distribution of the measured gas fluxes with a highly positive skewness.

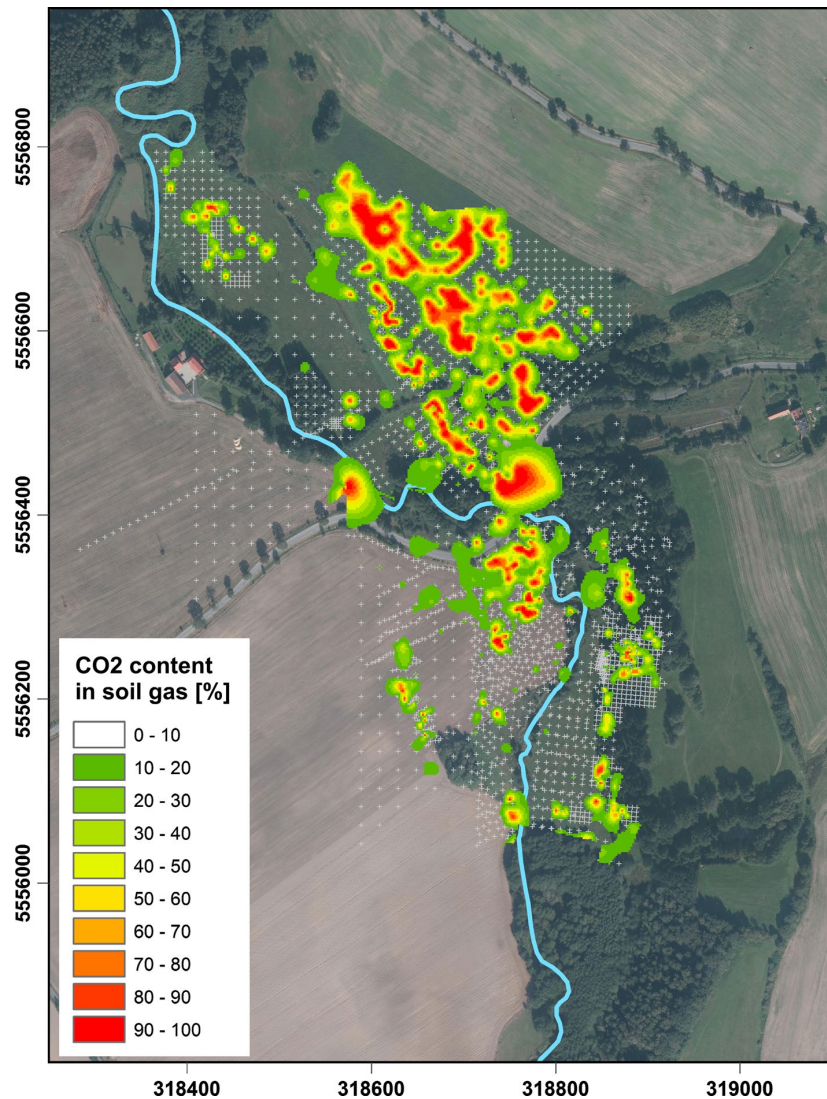
Table 1 shows the results from the repetition measurements in 2012. Variations in the measured gas fluxes could be observed within the course of a day: gas fluxes measured after several hours can differ significantly from another and be higher/lower by up to one order of magnitude for several spots. On average, standard deviations of nearly 40 % from the mean value were noticed along the profile. Considering these large variations is crucial when trying to quantify the amount of daily discharged CO₂. In most gas flux studies, standard deviations and variations are not shown or they are presented but not discussed in detail. Particularly, at heavily degassing sites, one-time measurements might lead to serious misinterpretations of this site’s CO₂ discharge. The high deviations in the gas flux occur in high- and low-degassing areas.

Calculations of the gas flux within the HMF lead to varying results due to the heavily positively skewed data. All methods have in common that they insufficiently reproduce the impact of the spatially narrow vents within the wide, less-degassing surroundings in the HMF. The non-Gaussian distribution of the degassing leads to very high standard deviations in all methods. The total sums are calculated for each cell of 1 m^2 in the area (347,872 cells).

Arithmetic mean The calculated arithmetic mean and standard deviation for all gas flux measurements results in an average CO₂ gas flux of $697.0 \text{ g m}^{-2} \text{ day}^{-1}$ and a standard deviation of $6,576 \text{ g m}^{-2} \text{ day}^{-1}$. This leads to a calculation of the whole area of $242 \times 10^6 \text{ g m}^{-2} \text{ day}^{-1}$.

Radial basis function Calculations based on the radial basis function result in an average value of $279.9 \text{ g m}^{-2} \text{ day}^{-1}$ with a standard deviation of $1,510 \text{ g m}^{-2} \text{ day}^{-1}$. The overall estimation of the gas flux in the area of the HMF was $97.4 \times 10^6 \text{ g m}^{-2} \text{ day}^{-1}$.

Fig. 6 Distribution of CO₂ content in soil gas in 0.6–0.8 m depth in the Hartoušov mofette field after interpolation of 3,003 measurements. *White dots* indicate the measuring position. CO₂ contents below 10 % are displayed as hollow

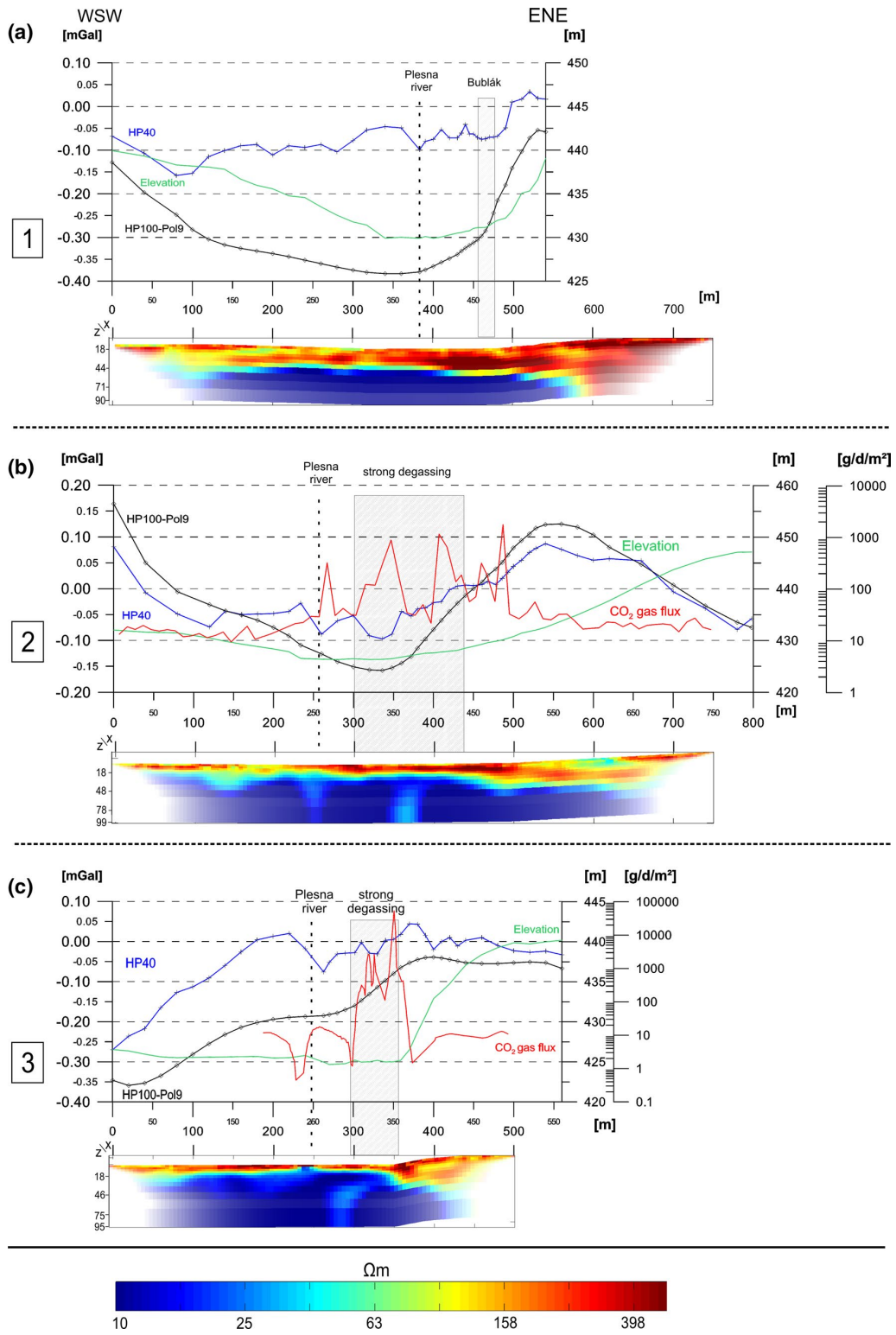


Kriging Geostatistical estimations of the CO₂ gas flux using ordinary kriging results in an average value of 250.7 g m⁻² day⁻¹ and a standard deviation of 2,400 g m⁻² day⁻¹. This method estimated 87.2 × 10⁶ g m⁻² day⁻¹ as the area's daily gas discharge rate.

Trans-Gaussian kriging The lowest standard deviations were achieved after transformation of the dataset and consecutive ordinary kriging. This procedure resulted in an average value of 65.2 g m⁻² day⁻¹ and a standard deviation of 480 g m⁻² day⁻¹. 22.7 × 10⁶ g m⁻² day⁻¹ were calculated as the daily CO₂ gas flux rate for the HMF.

In Fig. 6, results from the CO₂ content at depths of 0.6–0.8 m reveal that the soil contains high amounts of CO₂ over large areas, which replaces free oxygen in areas with

high CO₂ fluxes. Across the mofette field, some areas feature almost complete absence of O₂ at depths below 0.5 m. Saßmannshausen (2010) and Rennert et al. (2011) already showed that in general the CO₂/O₂ ratio decreases towards shallower depths, which is probably linked to atmospheric influence. Annunziatellis et al. (2008, Fig. 7) present a comparison of their CO₂ flux and concentration measurements. In general, high concentrations are found where high gas fluxes are measured, implying that CO₂ vents supply their surrounding with CO₂ and replace O₂ in pores. However, they do not present a direct proportionality between flux and concentration and also cut out fluxes higher than 500 g m⁻² day⁻¹. In the HMF, direct correlations between gas flux and CO₂ content in soil are impossible: while gas flux measurements take place at depths of 15–20 cm after



◀ **Fig. 7** Results of the ERT and relative gravity along the profiles 1–3 in Fig. 2 after filtering. The tomographies are inverted by using Wenner-alpha and Wenner-beta simultaneously. “HP40” is the gravity after applying a 40-m-wavelength filter on the measured Bouguer gravity. “Hp100-Pol9” is the gravity after the application of a 100-m-wavelength filter and a polynomial trend of 9th order. Profiles 2 and 3 also show CO₂ gas flux for comparison. Distinct local gravity lows correspond to high CO₂ flux and increased electric resistivity

removal of the topmost organic layer and require the soil to be dried out, the CO₂ content is measured at depths of 0.6–0.8 m. Within these few decimetres, the CO₂ content and gas flux change significantly (Rennert et al. 2011). The argillaceous composition of the soil and the high, but varying ground water level in the HMF lead to highly variable properties of the soil. High ground water levels lead to water saturation of pores and thus a channel-like degassing, while the first decimetres of soil are usually drier. This leads to open pore space and microfractures which promote rather diffuse degassing. Direct comparisons of CO₂ gas flux and concentration can only be accomplished if the gas flux measurements take place before the soil gas measurement drilling penetrates the exact same position and creates artificial migration paths for ascending CO₂.

Geophysical investigations: geoelectrical and gravity measurements

Geoelectrics

ERT experiments resulted in three profiles, shown in Fig. 2. The inversion results can be seen in Fig. 7a–c. The inversion of the ERT data along the profiles resulted in models with resistivity values between 5 and 1,000 Ohm, the latter appear locally in the near subsurface. To ensure a uniform representation, the resistivity distributions are shown between 10 and 500 Ohm. Generally, on profiles 2 and 3 (Fig. 7b, c), low resistivities of <50 Ohm were measured in the Plesná river valley at depths greater than 5–20 m. These low resistivity are related to clayey sands, clays and mudstones, according to Flechsig et al. (2008) and stratigraphic descriptions of drill cores from GEOFOND drills (drill SA-30/ID 103141, depth: 93 m, E: 3188716, N: 5556349 and drill 1H-31B/ID, depth: 30 m, E: 318713 N: 5556543). This unit is covered by a layer of higher resistivity (>150 Ohm) of 10–20 m, which can be related to sand, gravel and fluvial sediments in general. The eastern flanks of the valley (morphological steps of the PPZ) are also characterised by increased resistivities (>150 Ohm) and a significant thickening of this high-resistivity layer to more than 40 m. This layer’s resistivity is notably higher in areas where the strongest degassing occurs at surface. The resistivity distribution along profile No. 1 (Bublák degassing area, Fig. 7a) is slightly different compared to profiles 2 and 3.

An increase of the thickness of the topmost high-resistivity layer from 30 to 40 m and a local increase in the resistivity from about 200 to 400 Ohm around the Bublák mofette (profile 1 at 430–480 m) can be observed. In areas of strong surface CO₂ degassing, anomalies in the otherwise higher conductive clayey unit can be measured at a depth of 30–50 m (profiles No. 2 and 3 in Fig. 7). These anomalies are characterised by a resistivity increase to 80–100 Ohm and are stretched slightly in vertical direction. Some resistivity features occur systematically on profiles. A layer of high resistivity (>150 Ohm) with increasing thickness of 10–20 to 30–40 m to the north is measured at surface. The thickness increases east of the scarp (step-like in the eastern parts of profiles). Below this layer, a spatially limited area of increased resistivity translates to a highly conductive, clayey unit.

Gravity

Figure 7 shows changes in gravity along the profiles 1–3 from Fig. 2. The HP100-Pol9 curve shows the general trend of the gravity from west to east (100 m wavelength filter), while HP40 shows more local gravity residuals after a 40-m-wavelength filter.

In the western parts, we assume a significantly different lithological block (Plesná river sediment depositions). This can be observed in all three profiles in the gravity curve HP100-Pol9. The profiles 2 and 3 show the gas fluxes along these profiles for comparison; gas measurements along profile 1 were impossible (swamp area). In all three profiles, the Plesná river has a small gravitational impact on the nearby stations. A cut-off of the Plesná river across profile 2 (Fig. 7b) at 340 m also effects the nearby stations.

The gravity survey along profile 1 reveals that a 50 negative anomaly of about –0.03 to –0.06 mGal can be identified around the Bublák mofette. This anomaly is significant, especially when considering the gravity effect of the nearby steep slope in the east. The Bublák mofette features concentrated degassing, is about 5 m in diameter and is filled with a water column with a height between 0.7 and 2 m. However, the gravity anomaly is much wider (440–470 m) and hints at a deeper source. This indicates that the gravity low is rather caused by an increase in fractures, pore size and/or pore infilling with gas rather than the pure water infilling of the Bublák mofette.

Gravity observations along profile 2 reveal good correlations between lower gravity and increased CO₂ release, especially at the section between 300 and 440 m where a very distinct local gravity minimum of about –0.06 mGal corresponds to high CO₂ gas flux. At the same place, we see also the minimum of the “longer wavelength” gravity residuals (HP100-Pol9). Neither of these two different gravity residual lows is located around the river at 260 m

(profile 2), where they could be expected due to assumed maximum thickness of alluvial sediments. Since degassing occurs over a wide area and not focused in single spots, it is likely that a wide area is affected by the CO₂. This was also observed in the ERT measurements (Fig. 7, profile 2).

Along profile 3, a more chaotic gravity signal can be observed between the river at 260 m and the steep slope at ca. 360 m. A small but distinct gravity low of about -0.03 to -0.04 mGal can be observed at 330–340 m (HP40) where strong (up to 3×10^4 g m⁻² day⁻¹) surface degassing occurs. This gravity low is located where surface degassing via seeps occurs and above the zone of increased electric resistivity. Similar effects can be observed in other areas where degassing occurs.

In general, both methods detect anomalies in their respective potential where strong surface degassing is measured. The resistivity is increased in the subsurface, whereas the gravity is lower compared to the surrounding. Whether this effect is related to an increase in pore volume or microchannels (Bankwitz et al. 2003b; Kämpf and Bankwitz 2005) and/or subsequent infilling by gas or an upward oriented sediment transport as described by Bankwitz et al. (2003b), Flechsig et al. (2008), is debatable. Gravity and geoelectrics both also detect a shift of the lithological blocks in the eastern part of the Plesná valley where a morphological step emerges. This eastern block is characterised by an increase in the electrical resistivity as well as in its density. The geoelectrical inversion also hints at an increase of the topmost layer towards the north.

Discussion

Methodical aspects

Although the gas fluxes in the Hartoušov area are low in most areas, small depressions within the area can accumulate significant and lethal amounts of carbon dioxide. Strongly degassing areas are often accompanied by a change in the vegetation, e.g. timothy grass (*Phleum pratense*) (Saßmannshausen 2010; Pfanz et al. 2007). In a previous study, Kämpf et al. (2013) tried to quantify the gas flux in the HMF. Kämpf et al. (2013, Tab.2) list $\approx 19,000$ l h⁻¹ ($\approx 893,760$ g day⁻¹ at standard conditions) as the daily amount of released CO₂ for the Bublák mofette (B2), unequally distributed over seven spots. Compared to our dataset, this means that some of the dry degassing spots in the Hartoušov area release amounts of CO₂ that are comparable to the Bublák mofette and that the amount of carbon dioxide release has previously been underestimated severely. Kämpf et al. (2013) also concluded that the daily CO₂ discharge rate is about 1.56×10^6 g m⁻² day⁻¹ for the measured area and that more than 95 % of the CO₂ is

released via gas vents. However, this approach does not account for the spatial distribution of the measurements. This method is very susceptible to positioning and, thus, just a spot check. Small measurement spacing in heavily degassing areas and wide spacings in less-degassing areas lead to an overestimation of the impact of CO₂ discharge in the HMF's CO₂ balance. Using their measurements and ours combined, we tried to get better insight into the tempo-spatial CO₂ degassing behaviour in the HMF using different geostatistical tools.

In general, all applied geostatistical methods used here are heavily influenced by the high skewness of the measured data. Heavily skewed (non-Gaussian distributed) datasets lead to standard deviations that are much higher than the mean. For this reason, estimations using the simple arithmetic mean resulted in the highest mean and standard deviation and are hence not suited for interpretations. The radial basis function method overestimates the highs and underestimates lows as it tries to fit the interpolation surface through all data points. Therefore, the calculated 97.4×10^6 g m⁻² day⁻¹ can be considered as an overestimation. The CO₂ calculated gas flux of 87.2×10^6 g m⁻² day⁻¹ using ordinary kriging is a little lower but kriging itself weights correlation between points based on the semivariogram which is built by looking at the spatial distribution of the data. This way, the degassing vents are too wide and have too much impact on the CO₂ balance. Due to the method, the surface is smoothed out to result in an overall low error and therefore does not represent anomalies properly (highly degassing vents in a rather low-degassing surrounding). The pre-interpolation transformation using the Box–Cox transformation resulted in the lowest standard deviation of all the methods. According to Saito and Goovaerts (2000), kriging results are better, when the data is normally distributed. 22.7×10^6 g m⁻² day⁻¹ is also the lowest estimation from all methods for the area's gas flux, but underestimates the impact of the degassing vents in the smoothing of the interpolation process.

The real, dry CO₂ discharge rate is supposed to be between 23 and ≈ 97 tons per day for an area of $\approx 350,000$ m² in the HMF. The high uncertainty might be attributed:

1. The CO₂ gas flux mapping was spread over different years and different times of each year. The gas flux is highly variable on different time scales (Table 1). The variations between datasets of multiple surveys in this area from different times can also be seen in Sandig et al. (2014).
2. The measured CO₂ gas flux is highly dependent on the proper placement of the accumulation chamber. Particularly, around gas vents detailed measurements have to be done to not underestimate the impact of

CO₂ vents by mistake or to miss them at all. Moving the accumulation chambers can lead to underestimations of 1 or 2 orders of magnitude for the CO₂ gas flux (Fig. 3).

3. The measuring device uses a LiCOR 820 infrared gas analyser for CO₂ discharge quantification. Although widely used in gas flux studies, it bears high uncertainties when measuring gas fluxes of several tens of kilograms per day and square metre.
4. Geostatistical tools all have different approaches in the interpolation process, and depending on the method, the estimated CO₂ discharge in the HMF varies.

All these factors combined lead to relatively high uncertainties and errors in the quantification of the CO₂ gas flux in the HMF. Changing the measurement system can decrease these errors; however, the effect of temporal and spatial changes in the CO₂ would require many monitoring stations at surface. More advanced geostatistical approaches, such as the sequential Gaussian simulation (Cardellini et al. 2003; Lewicki et al. 2005; De Bortoli Teixeira et al. 2011), might improve the estimation by a bit.

However, these articles also report that this approach only results in slight improvements of estimation of the CO₂ emission rate. These slight improvements would be significantly lower than the natural variations of the CO₂ gas flux in the field. Therefore, a better approximation of the natural degassing behaviour is only achievable by multiple, continuously measuring monitoring stations.

CO₂ degassing at the HMF

Geoelectrical and gravity measurements reveal small magnitude, but distinct anomalies in the respective potential field where surface degassing occurs. In this case, the sub-surface features slightly higher resistivities than the surroundings (e.g. profile 3 at 300 m at a depth of 20–30 m) and measurements of the gravitational field reveal small, negative Bouguer anomalies close to focused CO₂ degassing sites. One possible explanation can be an increase of the size of micropores, as described in Bankwitz et al. (2003a) and Kämpf and Bankwitz (2005). The alteration process of rocks by the long-term influence of the high-pressure CO₂–water mixture mobilises or dissolves slowly, but continuously, the matrix with the consequence that the microcracks and pores will be relatively larger compared to the surrounding. The CO₂ ascent carries ground water along, and the bubbling CO₂–water mixture is then capable of transporting sediments with it. An increase in pore volume leads to a decrease in the bulk density, and if these pores are filled with uprising CO₂, it also leads to a decrease in the conductivity (=increase in the resistivity). Annunziatellis et al. (2008) mention that CO₂ migrates

not only vertically, but also horizontally in soil gas via advective forces and density-driven flows. This might lead to the horizontal change in the saturation of pore fluids and the relation of grain size to gas–water-filled (or-non-filled; Bankwitz et al. (2003b) pore space, which leads to decreased densities and increased resistivities (Revil and Florsch 2010). Another hypothesis includes a fluid-driven material transport from lower stratigraphic units upwards. Such transport of sediments due to high pressure was described by Bankwitz et al. (2003b), Kämpf et al. (2005) and Flechsig et al. (2008). This can also lead to the formation of larger cavern, as observed by Kämpf and Bankwitz (2005) in the Pliocene Vildštejn formation in the open-cast mine of Nová Ves II (E: 314500, N: 5561540, about 4.5 km NW from HMF) at depths of about 50 m. These caverns can have diameters of several decimetres and be partly filled with sediments (e.g. sand) from lower stratigraphic units which are mobilised and transported by a gas–water mixture. Crystallised gypsum was found at the rim of the cavern which indicates that the caverns were filled with fluids before (Störr, pers. comm., 2002). It is unknown to this point how large these cavities can get, but these caverns were about 1 m in diameter and about 10 m long (Fig. 8). Several of these caverns were found in clusters in the open-cast mine along a 300 m active CO₂ degassing long fault (Bankwitz et al. 2003a). Because no strong gas exhalations (only gas in mineral water) were found directly above the hypocentre in the vicinity of Nový Kostel (Kämpf et al. 2013, Fig. 4), it is assumed that low-permeable rock units (permeability barriers built up by low-permeable rock sequences and sealing processes in and above the seismogenic zone) are capping the active hydraulic system.

The following model was published by Bräuer et al. (2003): permeability barriers keep the permanent mantle fluid flux from further rising. Therefore, fluid overpressure is very likely to build up in the surroundings of the hypocentres and stimulate the nearly permanent seismic activity of the Nový Kostel focal zone. The model of Bräuer et al. (2003) is also supported by seismological investigations of Alexandrakakis et al. (2014), who found structures in the hypocentral area acting as a fluid trap zone.

ERT measurements reveal an increase of thickness of the topmost high-resistivity layer from south to north. The thickness is about 10 m in the southern and central area of Hartoušov, 15–20 m in the northern area and about 40 m in the Bublák area (Fig. 7) This is most likely related to the Pleistocene sediments of the Plesná valley. Flechsig et al. (2008) found this correlation between these sedimentary layers and an increase in electric resistivity in the main degassing area.

According to the results of pedological and sedimentological investigations at the central part of the HMF (Flechsig et al. 2008; Rennert et al. 2011), we assume the vents to

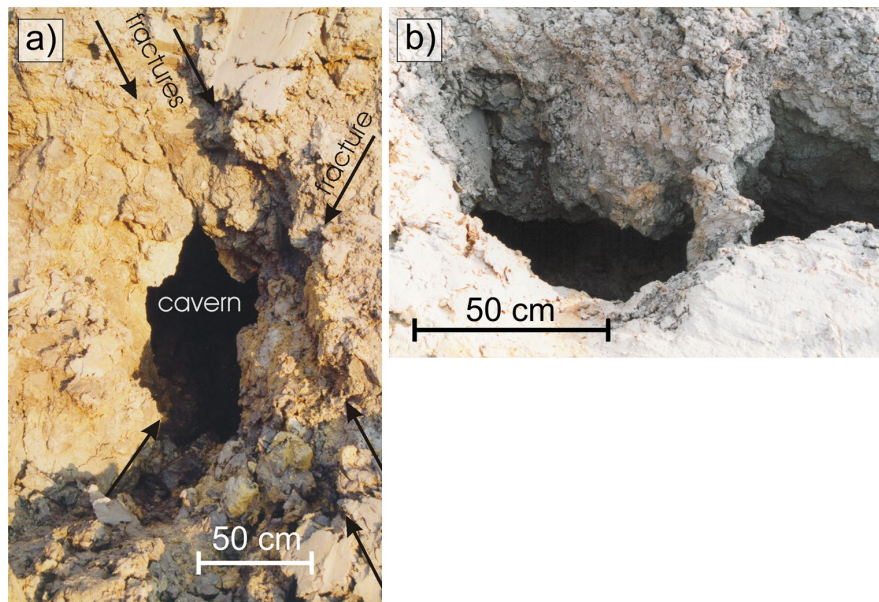


Fig. 8 A cavern in kaolinite-bearing clay in the Vildštejn formation (Pliocene) in the open-cast mine Nová Ves II at 50 m depth, which developed at the intersection of two fracture sets. Mobilised sand

from lower stratigraphic units filled the cavern at the base and was found nearby. Gypsum crystals are found at the rim of these caverns. **a** Front view, modified after Kämpf and Bankwitz (2005). **b** Top view

be more or less stable in the basement and the sedimentary subsurface along fractures. However, the first few metres of soil (Quaternary gravel and sand with varying contents of clay) seem to be responsible for a lateral change of the gas seepage. Weather effects, such as rain or soil frost, seem to change the pathways for the uprising CO_2 (Chiodini et al. 1998; Carapezza and Granieri 2004). This can be observed visually, when the position of the wilted vegetation changes (Pfanzen et al. 2007) within seasons and over the years, and technically via gas flux measurements (Table 1). Similar observations were made in the HMF by Sandig et al. (2014). They report different levels of CO_2 in the soil, depending on atmospheric conditions and soil properties. On the other hand, their measuring positions changed with every survey, which is a major source of errors as the CO_2 presence changes on a submeter scale. They find weak anomalies in soil temperature and soil moisture at the degassing spots, but also find these where no CO_2 degassing occurs. Hence, quantifications of the totally released CO_2 via the closed-chamber method can only be approximated. As large amounts of CO_2 are released via gas vents with diameters <1 m, changes in time and position of the measurement can result in high uncertainty of the CO_2 gas flux estimation. Girault et al. (2014) listed total amounts of CO_2 discharges for volcanic, geothermal, hydrothermal, mofette and fault-related areas. The HMF is also present in this list, referring to the statements from Kämpf et al.

(2013). As this study provides new information about the degassing process at this site and Kämpf et al. (2013) only made a minimum estimation of the gas flux, we suggest using the values provided in this article for the HMF for future comparisons.

The Počátky-Plesná fault zone

The regional fault network along the N–S-striking Regensburg–Leipzig–Rostock zone is characterised from the area of Regensburg to Leipzig by high number of N–S-, NW–SE- and sometimes also E–W-striking local faults (Bankwitz et al. 2003b). According to Bankwitz et al. (2003b), the Mariánské Lázně fault (MLF) consists south-east of Nový Kostel of four parallel trending faults which have been active recently. Both the Mariánské Lázně fault system and the Počátky-Plesná zone feature combinations of N–S- and NW–SW-oriented sub-faults. The boundaries of the pull-apart basin-like structures fit exactly this combination of fault segment orientations.

Bankwitz et al. (2003b, Fig. 6b) investigated the course of the PPZ from the NKFZ southward for about 6–7 km to U Mostku. Our investigations continued the research of the PPZ in the HMF. We agree with the results of Haviř (2000), Bankwitz et al. (2003b), Peterek et al. (2011) and Kämpf et al. (2013), as we can continue the split course of the PPZ in southward direction. We agree with the suggestion of

Bankwitz et al. (2003b) that the PPZ composed of differently running segments can be continued morphologically southward: NNE-running (015° strike) and NNW-running (150°–160° strike) segments. Degassing occurs along the eastern margin of the PPZ, which retraces at least one NNE- and one NNW-running segment. Kämpf et al. (2013) also present other degassing-related phenomena like ochre springs (as a sign for mineral water) along the PPZ north of the HMF and BMF which support the hypotheses of Bankwitz et al. (2003b) and its course along two differently striking segments. Our measurements show two types of CO₂ degassing behaviour related to these two differently striking areas: degassing along the N–S segments is spatially narrow and less intense compared to the NW–SE-striking segment, where degassing is stronger and affects a wider area. It is to be noted that the wet mofettes of the BMF are also located along NW–SE-striking segments of the PPZ.

As postulated by Bankwitz et al. (2003b) and supported by Peterek et al. (2011) and Rojčík et al. (2010), we also agree that the eastern block along the fault has experienced some kind of tectonic movement. Bankwitz et al. (2003b) postulate a “true level difference” between eastern and western flank of 5–15 m, whereas Peterek et al. (2011) postulate 12 m of difference. However, Bankwitz et al. (2003b) also mention a difference in elevation of up to 29 m. Unfortunately, Peterek et al. (2011) mistook the postulates from Bankwitz et al. (2003b) as they mixed level difference (vertical displacement of stratigraphic units) and scarp height. Thus, both articles are in agreement in terms of the displacement along the fault scarp.

Figure 9 shows the stratigraphic units of two GEOFOND drills near the Hartoušov village. SA-30 is located within the Plesná valley and HV12 is located on the eastern block. The lateral distance between drill wells is about 250 m. The thickness of the Neogene sediments is significantly increased (79 m in the western part, 107 m in the eastern part). While a 2.7-m-thick coal layer and a 25-m-thick layer of Palaeozoic eluvium were identified in the HV12 drill, these layers were not found in the SA-30 drill. The basement (Palaeozoic mica schists) has an offset of about 40 m between the two drills. This discrepancy between total elevation difference and stratigraphy difference might be related to the fact that the eastern flank experienced subsidence during the formation of the Cheb Basin during the late Oligocene to Mid Miocene (Špicáková et al. 2000; Peterek et al. 2011). Špicáková et al. (2000, Fig. 10) already showed that the thickest deposits of the Late Pliocene Vildštejn formation are not bound to the course of the MLFZ, but is aligned in a rather N–S-trending course. Subsequently, Peterek et al. (2011) show that the eastern flank experienced uplift during and after the Middle Pleistocene. This reactivation along the PPZ leads to the 12 m in geological shift

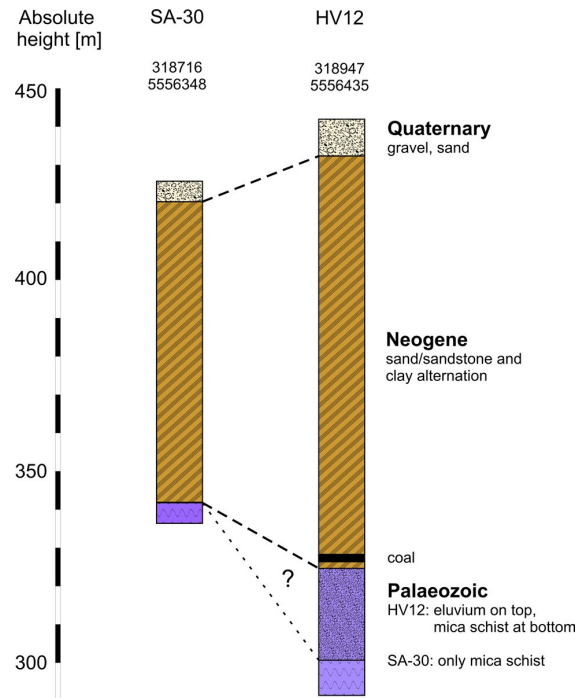


Fig. 9 Stratigraphic profile of the GEOFOND drill cores SA-30 and HV12 and their respective coordinates. The location of the drills can also be seen in Fig. 10

between the top of the Neogene sediments and 20–30 m elevation shift nowadays. Peterek et al. (2011) also mention that the southward continuation of the PPZ (the so-called Nebanice Fault Zone) features change in the displacement rate over time. This was found out after they did research on terraces at the Ohře river and their displacement to each other between the western and eastern blocks.

Sandig et al. (2014) find a change in their self-potential measurements in the eastern part of their profile and interpret this as the fault scarp of the PPZ. Our findings in the local electrical resistivity of profile 1–3 show a thickening of the high-resistivity block in the east in the ERTs, which we interpret as fault scarps (Fig. 7). The increase in the gravity towards the east contributes to this assumption. A GPR (Ground Penetrating Radar) profile crossing the Bublák mofette in E–W direction, and thus very near to the geoelectric profile No. 1, featured in Hubatka et al. (2004) shows a similar result. They find a of 200-m-wide and 10-m-deep depression (15 m near the Bublák mofette) on top of a complex fault pattern. Although visible in Hubatka et al. (2004, Fig. 1), the authors do not describe the distinct and sudden shift in the lateral rock composition underneath the morphological step, which is most likely related to the PPZ. They interpret this anomaly as an indicator for

the fault scarp near the surface. All of these articles and our studies fit the drilling results, shown in Fig. 9.

The PPZ's importance on the regional geodynamic activity is, from our point of view, underestimated. Particularly, seismological interpretations of earthquake swarm activity of the last decades linked the earthquake swarm activity with fault planes of the MLFZ, as it is the morphologically most striking one (Grünthal et al. 1990). However, as already mentioned by Bankwitz et al. (2003b), most of these focal mechanisms show a rather N–S sinistral strike-slip movement for several earthquake swarms (1985/1986, 1994, 1997, 2000) (Horálek et al. 2000), with only a minor relation to the course of the MLFZ. Fischer and Horálek (2003), Fischer and Michálek (2008) and Vavryčuk (2011) mentioned the planar character of the Nový Kostel focal zone (169° strike). They also admit that more than 90 % of the events were related to this strike orientation. Less activity could be correlated to the strike of the MLFZ. It is also mentioned that previous earthquake swarms in 1985/1986 (Vavryčuk 1993) and 2000 (Fischer 2003) have focal mechanisms with a similar orientation. The most recent comprehensive work on earthquake swarm in NW Bohemia (Fischer et al. 2014) also mentions that prevailing studies on focal mechanisms in the Nový Kostel area mostly feature strikes that are N–S related (165°–180°) and reflect the course of the PPZ rather than the MLFZ. Furthermore, from long-term geodetic monitoring, Mrlina and Seidl (2008) defined an active tectonic displacement zone of N–S to NNE–SSW direction, rather than NW–SE of the MLFZ.

According to Malkovský (1987), Špičáková et al. (2000), Bankwitz et al. (2003b) and Peterek et al. (2011), the MLFZ played a major role in the development of the Cheb Basin in the Late Tertiary (Oligocene), but showed little activity until the late Pliocene. In the late Pliocene, activity along the MLFZ increased, and the fault was reactivated (Fischer et al. 2014). At present, the PPZ is the seismically more active zone.

Pull-apart basin-like formations along the PPZ?

Bankwitz et al. (2003b) and Peterek et al. (2011) report the sinistral movement of the PPZ around the HMF. Peterek et al. (2011) observed this movement to the south to the Ohře River, and Wendt and Dietrich (2003) measured mainly NNW–SSE-striking sinistral strike-slip movement to the north. Field observations and measurements reveal that the most intense CO₂ degassing occurs over a wide area in the HMF and at BMF, which are located on the NW–SE-striking fault segments. We measured less intense, laterally narrow degassing in the southern part of the HMF, which is N–S oriented. Most of the wet mofettes (see Kämpf et al. (2013)) are also aligned like pearls on a string in a NNW–SSE orientation parallel to the morphological step, while some of them

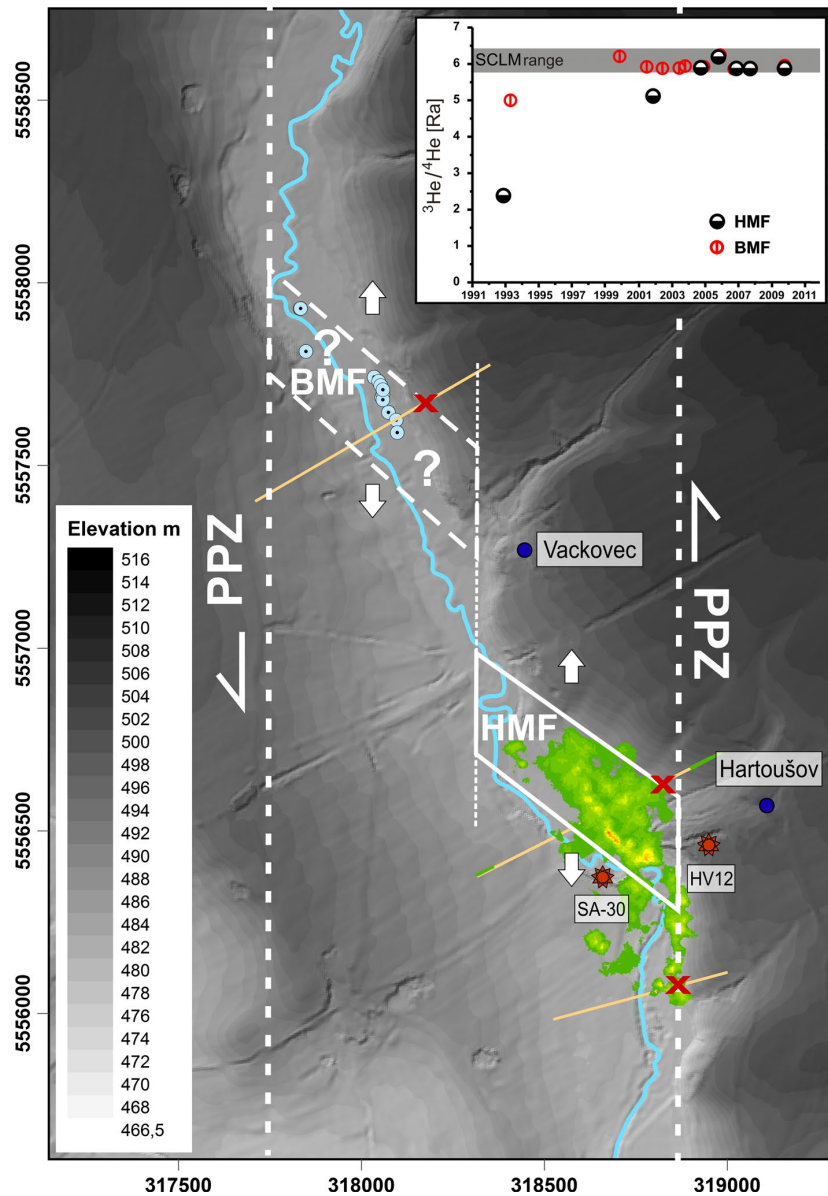
(BNW, B1 and B2) are located further to the north-west and rather isolated. In Bankwitz et al. (2003b) and Peterek et al. (2011), the faults segments were interpreted as sinistral P (=NNE) and sinistral Riedel shears (=NNW). We present a hypothesis that the HMF and BMF represent pull-apart basins, which requires verification in the future.

Pull-apart basins are often the result of two or more blocks moving along strike-slip faults (Aydin and Nur 1982; Brigster et al. 2002; Gürbüz 2010), which was also proven experimentally by e.g. McClay and Dooley (1995) and Atmaoui et al. (2006). The strike-slip movement along the fault leads to compressional or extensional deformation and results in a rhombic-shaped opening with length-to- ratios of mostly 3:1 or 4:1 (Gürbüz 2010). Pull-apart basins can feature sizes of just some tens of metres or several kilometres (Aydin and Nur 1982). This could explain why the N–S-oriented segments (focused and narrow vent degassing in the southern HMF and at BMF) feature a rather steep morphological step, which indicates parallel segments of the fault zone. On the other hand, the central and northern parts of the HMF feature a gentle slope to the west and more diffuse degassing over a wider area, which indicates the extensional basin opening. In this case, it is likely that more of these “basins” exist along the PPZ. One of these structures could be located at U Mostku, as Flechsig et al. (2010) found a basin-like depression via ERT surveys. Aydin and Nur (1982) and Gürbüz (2010) also mention the occurrence of springs and volcanic cones in pull-apart basin areas due to a thinning of the crust. Even though no recent volcanic activity is known in the HMF, it is interesting that the highest ratio of mantle-derived gasses in Central and Western Europe is observed at the BMF and the HMF (Bräuer et al. 2008; Kämpf et al. 2013), indicating easier upward migration paths for fluids.

Gas emanation studies of Weinlich et al. (1999), Bräuer et al. (2003, 2008, 2011) and Kämpf et al. (2013) showed that the CO₂-dominated gas exhalations exhibit signatures that are related to the subcontinental lithospheric mantle. Bräuer et al. (2011) observed ³He/⁴He ratios of approximately 5.89 Ra at Bublák and 5.56 Ra at U Mostku (located along the PPZ), whereas ³He/⁴He ratios of approximately 4.60 Ra at Kopanina and 5.13 Ra at Dolní Častkov (located along the MLFZ) were observed, which indicates less mixing of mantle gas with gas from the earth's crust. The highest increase in the ³He/⁴He ratios, however, was observed at the Hartoušov mofettes (2.38 Ra in 1993 to 5.11 Ra in 2002 and 5.89 in 2005 (Bräuer et al. 2009). From 2005 to 2012, the ³He/⁴He ratios of gas in the HMF (H5) and BMF (B2) both plot in the SCLM range (Fischer et al. 2014). This might also indicate that BMF and HMF are two separate structures and are on top of separate conduits for CO₂-dominated gas ascent (Fig. 10, inset).

A possible interpretation is shown in Fig. 10. In this case, the HMF and BMF would represent two small, independent

Fig. 10 Hypothetical model of the HMF and BMF as pull-apart basins (white rhombs) in the sinistral strike-slip-oriented PPZ (white, dashed line). Red stars mark the locations of the drills SA-30 and HV12 (Fig. 9). Red crosses mark the locations where evidence for the segments of the PPZ was found. The results from the gas flux studies (Fig. 5) and the locations of the wet mofettes as well as the geophysical profiles are presented for orientation purposes. Inset change of the $^3\text{He}/^4\text{He}$ ratio in the gas from the BMF and HMF over time (mofettes B2 and H5, respectively, from Kämpf et al. (2013), inset modified after Fischer et al. (2014)). SCLM subcontinental lithospheric mantle range for $^3\text{He}/^4\text{He}$ (Gautheron et al. 2005)



basin-like structures which developed at different faults of the PPZ. We interpret this as two independent basins because no gas emanations were observed between the two fields, the thickness of the sedimentary cover in both areas is different and because of the long-lasting trend of the helium isotope ratio only increased slightly in the BMF but significantly in the HMF over the last two decades (Fig. 10, inset). It is likely that similar degassing structures exist further to the north and south of HMF and BMF although they have not been observed yet. Only the occurrence of ochre springs (Kämpf et al. 2013) and the occurrence of mineral springs (Weinlich et al. 1999; Bräuer et al. 2011, 2014; Kämpf et al. 2013)

along the PPZ is well documented as emanations of the magmatic process below. Future studies should focus on systematic search of further degassing centres, and maybe pull-apart basins, following the morphology and regional fault network.

Conclusions

This study presents the results of a multi-method approach on a diffuse degassing structure, the Hartoušov mofette area in the geodynamically most active area of the European Cenozoic Rift System (Bräuer et al. 2008).

1. We discovered that in earlier studies, the degassing behaviour along the Počátky-Plesná fault zone was underestimated by only studying the degassing behaviour of wet mofettes (Weinlich et al. 1998, 1999). As degassing can easily be observed visually in water-filled pools, the detection of dry, and thus optically invisible, CO₂ vents is more problematic, because of their size and temporal and spatial instability.
2. The experiments carried out here show that coarse measuring grids for CO₂ gas flux studies cannot be applied in this diffuse degassing area, as the strongest degassing is related to spots with diameters in the sub-meter scale. Even the best statistical approaches might not correctly quantify the CO₂ discharge in the HMF if not based on thorough and extensive field work.
3. Field experiments show that in this special area, measured gas fluxes at the surface are highly variable, both spatially and temporally. Narrow measurement spacings at CO₂ vents improve the quality CO₂ surveys, and for correct evaluations of the carbon dioxide discharge, monitoring stations are necessary.
4. Due to the non-Gaussian distribution of the measured data, geostastical tools can only be used to roughly estimate the total CO₂ discharge. Depending on the method, we estimate that between 23 and 97 tons of CO₂ are ejected every day for this area in the HMF via dry seepage.
5. The application of geophysical methods such as ERT and gravity measurements reveals distinct anomalies in the subsurface below strong degassing areas. These anomalous areas are most likely the result of the force behind ascending fluids and consecutive sediment alteration and/or transport linked with the ascent of the CO₂-rich fluids.
6. ERT and gravity surveys also support the theory of a significant shift in the lithological composition between eastern and western flank along the PPZ. The correlation of stratigraphic units between different blocks of the PPZ leads to the assumption that the PPZ has been active since at least the late Miocene and earthquake focal mechanisms indicate that it is still active up to this day. Its importance should be reconsidered, as this fault zone of several tens of kilometres seems to play a major role in the regional tectonic frame.
7. Our results fit into a model in which the HMF and BMF are in the centres of two independent pull-apart basin-like structures, opened by sinistral strike-slip movement along the PPZ.
8. The gas emanations in these pull-apart basin-like structures bear signatures from the subcontinental lithospheric mantle and are thus connected via conduits to it.
9. Future studies should consider the geologic structure and evolution of these two basins related to mantle degassing by seismic profiling, CO₂ gas flux studies and by investigations of drill cores.
10. Since HMF and BMF only illustrate examples along the N–S-striking PPZ, the role of the PPZ and other N–S-striking faults of the RLRZ for upper mantle degassing might have been underestimated previously.
11. More degassing centres might be located along the PPZ south or north of HMF and BMF. Systematic search of further degassing centres, and maybe pull-apart basins, following the morphology and regional fault network might be able to trace more degassing centres.

Acknowledgments We would like to express our gratitude to the German Research Foundation (DFG) for funding this project (KA902/9 and/16 and FL271/13). We thank J. Schumann for his initial hard field work and I. Schüller, S. Kämpf, B. Friedrichs, E. Seidl, M. Seidl and V. Polák for their help in the field during this stage of the project. We want to give warm thanks to N. Wetzig for his language and spelling check. We thank P. Rojik for his help with the interpretation of the drill logs in the Hartoušov area. We also thank the GFZ for financial help for repairing measuring devices. Gravity observations were partly supported by the project CzechGeo/EPOS, Grant No. LM2010008. At last, we like to express our gratitude towards W. H. Geissler, our editor, and Svetlana Byrdina and Domenico Granieri, our reviewers, for their helpful suggestions which improved this article a lot.

References

- Alexandrakis C, Calò M, Bouchaala F, Vavryčuk V (2014) Velocity structure and the role of fluids in the West Bohemia Seismic Zone. *Solid Earth* 5:863–872
- Annunziatelli A, Beaubien SE, Bigi S, Giotoli G, Coltella M, Lombardi S (2008) Gas migration along fault systems and through the vadose zone in the Latera caldera (Central Italy): implications for CO₂ geological storage. *Int J Greenh Gas Control* 2:353–372
- Arts RJ, Baradello J, Girard F, Kirby G, Lombardi S, Williamson P, Zaja A (2009) Results of geophysical monitoring over a leaking natural analogue site in Italy. *Energy Proc* 1:2269–2276
- Atmaoui N, Kukowski N, Stöckhert B, König D (2006) Initiation and development of pull-apart basins with Riedel shear mechanism: insight from scaled clay experiments. *Int J Earth Sci* 95:225–238
- Aydin A, Nur A (1982) Evolution of pull-apart basins and their scale independence. *Tectonics* 1(1):91–105
- Babuška V, Plomerová J (2008) Control of paths of Quaternary volcanic products in western Bohemian Massif by rejuvenated Variscan triple junction of ancient microplates. *Stud Geophys Geod* 52:607–629
- Bankwitz P, Bankwitz E, Bräuer K, Kämpf H, Störr M (2003a) Deformation structures in Plio- and Pleistocene sediments (NW Bohemia, Central Europe). In: Van Rensbergen P, Hills R, Maltmann AJ, Morley CK (eds) *Subsurface sediments mobilization*. Geol. Soc. London, Spec. Publ
- Bankwitz P, Schneider G, Kämpf H, Bankwitz E (2003b) Structural characteristics of epicentral areas in Central Europe: study case Cheb Basin (Czech Republic). *J Geodyn* 35:5–32

- Bergfeld D, Fraser G, Janik CJ (2001) Elevated carbon dioxide flux at the Dixie Valley geothermal field, Nevada: relations between surface phenomena and the geothermal reservoir. *Chem Geol* 177:43–66
- Bergfeld D, Evans WC, Howle JF, Farrar CD (2006) Carbon dioxide emissions from vegetation-kill zones around the resurgent dome of Long Valley caldera, eastern California, USA. *J Volcanol Geotherm Res* 152:140–156
- Box GEP, Cox DR (1964) An analysis of transformations. *J R Stat Soc Ser B* 26:211–252
- Bräuer K, Kämpf H, Strauch G, Weise S (2003) Isotopic evidence ($^3\text{He}/\text{He}$, $\delta^{13}\text{C}_{\text{CO}_2}$) of triggered intraplate seismicity. *J Geophys Res* 108(B2):2070. doi:10.1029/2002JB002077
- Bräuer K, Kämpf H, Niedermann S, Strauch G (2005) Evidence for ascending upper mantle-derived melt beneath the Cheb basin, Central Europe. *Geophys Res Lett* 32:L08303. doi:10.1029/2004GL022205
- Bräuer K, Kämpf H, Niedermann S, Strauch G, Tesář J (2008) The natural laboratory NW Bohemia—comprehensive fluid studies between 1992 and 2005 used to trace geodynamic processes. *Geochem Geophys Geosyst* 9:L17309. doi:10.1029/2009GL039615
- Bräuer K, Kämpf H, Strauch G (2009) Earthquake swarms in non-volcanic regions: what fluids have to say. *Geophys Res Lett* 36:L17309. doi:10.1029/2009GL039615
- Bräuer K, Kämpf H, Koch U, Strauch G (2011) Monthly monitoring of gas and isotope compositions in the free gas phase at degassing locations close to the Nový Kostel focal zone in the western Eger Rift, Czech Republic. *Chem Geol* 290:163–176. doi:10.1016/j.chemgeo.2011.09.012
- Bräuer K, Kämpf H, Strauch G (2014) Seismically triggered anomalies in the isotope signatures of mantle-derived gases detected at degassing sites along two neighboring faults in NW Bohemia, central Europe. *J Geophys Res Solid Earth* 119:5613–5632. doi:10.1002/2014JB011044
- Brigster BS, Stephens WC, Norman GA (2002) Structure, stratigraphy, and hydrocarbon system of a Pennsylvanian pull-apart basin in north-central Texas. *AAPG Bull* 86:1–20
- Byrdina S, Revil A, Pant SR, Koirala BP, Shrestha PL, Tiwari DR, Gautam UP, Shrestha K, Sapkota SN, Contraires S, Perrier F (2009) Dipolar self-potential anomaly associated with carbon dioxide and radon flux at Syabru-Bensi hot springs in central Nepal. *J Geophys Res Solid Earth* 114(B10):B10101. doi:10.1029/2008JB006154
- Caine JS, Evans JP, Forster CB (1996) Fault zone architecture and permeability structure. *Geology* 24:1025–1028
- Carapezza ML, Granieri D (2004) CO_2 soil flux at Vulcano (Italy): comparison between active and passive methods. *Appl Geochem* 19:73–88
- Carapezza ML, Ricci T, Ranaldi M, Tarchini L (2009) Active degassing structures of Stromboli and variations in diffuse CO_2 output related to the volcanic activity. *J Volcanol Geotherm Res* 182:231–245
- Cardellini C, Chiodini G, Frondini F (2003) Application of stochastic simulation to CO_2 flux from soil: mapping and quantification of gas release. *J Geophys Res* 108:B9. doi:10.1029/2002JB002165
- Chiodini G, Frondini F (2001) Carbon dioxide degassing from the Albani Hills volcanic region, Central Italy. *Chem Geol* 177:67–83
- Chiodini G, Cioni R, Guidi M, Raco B, Marini L (1998) Soil CO_2 flux measurements in volcanic and geothermal areas. *Appl Geochem* 13:543–552
- Chiodini G, Frondini F, Cardellini C, Granieri D, Marini L, Ventura G (2001) CO_2 degassing and energy release at Solfatara volcano, Campi Flegrei, Italy. *J Geophys Res* 106(B8):16213–16221
- Chiodini G, Granieri D, Avoni R, Caliro S, Costa A, Minopoli C, Vilardo G (2010) Non-volcanic CO_2 Earth degassing: case of Mefite d'Ansanto (southern Apennines), Italy. *Geophys Res Lett*. doi:10.1029/2010GL042858
- Clifford J, Binley A (2010) Geophysical characterisation of riverbed hydrostratigraphy using electrical resistance tomography. *Near Surf Geophys* 8:493–501
- Credner H (1876) Das vogtländisch-erzgebirgische Erdbeben vom 23. November 1875. *Z Ges Naturwiss* 48:246–269
- Dahm T, Fischer T, Hainzl S (2008) Mechanical intrusion models and their implications for the possibility of magma-driven swarms in NW Bohemia region. *Stud Geophys Geod* 52:529–548
- De Bortoli Teixeira D, Panosso AR, Cerri CEP, Pereira GT, La Scala N (2011) Soil CO_2 emission estimated by different interpolation techniques. *Plant Soil* 345:187–194. doi:10.1007/s11104-011-0770-6
- Ebinger CJ, Keir D, Ayle A, Calais E, Wright TJ, Belachew M, Hammond JOS, Campbell E, Buck WR (2008) Capturing magma intrusion and faulting processes during continental rupture: seismicity of the Dabbahu (Afar) rift. *Geophys J Int* 174:1138–1152. doi:10.1111/j.1365-246X.2008.03877.x
- Fiala J, Vejnar Z (2004) The lithology, geochemistry, and metamorphic gradation of the crystalline basement of the Cheb (Eger) Tertiary Basin, Saxothuringian Unit. *Bull Geosci* 79:41–52
- Finizola A, Revil A, Rizzo E, Piscitelli S, Ricci T, Morin J, Angeletti B, Mocochain L, Sortini F (2006) Hydrogeological insights at Stromboli volcano (Italy) from geoelectrical, temperature, and CO_2 soil degassing investigations. *Geophys Res Lett*. doi:10.1029/2006GL026842
- Finizola A, Aubert M, Revil A, Schütze C, Sortini F (2009) Importance of structural history in the summit area of Stromboli during the 2002–2003 eruptive crisis inferred from temperature, soil CO_2 , self-potential, and electrical resistivity tomography. *J Volcanol Geotherm Res* 183:213–227
- Finizola A, Ricci T, Deiana R, Cabusson SB, Rossi M, Praticelli N, Giocoli A, Romano G, Delcher E, Suski B, Revil A, Menny P, Gangi FD, Letort J, Peltier A, Villasante-Marcos V, Douillet G, Avaré G, Lelli M (2010) Adventive hydrothermal circulation on Stromboli volcano (Aeolian Islands, Italy) revealed by geophysical and geochemical approaches: implications for general fluid flow models on volcanoes. *J Volcanol Geotherm Res* 196:111–119. doi:10.1016/j.jvolgeores.2010.07.022
- Fischer T (2003) The August–December 2000 earthquake swarm in NW Bohemia: the first results based on automatic processing of seismograms. *J Geodyn* 35:59–81
- Fischer T, Horálek J (2003) Space–time distribution of earthquake swarms in the principal focal zone of the NW Bohemia/Vogtland seismoactive region: period 1985–2001. *J Geodyn* 35:125–144
- Fischer T, Michálek J (2008) Post 2000-swarm microearthquake activity in the principal focal zone of West Bohemia/Vogtland: space-time distribution and waveform similarity analysis. *Stud Geophys Geod* 52:493–511
- Fischer T, Štěpančíková P, Karousová M, Flechsig C, Gaballah M (2012) Imaging the Mariánské Lázně Fault (Czech Republic) by 3-D ground-penetrating radar and electric resistivity tomography. *Stud Geophys Geod* 56:1019–1036
- Fischer T, Horálek J, Hrubcová P, Vavryčuk V, Bräuer K, Kämpf H (2014) Intra-continental earthquake swarms in West-Bohemia and Vogtland: a review. *Tectonophysics* 611:1–27. doi:10.1016/j.tecto.2013.11.001
- Flechsig C, Bussert R, Rechner J, Schütze C, Kämpf H (2008) The Hartoušov Mofette field in the Cheb Basin, Western Eger Rift (Czech Republic): a comparative geoelectric, sedimentologic and soil gas study of a magmatic diffuse CO_2 -degassing structure. *Z Geol Wiss* 36(3):177–193
- Flechsig C, Fabig T, Rucker C, Schütze C (2010) Geoelectrical investigations in the Cheb Basin/W-Bohemia: an approach to

- evaluate the near-surface conductivity structure. *Stud Geophys Geod* 54:417–437
- Gautheron C, Moreira M, Allègre C (2005) He, Ne and Ar composition of the European lithospheric mantle. *Chem Geol* 217:97–112
- Geissler WH, Kämpf H, Kind R, Bräuer K, Klinge K, Plenefisch T, Horálek J, Zedník J, Nehybka V (2005) Seismic structure and location of a CO₂ source in the upper mantle of the western Eger (Ohre) rift. *Central Europe. Tectonics* 24:TC5001. doi:10.1029/2004TC001672
- Gilbert RO (1987) *Statistical methods for environmental pollution monitoring*. Wiley, New York
- Girault F, Perrier F, Crockett R, Bhattarai M, Koirala BP, France-Lanord C, Agrinier P, Ader M, Fluteau F, Gréau C, Moreira M (2014) The Syabru-Bensi hydrothermal system in central Nepal: 1. Characterization of carbon dioxide and radon fluxes. *J Geophys Res Solid Earth* 119:4017–4055. doi:10.1002/2013JB010301
- Grünthal G (1989) About the history of earthquake activity in the focal region Vogtland/Western Bohemia. In: Bormann P (ed) *Monitoring and analysis of the earthquake swarm 1985/86 in the region Vogtland/Western Bohemia*. Akademie der Wissenschaft der DDR, Potsdam, pp 30–34
- Grünthal G, Schenk V, Zeman A, Schenková Z (1990) Seismotectonic model for the earthquake swarm of 1985–1986 in the vogtland/west bohemia focal area. *Tectonophysics* 174:369–383
- Günther T, Rücker C, Spitzer K (2006) Three dimensional modelling and inversion of dc resistivity data incorporating topography—II. Inversion. *Geophys J Int* 166(2):506–517
- Gürbüz A (2010) Geometric characteristics of pull-apart basins. *Lithosphere* 2(3):199–206
- Haviř J (2000) Stress analyses in the epicentral area of Nový Kostel (Western Bohemia). *Stud Geophys Geod* 44:522–536
- Hecht L, Vignerresse J, Morteani G (1997) Constraints on the origin of zonation of the granite complexes in the Fichtelgebirge (Germany and Czech Republic): evidence from a gravity and geochemical study. *Geol Rundsch* 86:S93–S109
- Hemmann A, Kämpf H (2002) Seismicity in the central part of the Naab–Pritzwalk–Rostock lineament, related to mantle fluid activity? EGS XXVII General Assembly, Nice, 21–26 April 2002, abstract 5193
- Hemmann A, Meier T, Jentzsch G, Ziegert A (2003) Similarity of waveforms and relative relocalisation of the earthquake swarm 1997/1998 near Werdau. *J Geodyn* 35:191–208
- Heuer B, Geissler WH, Kind R, Kämpf H (2006) Seismic evidence for asthenospheric updoming beneath the western Bohemian Massif, central Europe. *Geophys Res Lett* 33:L05311. doi:10.1029/2005GL025158
- Heuer B, Geissler WH, Kind R, the BOHEMA working group (2011) Receiver function search for a baby plume in the mantle transition zone beneath the Bohemian Massif. *Geophys J Int* 187:577–594
- Hill DP, Prejean S (2005) Magmatic unrest beneath Mammoth Mountain, California. *J Volcanol Geotherm Res* 146:257–283
- Horálek J, Fischer T (2008) Role of crustal fluids in triggering the West Bohemia/Vogtland earthquake swarms: just what we know (a review). *Stud Geophys Geod* 52:455–478
- Horálek J, Fischer T (2010) Intraplate earthquake swarms in West Bohemia/Vogtland (Central Europe). *Jökull* 60:67–87
- Horálek J, Šilény J, Fischer T, Sláncová A, Boušková A (2000) Scenario of the January 1997 West Bohemia earthquake swarm. *Stud Geophys Geod* 44:491–521
- Hrubcová P, Geissler W (2009) The crust–mantle transition and the Moho beneath the Vogtland/West Bohemian region in the light of different seismic methods. *Stud Geophys Geod* 53:275–294
- Hrubcová P, Vavryčuk V, Boušková A, Horálek J (2013) Moho depth determination from waveforms of microearthquakes in the West Bohemia/Vogtland swarm area. *J Geophys Res* 118:1–17. doi:10.1029/2012JB009360
- Hubatka F, Boušková A, Špičák A, Švancara J, Tilšarová R (2004) Ground penetrating radar profile measurements above the seismoactive area at the eastern margin of the Cheb Basin, Western Bohemia. *Geolines* 17:41–42
- Ibs-von Seht M, Blumenstein S, Wagner R, Hollnack D, Wohlenberg J (2001) Seismicity, seismotectonics and crustal structure of the southern Kenya rift—new data from the Lake Magadi Area. *Geophys J Int* 146:439–453
- Ibs-von Seht M, Plenefisch T, Klinge K (2008) Earthquake swarms in continental rifts—a comparison of selected cases in America, Africa and Europe. *Tectonophysics* 452:66–77
- Inguaggiato S, Calderone L, Inguaggiato C, Mazot A, Morici S, Vita F (2012) Long-time variation of soil CO₂ fluxes at the summit crater of Vulcano (Italy). *Bull Volcanol* 74:1859–1863
- Jakobsdóttir S, Roberts M, Gudmundsson G, Geirsson H, Slunga R (2008) Earthquake swarms at Upptyppingar, north-east Iceland: a sign of magma intrusion? *Stud Geophys Geod* 52:513–528
- Kämpf H, Bankwitz P (2005) The KTB deep crustal laboratory and the western Eger Graben. In: Koch R, Röhling HG (eds) *GeoErlangen 2005/Exkursionsführer, Schriftenreihe der Deutschen Gesellschaft für Geowissenschaften* 40:37–108
- Kämpf H, Peterek A, Rohrmüller J, Kumpel HJ, Geissler WH (2005) The KTB deep crustal laboratory and the western Eger Graben. In: Koch R, Röhling HG (eds) *GeoErlangen 2005/Exkursionsführer, Schriftenreihe der Deutschen Gesellschaft für Geowissenschaften* 40:37–108
- Kämpf H, Geissler WH, Bräuer K (2007) Combined gasgeochemical and receiver function studies of the Vogtland/NW Bohemia intraplate mantle degassing field. In: Christensen UR, Ritter JRR (eds) *Mantle plumes—a multidisciplinary approach*. Springer, Berlin
- Kämpf H, Bräuer K, Schumann J, Hahne K, Strauch G (2013) CO₂ discharge in an active, non-volcanic continental rift area (Czech Republic): characterisation (¹³C, ³He/⁴He) and quantification of diffuse and vent CO₂ emissions. *Chem Geol* 339:81–83
- Kárník V, Michal E, Molnár A (1957) *Erdbebenkatalog der Tschechoslowakei bis zum Jahre 1956*. Travaux de l'Institut Géophysique de l'Académie Tchecoslovaque des Sciences 69:411–598
- Key J, White RS, Soosalu H, Jakobsdóttir S (2011) Multiple melt injection along a spreading segment at Askja, Iceland. *Geophys Res Lett* 38:L05301. doi:10.1029/2010GL046264
- Korn M, Funke S, Wendt S (2008) Seismicity and seismotectonics of West Saxony, Germany—new insights from recent seismicity observed with the Saxonian seismic network. *Stud Geophys Geod* 52:479–492
- Krüger JC, Romer RL, Kämpf H (2013) Late Cretaceous ultramafic lamprophyres and carbonatites from the Delitzsch Complex, Germany. *Chem Geol* 353:140–150
- Lewicki JL, Bergfeld D, Cardellini C, Chiodini G, Granieri D, Varley N, Werner C (2005) Comparative soil CO₂ flux measurements and geostatistical estimation methods on Masaya volcano, Nicaragua. *Bull Volcanol* 68:76–90
- Lewicki JL, Hilley GE, Dobeck L, Marino BDV (2012) Eddy covariance imaging of diffuse volcanic CO₂ emissions at Mammoth Mountain, CA, USA. *Bull Volcanol* 74:135–141
- Loseth H, Gading M, Wensaas L (2009) Hydrocarbon leakage interpreted on seismic data. *Mar Pet Geol* 26:1304–1319
- Malkovský M (1987) The Mesozoic and Tertiary basins of the Bohemian Massif and their evolution. *Tectonophysics* 137:31–42
- McClay K, Dooley T (1995) Analogue models of pull-apart basins. *Geology* 23(8):711–714

- Mlčoch B (2003) Character of the contact between the Saxothuringian and Teplá-Barrandian unit. *Geolines* 16:75
- Mlčoch B, Skácelová Z (2009) Digital elevation model of the crystalline basement of the Cheb and Sokolov Basin areas (Western Bohemia, Central Europe). *Z Geol Wiss* 37:145–152
- Mrlina J, Seidl M (2008) Relation of surface movements in West Bohemia to earthquake swarms. *Stud Geophys Geod* 52:549–566
- Mrlina J, Kämpf H, Kroner C, Mingram J, Stebich M, Brauer A, Geissler WH, Kallmeyer J, Matthes H, Seidl M (2009) Discovery of the first Quaternary maar in the Bohemian Massif, Central Europe, based on combined geophysical and geological surveys. *J Volcanol Geotherm Res* 182:97–112
- Neunhöfer H, Hemmann A (2005) Earthquake swarms in the Vogtland/Western Bohemian region: spatial distribution and magnitude–frequency distribution as an indication of the genesis of swarms? *J Geodyn* 39:361–385
- Nguyen F, Garambois S, Chardon D, Hermitte D, Bellier O, Jongmans O (2007) Subsurface electrical imaging of anisotropic formations affected by a slow active reverse fault, Provence, France. *J Appl Geophys* 62(4):338–355
- Petek A, Reuther CD, Schunk R (2011) Neotectonic evolution of the Cheb Basin (Northwestern Bohemia, Czech Republic) and its implications for the late Pliocene to Recent crustal deformation in the western part of the Eger Rift. *Z Geol Wiss* 5(6):335–365
- Pettinelli E, Beaubien SE, Lombardi S, Annan AP (2008) GPR, TDR, and geochemistry measurements above an active gas vent to study near-surface gas-migration pathways. *Geophysics* 73(1):11–15
- Pettinelli E, Beaubien SE, Zaja A, Menghini A, Praticelli N, Mattei E, Di Matteo A, Ciotoli G, Lombardi S (2010) Characterization of a CO₂ gas vent using various geophysical and geochemical methods. *Geophysics* 75(3):137–146
- Pfanz H, Vodnik D, Wittmann C, Aschan G, Batic F, Turk B, Macek I (2007) Photosynthetic performance (CO₂-compensation point, carboxylation efficiency, and net photosynthesis) of timothy grass (*Phleum pratense* L.) is affected by elevated carbon dioxide in post-volcanic mofette areas. *Environ Exp Bot* 61:41–48
- Rennert T, Eusterhues K, Pfanz H, Totsche KU (2011) Influence of geogenic CO₂ on mineral and organic soil constituents on a mofette site in the NW Czech Republic. *Eur J Soil Sci* 62:572–580. doi:10.1111/j.1365-2389.2011.01355.x
- Revil A, Florsch N (2010) Determination of permeability from spectral induced polarization in granular media. *Geophys J Int* 181:1480–1498
- Revil A, Finizola A, Piscitelli S, Rizzo E, Ricci T, Crespy A, Angeletti B, Balasco M, Barde Cabusson S, Bennati L, Bolève A, Byrdina S, Carzaniga N, Di Gangi F, Morin J, Perrone A, Rossi M, Rouleau E, Suski B (2008) Inner structure of La Fossa di Vulcano (Vulcano Island, southern Tyrrhenian Sea, Italy) revealed by high resolution electric resistivity tomography coupled with self-potential, temperature, and soil CO₂ diffuse degassing measurements. *J Geophys Res* 113:B07207. doi:10.1029/2007JB005394
- Revil A, Finizola A, Ricci T, Delcher E, Peltier A, Barde Cabusson S, Avard G, Bailly T, Bennati L, Byrdina S, Cologne J, Di Gangi F, Douillet G, Lupi M, Letort J, Tsang Hin Sun E (2011) Hydrogeology of Stromboli volcano, Aeolian Islands (Italy) from the interpretation of resistivity tomograms, self-potential, soil temperature and soil CO₂ concentration measurements. *Geophys J Int* 186(3):88–98
- Rogie JD, Kerrick DM, Sorey ML, Chiodini G, Galloway DL (2001) Dynamics of carbon dioxide emission at Mammoth Mountain, California. *Earth Planet Sci Lett* 188:535–541
- Rojík P, Dašková J, Fejfar KJO, Kvaček Z, Pešek J, Sýkorová I, Teodoridis V (2010) Chebské pánve. In: Pešek J (ed) *Ložiska hnědé uhlí na území České republiky a jejich využití*. Czech Geological Survey, Prague, pp 206–229
- Saito H, Goovaerts P (2000) Geostatistical interpolation of positively skewed and censored data in a dioxin-contaminated site. *Environ Sci Technol* 34:4228–4235
- Sakia RM (1992) The Box–Cox transformation technique: a review. *The Statistician* 41:169–178
- Sandig C, Sauer U, Bräuer K, Serfling U, Schütze C (2014) Comparative study of geophysical and soil-gas investigations at the Hartoušov (Czech Republic) natural CO₂ degassing site. *Environ Earth Sci* 72:1421–1434
- Saßmannshausen F (2010) Vegetationsökologische Charakterisierung terrestrischer Mofettenstandorte am Beispiel des west-tschechischen Plesná-Tals. PhD thesis, University Duisburg-Essen
- Sauer U, Schütze C, Leven C, Schlömer S, Dietrich P (2013) An integrative hierarchical monitoring approach for detecting and characterizing CO₂ releases. *Energy Proc* 37:4257–4267
- Schütze C, Sauer U, Beyer K, Lamert H, Bräuer K, Strauch G, Flechsig C, Kämpf H, Dietrich P (2012) Natural analogues: a potential approach for developing reliable monitoring methods to understand subsurface CO₂ migration processes. *Environ Earth Sci* 67:411–423
- Schütze C, Dietrich P, Sauer U (2013) Diagnostic monitoring to identify preferential near-surface structures for CO₂ degassing into the atmosphere: tools for investigations at different spatial scales validated at a natural analogue site. *Int J Greenh Gas Control* 18:285–295
- Špičáková A, Ulčny D, Kouldeková G (2000) Tectonosedimentary evolution of the Cheb Basin (NW Bohemia, Czech Republic) between Oligocene and Pliocene: a preliminary note. *Stud Geophys Geod* 44:556–580
- Suski B, Brocard G, Authemayou C, Murallas BC, Teyssier C, Holliger K (2010) Localization and characterization of an active fault in an urbanized area in central Guatemala by means of geoelectrical imaging. *Tectonophysics* 480:88–98
- Ulrych FC (2011) Recurrent Cenozoic volcanic activity in the Bohemian Massif (Czech Republic). *Lithos* 123:133–144
- Vavryčuk V (1993) Crustal anisotropy from local observations of shear-wave splitting in West Bohemia, Czech Republic. *Bull Seismol Soc Am* 83:1420–1441
- Vavryčuk V (2011) Principal earthquakes: theory and observations from the 2008 West Bohemia swarm. *Earth Planet Sci Lett* 305:290–296
- Vylita T, Žak K, Cílek V, Hercman H, Mikšíkova L (2007) Evolution of hot-spring travertine accumulation in Karlovy Vary/Carlsbad (Czech Republic) and its significance for the evolution of Tepla valley and Ohře/Eger rift. *Z Geomorphol N F* 51:427–442
- Weinlich FH, Tesář J, Weise SM, Bräuer K, Kämpf H (1998) Gas flux distribution in mineral springs and tectonic structure in north-west Bohemia. *J Czech Geol Soc* 43:91–110
- Weinlich FH, Bräuer K, Kämpf H, Strauch G, Tesář J, Weise SM (1999) An active subcontinental mantle volatile system in the western Eger rift, Central Europe: gas flux, isotopic (He, C, and N) and compositional fingerprints. *Geochim Cosmochim Acta* 63:3653–3671
- Weinlich FH, Bräuer K, Kämpf H, Strauch G, Tesář J, Weise SM (2003) Geochemie und Verteilung der Quellgase und tektonische Struktur des Eger-Rifts in der Oberpfalz und in Oberfranken, Bayern. *Zeit Deutschen Geol Gesell* 154:67–83
- Wendt J, Dietrich R (2003) Determination of recent crustal deformations based on precise GPS measurements in the Vogtland earthquake area. *J Geodyn* 35:235–246
- White RS, Drew J, Martens HR, Key J, Soosalu H, Jakobsdóttir S (2011) Dynamics of dyke intrusion in the mid-crust of Iceland. *Earth Planet Sci Lett* 304:300–312
- Wise DJ, Cassidy J, Locke CA (2003) Geophysical imaging of the Quaternary Wairoa North Fault, New Zealand: a case study. *J Appl Geophys* 53:1–16

10 Architecture and temporal variations of a terrestrial CO₂ degassing site using electric resistivity and CO₂ gas measurements

Nickschick, T., Flechsig, C., Meinel, C., Mrlina, J., Kämpf, H.

submitted to International Journal of Earth Sciences in July 8th, 2016

International Journal of Earth Sciences

Architecture and temporal variations of a terrestrial CO₂ degassing site using electric resistivity and CO₂ gas measurements

--Manuscript Draft--

Manuscript Number:	
Full Title:	Architecture and temporal variations of a terrestrial CO ₂ degassing site using electric resistivity and CO ₂ gas measurements
Article Type:	Original Paper
Keywords:	Eger Rift; ERT; CO ₂ gas flux; Cheb Basin; mofettes
Corresponding Author:	Tobias Nickschick, Dipl. geophys. German Research Centre for Geosciences GFZ Potsdam, Section 3.2 Telegrafenberg, 14473 Potsdam, Germany Potsdam, Deutschland (DEU) GERMANY
Corresponding Author Secondary Information:	
Corresponding Author's Institution:	German Research Centre for Geosciences GFZ Potsdam, Section 3.2 Telegrafenberg, 14473 Potsdam, Germany
Corresponding Author's Secondary Institution:	
First Author:	Tobias Nickschick, Dipl. geophys.
First Author Secondary Information:	
Order of Authors:	Tobias Nickschick, Dipl. geophys. Christina Flechsig Cornelia Meinel Jan Mrlina Horst Kämpf
Order of Authors Secondary Information:	
Funding Information:	Deutsche Forschungsgesellschaft Dr. Christina Flechsig Dr Horst Kämpf
Abstract:	The Hartoušov mofette field in NW Bohemia, Czech Republic, is characterized by strong CO ₂ degassing from the Lithospheric Mantle. In a test survey using electrical resistivity tomography we observed changes over time in the subsurface structure beneath heavily CO ₂ degassing spots to depths of about 40 m and compare them to CO ₂ gas flux and soil gas mappings. Changes in the electrical resistivity were measured over the course of time of about one year in irregular intervals and reveal large variations in the resistivity distribution where the CO ₂ degassing was strongest (50 to 60 * 10 ³ g m ⁻² d ⁻¹), indicating a fluid-induced alteration of the underlying clayey sediments over the course of time. Positive and negative anomalies in the electric self potential parallel to the ERTs can be found where CO ₂ degassing occurs which indicates varying ascent or descent of fluids within these spots. Some degassing spots seem to not be actively degassing continuously over time, which can also be observed by other studies in the same area. Traditional gas flux mappings often consider steady states of the observed area's degassing regime. We suggest that future gas mappings are accompanied by methods that observe the state of fluid systems at subsurface over time, e. g. electric resistivity tomography and self potential.

[Click here to view linked References](#)

1 1. Introduction

2

3 Over the last decades several geoelectric, especially tomographic, studies have been carried
4 out at CO₂ storage and degassing sites. While many studies have been focused on CO₂ capture
5 and storage sites, far fewer studies exist that used geoelectrical methods at natural, terrestrial
6 degassing sites. Most of these CO₂ degassing studies either used geoelectrical methods (Flechsig
7 et al., 2008; Nickschick et al., 2015; Pettinelli et al., 2010; Schütze et al., 2012a,b) or combined
8 them with self-potential methods (Byrdina et al., 2009; Sandig et al., 2014; Sauer et al., 2013).
9 Although all of these studies can reveal the underground structure of degassing sites (Ramirez et
10 al., 2003; Bergmann et al., 2012, accepted), the aspect of changes over time within these has only
11 been scarcely researched (Drahor et al., 2012; Fedele et al., 2015). In this study we used both
12 methods in a natural degassing site to study changes in the subsurface architecture.

13

14 The Hartoušov mofette field (HMF) is a strongly CO₂ degassing site in the NW part of the Czech
15 Republic (Fig. 1, inset map). It has been a center of research for various mantle gas and fluid-
16 related studies within the last 2 decades. After the first geophysical studies in the area (Flechsig et
17 al., 2008, 2010; Schütze et al., 2012a, 2013; Kämpf et al., 2013; Sauer et al., 2013; Sandig et al.,
18 2014; Nickschick et al., 2015), which also included geochemical, geological and tectonic data,
19 interest rose about the stability of this natural, heavily degassing site over time. Nickschick et al.
20 (2015) found out that the gas flux measurements at the surface at the central mofette in the HMF
21 show high variations in the total CO₂ emission, while not being able to find the cause for these
22 variations. However, some anomalous areas were detected in the subsurface by electric resistivity
23 tomographies (ERT) and underneath strong CO₂ degassing spots in that study. They noticed that
24 anomalies with higher resistivities were detected where strong surface degassing occurred.

25

26 As a follow-up study to the findings of Nickschick et al. (2015), we conducted a test survey in
27 the southern part of the HMF to trace possible changes in the structure of two separate degassing
28 spots over the course of one year from 2012 to 2013 using ERT in irregular intervals. The southern
29 part of the HMF was chosen (Fig. 1) as it is not penetrated or altered by older drills unlike the
30 central part of the HMF and is better suited for studying a natural CO₂ degassing site. The ERT
31 profile crosses one mofette with two surface degassing spots, which are close to each other

32 (distance to each other: about 3 m) and one degassing spot that is on top of the assumed fault.
33 After combined inversions of two electrode configurations (Wenner alpha and Wenner beta), we
34 observe variations within the mofettes' architecture, most likely caused by the ascent of gaseous
35 CO₂ and water, which lead to the alteration of the subsurface within weeks. Measuring the electric
36 self-potential reveals anomalies in the fluid flow direction at these mofettes.

37

38 2. Site description

39

40 The area of interest is located in NW Bohemia in the Cheb Basin in the Czech Republic, close
41 to the German-Czech border. The Cheb Basin is an intracontinental sedimentary basin of mainly
42 Tertiary sediments with a thickness of 50-350 m. The area is famous for fluid-induced earthquake
43 swarms, mineral water springs and also natural degassing sites of magmatic CO₂ (Kämpf et al.,
44 2013; Fischer et al., 2014; Nickschick et al., 2015), which has risen interest in the frame of the
45 International Continental Scientific Drilling Program ICDP (Dahm et al., 2013). The isotopic
46 composition (C, He) of the gas points at a magmatic intrusion from which large amounts of mainly
47 CO₂ dominated gas from the Lithospheric Mantle is ejected (Weinlich et al., 1999; Bräuer et al.,
48 2008, 2009, 2014). Nickschick et al. (2015) calculated that between 23 and 97 tons of CO₂ are
49 ejected each day in an area of about 0,33 km² in the HMF. They related the heavy degassing to the
50 course of a deep-seated, reactivated N-S-running fault (Počátky-Plesná fault zone (PPZ), Bankwitz
51 et al. (2003); Nickschick et al. (2015)), which was indicated by analyzing a digital terrain model,
52 geoelectric and gravity measurements (Nickschick et al., 2015), as well as by self-potential (SP)
53 (Sandig et al., 2014) and ground penetrating radar (GPR) (Hubatka et al., 2004).

54

55 The stratigraphy of the first tens of meters is well known from drill logs. The topmost layer, after
56 the soil coverage, consists of up to 6 - 10 m of mainly and clayey sediments with sand and gravel
57 (Flehsig et al., 2008; Rojik et al., 2014). This layer covers a massive, up to 70 to 80 m thick Lower
58 Miocene sediment package (Cypris formation) of mainly mudstone with sandy interbeddings of
59 about 2 - 5 m thickness. This sediment package is followed by the Paleozoic crystalline, consisting
60 of weathered and unweathered mica schist. The area is divided by the fault zone, which can
61 roughly be traced by following the morphology (Nickschick et al., 2015), Spicakova et al. (2000)
62 and (Peterek et al., 2011).

63

64 Measurements of the CO₂ gas flux (Fig. 2) and the content of CO₂ in the soil gas (Fig. 3) from
65 Nickschick et al. (2015) revealed that carbon dioxide emission occurs in a N-S oriented way at
66 the foot of the slope in the southern part of the HMF.

67

68 Low (<25 g m⁻² d⁻¹) gas fluxes can be observed for large parts of the area, often even lower
69 than 10 g m⁻² d⁻¹. The highest measured gas fluxes were measured close to and within a
70 degassing spot at the slope (mofette 1), ranging between 50 and 60 *10³ g m⁻² d⁻¹. Around and
71 close to two spots near a mofette in the center of the meadow (mofette 2) the gas flux varies
72 between 1 (edge) and 5000 g m⁻² d⁻¹ (center). Between the two surface degassing spots and
73 thus, along the ERT profiles, gas fluxes around 100 to 1300 g m⁻² d⁻¹ were measured. High gas
74 emissions are bound to surface degassing spots and decrease very rapidly with distance from
75 the degassing spot. High CO₂ concentrations are also observed near the two mofettes where
76 higher gas fluxes were measured (Fig. 3). Although large portions of the test area show CO₂
77 contents of less than 10 %, CO₂ contents of 80 % and higher can be observed at single locations
78 and mostly in those places, where high CO₂ gas fluxes have been observed (mofettes 1 and 2).

79

80

81 *Fig. 1: Modified model of the HMF from Nickschick et al. (2015), which hypothesized that the*
82 *CO₂ degassing is correlated to pull-apart basin-like structures that formed along a seismically*
83 *active fault, the Počátky-Plesná fault zone (PPZ). The inset shows the location of the area in the*
84 *NW Cheb Basin, Czech Republic, close to the German-Czech border. Yellow line marks the*
85 *profile for the repeated geoelectric measurements, blue line marks the course of the Plesna river.*
86 *1H031b is the drilling site where the ground water level is measured. Coordinates are in UTM 33*
87 *N.*

88

89

90 *Fig. 2: CO₂ gas flux in the southern part of the HMF, modified after Nickschick et al. (2015).*
91 *Strong gas fluxes are bound to the mofettes at the foot of the slope (mofette 1) and in the center*
92 *of the meadow (mofette 2). The gas fluxes are shown as the interpolation plot using Trans-*
93 *Gaussian Kriging (Nickschick et al., 2015). Black dots represent CO₂ gas flux measurement*

94 stations. Yellow line marks the ERT profile for time lapse measurements. Fluxes below 25 g m^{-2}
95 d^{-1} are not displayed to retain overview.

96

97

98 *Fig. 3: CO₂ content in soil gas at depths of 0.6 to 0.8 m, modified after Nickschick et al. (2015).*
99 *The eastern part could not be measured due to not being able to drill into the ground, mainly*
100 *consisting of gravel. Yellow line: ERT profile for time lapse measurements. Soil gas*
101 *measurement stations are indicated by black dots. CO₂ contents of less than 10 % are not*
102 *displayed.*

103

104

105 Fig. 4 shows the 500 m long profile from Nickschick et al. (2015) with an electrode spacing of
106 5m which revealed resistivity anomalies in the Neogene sediments which are supposed to be
107 caused by fluid ascent, as mofette activity can be observed on top of these anomalies. We chose
108 the eastern part of this profile with a denser electrode spacing of 2 m for the repeated
109 measurements to be comparable to the profile 3 from Nickschick et al. (2015), while providing a
110 better resolution near the surface and still including two surface degassing spots, which are
111 located at ca. 300 and 350m in the profile from Fig. 4, and including the top of the anomaly at
112 270-300 m.

113

114

115 *Fig. 4: Modified geoelectric profile from Nickschick et al. (2015, Fig. 7) and the extent of the*
116 *profile from this article. Arrows mark the locations of the 2 main mofettes.*

117

118

119 3. Methods

120

121 Variable portions of free (gaseous) and/or dissolved CO₂ in the pore space have impact on
122 the resistivity, which can be measured with geoelectrical methods, such as Electrical Resistivity
123 Tomography (ERT). Temporal fluctuating fluid movements lead to the occurrence of natural
124 electrical potentials (electro-kinetic effect) which is measurable with self-potential (SP) mapping.

125 The combination of various kinds of geophysical information (resistivity, self-potential with
126 surface-based measurements of CO₂ concentration and CO₂ flux) is capable of providing more
127 reliable insight in order to constrain the potential temporal changes of CO₂ degassing in a
128 mofette area and to understand patterns of fluid flow.

129

130 3.0.1. Electrical Resistivity Tomography

131

132 To investigate fluid-induced subsurface changes the Electrical Resistivity Tomography
133 method is well-established and widely employed in all fields of hydrogeological applications
134 (Loke et al., 2013) and volcanological research (Byrdina et al., 2009, 2014; Finizola et al., 2009)
135 Here, ERT is used in time-lapse mode to measure temporal changes in resistivity. To evaluate
136 the stability of subsurface mofette structure over time via ERT and compare it to the findings of
137 Nickschick et al. (2015), the same measuring devices and measuring setup were chosen. A
138 GeoTom multi-electrode device was used in conjunction with multi-electrode cables and steel
139 electrodes for the resistivity measurements and Wenner alpha and Wenner beta electrode
140 configurations were consistently used during the surveys. While the Wenner alpha electrode
141 configuration (C1 P1 P2 C2) provides a higher signal-to-noise ratio at greater depths, the
142 Wenner beta configuration (C1 C2 P1 P2) is better suited for tracing lateral resistivity changes.
143 The spacing between the 100 electrodes was 2 m, resulting in a total profile length of 200 m for
144 the repeated surveys. As especially the Wenner beta configuration is characterized by higher
145 noise at greater depths, the exploration depth is about 40 m where the overall measurement
146 error was low (<10 %). Rarely, the error exceeded the 10 % threshold in which case they were
147 deleted. For every repeated measurement the profile was marked with wooden pegs so that
148 every electrode would be put into almost the same spot every time. The profile was chosen to
149 cover the fault-related heavy degassing spot at the foot of the slope in the area and to cross the
150 degassing site at the center of the meadow (Fig. 1). The profile runs through the area between
151 the two surface spots to gain more information about the assumed common source at depth.

152

153 The measurements along the profile presented here were carried out in September 2012,
154 May 2013, July 2013, August 2013 and October 2013, together with the self-potential
155 measurements. DC2DInvRes, a 2D finite difference inversion code (Günther et al., 2006; Rucker

156 et al., 2006, www.resistivity.net) was used for inversions. Local topography was included for all
157 ERT profile analyses. The RMS error for inversions was less than 17 %.

158

159

160 3.1. Self-potential

161

162 The self-potential (SP) method is widely used as an efficient and robust method to map
163 structures at volcanoes, such as faults, and structures permeable to gas/fluids, to detect
164 subsurface flow processes (groundwater, infiltration, fluid ascent), or to investigate contamination
165 sites and land-fills where solution processes cause changes in the subsurface (Zlotnicki and
166 Nishida, 2003; Revil et al., 2011; Pettinelli et al., 2010; Jardani et al., 2007; Naudet and Revil,
167 2003). The method is based on the fact that on the earth's surface the electrical field can be
168 observed without injecting an artificial current. The reason for this is the occurrence of natural
169 polarization effects such as redox reactions at ore bodies or chemical gradients in water-
170 saturated zones (electrochemical potentials), flow of ionic fluids through porous media
171 (electrokinetic potentials or streaming potentials) and temperature gradients (thermoelectric
172 potentials). A strong fluid flow can generate SP anomalies of the order of several ten to hundreds
173 of millivolts. The SP signals caused by streaming potentials can provide information about
174 transported fluids during strong fluid ascent in permeable cold degassing structures in cases
175 such as mofettes. Due to the difficulty in estimating the possible influences in the measured data
176 quantitatively, it is not advisable to use the SP method as a stand-alone method. Other
177 investigation methods should be applied (e.g., ERT), but SP provides useful additional
178 information about subsurface processes and movements of fluids

179

180 In September 2012, self-potentials were quantified using two non-polarizing Cu/CuSO₄
181 electrodes along the 200 m profile at 5 m measuring intervals. In May 2013, July 2013, August
182 2013, and October 2013 SP measurements were repeated with a measuring interval of 2 m. A
183 voltmeter (Sinometer JT-178) with a high internal impedance of 10 MOhm and a resolution of 0.1
184 mV was used to investigate the electric potential difference between the survey and a reference
185 electrode. At the reference station, a third permanent electrode was installed to consider diurnal
186 SP variations. The daily variations were in an acceptable range of approximately ± 2 mV. The

187 reference electrode was placed in a location without any anomalous degassing at the surface
188 where no carbon dioxide emission occurred. The contact resistance between the reference
189 station and the survey electrode was measured at each point to detect and eliminate coupling
190 problems of the electrodes.

191

192

193 4. Results

194

195 *Fig. 5: Combined inversions of the ERTs of the Wenner alpha and Wenner beta configuration*
196 *across the two main degassing spots in the southern part of the HMF. The two arrows mark the*
197 *location of mofette 1 at 100m and the projection of mofette 2 at 50 m onto the profile.*

198

199 Although our profile is nearly perpendicular to the assumed N-S- running fault, it can be
200 assumed that the subsurface structure has a three-dimensional geometry. Hence, we decided to
201 do combined inversions of both the Wenner alpha and Wenner beta configurations for all of the
202 measurements. The interpretation of the inverted data, the resistivity models, alone is a difficult
203 challenge, because the electrical resistivity varies with several parameters (salinity of the pore
204 fluids, clay mineral contents, clay mineralogy, and porosity). For the same data set, several
205 resistivity models fit the data equally well within the same error limit. However, the resulting
206 resistivity models highlight spatial resistivity contrasts that can be interpreted in terms of
207 degassing features.

208

209 The results seen in Fig. 5 show the combined inversion results of both configurations. The
210 repeated measurements along the profile reveal changes in the overall subsurface resistivity and
211 thus, variations in the underground itself. The first five to ten meters consist of a layer with a
212 resistivity of 200-400 Ohmm, covering the much thicker low resistivity layer (<30 Ohmm). The
213 two degassing sites are clearly characterized by an increase in the resistivity compared to the
214 surrounding: The overall low resistivity increases in a vertical structure to about 100-300 Ohmm
215 in the area below the central mofette (mofette 2) and to 600-1000 Ohmm below the strong
216 degassing site (mofette 1) at the foot of the slope. Both anomalies are independent from another
217 and separated by the low resistivity zone. The eastern part of the profile is characterized by a

218 block of higher resistivities of >300 Ohmm (see Fig. 4). This is, according to Nickschick et al.
219 (2015), related to a different lithological block, which is divided by the N-S-trending fault zone.

220

221 In all profiles the first five meters are characterized only by slightly varying resistivities over
222 time, related to meteoric surface effects like precipitation and evaporation. When we compare
223 the apparent resistivity of these topmost 4 meters, we get an average of 233 Ohmm for
224 September 2012, 195 Ohmm for May 2013, 178 Ohmm for July 13, 182 Ohmm for Aug 2013 and
225 199 Ohmm for the final measurement in October 2013.

226

227 Significant changes that exceed the influence of pure weather phenomena can be found
228 below the first eight to ten meters. The anomalies found in Nickschick et al. (2015) all over the
229 HMF below the mofettes are not stable in their architecture and vary over the course of time.

230

231 To compare the different inversion results better, we calculated the relative in- and decreases
232 from one survey to the next (Fig. 6). Smaller variations of less than $\pm 20\%$ are expected and can
233 be linked to changes in the surface conductivity due to changing weather conditions and soil
234 moisture, very small deviations in the electrode placing (< 10 cm) and numeric inversion
235 artefacts. Thus, these small variations have been shaded in Fig. 6. The distinct vertical anomaly
236 below the central mofette at 50 m changes from 300 Ohmm in September 2012 to about 100
237 Ohmm and less in May but extends farther to the east. A separate channel split from the original
238 channel (at 75 m), while leaving the original channel at 50m less distinct in width and resistivity.
239 This subchannel seems to unify with the main channel again, as it is not observed a second time.
240 In October 2013 the anomalous area has a resistivity of 250-300, similar to the values one year
241 ago. These changes are reliably observable against the low resistivity background.

242

243 The area below the stronger degassing mofette at 120 m in the profile, in the transition from
244 the low resistivity block in the west to the higher resistivity block in the east, is also not a steady
245 and fixed in its architecture over time. Although the variations are not easily visible in the
246 inversions themselves (Fig. 5), they are more striking when numerically compared (Fig. 6).
247 Varying, significant in- and decreases over time mark a non-steady structure at this transition

248 area with a changes in the width and position of that transition zone, which is most likely the
249 feeder channel for the mofette on top.

250

251

252 *Fig. 6: Relative change in the subsurface resistivity of the combined inversion of Wenner alpha*
253 *and beta configuration from one survey to the next. A positive variation of +100 % means that*
254 *the resistivity has doubled in that area, a variation of -50 % means it has halved. Changes of ±20*
255 *% are shaded due to natural variations and inversion errors.*

256

257

258 The results of the repeated self-potential (SP) measurements on the ERT profile are shown in
259 Fig. 7 with maximum values up to + 30 mV and minimum values of - 20mV measured on the
260 ERT profile. These values are low compared to the results in active volcanic environments
261 (Byrdina et al., 2009, 2014; Finizola et al., 2009), but their distribution shows notable signatures
262 in coincidence with subsurface anomalies of the resistivity models and gas flux measurements.
263 Whereas most SP values are between -10 up to +10 mV, two areas with fluctuating higher and
264 lower magnitudes can be localized both at the mofettes at 40-50 m and 100-110 m. Self-potential
265 anomalies are generally generated by three mechanisms: a) the streaming current (electrokinetic
266 potentials) related to the pore fluid flow and dragging part of the electrical layer of the inner
267 surface of porous media; b) the thermoelectric effect related to influences of temperature to the
268 chemical potential of the charge carriers; c) currents related to a gradient of the redox potential of
269 electronic conductors such as ore bodies are present (Revil and Jardani, 2013). An influence of
270 high temperature gradients can be excluded at the survey location. The values of the
271 temperature at 10 cm depth over the whole profile varies between 10.5-15.2°C (September
272 2012), 10.1-11.9°C (July 2013) and 10.5-13.2°C (May 2013). Likewise, the occurrence of redox
273 potentials can be excluded, so that streaming potentials caused by fluid movements (uprising
274 gaseous CO₂ and percolating rain water) are the main causes of the anomalies in the
275 investigated area. The observable anomalies are characterized by positive as well as negative
276 amplitudes depending of the direction of the fluid movement (positive: upward streaming,
277 negative: infiltration and downward movement of fluids). At both high degassing spots the SP
278 anomalies correlates or anti-correlates with the mofette activity. The strength of the amplitude of

279 electrokinetic potentials are balanced by weaker effects, which are caused by the uprising gas
280 (CO₂) and stronger effects by infiltration of a liquid (rain water).

281

282

283 *Fig. 7: Results of the self-potential measurements prior to each geoelectric campaign along the*
284 *profile. Distinct positive and negative anomalies indicate alternating up- or downward movement*
285 *of CO₂ and/or water near the mofettes at 50 m and 100 m, as indicated by the two arrows.*

286

287

288 5. Discussion

289

290 The CO₂ gas flux measurements underline the findings of Nickschick et al. (2015) and Kämpf
291 et al. (2013). Although measured gas fluxes are not as high as in the central part of the HMF,
292 CO₂ discharge rates of about 50 *10³ g m⁻² d⁻¹ were measured in one spot. Emission rates vary
293 on the placing of the accumulation chamber and are vent-bound: High degassing rates occur in
294 the proximity of those small (<1 m diameter) vents, which are marked by dead vegetation and/or
295 animals (Rennert et al. 2011, 2012). The CO₂ drastically decreases with distance from the
296 central vent to emission rates far lower than 100 g m⁻² d⁻¹ for the rest of the area.

297

298 As seen in Nickschick et al. (2015), we were able to observe anomalies in the subsurface
299 underneath the degassing sites. These anomalies were not a one-time feature but their
300 existence and occurrence seems to be a steady phenomenon. According to (Annunziatellis et al.,
301 2008), gases like CO₂ are capable of migrating not only vertically, but also horizontally in soil gas
302 as density-driven flows or advective forces, leading to the rather horizontally oriented anomalies.
303 This might also help understanding why we can observe resistivity changes in the western part of
304 the profile even though the mofette 2 is not located directly on top of the profile. However, the
305 shape of the anomalies is rather unsteady and seems to change over the course of time.
306 Observable increases in the electrically very conductive underground hint at time-dependent,
307 fluid-induced alteration of the very conductive clayey sediments of the Neogene Cypris formation
308 (Hurnik, 1990; Rojik et al., 2014). Since the combined inversion of the Wenner alpha and beta
309 have different sensitivities, they also reveal three-dimensional changes in the degassing sites

310 architecture. Judging from the observations, we assume that these variations in the subsurface
311 resistivity distribution are linked with sediment and/or transport. This could mean that the fluid
312 pressure is high enough to either mobilize sediments to the top or that the fluids rise to a certain
313 “reservoir” and accumulate there. Depending on the fluid pressure, vents of CO₂ and water force
314 their way from the reservoir to the surface, altering the rock properties and leading to variable
315 fluid pathways. If the fluid pressure is high enough in this reservoir, the carbon dioxide is
316 exhausted to the surface. We support the assumption due to the strong variations in the surface
317 gas flux from Nickschick et al. (2015). From there we know that at a heavy degassing spot about
318 300 north of our area the gas flux can vary drastically within hours and change by orders of
319 magnitude. At that point, it was uncertain what caused these huge variations but here we might
320 have found the reason. Considering these observed variations in the resistivity, we think that
321 these massive variations in the measured gas flux are not only linked to changes in soil
322 properties, but are linked to changes in rock properties (porosity, permeability) up to at least 40
323 meters. As indicated by Fig. 4 these alterations may also occur at greater depths in the
324 sedimentary cover but also in the crystalline basement.

325

326 Flores et al. (accepted) did a recent experiment in the exact same location and used a
327 passive registration method to detect seismic noise, caused by ascending fluids. They found two
328 sources that emitted seismic noise, both located where we find our surface degassing spots.
329 They noticed that the source, located at mofette 2, stopped emitting noise from one day to the
330 other, implying that the gas vents are not stable systems and their activity changes over time.
331 The heavier degassing mofette at the foot of the slope emitted a constant noise in their
332 experiment.

333

334

335 *Fig. 8: Ground water level in the HMF. Daily ground water levels are measured by the Czech*
336 *Hydrometeorological Institute in Prague at the drill hole 1H031b; Easting 318713, Northing*
337 *5556542 (see Fig. 1 the dates of the repeated measurements are highlighted red. The ground*
338 *water level changes only slightly over the course of time due to low infiltration rates in the clayey*
339 *sediments.*

340

341

342 During the repetitions of the geoelectrics, the high precipitation in June 2013 and an overall
343 cold and rainy spring lead to an increased influx of meteoric water from the top. The infiltration of
344 large amounts of water might work as an antagonistic force to the ascending CO₂ and work as a
345 seal, when soil pores are saturated by water. Observations of the ground water level at the drill
346 hole drill hole 1H031b (Easting 318713, Northing 5556542) in the central part of the HMF reveal
347 that the ground water level (Fig. 8) during the campaign (13 months) only shifts within one meter
348 with daily variations of about 20 cm. Even the heavy rainfall and flooding of May-June 2013 only
349 have little impact on the ground water level. While pressure (barometric or hydraulic) has been
350 discussed as a controlling factor for wet mofettes and natural springs (e. g. Koch and Heinicke
351 (2007)), the effects on the CO₂ gas flux and the fluid-rock-interaction in this sediment covered
352 mudstone at depths of several tens of meters has yet to be studied in situ. However we do not
353 think that this is controlling factor for the high variations measured in Nickschick et al. (2015).

354

355 If water influx is not the controlling factor, there are some other sources left to be considered
356 for the variations. The most logical one is, without question, unsteadiness in the gas ejection rate
357 itself. Geodynamic processes are not steady features and it is to be assumed that a certain
358 variability in the CO₂ release occurs naturally from the gas' way from its source in the
359 Lithospheric Mantle to the surface. The influence of deep-seated effect affecting the surface
360 degassing is a very complex and barely understood phenomenon.

361

362 We can exclude everything beyond a very minor influence of the measurements' setup. In all
363 experiments we used the same device and the electrodes were put into the same position which
364 was marked by wooden pegs. The inversions resulted in accuracies (RMS) of less than 17 %.
365 The meadow itself is not penetrated by drillings nor used for agriculture, except for mown grass
366 few times a year, so artificial alterations can be excluded as well.

367

368 As seen in Nickschick et al. (2015), the high pressure of fluids (CO₂ and water carried along)
369 is capable of altering the clayey sedimentary rocks mechanically and/or chemically: The fluid's
370 power is capable of moving sandy material along from lower stratigraphic units into the
371 overlaying clay or widening the pores. In Fig. 9 we tried to convert the resistivity distribution into

372 a simplified geologic model. In this case a reservoir in the clayey sediments, which is indicated at
373 the bottom of the model, releases gaseous CO₂ to the surface. The amount of released CO₂ is
374 stronger at the main mofette 1 at the foot of the slope, which relates to a more distinct high-
375 resistivity anomaly. If this is related to the course of the fault zone as indicated by Nickschick et
376 al. (2015) CO₂ (and water) could migrate upwards along the fault leading to strong CO₂
377 degassing at the top. Less CO₂ degasses at the mofette 2, indicated by the weaker anomaly and
378 also by the separate channel, which was only observed in July 2013.

379

380 In a very simplified estimation we can use Archie's law to roughly evaluate the changes in the
381 pore space parameters (saturation with water and gas), even though we are in a clay-rich
382 environment:

383

384 (1) $\rho_t = a \varphi^{-m} S_w^{-n} R_w$ with $a, m = \text{const}, n = 2$

385

386 ρ_t : Fluid saturated rock resistivity S_w : Brine saturation R_w : Brine resistivity φ : Porosity

387 a : Tortuosity factor m : Cementation exponent n : Saturation exponent

388

389 Since we used the same setup in the very same location every time, we assume that the
390 measuring situation did not change (no porosity and fluid resistivity changes $\rightarrow \varphi, R_w = \text{const}$).

391 In this very simple estimation we get the relation

392

393 $\rho_t \sim S_w^{-2}$

394

395 which means that if we observe a change in the resistivity of e.g. 100 Ohmm to 200 Ohmm,
396 we can relate that to a change in the saturation S_w to $\sim 70\%$ of the original saturation. Although
397 this is a very simplified estimation, it shows that slight changes in the saturation of the pores can
398 lead to significant changes in the measured resistivity in this conductive environment. As the
399 porosity is generally low, CO₂ could replace the fluid-filled pores rather quickly.

400

401 It is still not clear what actually causes the anomalies within the Neogene sediments as no
402 recent drill recording from nearby drill wells describes the sediments in detail. From what we

403 observe at the heavily degassing mofette near the slope and in the central part of the HMF, we
404 link this to the N-S-trending Počátky-Plesná fault zone, as fault zones provide pathways for
405 ascending fluids.

406

407

408 *Fig. 9: Schematic model of the subsurface architecture below the southern part of the HMF as*
409 *derived from the inversion result from July 2013 (bottom). Separate channels branch out from the*
410 *large anomaly from Fig. 4, indicated at the bottom of this model. They are overlain by a layer of*
411 *about 4 m of high resistivity, which also acts as a seal, which is penetrated by CO₂. Especially in*
412 *the eastern part where the fault zone is assumed to run, the ascending CO₂ is redirected to*
413 *degas at the foot of the slope.*

414

415

416 6. Conclusions and Outlook

417

418 1. Our test survey in the southern HMF reveals variations in the subsurface underneath high
419 gas flux areas (mofettes), indicated by changes in the electric resistivity. These changes
420 can were observed by using a combination of different electrode configurations (Wenner
421 alpha and beta) in a common inversion.

422 2. Varying positive and negative anomalies in the self-potential at the mofettes indicate a non-
423 steady ascent of CO₂ or a high infiltration of water acting as antagonistic force to the
424 ascending CO₂.

425 3. These changes indicate that CO₂ degassing sites are not steady structures and their
426 architecture changes over the course of weeks or maybe even days, which can also be
427 observed by other methods (e.g. seismic noise registrations (Flores et al., accepted)).

428 4. For this area, but maybe also for other volcanic or non-volcanic areas, extensive CO₂ map-
429 pings of the gas flux are erratic to an unknown extent yet as the degassing changes over
430 time.

431

432 One reason for this can be deeply-rooted changes in the CO₂'s source or in the pathways
433 from the source through the crust. However, changes in the amount of emitted carbon dioxide at

434 surface can be traced to changes in the underlying sedimentary rocks to at least 40 m of depth,
435 which are caused by the ascent of CO₂ and water mobilized along and the physical and/or
436 chemical alteration caused by it. Since there is no monitoring and, thus, no long term
437 measurement for the gas flux, it yet to be shown how changes in the electric resistivity correlate
438 with the actual amount of ejected CO₂, but a future systematic approach would be able to link
439 these two methods while monitoring and considering factors like precipitation and ground water
440 level changes. CO₂ gas flux mappings over longer periods of time consider a steady state of
441 degassing activity. However, as CO₂ degassing activity changes over time, these mappings bear
442 flaws to unknown extent and should be considered when mapping and calculating gas
443 emissions. Due to the setup of the experiment and the configuration's sensitivity, we were able to
444 only measure resistivity changes underneath the central mofette to a depth of about 40 meters,
445 while it is clear, that this is just the uppermost part of the anomalies. Using a wider electrode
446 spacing could provide further insight into possible changes with these anomalous areas at the
447 cost of resolution or effort but it is to be assumed that the observed variations in mofette
448 architecture continues at depth.

449

450 In the context of ICDP (see Dahm et al. (2013)) scientists will gather information about fluid
451 ascent and migration in NW Bohemia on different scales. From a drilling in the HMF, as
452 suggested by Alawi et al. (2015), we might gather insight about fluid migration in such a CO₂
453 vent. By analyzing core material and linking these results with geophysical surveys like those
454 presented in this article we will be able to understand fluid pathways and their interaction with the
455 surrounding better.

456

457 7. Acknowledgements

458

459 We would like to express our gratitude to the German Research Foundation (DFG) for
460 funding this project (KA902/16 and FL271/13). Special thanks goes to Claudia Schütze from the
461 UFZ Leipzig and Tomas Fischer from Charles University in Prague for providing ground water
462 data from the Czech Hydrometeorological Institute in Prague.

463

464

465 8. References

466

467 Alawi M, Nickschick T, H K (2015) Mikrobiologische Prozesse in CO₂-Aufstiegskanälen. In:
468 System Erde, DOI 10.2312/GFZ.syserde.05.01.5

469

470 Annunziatellis A, Beaubien SE, Bigi S, Giotoli G, Coltella M, Lombardi S (2008) Gas migration
471 along fault systems and through the vadose zone in the Latera caldera (Central Italy):
472 Implications for CO₂ geological storage. International Journal Of Greenhouse Gas Control
473 2:353–372

474

475 Bankwitz P, Schneider H Gand Kämpf, Bankwitz E (2003) Structural characteristics of epicentral
476 areas in Central Europe: study case Cheb Basin (Czech Republic). Journal Of Geodynamics
477 35:5–32

478

479 Bergmann P, Schmidt-Hattenberger C, Kiessling D, Rücker C, Labitzke T, Henniges J,
480 Baumann G, Schütt H (2012) Surface-downhole electrical resistivity tomography applied to
481 monitoring of CO₂ storage at Ketzin, Germany. Geophysics 77:B253–267

482

483 Bergmann P, Schmidt-Hattenberger C, Labitzke T, Wagner F, Just A, Flechsig C, Rippe D
484 (accepted) Fluid injection monitoring using electrical resistivity tomography – five years of CO₂
485 injection at Ketzin, Germany. Geophys Prosp

486

487 Bräuer K, Kämpf H, Niedermann S, Strauch G, Tesař J (2008) The natural laboratory NW
488 Bohemia-comprehensive fluid studies between 1992 and 2005 used to trace geodynamic
489 processes. Geochemistry, Geophysics, Geosystems 9: L17309, DOI 10.1029/2009GL039615

490 Bräuer K, Kämpf H, Strauch G (2009) Earthquake swarms in non-volcanic regions: what fluids
491 have to say. Geophysical Research Letters 36: L17309, DOI 10.1029/2009GL039615

492

493 Bräuer K, Kämpf H, Strauch G (2014) Seismically triggered anomalies in the isotope signatures of
494 mantle-derived gases detected at degassing sites along two neighboring faults in NW Bohemia,

495 central Europe. *Journal of Geophysical Research: Solid Earth* 119(7):5613–5632, DOI 10.1002/
496 2014JB011044

497

498 Byrdina S, Revil A, Pant SR, Koirala BP, Shrestha PL, Tiwari DR, Gautam UP, Shrestha K,
499 Sapkota SN, Contraires S, Perrier F (2009) Dipolar self-potential anomaly associated with
500 carbon dioxide and radon flux at Syabru-Bensi hot springs in central Nepal. *Journal of*
501 *Geophysical Research: Solid Earth* 114(B10):B10,101, DOI 10.1029/2008JB006154

502

503 Byrdina S, Vandemeulebrouck J, Cardellini C, Legaz A, Camerlynck C, Chiodini G, Lebourg T,
504 Gresse M, Bascou P, Motos G, Carrier AS, Caliro S (2014) Relations between electrical
505 resistivity, carbon dioxide flux, and self-potential in the shallow hydrothermal system of Solfatara
506 (Phlegrean Fields, Italy). *Journal of Volcanology and Geothermal Research* 283:172–182

507

508 Dahm T, Hrubcová P, Fischer T, Horálek J, Korn M, Buske S, Wagner D (2013) Eger Rift ICDP: an
509 observatory for study of non-volcanic, mid-crustal earthquake swarms and accompanying
510 phenomena. *Scientific Drilling* 16:93–99

511

512 Drahor MG, Berge MA, Özde B, Öztürk C (2012) An Example of Electrical Resistivity Tomography
513 Monitoring in Geothermal Sites: Balcova-Izmir Case Study. In: *Geoelectric Monitoring: Current*
514 *Research and Perspectives for the Future: GELMON 2011: 1st International Workshop on*
515 *Geoelectric Monitoring: Book of extended abstracts; International Workshop within the fra-me of*
516 *the FWF project TEMPEL (TRP 175-N21) and the 7th FP European project SafeLand November*
517 *30th - December 2nd, 2011, Vienna*

518

519 Fedele A, Giulia Di Giuseppe M, Troiano A, Somma R, Caputo T, Patella D, Troise C, De Natale G
520 (2015) Monitoring the geothermal fluid using time lapse electrical resistivity tomography: The
521 Pisciarelli fumarolic field test site (Campi Flegrei, South Italy). In: *EGU General Assembly*
522 *Conference Abstracts, EGU General Assembly Conference Abstracts, Vol 17, p 13496*

523

524 Finizola A, Aubert M, Revil A, Schütze C, Sortino F (2009) Importance of structural history in the
525 summit area of Stromboli during the 2002-2003 eruptive crisis inferred from temperature, soil

526 CO₂, self-potential, and electrical resistivity tomography. *Journal of Volcanology and Geothermal*
527 *Research* 183:213–227
528

529 Fischer T, Horálek J, Hrubcová P, Vavryčuk V, Bräuer K, Kämpf H (2014) Intra-continental
530 earthquake swarms in West-Bohemia and Vogtland: A review. *Tectonophysics* 611:1–27, DOI
531 10.1016/j.tecto.2013.11.001
532

533 Flechsig C, Bussert R, Rechner J, Schütze C, Kämpf H (2008) The Hartoušov Mofette Field in the
534 Cheb Basin, Western Eger Rift (Czech Republic): A Comparative Geoelectric, Sedimentologic
535 and Soil Gas Study of a Magmatic Diffuse CO₂-Degassing Structure. *Zeitschrift für Geologische*
536 *Wissenschaften* 36(3):177–193
537

538 Flechsig C, Fabig T, Rücker C, Schütze C (2010) Geoelectrical investigations in the Cheb
539 Basin/W-Bohemia: An approach to evaluate the near-surface conductivity structure. *Studia*
540 *Geophysica et Geodetica* 54:417–437
541

542 Flores H Estrella, Umlauf J, Schmidt A, Korn M (accepted) Locating mofettes using seismic noise
543 records from small dense arrays and Matched Field Processing Analysis in the NW
544 Bohemia/Vogtland Region, Czech Republic. *Near Surface Geophysics*
545

546 Günther T, Rücker C, Spitzer K (2006) Three dimensional modelling and inversion of dc resistivity
547 data incorporating topography - II. Inversion. *Geophysical Journal International* 166 (2):506–517
548

549 Hubatka F, Boušková A, Špičák A, Švancara J, Tiišarová R (2004) Ground Penetrating Radar
550 Profile Measurements above the Seismoactive Area at the Eastern Margin of the Cheb Basin,
551 Western Bohemia. *Geolines* 17:41–42
552

553 Hurnik S (1990) Clastic dikes in the brown coal seam near Most in the North Bohemian Basin
554 (Miocene). *Geologie* 45:123–150
555

556 Jardani A, Revil F Aand Santos, Fauchard C, Dupont J (2007) Detection of preferential infiltration
557 pathways in sinkholes using joint inversion of self-potential and EM-34 conductivity data.
558 Geophysical Prospecting 55:749–760
559

560 Kämpf H, Bräuer K, Schumann J, Hahne K, Strauch G (2013) CO₂ discharge in an active, non-
561 volcanic continental rift area (Czech Republic): Characterisation (¹³C, ³He/⁴He) and quantifi-
562 cation of diffuse and vent CO₂ emissions. Chemical Geology 339:81–83
563

564 Koch U, Heinicke J (2007) Hydrological influences on long-term gas flow trends at locations in the
565 Vogtland/NW Bohemian seismic region (German-Czech border). Annals of geophysics
566 50(4):557– 568
567

568 Loke MH, Chambers J, Rucker D, Kuras O, Wilkinson PB (2013) Recent developments in the
569 direct-current geoelectrical imaging method. Journal of Applied Geophysics 95:132–156
570

571 Naudet V, Revil A, Bottero, JY, Bégassat P (2003) Relationship between self-potential (SP) signals
572 and redox conditions in contaminated groundwater. Geophysical Research Letters 30:2091, DOI
573 10.1029/2003GL018096,21
574

575 Nickschick T, Kämpf H, Flechsig C, Mrlina J, Heinicke J (2015) CO₂ degassing in the Hartoušov
576 mofette area, western Eger Rift, imaged by CO₂ mapping and geoelectrical and gravity surveys.
577 International Journal Of Earth Sciences 104:2107–2129
578

579 Peterek A, Reuther CD, Schunk R (2011) Neotectonic evolution of the Cheb Basin (Northwestern
580 Bohemia, Czech Republic) and its implications for the late Pliocene to Recent crustal deforma-
581 tion in the western part of the Eger Rift. Zeitschrift für Geologische Wissenschaften 5/6:335–365
582

583 Pettinelli E, Beaubie SE, Zaja A, Menghini A, Praticelli N, Mattei E, Di Matteo A, Ciotoli G,
584 Lombardi S (2010) Characterization of a CO₂ gas vent using various geophysical and
585 geochemical methods. Geophysics 75, 3:137–146
586

587 Ramirez A, Newmark R, Daily W (2003) Monitoring carbon dioxide floods using electrical
588 resistance tomography (ERT):sensitivity studies. *Journal of Environmental & Engineering*
589 *Geophysics* 8:187–208
590

591 Rennert T, Eusterhues K, Pfanz H, Totsche KU (2011) Influence of geogenic CO₂ on mineral and
592 organic soil constituents on a mofette site in the NW Czech Republic. *European Journal Of Soil*
593 *Science* 62:572–580, DOI 10.1111/j.1365-2389.2011.01355.x
594

595 Rennert T, Eusterhues K, de Andrade V, Totsche KU (2012) Iron species in soils on a mofette site
596 studied by Fe K-edge X-ray absorption near-edge spectroscopy. *Chemical Geology* 332-
597 333:116–123
598

599 Revil A, Jardani A (2013) *The Self-Potential Method: Theory and Applications in Environmental*
600 *Geosciences*
601

602 Revil A, Finiziola A, Ricci T, Delcher E, Peltier A, Barde Cabusson S, Avard G, Bailly T, Ben-nati L,
603 Byrdina S, Cologne J, Di Gangi F, Douillet G, Lupi M, Letort J, Tsang Hin Sun E (2011)
604 Hydrogeology of Stromboli volcano, Aeolian Islands (Italy) from the interpretation of resistivity
605 tomograms, self-potential, soil temperature and soil CO₂ concentration measurements.
606 *Geophysical Journal International* 186(3):88–98
607

608 Rojik P, Fejfar O, Dašková J, Kvaček Z, Pešek J, Sýkorová I, Teodoridis V (2014) Krušné hory
609 Piedmont basins - Cheb Basin. In: Pešek J (ed) *Tertiary Basins and Lignite Deposits of the*
610 *Czech Republic, Tertiary Basins and Lignite Deposits of the Czech Republic, Prague*
611

612 Rucker C, Günther T, Spitzer K (2006) 3-D modeling and inversion of DC resistivity data
613 incorporating topography - Part I: modeling. *Geophysical Journal International* 166:495–505
614

615 Sandig C, Sauer U, Bräuer K, Serfling U, Schütze C (2014) Comparative study of geophysical and
616 soil-gas investigations at the Hartoušov (Czech Republic) natural CO₂ degassing site. *Environ-*
617 *mental Earth Sciences* 72:1421–1434

618

619 Sauer U, Schütze C, C L, Schlömer S, Dietrich P (2013) An Integrative Hierarchical Monitoring
620 Approach for Detecting and Characterizing CO₂ Releases. *Energy Procedia* 37:4257–4267

621

622 Schütze C, Sauer U, Beyer K, Lamert H, Bräuer K, Strauch G, Flechsig C, Kämpf H, Dietrich P
623 (2012a) Natural analogues: a potential approach for developing reliable monitoring methods to
624 understand subsurface CO₂ migration processes. *Environmental Earth Sciences* 67:411–423

625 Schütze C, Vienken T, Werban U, Dietrich P, Finizola A, Leven C (2012b) Joint application of
626 geophysical methods and Direct Push-soil gas surveys for the improved delineation of buried
627 fault zones. *Journal of Applied Geophysics* 82:129 – 136, DOI 10.1016/j.jappgeo.2012.03.002

628

629 Schütze C, Dietrich P, Sauer U (2013) Diagnostic monitoring to identify preferential near-surface
630 structures for CO₂ degassing into the atmosphere: Tools for investigations at different spatial
631 scales validated at a natural analogue site. *International Journal Of Greenhouse Gas Control*
632 18:285–295

633

634 Spicakova L, Ulicny D, Koudelkova GC (2000) Tectonosedimentary evolution of the Cheb Basin
635 (NW Bohemia, Czech Republic) between late Oligocene and Pliocene: a preliminary note. *Studia*
636 *Geophysica et Geodetica* 44:556–580

637

638 Weinlich FH, Bräuer K, Kämpf H, Strauch G, Tesař J, Weise SM (1999) An active subcontinental
639 mantle volatile system in the western Eger rift, Central Europe: Gas flux, isotopic (He, C, and N)
640 and compositional fingerprints. *Geochim Cosmochim Acta* 63:3653–3671

641

642 Zlotnicki J, Nishida Y (2003) Review on morphological insights of self-potential anomalies on
643 volcanoes. *Surveys in Geophysics* 24:291–338

644

Figure 1

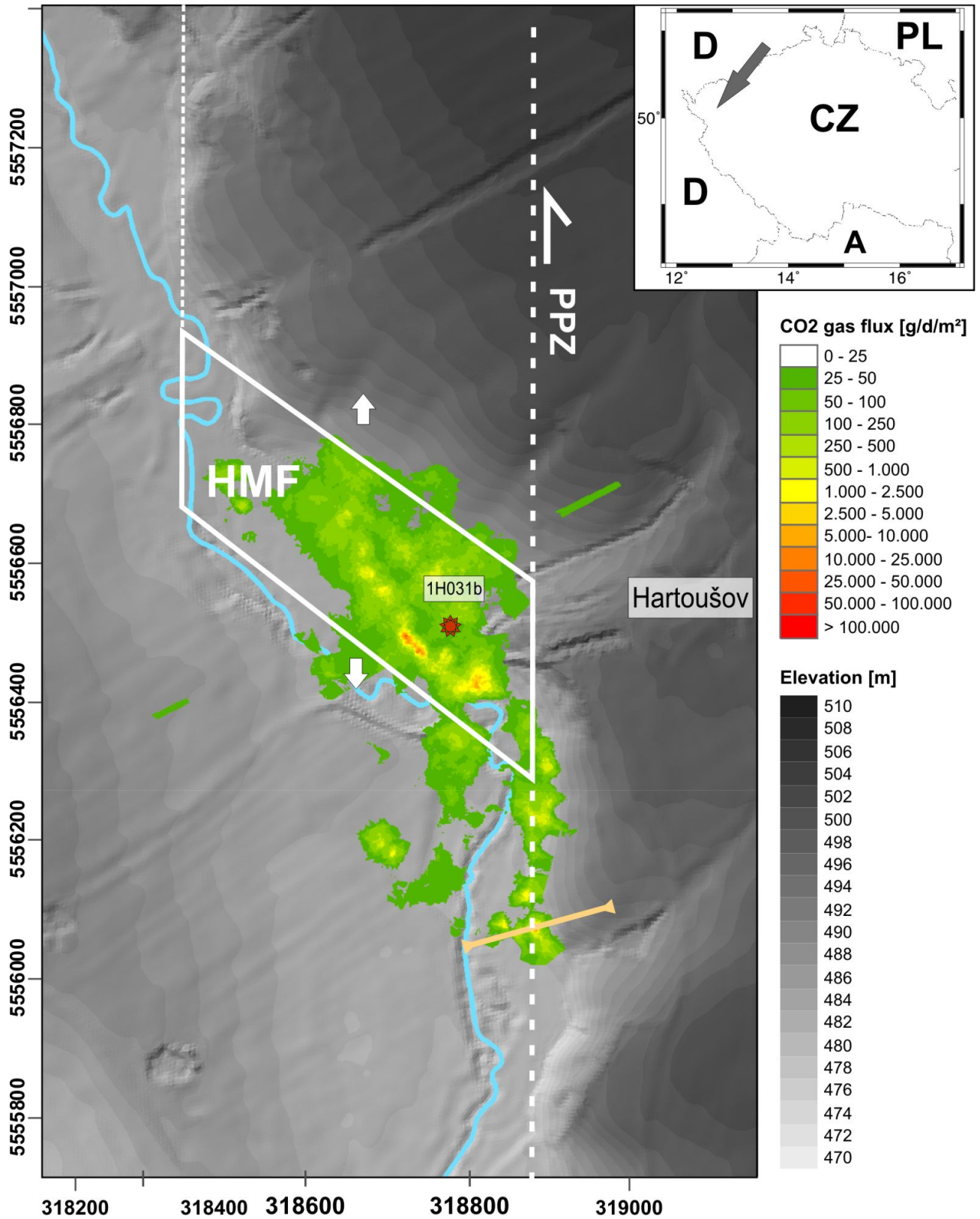


Figure 2

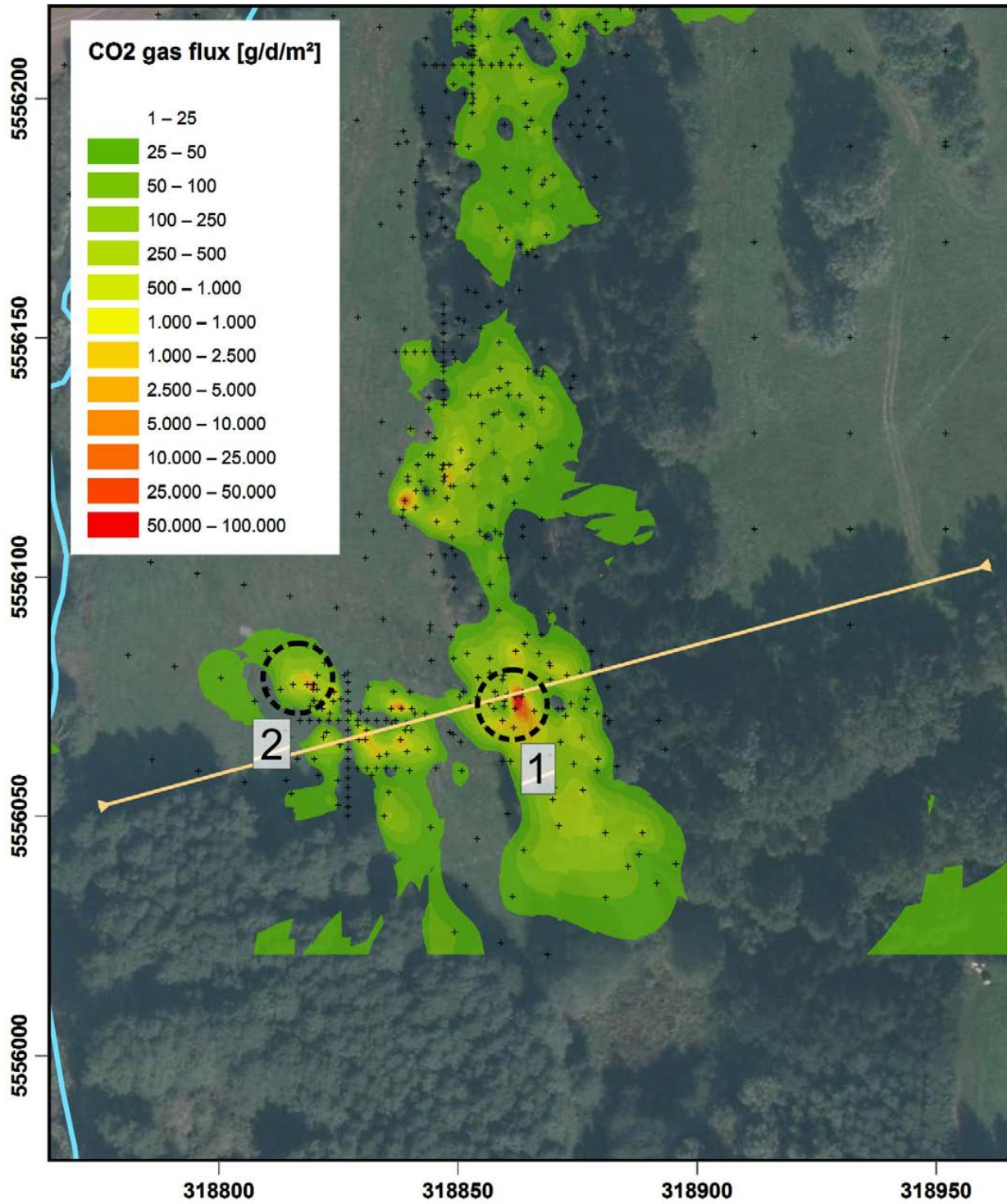


Figure 3

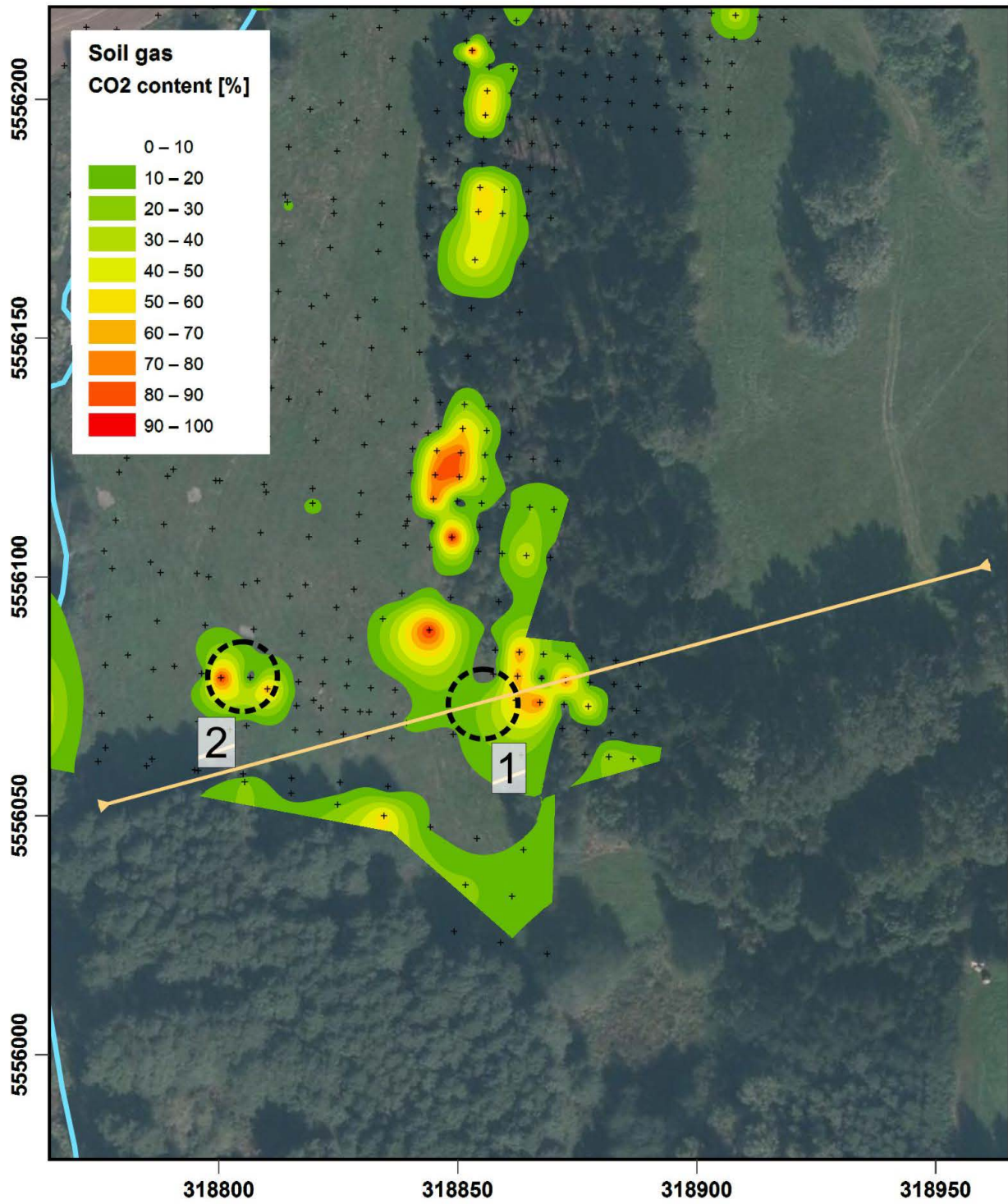


Figure 4

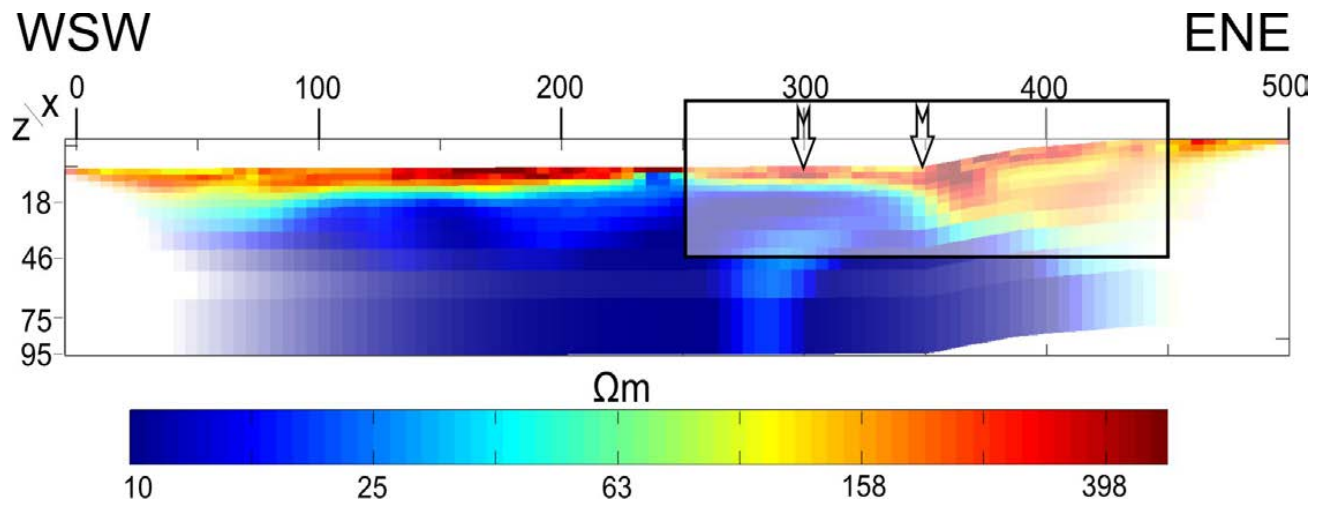


Figure 5

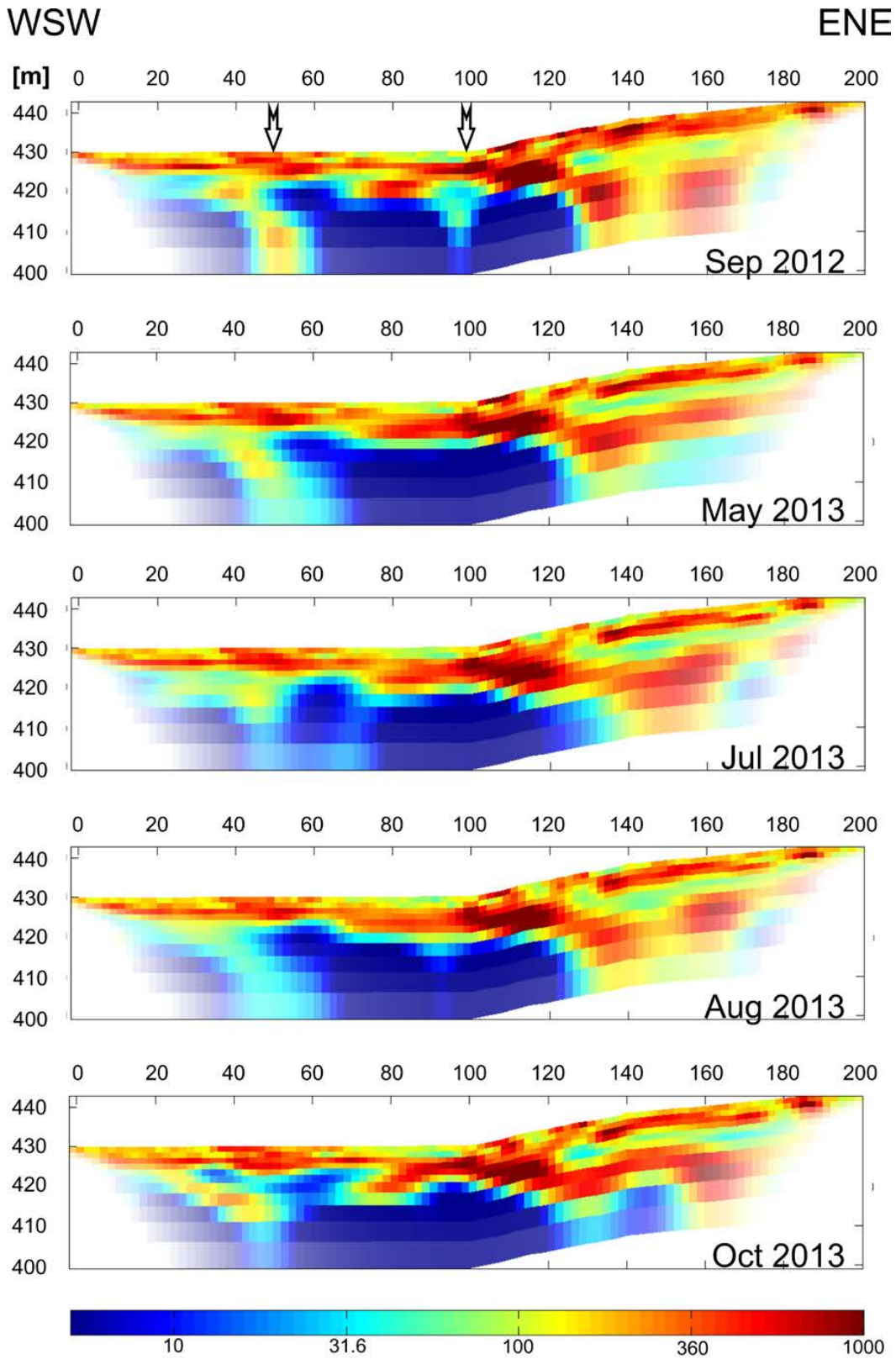


Figure 6

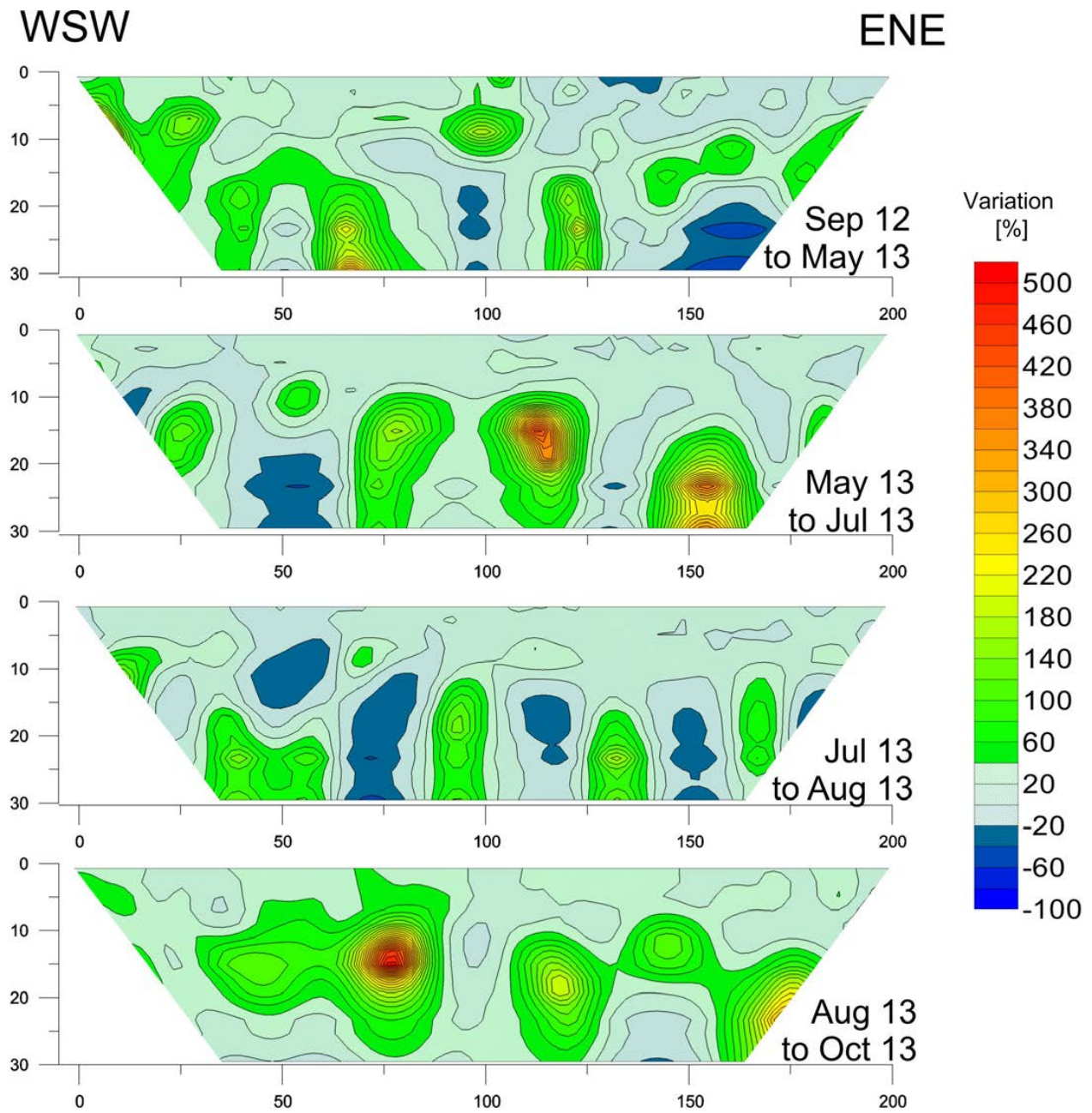


Figure 7

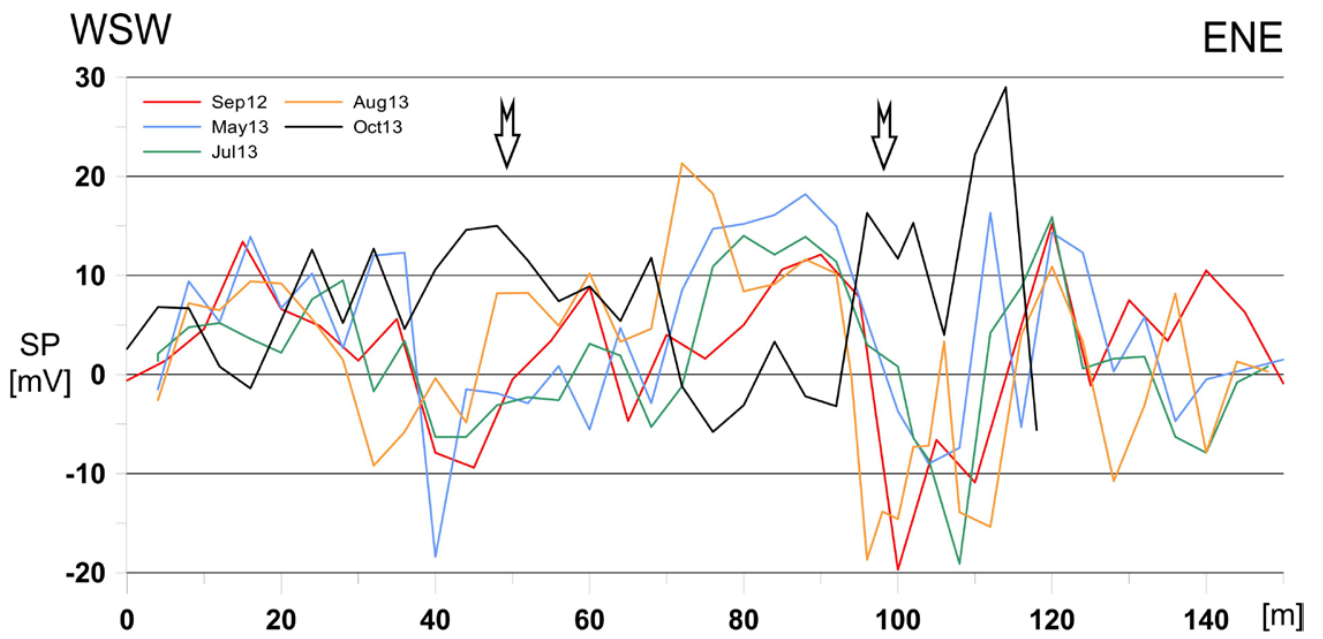
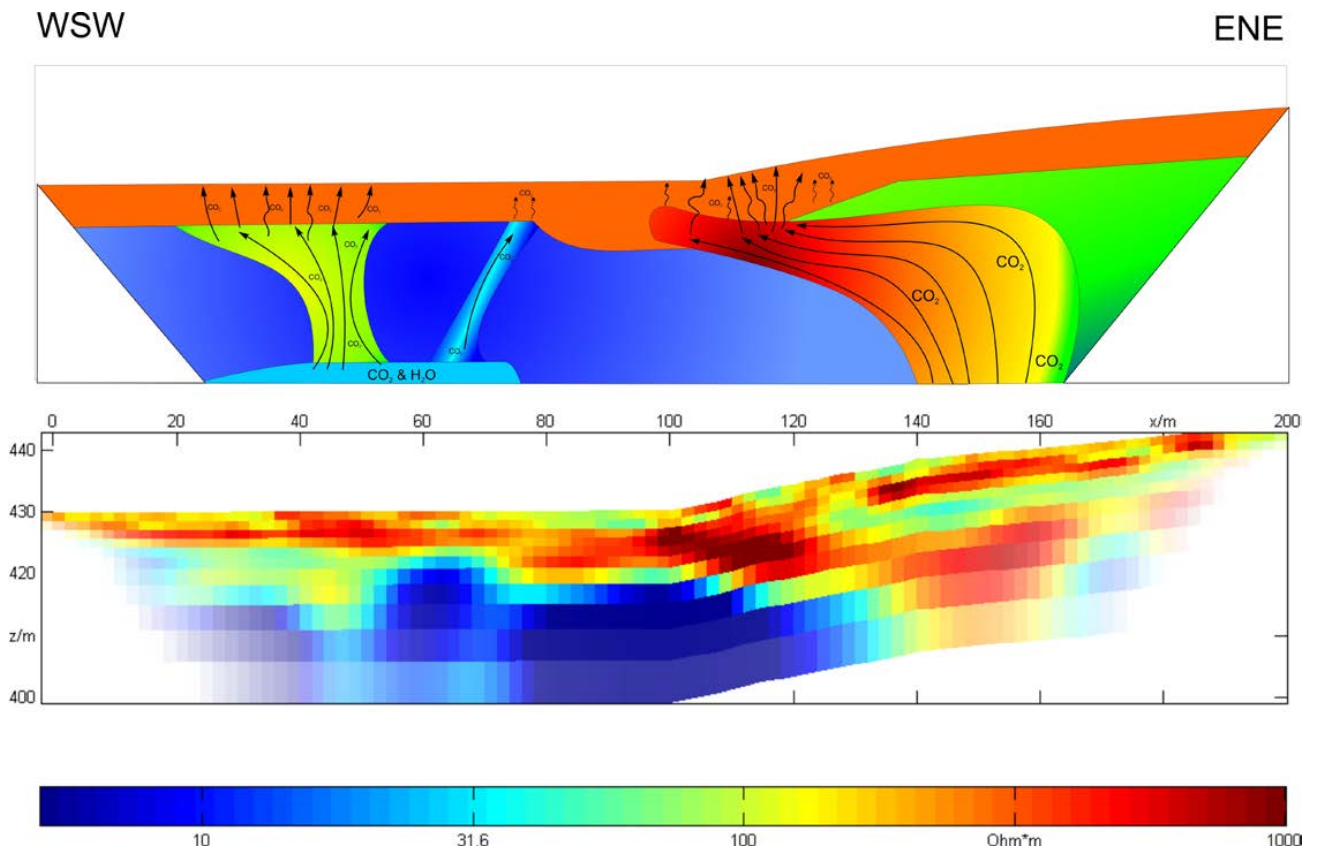


Figure 8



Reprint permissions for listed articles

SPRINGER LICENSE TERMS AND CONDITIONS

Aug 13, 2016

This Agreement between Tobias Nickschick ("You") and Springer ("Springer") consists of your license details and the terms and conditions provided by Springer and Copyright Clearance Center.

License Number	3927170136629
License date	Aug 13, 2016
Licensed Content Publisher	Springer
Licensed Content Publication	Bulletin of Volcanology
Licensed Content Title	The "Triasscholle" near Greiz, Germany—a volcanic origin?
Licensed Content Author	T. Nickschick
Licensed Content Date	Jan 1, 2014
Licensed Content Volume Number	76
Licensed Content Issue Number	4
Type of Use	Thesis/Dissertation
Portion	Full text
Number of copies	4
Author of this Springer article	Yes and you are a contributor of the new work
Order reference number	
Title of your thesis / dissertation	Palaeovolcanic and present magmatic structures along the N-S trending Regensburg-Leipzig-Rostock zone
Expected completion date	Aug 2016
Estimated size(pages)	150
Requestor Location	Tobias Nickschick Telegrafenberg Potsdam, 14473 Germany Attn: Tobias Nickschick
Billing Type	Invoice
Billing Address	Tobias Nickschick Telegrafenberg Potsdam, Germany 14473 Attn: Tobias Nickschick
Total	0.00 EUR
Terms and Conditions	

Introduction

The publisher for this copyrighted material is Springer. By clicking "accept" in connection with completing this licensing transaction, you agree that the following terms and conditions apply to this transaction (along with the Billing and Payment terms and conditions established by Copyright Clearance Center, Inc. ("CCC"), at the time that you opened your Rightslink account and that are available at any time at <http://myaccount.copyright.com>).

SPRINGER LICENSE TERMS AND CONDITIONS

Aug 13, 2016

This Agreement between Tobias Nickschick ("You") and Springer ("Springer") consists of your license details and the terms and conditions provided by Springer and Copyright Clearance Center.

License Number	3927170292379
License date	Aug 13, 2016
Licensed Content Publisher	Springer
Licensed Content Publication	International Journal of Earth Sciences
Licensed Content Title	CO2 degassing in the Hartoušov mofette area, western Eger Rift, imaged by CO2 mapping and geoelectrical and gravity surveys
Licensed Content Author	Tobias Nickschick
Licensed Content Date	Jan 1, 2015
Licensed Content Volume Number	104
Licensed Content Issue Number	8
Type of Use	Thesis/Dissertation
Portion	Full text
Number of copies	4
Author of this Springer article	Yes and you are a contributor of the new work
Order reference number	
Title of your thesis / dissertation	Palaeovolcanic and present magmatic structures along the N-S trending Regensburg-Leipzig-Rostock zone
Expected completion date	Aug 2016
Estimated size(pages)	150
Requestor Location	Tobias Nickschick Telegrafenberg Potsdam, 14473 Germany Attn: Tobias Nickschick
Billing Type	Invoice
Billing Address	Tobias Nickschick Telegrafenberg Potsdam, Germany 14473 Attn: Tobias Nickschick
Total	0.00 USD
Terms and Conditions	

Introduction

The publisher for this copyrighted material is Springer. By clicking "accept" in connection with completing this licensing transaction, you agree that the following terms and conditions apply to this transaction (along with the Billing and Payment terms and conditions

SPRINGER LICENSE TERMS AND CONDITIONS

Aug 13, 2016

This Agreement between Tobias Nickschick ("You") and Springer ("Springer") consists of your license details and the terms and conditions provided by Springer and Copyright Clearance Center.

License Number	3927170385024
License date	Aug 13, 2016
Licensed Content Publisher	Springer
Licensed Content Publication	International Journal of Earth Sciences
Licensed Content Title	Integrated geophysical and geological methods to investigate the inner and outer structures of the Quaternary Mýtina maar (W-Bohemia, Czech Republic)
Licensed Content Author	Christina Flechsig
Licensed Content Date	Jan 1, 2015
Licensed Content Volume Number	104
Licensed Content Issue Number	8
Type of Use	Thesis/Dissertation
Portion	Full text
Number of copies	4
Author of this Springer article	Yes and you are a contributor of the new work
Order reference number	
Title of your thesis / dissertation	Palaeovolcanic and present magmatic structures along the N-S trending Regensburg-Leipzig-Rostock zone
Expected completion date	Aug 2016
Estimated size(pages)	150
Requestor Location	Tobias Nickschick Telegrafenberg Potsdam, 14473 Germany Attn: Tobias Nickschick
Billing Type	Invoice
Billing Address	Tobias Nickschick Telegrafenberg Potsdam, Germany 14473 Attn: Tobias Nickschick
Total	0.00 USD
Terms and Conditions	

Introduction

The publisher for this copyrighted material is Springer. By clicking "accept" in connection with completing this licensing transaction, you agree that the following terms and conditions apply to this transaction (along with the Billing and Payment terms and conditions

Declaration of personal contribution

Erklärung zu den Eigenanteilen des Promovenden Tobias Nickschick an den Publikationen und Zweitpublikationsrechten bei der kumulativen Dissertation

The "Triasscholle" near Greiz, Germany - a volcanic origin?

Nickschick, T., Kämpf, H., Jahr, T.
published 2014 in Bulletin of Volcanology 76(4):1-20

	T.Nickschick	H. Kämpf	T. Jahr
Generelle Beteiligung	70%	20%	10%
Konzeption des Forschungsansatzes		X	X
Planung der Untersuchungen	X	X	X
Datenerhebung und Interpretation	X	X	
Schreiben des Manuskripts	X	X	
Vorschlag Anrechnung Publikationsäquivalente			

Integrated geophysical and geological methods to investigate the inner and outer structures of the Quaternary Mýtina maar (W-Bohemia, Czech Republic)

Flehsig, C., Heinicke, J., Mrlina, J., Kämpf, H., **Nickschick, T.**, Schmidt, A., Bayer, T., Günther, T., Rücker, C., Seidel, E., Seidl, M.
published 2015 in International Journal of Earth Sciences 104(8):2087-2105

	C. Flehsig	J. Heinicke	J. Mrlina	H. Kämpf	T. Nickschick	Assistenten & Studenten
Generelle Beteiligung	30%	20%	20%	15%	10%	5%
Konzeption des Forschungsansatzes	x			x		
Planung der Untersuchungen	x			x		
Datenerhebung und Interpretation	x	x	x	x	x	x
Schreiben des Manuskripts	x	x	x	x	x	
Vorschlag Anrechnung Publikationsäquivalente						

CO₂ degassing in the Hartoušov mofette area, western Eger Rift, imaged by CO₂ mapping and geoelectrical and gravity surveys

Nickschick, T., Kämpf, H, Flechsig, C., Mrlina, J., Heinicke, J.
published 2015 in International Journal of Earth Sciences 104(8):2107-2129

	T. Nickschick	H. Kämpf	C. Flechsig	J Mrlina	J. Heinicke
Generelle Beteiligung	60%	20%	10%	5%	5%
Konzeption des Forschungsansatzes	x	x	x		
Planung der Untersuchungen	x	x	x		
Datenerhebung und Interpretation	x	x	x	x	x
Schreiben des Manuskripts	x	x	x	x	
Vorschlag Anrechnung Publikationsäquivalente					

Architecture and temporal variations of a terrestrial CO₂ degassing site using electric resistivity and CO₂ gas measurements

Nickschick, T., Flechsig, C., Meinel, C., Mrlina, J., Kämpf, H.
submitted to International Journal of Earth Sciences July 8th, 2016

	T. Nickschick	C.Flechsig	C. Meinel	J Mrlina	Kämpf. H.
Generelle Beteiligung	65%	15%	10%	5%	5%
Konzeption des Forschungsansatzes	x	x			x
Planung der Untersuchungen	x	x	x		
Datenerhebung und Interpretation	x	x	x	x	
Schreiben des Manuskripts	x	x			x
Vorschlag Anrechnung Publikationsäquivalente					

Für die in dieser kumulativen Dissertation verwendeten Publikationen habe ich die notwendigen Genehmigungen des Verlags (Springer) eingeholt, die hier eingebunden sind (reprint permission).

Die Coautoren der in dieser Dissertation verwendeten Manuskripte sind über deren Nutzung und die hier angegebenen Eigenanteilsvorschläge informiert. Ihr Einverständnis habe ich in digitaler Form als E-Mail erhalten. Unter dem Punkt „Generelle Beteiligung“ ist die von mir vorgeschlagene Einschätzung der Anteile angegeben.

Dipl.-Geophys. Tobias Nickschick

Jena, 15.08.2016

Ich bin mit der Abfassung der Dissertation als publikationsbasiert, d. h. kumulativ, einverstanden und bestätige die hier gemachten Angaben. Eine entsprechend begründete Befürwortung mit Angabe des wissenschaftlichen Anteils des Doktoranden an den verwendeten Publikationen werde ich an den Rat der Chemisch-Geowissenschaftlichen Fakultät richten.

Prof. Dr. Florian Bleibinhaus

Prof. Dr. Lothar Viereck

Erklärung

Hiermit bestätige ich, dass ich die vorliegende Arbeit selbständig verfasst und keine anderen als die angegebenen Hilfsmittel benutzt habe. Die Stellen der Arbeit, die dem Wortlaut oder dem Sinn nach anderen Werken (dazu zählen auch Internetquellen) entnommen sind, wurden unter Angabe der Quelle kenntlich gemacht.

Diplom-Geophysiker Tobias Nickschick

Jena, den 15. August 2016

Acknowledgements

An allererster Stelle möchte ich meinen tiefen Respekt und mein herzlichstes Dankeschön gegenüber meinem Mentor Horst Kämpf ausdrücken. Ich kann an dieser Stelle nur schwer beschreiben, wie oft ich durch seine Hilfe die letzten Jahre gewachsen bin. Mein Wissen, mein Horizont, meine wissenschaftliche Neugier, meine Kontakte, die Orte, die ich bereisen durfte. Eine schier unendliche Anzahl an Dingen, die mich bereichert haben, sowohl als Person als auch als Wissenschaftler, verdanke ich Horst Kämpf. Da Worte können nur schwer meine tief empfundene Dankbarkeit ausdrücken: Eine tiefe, stille, lange Verbeugung ist hier ein bildliches Äquivalent.

Mein außerordentliches Danke geht an meine Betreuer Prof. Lothar Viereck und Dr. Thomas Jahr. Vielen Dank für eure Zeit und Mühe mir die Möglichkeit zu geben, an meiner Alma Mater zu promovieren, mir persönlich bedeutet es sehr viel auch nach Abschluss des Studiums die Zugehörigkeit zur Universität Jena und zum IGW zu erfahren. Auch wenn das Thema sehr multidisziplinär ist, freue ich mich sehr darüber, dass Ihr Euch die Zeit nehmt und genommen habt, euch einzuarbeiten, diese Arbeit zu formen und in die richtige Bahn zu lenken und damit ein wichtiger Teil meiner Entwicklung zu sein. Habt Dank.

Meine Projektfamilie, bestehend aus Dr. Christina Flechsig, Dr. Jan Mrlina, Dr. Karin Bräuer und Irka Schüller als Ganzes: Wir haben uns durch viele Schwierigkeiten im Projekt gekämpft. Habt Dank für eure Hilfe, euren Rat, die vielen Reisen, unsere Artikel und die generelle Unterstützung in guten und schlechten Zeiten wie Finanzierungspausen, Kürzungen, Ablehnungen etc. Es erfüllt mich mit tiefer Freude, dass ihr mich betreut und begleitet habt. Habt aber auch Dank individuell: Christina, mein herzlichst Danke für deine Unterstützung, geistig wie natürlich auch die finanzielle, die mir erst erlauben diese Arbeit kumulativ mit der erforderlichen Anzahl an Artikeln so fertig zu stellen. Jan, I appreciate your help and support with all the small and big things soooo much, let alone all the logistical and translation issues you have solved. My deepest appreciation to you - personally and professionally. Karin, auch natürlich an dich geht mein tiefer, tiefer Dank. Ich freue mich jedesmal, wenn du angerufen oder dich anderweitig bei mir erkundigt hast oder mir auf Reisen ein bisschen die Welt der Isotope erklären konntest. Irka, auch wenn wir leider nur die ersten Monate in diesem Projekt zusammen arbeiten konnten: Ein großer Teil dieser Arbeit hätte nicht entstehen können, wenn du nicht so tatkräftig geholfen hättest. Habt vielen Dank für die vielen gemeinsamen Feldarbeitstage und deinen grenzenlosen Optimismus. Ich wüsste niemanden, der mich solange hätte ertragen können.

Bedanken möchte ich mich bei all den lieben Freunden und Kollegen, die mich moralisch unterstützt haben: Stefan Kiefer - Danke für deine langjährige Freundschaft und dafür, dass du mich immer zum Lachen bringst. Auch wenn ich mich gefühlte Jahre nicht melde, freue ich mich nach wie vor, dass ein Wiedersehen ist, als hätte das Studium nie aufgehört. Unsere kleine Band: Habt dank für die zahllosen Stunden mit Musik, Lachen und ernsten Gesprächen. Paule, Mike, Henning, Oppa: Danke, dafür, dass ich Teil dieses kleinen, exklusiven Clubs sein kann. Stefan Wagenführ, mein langjähriger Freund, danke natürlich auch für deine Freundschaft und dafür, dass du immer ein offenes Ohr hast. Natürlich auch ein herzliches Danke an all die anderen Begleiter auf dem Weg zu dieser Promotion: Jens Heinicke, Susann Kämpf, Alina Schmidt, Gabe Newell, Anna-Neva Visser, Familie Zelinka, den Leuten und Kollegen am GFZ, besonders Prof. Brian Horsfield und Claudia Röhl, meinen Kollegen und Freunden von der Geophysik und wahrscheinlich ein ganzer Teil Menschen, die ich hier vergessen habe. Habt vielen, vielen

Dank.

Für den Schluss habe ich mir die wichtigsten Menschen in meinem Leben aufgehoben: Meine Mutter Petra Nickschick, meinen Vater Matthias Nickschick, meine Großmutter Anneliese Jokubeit, meine bessere Hälfte Tatjana Welk: Ihr haltet meine kleine Welt aufrecht. Worte können nicht meinen Dank beschreiben, Worte sind auch nicht nötig. Danke, dass ihr da seid.

Tobias Nickschick

Lebenslauf – curriculum vitae

Persönliche Daten

Name: Dipl.-Geophys. Tobias Nickschick
Anschrift: Max-Volmer-Straße 4
14473 Potsdam
Telefon: 0178/5595596
E-Mail: tnickschick@gmx.de
Geburtsdaten: 18.11.1985, Wernigerode

Beruflicher Werdegang

Juli 2015 – Juni 2016 wissenschaftlicher Mitarbeiter an Universität Leipzig, Sitz am Deutschen GeoForschungsZentrum Potsdam GFZ, drittmittelfinanziert durch DFG (FL 271/13)
Juli 2014 – Juni 2015 wissenschaftlicher Mitarbeiter/ Doktorand am Deutschen GeoForschungsZentrum Potsdam GFZ, drittmittelfinanziert durch DFG (KA 902/16)
Nov. 2011 – Okt. 2013 wissenschaftlicher Mitarbeiter/ Doktorand am Deutschen GeoForschungsZentrum Potsdam GFZ, drittmittelfinanziert durch DFG (KA 902/16)

Grundwehrdienst/ Zivildienst

Aug. 2005 – Apr. 2006 Zivildienst in der integrativen Kindertagesstätte „Quasselstrippe“ der Lebenshilfe Wernigerode

Schulbildung/ Studium

Seit Apr. 2014 offizielle Promotion an der Friedrich-Schiller-Universität Jena, Thema „Palaeovolcanic and present magmatic structures along the N-S trending Regensburg-Leipzig-Rostock zone“
Okt. 2006 – Sep. 2011 Studium der Geophysik, Friedrich-Schiller-Universität Jena, Abschluss: Diplom (1,6), Abschlussthema: „Gravimetrische Untersuchungen und Modellierung der Triasscholle bei Greiz“
1996 – 2005 Gerhart-Hauptmann-Gymnasium, Wernigerode; Abschluss: Abitur (2,1)
1992 – 1996 Grundschule Harzblick, Wernigerode

Tobias Nickschick

Jena, 15.08.2016